Hiroshima University Doctoral Thesis

Multinuclear Coinage Metal Complexes of Bis(diphenylphosphinyl)-functionalized Dipyrido-annulated N-heterocyclic Carbene

(ビス(ジフェニルホスフィニル)官能基を有するジピリド縮環 N-ヘテロサイクリックカルベンの多核貨幣金属錯体)

2019

Department of Chemistry,
Graduate School of Science,
Hiroshima University

Zhang, SIHAN

Table of Contents

Main Thesis

Multinuclear Coinage Metal Complexes of Bis(diphenylphosphinyl)-functionalized Dipyrido-annulated N-heterocyclic Carbene

Department of Chemistry,
Graduate School of Science,
Hiroshima University

Zhang, SIHAN

Contents

Chapter 1

General Introduction

1-1. N-heterocyclic Carbenes

Pursuing the carbon-based species which feature unique electronic properties and concomitant reactivity has always been the active area of chemical research. The neutral compounds N-heterocyclic carbenes (NHCs), containing a divalent carbon atom with a six-electron valence shell and stabilized by at least one neighboring nitrogen atom within the heterocycle, have attracted considerable attention since the landmark isolation of the first stable NHC via the deprotonation of 1.3-di-1-adamantylimidazolium chloride with potassium tert-butoxide or sodium hydride in the presence of catalytic dimsyl anion by Anduengo et al. in 1991,[1] due to their peculiar topology. So far, a large number of NHCs with diverse electronic and steric properties were synthesized and structurally characterized, in which 5-membered rings account for the largest part.[2] Among them, imidazole-based NHCs (**Figure 1. A**), the carbene carbon stabilized by two neighboring nitrogen atoms, are the most representative and famous species, which, to date, have received enormous interests from the world-wide chemists.

Other NHCs with 5-membered rings (**Figure 1**) include N-substituted (N,N'-disubstituted) imidazolidinylidenes (**B**), triazolinylidenes (**C**), benzimidazolinylidenes (**D**),[3] the 'abnormal' imidazolinylidenes (**E**)[4] and the cyclic(alkyl)(amino)carbenes (CAACs) (**F**) which gathered increasing interests since its first isolation by Bertrand et al. in 2005,[5] and so forth. Though the reduced conjugated π-system, **B** can still stably exist at room temperature, demonstrating the unsaturation in the imidazole ring is not required to produce a stable nitrogen-substitued carbene. **D** showed a enhanced thermal stability compared to **A** due to their widened and 10 electron conjugated π-system. In comparison to **A** which exhibit strong σ-donation but weak π-acceptor properties, **F** showed not only strong σ-donation but also relativey stronger π-acceptor properties so that these ligands can firmly bind to transition metals and main group elements. Due to their enormous practical significance, many of the NHCs are commercially available. Meanwhile, these compounds have found numerous applications, for instance, as supporting ligands for transition metal complexes, stabilizing *p*-block elements and as organocatalysts.[6] This, after all, benefits mostly from the distinct features, electronically and sterically, of NHCs.

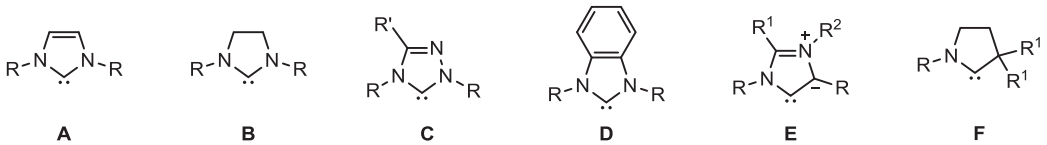

Figure 1. Structures of some of the most classical NHCs

In detail, due to the bent and sp^2-like arrangement of the carbene carbon as shown in **Figure 2** of their ground-state electronic structure, NHCs are generally considered as singlet carbenes.[7] This endows these compounds with nucleophilic ability since the lone pair in carbene carbon situates in the plane of the heterocycle of NHCs. Consequently, NHCs can serve as the strong σ-donor groups to bind

to a broad range of (non)metallic species, which leads to the formation of metal NHC complexes with strong metal-$C_{carbene}$ bonds. Comparatively, these bonds are generally stronger than that of their mimics, tertiary phosphines.[8] The enhanced strength and distinct features of the interactions between NHC and coordinated metals have notable influence on the stability, structure and reactivity of the resulting complexes.[9]

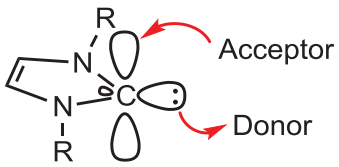

Figure 2. Representative ground-state electronic structure of NHCs

In general, it is fair to say that most of the NHCs can be described as fan- or umbrella-shaped with the nitrogen-substituents flanking the carbene carbon prefering to point towards the coordinated metals (**Figure 3**).[9,10] Therefore, any change of the nitrogen substituents could have a effect on the steric environment of the metal centers, thereby on the steric and electronic properties of NHCs, independently. While, in stark contrast to NHCs, the sp^3-hybridized phosphines exhibit a cone-shaped spatial arrangement (**Figure 3**), such that changing the substituents of phosphines invariably influences the steric and electronic properties.[9] This is also one of the advantages why the NHCs can rival their mimics of phosphines to become mainstream of chemical research as ancillary ligands. Furthermore, it is worth noting that thanks to decades of research on the preparation of heterocyclic compounds,[11] facile modifications of the peripheral architecture of NHCs are accessible by simple variation of the starting materials.

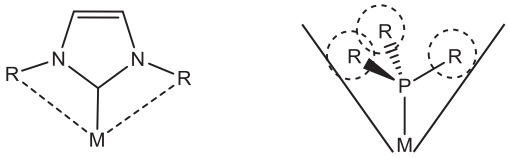

Figure 3. Steric influence of NHCs and phosphines on the metals which they are coordinated to.

While one should keep in mind that although NHCs have gained such interest, their scaffolds are still very limited, namely, the imidazole-based NHCs take up the largest part of research. The NHCs with different scaffolds, such as those with larger ring size and increased aromaticity, are still underexplored.[12] So far, only a handful of this kind of NHCs have been reported, including the imidazo[1,5-a]pyridin-3-ylidenes,[12a,d] indazolin-3-ylidenes,[12b,c] multicyclopentyl(or hexyl, heptyl)phenyl)-imidazol-2-ylidenes,[12e,k,l,m,o,p,r] isoquinolin-1-ylidenes,[12f] 5,7-bis(1,1-dimethylethyl)-5H-imidazo[4,5-f]-2,1,3-benzothiadiazol-6-ylidene,[12g] mixed amino-amido NHCs,[12h,j] porphyrin–NHCs[12i] and phenanthro[4,5-abc]phenazino[11,12-d] or acetonaphtho[1,2-b]quinoxaline[11,12-

d]imidazol-2-ylidenes[12n,q]. Given this, as the supporting ligands NHCs have great potential to be exploited for a long time.

1-2. Functionalized N-heterocyclic Carbenes

In principle, NHCs are considered as typical monodentate σ-donor ligands, thus the coordination of NHCs towards transition metals leads, in most cases, to the formation of mononuclear metal-carbene complexes. These complexes are suitable in a broad applications such as catalytic transformations, medicinal and luminescent materials.[9] Whereas with the rapid development of modern chemistry, research scope has been gradually extended from those monometallic NHC complexes to multimetallic NHC complexes, which gained in more and more popularity recently owing to their optoelectronic,[13] catalytic, medicinal and material applications.[14] Usually, two or more donor centers, such as NHC, phosphines, oxygens or nitrogens, are required for synthesizing the multimetallic complexes. The polydentate ligands which integrate the donor centers into one ligand seem to be a good choice as building blocks for multimetallic complexes. In this contribution, functionalized NHC ligands, as one of the polydentate ligands, attracted considerable attention.

Introducing the functional groups into the NHC ligands allows for hemilability, modification of the bite angles, establishing a specific ligand geometry or fine-tuning the electronic or steric properties of the ligand.[15] Hence, in a forward sense, functionalization of this class of ligands seems to be necessary. Furthermore, the functional groups of NHCs can strongly influence the reaction behaviors between ligands and the metals and structural motifs and properties of the concomitant products: (1) functionalized NHCs serving as pincer ligands type can afford more stable coordination environment for the metal centers of mononuclear NHC complexes since the functional groups can serve as the σ-donor ligand to coordinate with the metal center such that to further stabilize it; (2) it is conceivable that the designed functionalized NHCs are capable to precisely tune the metal coordination sphere through their multiple donor atoms;[16] (3) the multidentate NHC ligands functioning as the building blocks can provide a broad platform for selectively constructing the polynuclear metal NHC complexes. Meanwhile, interesting coordination chemistry of the functionalized NHC ligands towards transition metals are usually found and has attracted considerable attention of researchers.

1-3. Polynuclear Coinage Metal NHC Complexes

Coinage metal complexes bearing NHC ligands have been widely studied for their diverse coordination geometries and a variety of applications. For example, Ag(I)-NHC complexes have been widely utilized as reagents of transmetallation for the synthesis of other transition metal-NHC complexes.[17] Meanwhile, they showed excellent performance as catalysts in many important organic transformations.[18] Multinuclear Ag(I)-NHC complexes usually feature attractive intramolecular Ag-Ag interactions and diverse structures which are of current interest to researchers. Au(I)-NHC complexes are well-defined precatalysts in some of the most important transformations.[19] Oftentimes, multinuclear Au(I)-NHC complexes show attractive luminescence properties and metal-metal interactions. The Cu(I)-NHC complexes can serve as catalysts in many organic transformations.[20] Recently, many researchers have focused on the exploration of the photophysical properties of multinuclear Cu(I)-NHC complexes, especially, featuring strong intramolecular Cu-Cu interactions.

A seminal overview by J. C. Y. Lin et al.[21] in 2009 outlined comprehensively the development of this class of complexes, including their modular syntheses, diverse structural properties, excellent catalytic performance and medicinal applications, as well as their great potentials as luminescent materials. Since then, numerous coinage metal-NHC complexes have been synthesized, among which polynuclear coinage metal complexes based on phosphine-functionalized NHC ligands play an important role and are gathering increasing interests due to their diverse structures, metal-metal interactions and interersting photophysical properties (**Figure 5**).[22]

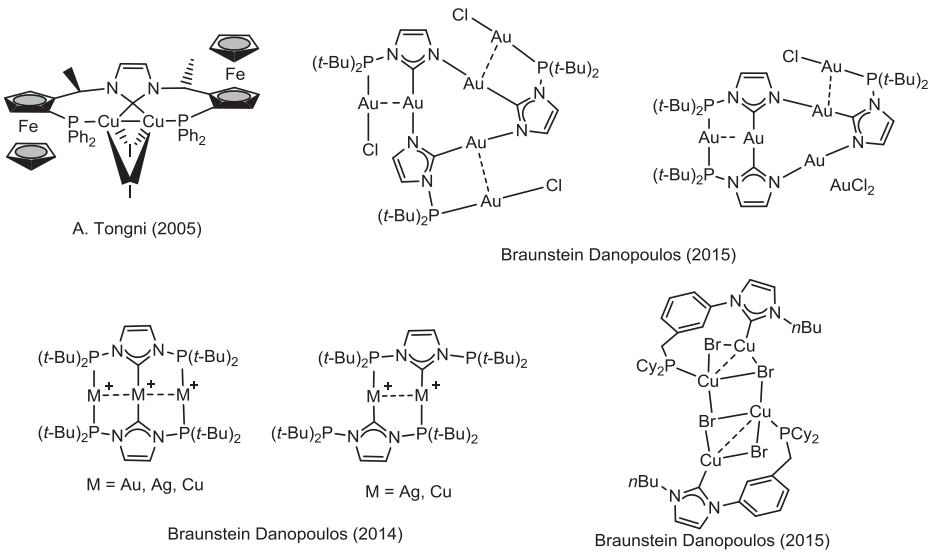

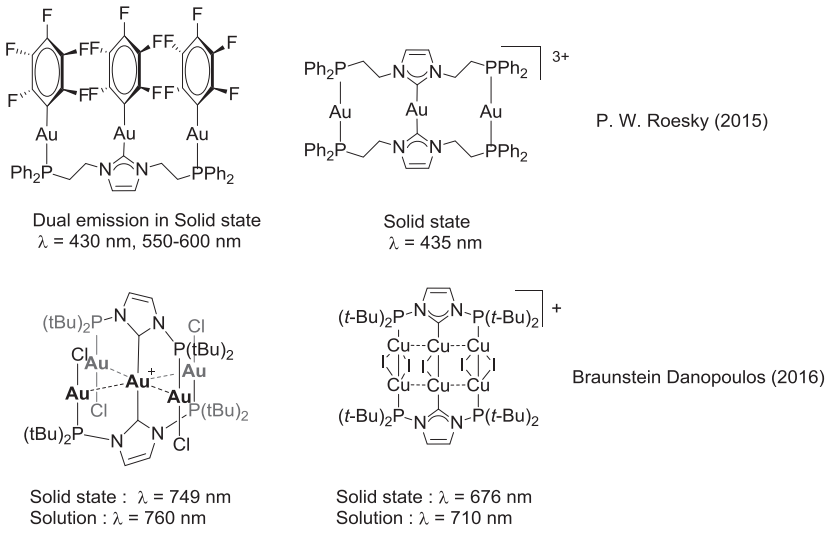

Figure 5. Examples of multinuclear coinage metal complexes bearing P-functionalized NHCs with diverse structures, metal-metal interactions and interesting photophysical properties

Our group has been always interested in the design and synthesis of pincer type ligands which can serve as the supporting ligands for monomeric mononuclear transition metal complexes.[23] These complexes showed good performance as catalysts in many organic transformations. Fortunately, the aforementioned supporting ligands that support coinage metal complexes can also be regarded as the standard pincer type ligands. Consequently, by virtue of our accumulation in the design and synthesis of pincer type ligands before, we are determined to expand our research area to the multinuclear coinage metal complexes.

1-4. Phosphine-functionalized N-heterocyclic Carbenes

As we have mentioned that functinalized NHC ligands attracted considerable attention and are highly desirable. To date, much efforts have been made to introduce functional groups into NHCs and fortunately, achievements in this field are remarkably prominent.[13,24] Among these, the NHC ligands functionalized by phosphine groups occupy the overwhelming position. Multidentate ligands containing both N-heterocyclic carbene and phosphine moieties can offer combined, complementary electronic properties and coordination geometries to transition metal centers to enhance the desired physical and chemical properties. Since the first isolation of a phosphinyl-functionalized imidazolium iodide by Herrmann *et al*. in 1996,[25] P-functionalized NHCs have been widely investigated as supporting ligands to afford numerous metal-NHC complexes which have been one of the hot research topics in the chemistry due to their great potentials in optoelectronic, medicinal and material applications as mentioned above. To date, a variety of phosphine-functionalized NHC ligands, as well as their modular syntheses have been developed (**Figure 4, G-I**).[22]

It is worth noting that most of these phosphine-functionalized NHC ligands are derived from the Arduengo type imidazole scaffold. Meanwhile, these phosphine-functionalized NHCs can be generally categorized into the rigid mono- and disubstituted bisphosphanyl NHC ligands (**Figure 4, G**), and the flexible mono- and disubstituted bisphosphanyl NHC ligands with a spacer between the phosphine and carbene moieties (**Figure 4, H** and **I**). For the former ligands, the carbene and phosphine donors align the metal cations along one axis (x axis in **Figure 4**), allowing intramolecular metal-metal interactions. Although free rotation along the N-P bond (the x axis) is possible, coordination to the metal leads to mostly rigid 2-D structures where all carbene and phosphine ligands, and metal centers lie within the same plane. Consequently, this kind of linking mode, to a large extent, limits their coordination geometries. In contrast, the latter ligands allow controllable degrees of freedom in all directions depending on the spacer between the coordination sites, permitting more diversified coordination geometries. However, due to the long distance between σ donors, the complexes based on these ligands usually have longer metal-metal distances, which prevent intramolecular d^{10}-d^{10} interactions which are desired and important in our initial design of the target compounds. In addition, the flexibility of ligands is known to hamper the efficiency of luminescence through thermal vibrations.

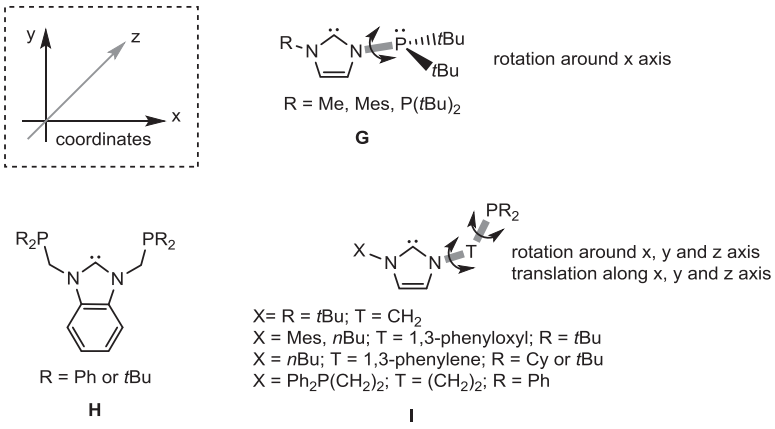

Figure 4. Selected examples of phosphine-functionalized NHC ligands

Compared to conventional chemical bonds, the metal-metal (coinage metals) interactions are regarded as weak forces. Even that, theoretical calculations and experiments have shown that these weak forces play an important role in the photophysical properties and electronic conductivity of coinage metal complexes.[26]

In this contribution, a structurally rigid design containing carbene and phosphine that offers different coordination geometries and short metal-metal distance would be highly desirable.

1-5. Bis(diphenylphosphinyl)-functionalized Dipyrido-annulated N-heterocyclic Carbene (dpa^{P2}-NHC)

Dipyridoimidazolinylidene, an electron-rich NHC with the empty carbene p-orbital additionally stabilized by a broad conjugation between which and the 14 electron conjugated π-system of the dipyrido moiety, was first reported by Weiss et al. in 1998 (**Figure 6. J**).[27] Interests in this ligand lay dormant for almost a decade until 2005 when it was used by Kunz group as supporting ligand to construct the chromium and tungsten pentacarbonyl complexes.[28] Simultaneously, for increasing its thermal stability and solubility in solution, the author introduced the *tert*-butyl groups into this compound by fixing them at the 2- and 10-positions, respectively, of the dipyrido moiety (**Figure 6. K**), which was structurely characterized in the next year.[29] Since then, compound **K** served as the ancillary ligand for otherwise transition metal complexes appeared in a limited number of literatures from Prof. Kunz's group.[30]

Due to our long-standing interest in the chemistry of pincer type ligands[23] and the unique features of compound **K**, we attempted to introduce functional groups (-SPh) into the monodentate compound **K** and fortunately as a result, two new hybrid NHC ligands (**Figure 6. M**) were synthesized, which both were successfully introduced as supporting ligands into rhodium carbene complexes (**Figure 6. N**).[23c] Shortly after this, based on compound **K** a new hybrid tridentate NHC ligand **dpa^{P2}-NHC** functionalized by diphenylphosphine groups (**Figure 6**) was synthesized by our group, which was then introduced as supporting tridentate ligand for monomeric mononuclear rhodium carbene complexes (**Figure 6, O**).[23d] While unfortunately, at that time this compound was just used as the transient intermediate, such that its isolation and structurally characterization were not obtained.

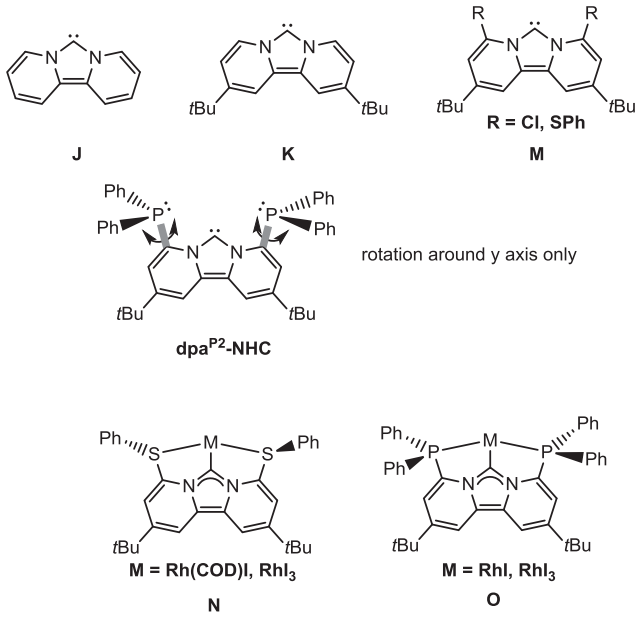

Figure 6. Reported dipyrido-annulated N-heterocyclic carbene ligands (top) and *ortho*-substituted dipyrido-annulated NHC rhodium complexes (bottom).

It is not until most recently **dpa^{P2}-NHC** was successfully isolated and structurally characterized by us. The **dpa^{P2}-NHC** was generated by the deprotonation of the carbene precursor **L(H)I** with KO*t*Bu in anhydrous THF for 3-4 h. After evaporation under reduced pressure of the resulting reaction solution, the addition of anhydrous hexane and the subsequently filtration and evaporation, pure **dpa^{P2}-NHC** was obtained as a yellow solid in 69% yield. In stark contrast to the compound **K** which can only stably exist at <-30 °C, **dpa^{P2}-NHC** did not show any sign of decomposition at ambient temperature in inert atmosphere for several months as judged by the NMR spectroscopy. The stability will considerably favor its subsequent complexation with metals. The characterisrtic downfield resonance at 8.3 ppm assignable to pro-carbenic proton in **L(H)I** in the ^{1}H NMR spectrum is missing, suggesting the successful deprotonation. The carbene carbon gave rise to a triplet resonance at 198.3 ppm (t, $^{3}J_{CP}$ = 34 Hz, C1) in the $^{13}C\{^{1}H\}$ NMR spectrum which is slightly downfield shifted by 2.0 ppm in comparison to that of compound **K** (δ 196.3),[29] which is indicative of a more stable structure for **dpa^{P2}-NHC** via phosphine groups inducively lowering the energy of the occupied σ-donor. $^{31}P\{^{1}H\}$ NMR spectrum displays only one singlet at -13.86 ppm, indicating the equivalence of two phosphine groups in **dpa^{P2}-NHC** in solution.

Single crystals suitable for X-ray analysis were obtained by slow evaporation of the **dpa^{P2}-NHC** solution in the mixed solvents THF/hexane at ambient temperature. The molecular structure (**Figure 7**) shows an almost inversion symmetry with the orientation of the lone pairs at phosphine *syn* to the lone pair of $C_{carbene}$, which allows more access to the metal centers. Three cycles of the backbone are coplanar, in which dipyrido moiety exhibits alternating single and double bonds as in the case of compound **K**.[29] While the phosphine groups show slightly bend out of the backbone plane (Φ_{PCCP}=9.6°). The N-$C_{carbene}$ bonds lengths of 1.368(2) Å (N1-C1) and 1.378(2) Å (N2-C1) are in the typical range for imidazoline derived NHCs. Meanwhile, the N-$C_{carbene}$-N shows an angle of 100.15(16)˚ that is slightly bigger compared with that of compound **K** (99.6(2)˚).[29] The N-C-N angle of 100.2(2)° is slightly larger than compound **K** (99.6(2)°). Furthermore, The close spatial proximity between the donor atom sites (P and $C_{carbene}$, averaged 2.971 Å) can be observed from the crystal conformation. This, together with the high rigidity of this ligand, will be conducive to the formation of polynuclear metal complexes with strong intramolecular metal-metal interactions.

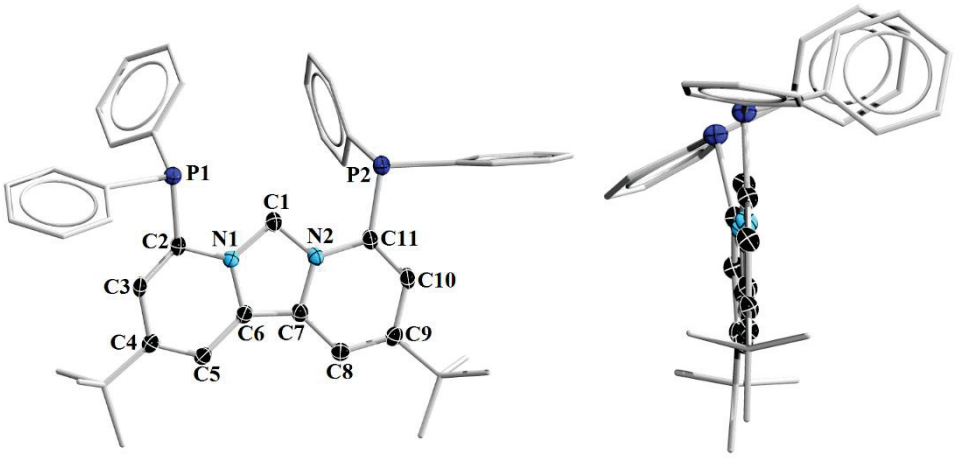

dpa^{P2}-NHC, front view **dpa^{P2}-NHC**, side view

Figure 7. Molecular structure of compound **dpa^{P2}-NHC**. Ellipsoids are shown at the 50% probability level. Hydrogen atoms are omitted for clarity. Selected bond lengths (Å) and angles [˚]: N1-C1 1.368(2), N2-C1 1.378(2), N1-C6 1.416(2), N2-C7 1.409(2), C6-C5 1.419(3), C7-C8 1.420(3), C5-C4 1.361(3), C8-C9 1.362(3), C4-C3 1.442(3), C9-C10 1.443(3), C3-C2 1.350(3), C10-C11 1.352(3), C2-N1 1.404(2), C11-N2 1.400(2), C2-P1 1.839(2), C11-P2 1.830(2); N1-C1-N2 100.15(16); torsion angle $\Phi_{P1C2C11P2}$ = 9.6.

However, although the NHC ligand **dpa^{P2}-NHC** has been designed and synthesized by us before, deeply exploring this interesting compound as the supporting ligand of polynuclear metal complexes remains dormant.

1-6. Purpose of This Work

With **dpa^{P2}-NHC** in hand and our interest in the research area of the polynuclear coinage metal complexes, we are determined to investigate the coordination chemistry of **dpa^{P2}-NHC** towards coinage metals as well as the photophysical properties of the concomitant products. In this thesis, the syntheses, spectroscopically and structurally characterization, interesting coordination chemistry and photophysical properties of the multinuclear coinage metal complexes based on **dpa^{P2}-NHC** will be discussed.

Chapter 2 described the synthesis and photophysical properties of three dinuclear and one tetranuclear gold(I) complexes based on **dpa^{P2}-NHC** and its imidazolium salt precursor. All of these complexes are structurally characterized by X-ray diffraction analysis and investigated with NMR spectroscopy.

Chapter 3 described the synthesis and photophysical properties of five homonuclear copper(I) and silver(I) complexes and one heteronuclear bimetallic Ag-Cu complexes based on **dpa^{P2}-NHC**. These complexes have been investigated with NMR spectroscopy and X-ray diffraction study.

Chapter 4 summarized the work of **Chapter 1-3** and brought forward the outlook towards our future work.

References

[1]. A. J. Arduengo, R. L. Harlow, M. Kline, *J. Am. Chem. Soc.* **1991**, 113, 361-363.

[2]. (a) H. V. Huynh, *Electronic Properties of N-Heterocyclic Carbenes and Their Experimental Determination*, *Chem. Rev.* **2018**. (b) *N-Heterocyclic Carbenes*. Wiley-VCH, Verlag GmbH & Co. KGaA, **2014**. (c) M. C. Jahnke and F. E. Hahn, *RSC Catal Series*, **2011**, 6, 1-41.

[3]. (a) A.J. Arduengo, J.G. Goerlich, W.J. Marshall, *J. Am. Chem. Soc.* **1995**, 117, 11027-11028. (b) D. Enders, K. Breuer, G. Raabe, J. Runsink, J.H. Teles, J.-P. Melder, K. Ebel, S. Brode, *Angew. Chem.* **1995**, 107, 1119; *Angew. Chem. Int. Ed.* **1995**, 34, 1021-1023. (c) D. Enders, K. Breuer, J. Runsink, J. H. Teles, *Liebigs. Ann.* **1996**, 2019. (d) D. Enders, K. Breuer, J.H. Teles, K. Ebel, J. Prakt. *Chem.* **1997**, 339, 397-399. (e) D. Enders, H. Gielen, *J. Organomet. Chem.* **2001**, 617-618, 70-80. (f) D. Zhao, L. Candish, D. Paul, F. Glorius, *ACS Catal.* **2016**, 6, 5978-5988. (g) C. Metallinos, X. Du, *Organometallics* **2008**, 28, 1233-1242. (h) M. Jonek, A. Makhloufi, P. Rech, W. Frank, C. Ganter, *J. Organomet. Chem.* **2014**, 750, 140-149. (i) L. Cao, S. Huang, W. Liu, X. Yan, *Organometallics* **2018**, 37, 2010-2013.

[4]. (a) S. Grundemann, A. Kovacevic, M. Albrecht, J. W. Faller Robert, R. H. Crabtree, *Chem. Commun.* **2001**, 2274-2275. (b) R. S. Ghadwal, S. O. Reichmann, R. HerbstIrmer, *Chem. Eur. J.* **2015**, 21, 4247-4251. (d) B. M. Day, T. Pugh, D. Hendriks, C. F. Guerra, D. J. Evans, F. M. Bickelhaupt, R. A. Layfield, *J. Am. Chem. Soc.* **2013**, 135, 13338-13341. (e) M. Melaimi, M. Soleilhavoup, G. Bertrand, *Angew. Chem., Int. Ed.* **2010**, 49, 8810-8849. (f) R. S. Ghadwal, *Dalton Trans*. **2016**, 45, 16081-16095. (c) R. H. Crabtree, *Coord. Chem. Rev.* **2013**, 257, 755-766. (g) M. Uzelac, A. Hernan-Gomez, D. R. Armstrong, A. R. Kennedy, E. Hevia, *Chem. Sci.* **2015**, 6, 5719-5728. (h) A. Kruger, M. Albrecht, *Aust. J. Chem.* **2011**, 64, 1113-1117. (i) M. Bhunia, P. K. Hota, G. Vijaykumar, D. Adhikari, S. K. Mandal, *Organometallics* **2016**, 35, 2930-2937. (j) M. Flores-Jarillo, V. Salazar-Pereda, F. J. Ruiz-Mendoza, A. Alvarez-Hernandez, O. R. Suarez-Castillo, D. Mendoza-Espinosa, *Organometallics* **2018**, 57, 28-31.

[5]. (a) V. Lavallo, Y. Canac, C. Prasang, B. Donnadieu, G. Bertrand, *Angew. Chem. Int. Ed.* **2005**, 44, 5705-5709. (b) M. Soleilhavoup, G. Bertrand, *Acc. Chem. Res.* **2015**, 48, 256−266. (c) M. Asay, B. Donnadieu, A. Baceiredo, M. Soleilhavoup, G. Bertrand, *Inorg. Chem.* **2008**, 47, 3949−3951. (d) M. Jazzar, R. Melaimi, M. Soleilhavoup, G. Bertrand, *Angew. Chem., Int. Ed.* **2017**, 56, 10046−10068. (e) R. Jazzar, J. B. Bourg, R. D. Dewhurst, B. Donnadieu, G. J. Bertrand, *Org. Chem.* **2007**, 72, 3492−3499. (f) V. Lavallo, Y. Canac, B. Donnadieu, W. W. Schoeller, G. Bertrand, *Angew. Chem., Int. Ed.* **2006**, 45, 3488−3491. (g) R. Kinjo, B. Donnadieu, M. A. Celik, G. Frenking, G. Bertrand, *Science* **2011**, 333, 610−613. (h) R. Jazzar, R. D. Dewhurst, J. B. Bourg, B. Donnadieu, Y. Canac, G. Bertrand, *Angew. Chem., Int. Ed.* **2007**, 46, 2899−2902.

[6]. (a) S. Díez-Gonzalez, N. Marion, S. P. Nolan, *Chem. Rev.* **2009**, 109, 3612−3676. (b) D. Enders,

O. Niemeier, A. Henseler, *Chem. Rev.* **2007**, 107, 5606−5655. (c) M. Poyatos, J. A. Mata, E. Peris, *Chem. Rev.* **2009**, 109, 3677-3707. (d) D. Enders, O. Niemeier, A. Henseler, *Chem. Rev.* **2007**, 107, 5606-5655. (e) C. Radloff, H.-Y. Gong, C. Schulte to Brinke, V. M. Lynch, J. L. Sessler, F. E. Hahn, *Chem. Eur. J.* **2010**, 16, 13077-13081. (f) W. A. Herrmann, *Angew. Chem. Int. Ed.* **2002**, 41,1290-1309. (g) S. Würtemberger-Pietsch, U. Radius, T. B. Marder, *Dalton Trans.* **2016**, 45, 5880–5895.

[7]. D. J. Nelson and S. P. Nolan. *Chem. Soc. Rev.* **2013**, 42, 6723-6753.

[8]. C. M. Crudden and D. P. Allen, *Coord. Chem. Rev.* **2004**, 248, 2247-2273.

[9]. M. N. Hopkinson, C. Richter, M. Schedler, F. Glorius, *Nature* **2015**, 510, 485-496.

[10]. A. J. Arduengo, *Acc Chem Res.* **1999**, 32, 913-921.

[11]. L. Benhamou, E. Chardon, G. Lavigne, S. Bellemin-Laponnaz, V. Cesar, *Chem. Rev.* **2011**, 111, 2705-2733.

[12]. (a) Y. Koto, F. Shibahara, T. Murai, *Org. Biomol. Chem.* **2017**, 15, 1810-1820. (b) R. Jothibasu and H. V. Huynh, *Chem. Commun.* **2010**, 46, 2986-2989. (c) Y. Zhou, Q. Liu, W. Lv, Q. Pang, R. Ben, Y. Qian, J. Zhao, *Organometallics* **2013**, 32, 3753-3759. (d) M. Alcarazo, S. J. Roseblade, A. R. Cowley, R. Fernández, J. M. Brown, J. M. Lassaletta, *J. Am. Chem. Soc.* **2005**, 127, 3290-3291. (e) R. Savka, H. Plenio, *Eur. J. Inorg. Chem.* **2014**, 2014, 6246-6253. (f) S. Gómez-Bujedo, M. Alcarazo, C. Pichon, E. Alvarez, R. Fernández, J. M. Lassaletta, *Chem. Commun.* **2007**, 1180-1182. (g) D. Tapu, O. J. Buckner, C. M. Boudreaux, M. Norvell, M. Vasiliu, D. A. Dixon, C. D. McMillen, *J. Organomet. Chem.* **2016**, 823, 40-49. (h) A. Makhloufi, M. Wahl, W. Frank, C. Ganter, *Organometallics* **2013**, 32, 854-861. (i) J. F. Lefebvre, M. Lo, D. Leclercq, S. Richeter, *Chem. Commun.* **2011**, 47, 2976-2978. (j) A. Makhloufi, W. Frank, C. Ganter, *Organometallics* **2012**, 31, 7272-7277. (k) S. Urban, M. Tursky, R. Fröhlich, F. Glorius, *Dalton Trans.* **2009**, 6934-6940. (l) E. L. Rosen, C. D. Varnado, A. G. Tennyson, D. M. Khramov, J. W. Kamplain, D. H. Sung, D. T. Gresswell, V. M. Lynch, C. W. Bielawski, *Organometallics* **2009**, 28, 6695-6706. (m) M. Pompeo, R. D. J. Froese, N. Hadei, M. G. Organ, *Angew. Chem. Int. Ed.* **2012**, 51, 11354-11357. (n) H. Valdés, M. Poyatos, E. Peris, *Inorg. Chem.* **2015**, 54, 3654-3659. (o) H. Valdés, M. Poyatos, E. Peris, *Organometallics* **2014**, 33, 5447-5450. (p) T. W. Hudnall, A. G. Tennyson, C. W. Bielawski, *Organometallics* **2010**, 29, 4569-4578. (q) D. Tapu, Z. McCarty, L. Hutchinson, C. Ghattas, M. Chowdhury, J. Salerno, D. A. VanDerveer, *J. Organomet. Chem.* **2014**, 749, 134-141. (r) R. Savka, S. Foro, H. Plenio, *Dalton Trans.* **2016**, 45, 11015-11024.

[13]. R. Visbal and M. C. Gimeno, *Chem. Soc. Rev.* **2014**, 43, 3551-3574.

[14]. (a) K. M. Lee, C. K. Lee, I. J. B. Lin, *Angew. Chem. Int. Ed.* **1997**, 36, 1850–1852. (b) K. M. Hindi, M. J. Panzner, C. A. Tessier, C. L. Cannon, W. J. Youngs, *Chem. Rev.* **2009**, 109, 3859–3884. (c) L. Mercs and M. Albrecht, *Chem. Soc. Rev.* **2010**, 39, 1903–1912. (d) A. J. Boydston,

K. A. Williams, C. W. Bielawski, *J. Am. Chem. Soc.* **2005**, 127, 12496–12497. (e) R. Visbal, G. M. Concepcion, *Chem. Soc. Rev.* **2014**, 43, 3551–3574. (f) K. Oisaki, Q. Li, H. Furukawa, A. U. Czaja, O. M. A. Yaghi, *J. Am. Chem. Soc.* **2010**, 132, 9262–9264. (g) K. Nomiya, S. Morozumi, Y. Yanagawa, M. Hasegawa, K. Kurose, K. Taguchi, R. Sakamoto, K. Mihara, N. C. Kasuga, *Inorg. Chem.* **2018,** 57, 11322-11332. (h) B. Bertrand, M. O'Connell, A. Maria, Z. A. E. Waller, M. Bochmann, *Chem. Eur. J.* **2018**, 24, 3613-3622.

[15]. O. Kuhl. *Functionalised N-Heterocyclic Carbene complexes*, Wiley, **2010**.

[16]. D. Janssen-Muller, C. Schlepphorst, F. Glorius, *Chem. Soc. Rev.* **2017**, 46, 4845-4854.

[17]. (a) H. M. J. Wang, I. J. B. Lin, *Organometallics* **1998**, 17, 972-975. (b) M. E. Humphries, W. H. Pecak, S. A. Hohenboken, S. R. Alvarado, D. C. Swenson and G. J. Domski, *Inorg. Chem. Commun.* **2013**, 37, 138–143. (c) E. Bappert and G. Helmchen, *Synlett* **2004**, 1789–1793. (d) J. Y. Zeng, M.-H. Hsieh and H. M. Lee, *J. Organomet. Chem.* **2005**, 690, 5662–5671. (e) A. Marchenko, H. Koidan, A. Hurieva, O. Kurpiieva, Y. Vlasenko, A. Kostyuk, C. Tubaro, A. Lenarda, A. Biffi, C. Graiff, *J. Organomet. Chem.* **2014**, 771, 14–23.

[18]. J. C. Garrison, W. J. Youngs, *J. Chem. Rev.* **2005**, 105, 3978-4008.

[19]. S. P. Nolan, *Acc. Chem. Res.* **2011**, 44, 91-100.

[20]. J. D. Egbert, C. S. J. Cazin, S. P. Nolan, *Catal. Sci. Technol.* **2013**, 3, 912-926.

[21]. J. C. Y. Lin, R. T. W. Huang, C. S. Lee, A. Bhattacharyya, W. S. Hwang, I. J. B. Lin, *Chem. Rev.* **2009**, 109, 3561-3598.

[22]. (a) S. Gaillard and J.-L. Renaud, *Dalton Trans.* **2013**, 42, 7255-7270. (b) H. M. Lee, J. Y. Zeng, C.-H. Hu, M.-T. Lee, *Inorg. Chem.* **2004**, 43, 6822-6829. (c) J. A. Cabeza, M. Damonte, P. Garcia-Alvarrez, A. R. Kennedy, E. Perez-Carrefio, *Organometallics* **2011**, 30, 826-833. (d) J. A. Cabeza, M. Damonte, P. Garcia-Alvarrez, M. G. Hernandez-Cruz, A. R. Kennedy, E. Perez-Carrefio, *Organometallics* **2012**, 31, 327-334. (e) M. Brill, E. Kuhnel, C. Scriban, F. Rominger, P. Hofmann, *Dalton Trans.* **2013**, 42, 12861-12864. (f) E. Kuhnel, I. V. Shishkov, F. Rominger, T. Oeser, P. Hofmann, *Organometallics* **2012**, 31, 8000-8011. (g) A. P. Marchenko, H. N. Koidan, A. N. Hurieva, O. V. Gutov, A. N. Kostyuk, C. Tubaro, S. Lollo, A. Lanza, F. Nestola, A. Biffis, *organometallics* **2013**, 32, 718-721. (h) S. Gischig and A. Tongi, *Organometallics* **2004**, 23, 2479-2487. (i) T. Simler, P. Braunstein, A. A. Danopoulos, *Dalton Trans.* **2016**, 45, 5122-5139. (j) T. Simler, P. Braunstein, A. A. Danopoulos, *Angew. Chem. Int. Ed.* **2015**, 54, 13691-13695. (k) L. Cao, S. Huang, W. Liu, X. Yan, *Organometallics* **2018**, 37, 2010-2013. (l) S. Bestgen, M. T. Gamer, S. Lebedkin, M. M. Kappes, P. W. Roesky, *Chem. Eur. J.* **2015**, 21, 601-614. (m) C. Kaub, S. Lebedkin, S. Bestgen, R. Koppe, M. M. Kappes, P. W. Roesky, *Chem. Commun.* **2017**, 53, 9578-9581. (n) P. Ai, M. Mauro, L. D. Cola, A. A. Danopoulos, P. Braunstein, *Angew. Chem. Int. Ed.* **2016**, 55, 3338-3341. (o) P. Ai, K. Y. Monakhov, J. V. Leusen, P. Kogerler, C. Gourlaouen, M. Tromp, R. Welter, A. A. Danopoulos, P. Braunstein,

Chem. Eur. J. **2018**, 24, 8787-8796. (p) P. Ai, M. Mauro, C. Gouristophe, S. Carrara, L. D. Cola, Y. Tobon, U. Giovanella, C. Botta, A. A. Danopoulos, P. Braunstein, *Inorg. Chem.* **2016**, 55, 8527-8542. (q) P. Ai, A. A. Danopoulos, P. Braunstein, *Inorg. Chem.* **2015**, 54, 3722-3724. (r) P. Ai, A. A. Danopoulos, P. Braunstein, K. Y. Monakhov, *Chem Commun.* **2014**, 50, 103-105. (s) P. L. Chiu and H. M. Lee, *Organometallics* **2005**, 24, 1692-1702. (t) F. E. Hahn, M. C. Jahnke, T. Pape, *Organometallics* **2006**, 25, 5927-5936. (u) A. Plikhta, A. Pöthig, E. Herdtweck, B. Rieger, *Inorg. Chem.* **2015,** *54* (19), 9517-9528. (v) S. Takaoka, A. Eizawa, S. Kusumoto, K. Nakajima, Y. Nishibayashi, K. Nozaki, *Organometallics* **2018,** *37* (18), 3001-3009.

[23]. (a) Y. Shi, S. Kojima, Y. Yamamoto, *Phosphorous Sulfur Silicon* **2012**, 188, 116-120. (b) Y. Shi, T. Suguri, C. Dohi, H. Yamada, S. Kojima, Y. Yamamoto, *Chem. Eur. J.* **2013**, 19, 10672-10689. (c) S. Fuku-en, J. Yamamoto, M. Minoura, S. Kojima, Y. Yamamoto, *Inorg. Chem.* **2013**, 52, 11700-11702. (d) S. Fuku-en, J. Yamamoto, S. Kojima, Y. Yamamoto, *Chem. Lett.* **2014**, 43, 468-470. (e) Y. Imada, H. Nakano, K. Furukawa, R. Kishi, M. Nakano, H. Maruyama, M. Nakamoto, A. Sekiguchi, M. Ogawa, T. Ohta, Y. Yamamoto, *J. Am. Chem. Soc.* **2016**, 138, 479-482.

[24]. (a) C. Fliedel and P. Braunstein, *J. Organomet. Chem.* **2014**, 751, 286-300. (b) S. Hameury, P. de Fremont, P. Braunstein, *Chem. Soc. Rev.* **2017**, 46, 632-733. (c) P. Hofmann and M. Brill, *NHCP Ligands for Catalysis*, Wiley, **2014**, chapter 10, pp 207-233.

[25]. W. A. Herrmann, C. Kocher, L. J. Gooben, G. R. Artus, *J. Chem. Eur. J.* **1996**, 2, 1627-1636.

[26]. a) E. R. T. Tiekink, J.-G. Kang, *Coord. Chem. Rev.* **2009**, 253, 1627-1648. b) X. He, V. W.-W. Yam, *Coord. Chem. Rev.* **2011**, 255, 2111-2123. c) P. Meyer, A. Rimsky, R. Chevalier, Acta Crystallogr. Sect. B **1978**, 34, 1457-1462. d) G. A. P. Dalgaard, A. C. Hazell, R. G. Hazell, *Acta Crystallogr. Sect. B* **1974**, 30, 2721-2724. e) M. T. Buckner, D. R. McMillin, *J. Chem. Soc., Chem. Commun.* **1978**, 759-761. f) H. D. Hardt, H.-J. Stoll, *Z. Anorg. Allg. Chem.* **1981**, 480, 193-198. g) R. A. Rader, D. R. McMillin, M. T. Buckner, T. G. Matthews, D. J. Casadonte, R. K. Lengel, S. B. Whittaker, L. M. Darmon, F. E. Lytle, *J. Am. Chem. Soc.* **1981**, 103, 5906-5912. h) H. D. De Ahna, H. D. Hardt, Z. Anorg. Allg. Chem. 1972, 387, 61-71. i) J. R. Kirchhoff, R. E. Gamache, M. W. Blaskie, A. A. Del Paggio, R. K. Lengel, D. R. McMillin, *Inorg. Chem.* **1983**, 22, 2380-2384. j) H. D. Hardt, *Naturwissenschaften* **1974**, 61, 107-110. k) M. W. Blaskie, D. R. McMillin, Inorg. Chem. 1980, 19, 3519-3522.

[27]. R. Weiss, S. Reichel, M. Handke, F. Hampel, *Angew. Chem. Int. Ed.* **1998**, 37, 344-346.

[28]. M. Nonnenmacher, D. Kunz, F. Rominger, T. Oser, *J. Organomet. Chem.* **2005**, 690, 5647-5653.

[29]. M. Nonnenmacher, D. Kunz, F. Rominger, T. Oser, *Chem. Commun.* **2006**, 1378-1380.

[30]. (a) M. Nonnenmacher, D. Kunz, F. Rominger, *Organometallics* **2008**, 27, 1561-1568. (b) M. Nonnenmacher, D. M. Buck, D. Kunz, Beilstein *J. Org. Chem.* **2016**, 12, 1884-1896. (c) D.

Kunz, C. Deibler, V. Gierz, F. Rominger, T. Oser, *Z. Natureforsch.* **2010**, 65b, 861-872. (d) V. Gierz, A. Seyboldt, C. Maichle-Mossmer, R. Frohlich, F. Rominger, D. Kunz, *Eur. J. Inorg. Chem.* **2012**, 1423-1429.

Chapter 2

Di- and Tetranuclear Au(I) Complexes of Bis(Diphenylphosphine)-Functionalized Dipyrido-Annulated N-Heterocyclic Carbene

2-1. Introduction

Gold(I)-NHC complexes have been the active area of research in the past three decades owing to their numerous applications, for instance, in catalysis,[1] medicine[2] and luminescence materials.[3] These compounds usually display remarkable luminescence properties, as the gold metal centers are capable of enhancing intersystem crossing and providing an effective means for the access of the spin-forbidden triplet states upon photoexcitation to the singlet excited states.[4] Since the first report of luminescent Au^{I}-NHC complex by Lin et al. in 1999,[5] this class of compounds has been considerably enriched with numerous NHC Au^{I} complexes featuring interesting optical properties being prepared. With the increasing understanding of this family of complexes, researchers have a high propensity to the polynuclear Au^{I}-NHC complexes with aurophilic interaction, since most of which exhibit more various and excellent luminescence properties in comparison to the mononuclear ones which generally show excellent catalytic performance in some of the most important transformations. That is mainly due to the ease and characters of electron communications of polynuclear Au^{I}-NHC complexes not just between ligands, ligand and metal centers, but also between the metal centers which are normally absent in the mononuclear Au^{I}-NHC complexes. More importantly, recent experimental and theoretical studies have shown that the aurophilic interactions have a crucial impact on the luminescence properties of gold complexes, as well as favor the formation of polymetallic structures.[6]

On the other hand, multidentate NHC ligands provide great opportunities for the research of coordination chemistry with metals and construction of metal complexes with diverse structures, oftentimes some of which are unexpected. For instance, Danopoulos and Braunstein group[7] has recently prepared a series of gold(I) NHC complexes with novel coordination sphere **(Figure 1)** based on their new developed tridentate P-functionalized NHC ligand, *N,N'*-diphosphanyl-imidazol-2-ylidene. These unexpected coordination behaviors and structures can considerably promote fundamental understanding of the nature of coordination chemistry between σ-donor ligands and metals.

Therefore, in this chapter, we aim to investigate the coordination chemistry of **dpa^{P2}-NHC** towards gold(I), establish the solid state structures of concomitant complexes and conduct the preliminary investigation on their luminescence properties.

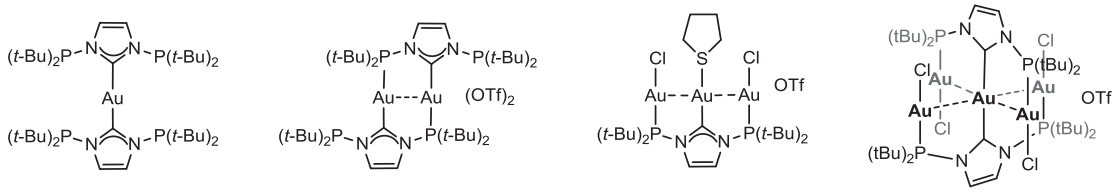

Figure 1. Selected examples of Au complexes based on *N,N'*-diphosphanyl-imidazol-2-ylidene reported by Danopoulos and Braunstein group.

2-2. Syntheses and Characterization of Dinuclear Au Complexes Based on dpa^{P2}-NHC

As mentioned above, aurophilic interaction has a crucial impact on the luminescence properties of gold complexes. Thus, for taking a glimpse of the influence of intramolecular d^{10}-d^{10} interaction to the luminescence properties of gold complexes, we were first to aim to synthesize a dinuclear Au^I-carbene complex without intramolecular d^{10}-d^{10} interaction, that is, a complex without activation of the carbene function. So the starting material should be the carbene precursor **L(H)I** rather than the free carbene **dpa^{P2}-NHC**. To avoid the potential substitution of chloride associated with Au^I ($AuCl{\cdot}SMe_2$ chosen to be the gold precursor in next complexation reaction) by iodide, an anion, such as PF_6^-, that will not adopt strong coordination with Au^I atom needs to be introduced instead of the iodide anion before complexation. Concerning the cost and the convenience of reagent acquisition, the PF_6^- was eventually chosen as the counter anion which replaces the iodide ion in subsequent anion metathesis.

Eventually, salt metathesis reaction was carried out by the combination of **L(H)I** and KPF_6 in CH_2Cl_2, generating the compound **L(H)PF$_6$** (**Scheme 1**). A multiplet resonance centered at δ -143.2 in ^{31}P NMR spectrum suggests the success of this anion metathesis.

With **L(H)PF$_6$** in hand, we are going to synthesize the dinuclear gold complex without the intramolecular aurophilic interactions as we designed before. Given the stability of the starting materials and the designed product to air and moisture, the next complexation was thus carried out at ambient atmosphere and the reaction solvent CH_2Cl_2 did not undergo rigorous drying procedure. The combination of [$AuCl(SMe_2)$] and **L(H)PF$_6$** in a ratio of 2:1 in CH_2Cl_2 gave rise to the desired digold complex **1** as bright yellow solid in excellent yield (90%) (**Scheme 1**). As predicted before, complex **1** is water tolerant and notably stable towards the air. In comparison to the phosphorous resonance of **L(H)PF$_6$** at δ -13.6, complex **1** shows a significant downfield shift by 48.0 ppm (δ_P 27.2 for **1**), indicating the formation of gold(I) coordinated phosphines. This, together with the upfield shift of the pro-carbenic proton resonance [**1**: δ_H 8.3 vs **L(H)PF$_6$**: δ_H 8.6], demonstrates the formation of the digold complex **1**, with two gold atoms respectively ligated to the phosphine groups. It is of note that the *p*-carbon resonance signal of phenyl groups cannot be found in the ^{13}C NMR spectrum, whereas which was detected at δ 134.6 (d, $^4J_{PC}$ = 2 Hz) in DEPT (135) NMR measurements. Meanwhile, ESI-MS spectrum shows an ion peak at *m/z* = 1113.1609 a.u. expected for the $[(AuCl)_2\mathbf{1}(H)]^+$ cation.

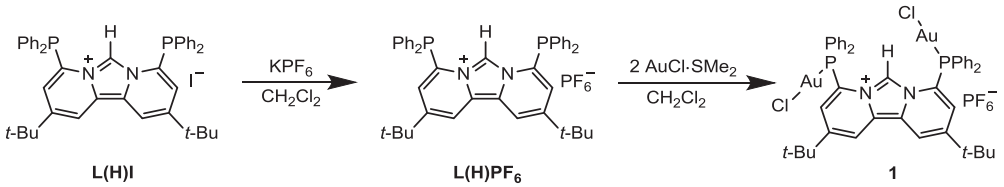

Scheme 1. Syntheses of digold complex **1**.

Further characterization for complex **1** was performed by X-ray diffraction analysis. Slow diffusion of diethyl ether into the solution of **1** in dimethylformamide (DMF) grew suitable single

crystals for structure analysis. Molecular structure (**Figure 2**) shows that complex **1** is C_2 symmetrical, with each gold nearly linearly coordinating with one phosphine and chloride atoms (P-Au-Cl 176.35(4)°). Presumably due to the steric repulsion from the diphenylphosphine groups, two Au-Cl bonds point towards the opposite orientations. The P-Au bond length of 2.2290(11) Å and Au-Cl bond length of 2.2984(12) Å are both in the typical range for gold(I) phosphine complexes[8] and AuCl complexes.[9] In agreement with our initial design, no intramolecular Au-Au interaction was observed based on their long distance of 7.006 Å.[10] In the crystal lattice, the AuCl moieties are aligned with intermolecular Au-Cl distance of 3.55 Å, and Au-Au distance of 4.219 Å, indicating no intermolecular metal-metal interactions.

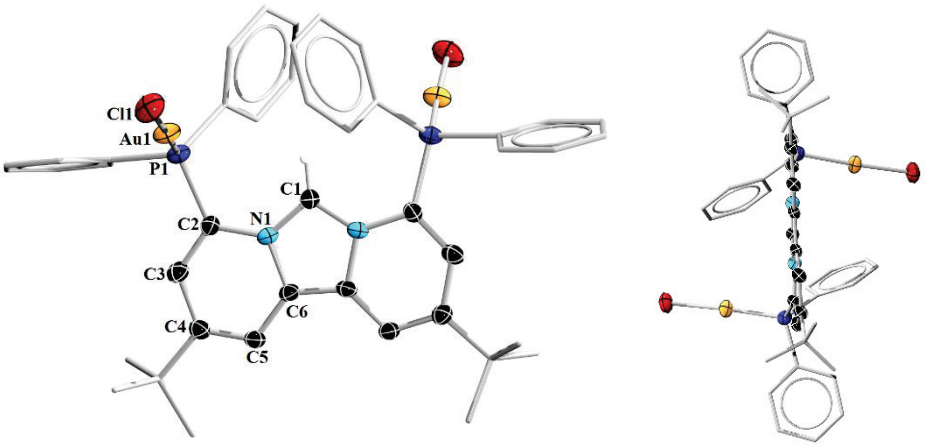

front view side view

Figure 2. Molecular structure of the cation of **1** in **1**·4DMF. Ellipsoids are shown at the 50% probability level. Solvent molecules and dissociated anion are omitted for clarity. Selected bond lengths (Å) and angles [°]: Au1-P1 2.2290(11), Au1-Cl1 2.2984(12); P1-Au1-Cl1 176.35(4).

Next, we aimed to afford the multinuclear gold complexes with intramolecular aurophilic interactions. Generally, gold(I)-carbene complexes can be produced either from the free carbene[11] or by transmetallation from their corresponding silver(I)-carbene complexes.[12] Considering the cost and time factors, we temporarily choose the former method. While unfortunately, one-pot reaction of **dpa^{P2}-NHC** with the gold precursor [AuCl(SMe_2)] in THF failed to generate the desired gold complexes, with ill-defined mixture formed. Changing the reaction conditions, such as reaction solvent, gold precursor and reactions temperature, did not make any progress for the reaction outcome.

Given the strong σ-donation and coordination abilities of carbene[13] and the Au atom weakly coordinated by SMe_2,[14] we surmise that the metalation between **dpa^{P2}-NHC** and gold precursor [AuCl(SMe_2)] would rapidly proceed. Thus, an optimized procedure different from the one-pot reaction was developed. Under the argon protection, an approximately saturated solution of AuCl·SMe_2 in anhydrous CH_2Cl_2 was added dropwise to the solution of **dpa^{P2}-NHC** in hexane, with

yellow solid instantly precipitating (**Scheme 2**). After filtration, a novel dimeric digold complex **2** was obtained in a 72% isolated yield. Its molecular structure was established by X-ray diffraction analysis.

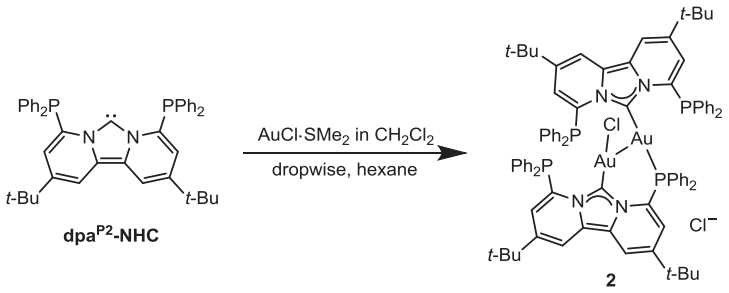

Scheme 2. Syntheses of dinuclear gold(I) complex **2**.

Complex **2** is asymmetric (**Figure 3**), in which two gold centers are both three-coordinate but exhibiting different arrangement, i.e., Au1 is ligated by one C_{NHC} donor and one P donor which are from two hybrid ligands **dpa^{P2}-NHC**, with the coordination sphere being completed by the neighboring Au^{I} atom, and Au2 is ligated by one C_{NHC} and one chloride, with the third coordination site being occupied by the adjacent Au^{I}. Two identical carbene ligands **dpa^{P2}-NHC** are respectively nearly planar, and significantly twisted into each other by 28.4° from a 90° angle, which can be attributed to the strong intramolecular Au^{I}-Au^{I} interaction. Both gold(I) atoms feature an almost linear arrangement with respect to C44-Au1-P4 angle of 178.48(12)° and C1-Au2-Cl1 angle of 178.27(13)°. The bond lengths for C_{NHC}-Au (C44-Au1 = 2.026(4) Å, C1-Au2 = 1.995(4) Å), P4-Au1 of 2.2914(12) Å and Au2-Cl1 of 2.3087(13) Å lie in the expected range for gold(I)-NHC,[15] gold(I)-phosphine and AuCl complexes.[8,9] Nevertheless, the P2-Au1 (2.8944(12) Å) and P3-Au2 (2.9374(14) Å) bond distances are significantly longer than the typical P-Au bond distance. In spite of that, these distances are still much shorter than the sum of van der Waals radii of 3.44 Å for P-Au, indicating the weak interaction between them. This probably results from the strain and reduced orbital overlap within the Au^{I}-contained five-membered rings due to the acute bite angle of 78.13(14)° (C1-Au2-P3) and 77.09(12)° (C44-Au1-P2), respectively. An intramolecular aurophilic d^{10}-d^{10} interaction is present judging by the short bond length between two gold(I) atoms (Au1-Au2 = 2.9557(3) Å).[10]

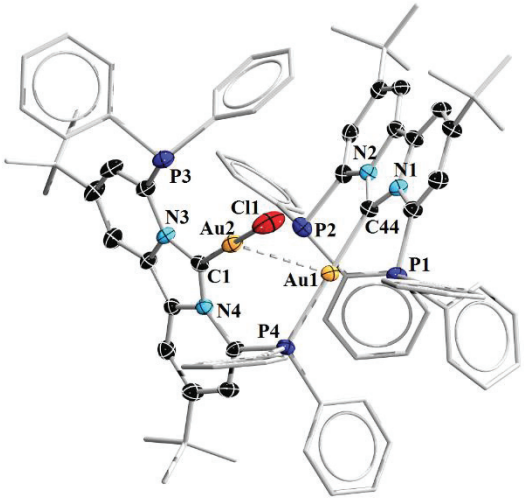

Figure 3. Molecular structure of complex **2** in **2**·2DMF. Ellipsoids are shown at the 50% probability level. Hydrogen atoms, dissociated chloride anion and solvent molecules are omitted for clarity. Selected bond lengths (Å) and angles [°]: Au1-Au2 2.9557(3), Au1-P4 2.2914(12), Au1-C44 2.026(4), Au2-Cl1 2.3087(13), Au2-C1 1.995(4); C1-Au2-Au1 88.11(13), C1-Au2-Cl1 178.27(13), C44-Au1-Au2 105.60(13), C44-Au1-P4 178.48(12), P4-Au1-Au2 75.42(3).

Although crystals of **2**·2DMF can be obtained reproducibly in good yield, the solid state structure cannot be maintained in solution. Specifically, the NMR spectra at ambient temperature did not show any discernible signal for complex **2**, while cooling down to -10 °C gave rise to four singlets at δ 26.2, 27.3, 28.5, 30.3, respectively, in ^{31}P NMR spectrum with slightly different intensity. Correspondingly, ^{1}H NMR spectrum displays a base peak (singlet) at δ 1.20 neighbored by four less intense peaks, both of which can be assigned to the proton signals of *tert*-butyl groups. Together, these NMR data suggest an arguably fluxional process for **2** in solution.

To investigate further this dynamic behavior, VT (variable temperature) NMR experiments were thus conducted for complex **2** (**Figure 4**). With the temperature cooling down from -10 to -40 °C, the singlet at δ 28.5 in ^{31}P NMR spectrum became more intense, while simultaneously the intensity of other three signals correspondingly decreased, finally this process averaged out at -40 °C. In the meantime, the base peak at δ 1.20 became slightly less intense with the neighboring small peaks correspondingly becoming more intense. This phenomenon can be tentatively explained by the rapid interconversion of the mixture of monomer, dimer or oligomers, which resulted from the presence of three dangling phosphine ligands as well as the lability of chloride that may dissociate or coordinate to the gold center in solution. Unfortunately, numerous attempts to grow suitable crystals of the monomer or oligomers at low temperature (below 0 °C) for X-ray analysis failed due to the consistently identical results that only the crystals of complex **2** can be obtained. Thus, proof is not sufficient enough to support the hypothesis above and more efforts for affording the crystals of the

monomer and oligomers is underway.

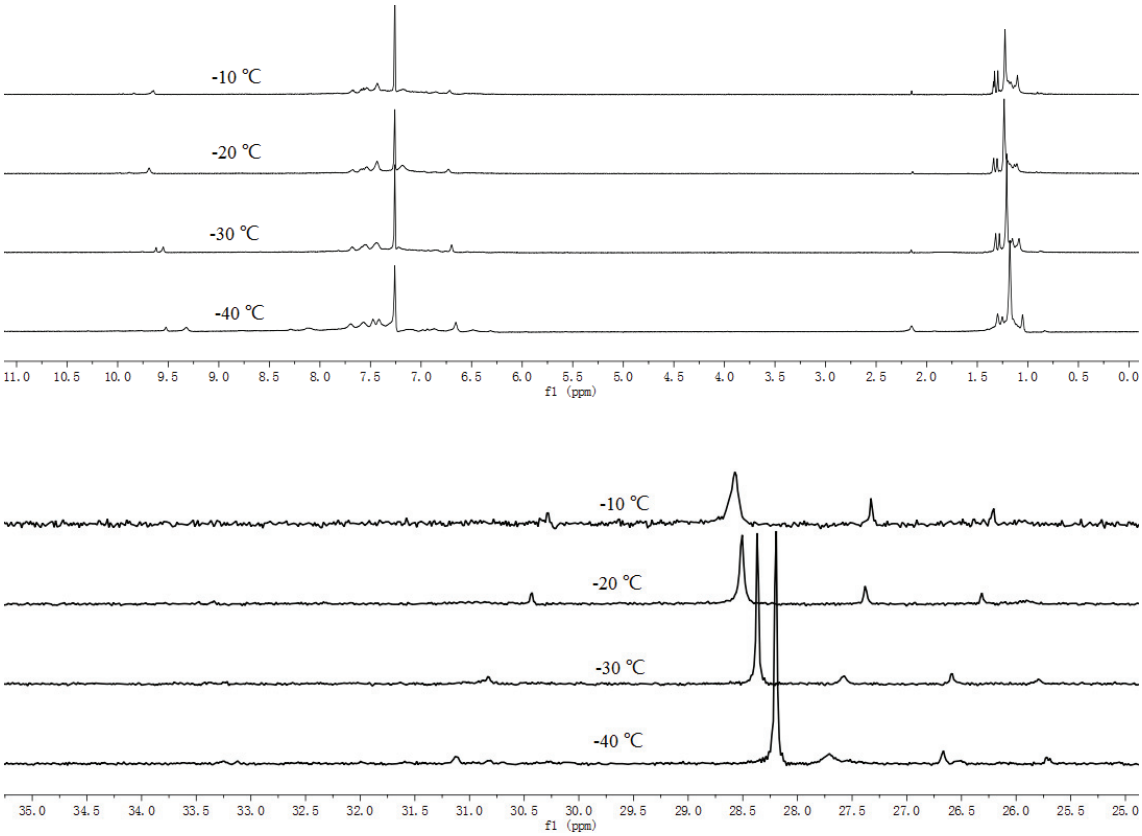

Figure 4. VT ^{1}H (top) and ^{31}P (bottom) NMR spectra of complex **2** in $CDCl_3$ from -10 to -40 ºC.

The complexation behavior of gold(I) precursors often depends on their ligands. The presence or absence of halide (X ligand), and the coordination strength of Lewis base (L ligand) have been reported to provide structurally different products. For instance, in 2016 P. Ai et al.[16] reported that reactions of phosphine-functionalized NHC with different gold(I) precursors yielded completely different gold(I)-carbene complexes (**Scheme 3**). Through the reaction of **dpa^{P2}-NHC** with $AuCl(SMe_2)$, the digold complex **2** has been formed as described above. Thus, we were curious about the outcome of the reaction of **dpa^{P2}-NHC** with $[Au(tht)_2(OTf)]$. Surprisingly, combination of the free carbene **dpa^{P2}-NHC** with 1 equiv $[Au(tht)_2(OTf)]$ in THF resulted in the formation of a new dinuclear gold(I)-carbene complex, the complex **3** (**Scheme 4**), in an 83% isolated yield. Two triplets at δ 29.65 (virtual triplet (vt), J_{PP} = 31.5 Hz) and 6.75 (vt, J_{PP} = 30.7 Hz), respectively, in $^{31}P\{^{1}H\}$ NMR spectrum suggest the presence of two different kinds of gold coordinated phosphine groups in **3**. Correspondingly, two singlets in the ^{1}H NMR spectrum at δ 1.04 and δ 1.20, respectively, that can be ascribed to the protons of tert-butyl groups, indicates the presence of two sets of *tert*-butyl groups. Both the NMR spectra are in good agreement with the observation of its solid state structure as shown in **Figure 5**. Meanwhile, ESI-MS spectrum shows a signal at *m/z* = 845.2486 expected for the ion peak of the dication of **3**,

revealing its persistence in solution.

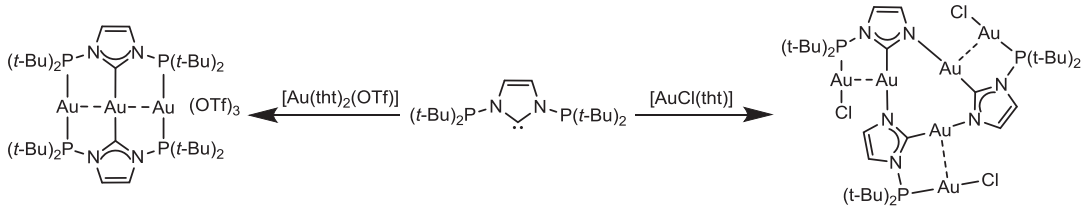

Scheme 3. Syntheses of two different gold(I) complexes starting from the same NHC by changing the anions of gold precursors (P. Ai et al. in 2015)

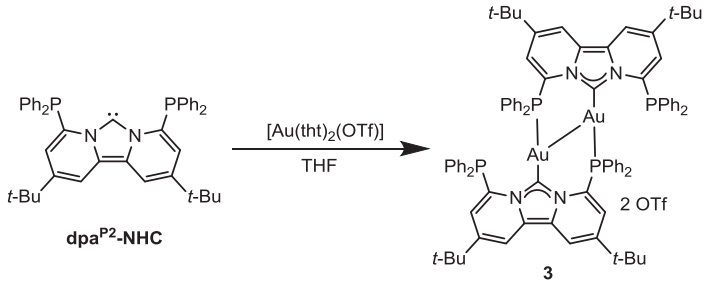

Scheme 4. Syntheses of digold complex **3** from **dpa^{P2}-NHC**.

Single crystals suitable for X-ray diffraction analysis were obtained by slow diffusion of diethyl ether into the solution of complex **3** in dimethylformamide (DMF). Its molecular structure is centrosymmetric and the planes of the two carbene heterocycles are not coplanar but at 122.55°. Two gold(I) atoms are three-coordinate and display identical coordination sphere with each metal ligated by one P donor and one NHC from two **dpa^{P2}-NHC** ligands, and the neighboring Au^{I}. Interestingly, the P1-Au1-Au2-P3 chain shows a nearly linear arrangement in terms of the P1-Au1-Au2 angle of 176.56(2)° and Au1-Au2-P3 angle of 174.52(3)°, respectively. Comparing with complex **2**, the bond distances of Au-P (Au1-P4 2.3072(13), Au2-P2 2.3015(13)) and Au-C_{NHC} (Au1-C1 2.048(5), Au2-C44 2.041(5) Å) in **3** show negligible deviations (maximum average deviation 0.034 Å for C_{NHC}-Au), while the Au-Au bond length of 3.0173(3) Å is 0.0616 Å longer but still implies a strong intramolecular d^{10}-d^{10} interaction.[10] This change can be ascribed to the strain of the metallocycles, especially the internal ten-membered ring, in **3**. Furthermore, this novel arrangement is reminiscent of a dinuclear Pd(I) complex with phosphine-functionalized tridentate NHC ligand.[17] Directed by hydrogen bonding between triflate and phenyl hydrogen atoms, the two rigid dpa^{P2}-NHC forms a bowl shape with phosphines orientated outwards (Figure 5, side view).

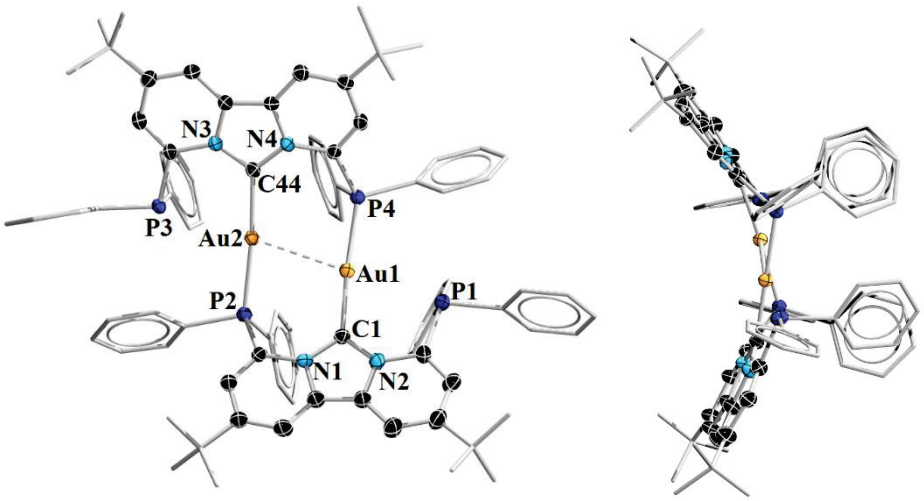

front view side view

Figure 5. Molecular structure of complex **3** in **3**·2DMF·Et_2O. Ellipsoids are shown at the 50% probability level. Hydrogen atoms, counter anions, and solvent molecules are omitted for clarity. Selected bond lengths (Å) and angles [°]: Au1-Au2 3.0173(3), Au1-P4 2.3072(13), Au1-C1 2.048(5), Au2-P2 2.3015(13), Au2-C44 2.041(5); C1-Au1-Au2 106.22(13), C1-Au1-P4 174.50(14), C44-Au2-Au1 106.53(14), C44-Au2-P2 176.07(14), P2-Au2-Au1 77.39(3), P3-Au2-Au1 174.52(3), P4-Au1-Au2 78.10(3).

Given the two nuclear Au(I) complexes, namely **2** and **3**, obtained above, we can make a conclusion that the products of the reactions of free carbene **dpa^{P2}-NHC** with gold(I) precursors depend on the nature of the anions associated with latter. Compared with triflate anion, chloride anion is a better ligand in terms of their abilities to coordinate to metals. Thus, in complex **2** one of the chlorides is prone to serve as a ligand coordinating to one Au(I), instead of a free anion which is like triflate anions in complex **3**. Consequently, two different dinuclear complexes **2** and **3** were achieved when dpa^{P2}-NHC reacted with equimolar amounts of two different gold(I) precursors, namely [AuCl(SMe_2)] and [Au(tht)$_2$(OTf)], respectively.

2-3. Syntheses and Characterization of Tetranuclear Au Complexes Based on dpa^{P2}-NHC

The successful syntheses of complex **1** has proven that two phosphine donors in **dpa^{P2}-NHC** are capable of coordinating metal cations independently. Thus, both **2** and **3**, the two dinuclear gold(I) complexes, can be considered to be coordinatively unsaturated since each tridentate **dpa^{P2}-NHC** captured only one metal center and the phosphine donors (three in **2** and two in **3**) are found to be non-metallated, which can be activated for coordination to metal center. In other words, these complexes have the potential to capture more metals. Meanwhile, recent reports have shown that diphosphine-functionalized NHC ligands are able to capture three, five and even six transition-metal cations in the form of dimeric species (**Figure 6**).[3e,7a]

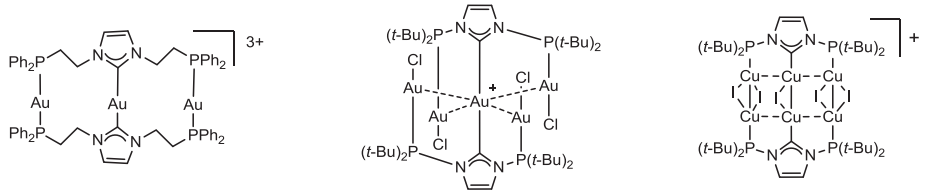

Figure 6. reported tri-, tetra- and pentanuclear complexes supported by diphosphine-functionalized NHC ligands.

To complete the series of gold complexes of P-functionalized NHC ligand **dpa^{P2}-NHC**, we thus aimed to synthesize the multinuclear gold(I)-carbene complexes such as those reported in recent literature.[7a] Considering the synthetic method for gold dpa^{P2}-NHC complexes containing more than two metals, there are currently two choices, coordination of the free carbene **dpa^{P2}-NHC** to a labile gold precursor (in this case [Au(tht)$_2$(OTf)]) in a ratio of <1:1 or reaction of dinuclear gold complex **2** (or **3**) containing non-metallated phosphine donors with gold precursor. Both seem to be reasonable and applicable and will be utilized in the next study.

To our excitement, a tetranuclear gold(I) complex **4** was afforded through the reaction of **dpa^{P2}-NHC** with either 1.5 equiv or 2 equiv [Au(tht)$_2$(OTf)] in 71.3% isolated yield (**Scheme 5**). Interestingly, increasing the amount of gold precursor [Au(tht)$_2$(OTf)] did not lead to the formation of new complexes with higher metal content but **4**. The ^{31}P NMR singlets at δ 36.3 suggests equivalence of all the phosphine groups. Meanwhile, the protons on the *tert*-butyl groups gave rise to only one singlet at δ 1.12 in the ^{1}H NMR spectrum, indicating the highly symmetric structure of **4** in solution. Both NMR data are in line with the observation of molecular structure as shown in **Figure 7**.

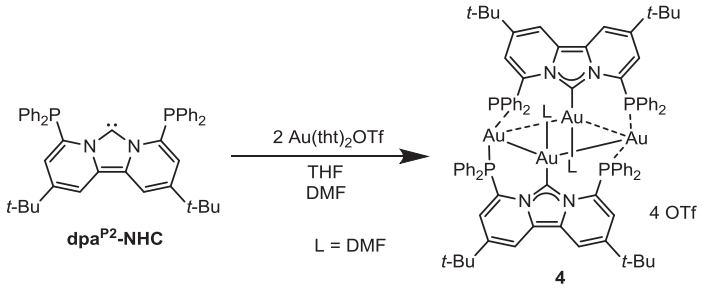

Scheme 5. Syntheses of tetranuclear gold complex **4** from **dpa^{P2}-NHC**.

Single crystals suitable for X-ray diffraction analysis were obtained by slow diffusion of diethyl ether into the solution of complex **4** in dimethylformamide (DMF). Complex **4** crystallized in the triclinic space group P$\bar{1}$ with two molecules in the asymmetric unit, which differ slightly with regard to their bond lengths and angles. Only one of the two molecules is discussed here. The structure of **4** shows a centrosymmetry with two identical Au_2**(dpa^{P2}-NHC)**-2OTf subunits, and two **dpa^{P2}-NHC** ligands are not coplanar but parallel and pointing precisely in opposite direction, which are bridged by a four-membered planar gold(I) ring connected by strong aurophilic interactions (Au4-Au3 3.0341(7), Au4-Au3# 3.1630(7) Å), although these Au-Au bond lengths are slightly longer than those in complexes **2** and **3**. Each outer Au^I displays a deviation from the linear P4-Au3-P3# arrangement (157.02(10)°) toward the central gold(I) atoms, which is likely attributed to the attractive intermolecular Au^I-Au^I interaction with the central golds. Regardless of the Au-Au interactions, all the four gold atoms are two-coordinate. Unlike the trinuclear Au^I bis(NHC) complexes[7a] in which all the three metals are respectively coordinated by either the two C_{NHC} donors (central gold) or two of the P donors (two outer golds) that belong to two hybrid carbene ligands, each of the two central golds in **4** is identically coordinated by one C_{NHC} donor and one DMF molecule, while the two outer Au^I atoms are respectively bound to two P donors from different ligands. This dimeric molecular 3D lattice arrangement is unique from all previously reported heteroleptic phosphine/carbene multinuclear complexes because the three donors are restricted to one plane with only rotation possible at the phosphines (Figure 7. side view). To the best of our knowledge, a similar structure with **4** has not been reported to date.

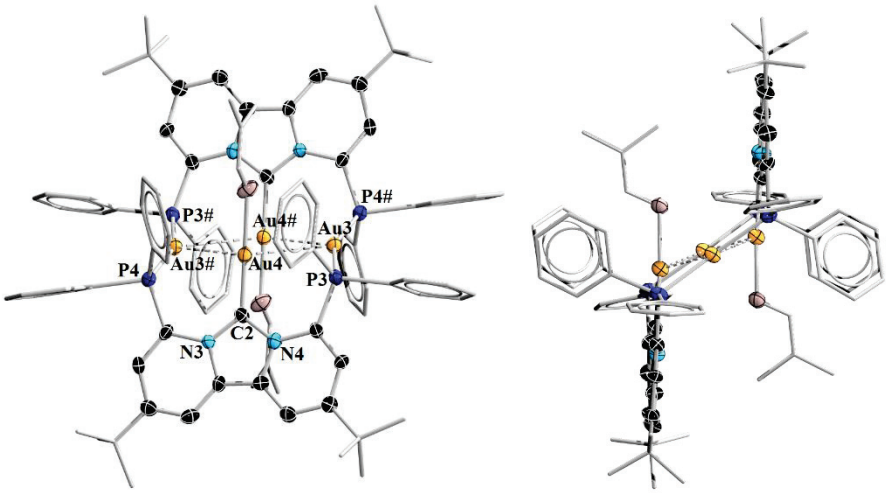

front view side view

Figure 7. Molecular structure of complex **4**·2DMF in **4**·4DMF. Ellipsoids are shown at the 50% probability level. Hydrogen atoms, counter anions, and disassociated solvent molecules (DMF) are omitted for clarity. Selected bond lengths (Å) and angles [°]: Au3-Au4 3.0341(7), Au3#-Au4 3.1630(7), Au4-C2 1.970(10), Au3-P4 2.302(3), Au3-P3 2.301(3); Au3-Au4-Au3# 113.284(16), Au4-Au3-Au4# 66.719(16), P4-Au3-P3# 157.02(10), C2-Au4-Au3 102.0(3), C2-Au4-Au3# 102.0(3).

2-4. Alternative Syntheses of Di- and Tetragold Complexes 3 and 4 from Complex 2

Looking more closely to the formulas of complexes **2** and **3**, it is easy to find that the only distinction between them is their counter anions, namely, complexes **2** and **3** possess two chlorides (one is coordinated to gold atom, another is serving as free counter anion) and two disassociated triflates, respectively, as their counter anions, regardless of their steric configurations. Thus, we wonder if it is possible to generate **3** starting from **2** by chloride abstraction. In view of that, reaction of complex **2** with 2 equiv AgOTf in CH_2Cl_2 in the absence of light was carried out and fortunately, complex **3** was expectedly formed as the only product in an 64% isolated yield as judged by the NMR spectroscopy (**Scheme 6**).

Most recently, in a landmark paper O. Rivada-Wheelaghan et al.[18] reported the controlled stepwise growth of linear copper (I) chains in their specially designed ligands. In detail, the author can easily increase the nuclearity (from one to four) of the complex by the stepwise addition of copper precursor and in the meantime, stepwise nuclearity reducing (from four to one) of the complex can also be achieved by changing the reaction solvent. Even though the author stressed that the ligand scaffolds are the key factor for achieving the metal growth, we hold the opinion that ligand transfer seems to play a more important role in these metal growth reactions. In other words, the quantitatively equal or excess σ-donors for supporting additional metals are likely responsible for accessing the metal growth. For example, in the dinuclear gold(I) complex **2**, it is conceivable that one, two, three even four additional metals can be introduced into this compound, since complex **2** owns totally six σ-donors (four phosphines and two NHCs) and two of the phosphine donors are non-metallated which are capable of coordinating to metal centers. Thus, we wonder if it is really feasible to implement the metal growth in our ligand system. As expected, this idea was successfully realized after the addition of 2 equiv $[Au(tht)_2(OTf)]$ into the solution of complex **3** in THF, with **4** being afforded as the only product in a yield of 51% (**Scheme 6**). Despite the unclear mechanism of the formation of **4**, it is plausible that the phosphine ligands transfer from the coordinated Au^I and the coordination of dangling phosphine donors to new added Au ions (simultaneously or sequentially) led to the formation of **4**.

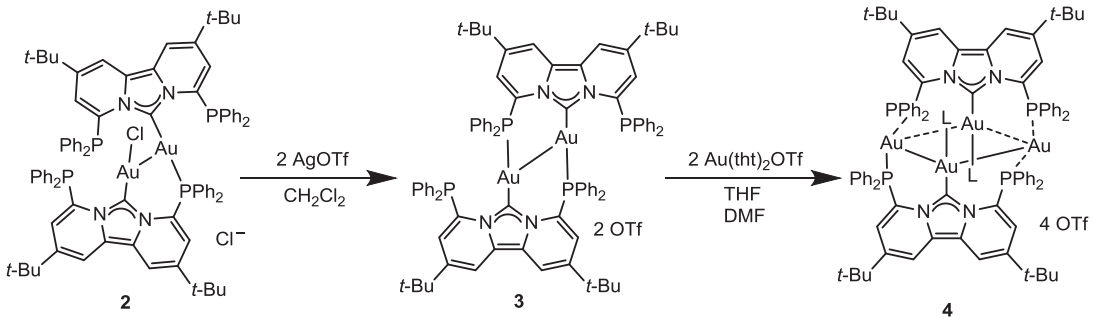

Scheme 6. Syntheses of complexes **3** and **4** starting from complex **2**.

Consequently, the above two reactions clearly demonstrate that complex **2** is able to function as

the precursor on the way to complexes **3** and **4**. More importantly, it also provides alternative method for the syntheses of multimetallic gold-NHC complexes, which not only is suitable to our ligand (**dpa^{P2}-NHC**), but also is highly likely to be applicable to other similar ligand systems. By the way, these discoveries inspire us to explore further the coordination chemistry of **dpa^{P2}-NHC** towards other transition metals, especially the other two group 11 metals, silver and copper.

2-5. Photophysical Properties of the Free Carbene Ligand dpa^{P2}-NHC and Complexes 1-4

As mentioned above, interesting photophysical properties most often can be found in gold NHC complexes. This, together with the novel structures of the complexes **1-4**, prompted us to investigate their luminescence in solution.

The obtained absorption spectra for free carbene **dpa^{P2}-NHC** and complexes **1-4** in dilute 2-methyl-THF are depicted in **Figure 8**. All the measured compounds absorbed in the visible region with the absorption maxima ranging from 320 to 420 nm, and these absorption bands can be tentatively attributed to the ligand-centered (LC) transitions and metal-to-ligand charge transfer (MLCT) transitions.[19] In comparison to the analogous multinuclear coinage metal complexes bearing P-functionalized imidazole-2-ylidene ligand (absorption maxima ranging from 260 to 350 nm),[7a,b] the absorption bands of complexes **1-4** are dramatically red-shifted, which can be rationalized by the expansion of the π-system from the dipyrido-annulated NHC ligand **dpa^{P2}-NHC** which leads to a lower lying LUMO energy than that of imidazole-based ligands.[20] Interestingly, **1** exhibits a low energy absorption band relative to complexes **2** and **3** (**1**: λ_{max} = 394 nm versus **2**: λ_{max} = 366 nm and **3**: λ_{max} = 388 nm), which is probably associated with (σ + Cl)-π* charge transfer from the Au-Cl bond to the LUMO in complex **1**.[21] Nevertheless, the significantly red-shifted absorption band was observed for complex **4** (λ_{max} = 431 nm) relative to complex **1**, which is most likely due to the presence of intramolecular aurophilic interactions.

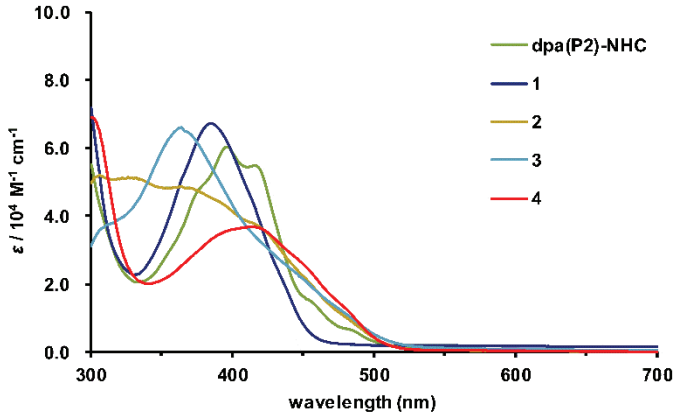

Figure 8. UV-vis absorption spectra of compounds **dpa^{P2}-NHC** and **1-4** in 2-methyl-THF solution (2.0×10^{-5} M) at room temperature.

Upon excitation at λ_{exc} = 345 nm, complexes **2-4** exhibit broad, structureless emission bands with the emission maxima in the sequence **3**＜**2**＜**4** (complexes **3**, **2** and **4** of 510, 522 and 550 nm, respectively) (**Figure 9**), tentatively pointing towards a greater contribution of an excited state where strong intramolecular Au^{I}-Au^{I} interaction is involved.[22] Given their low-energy emission, we thus tentativey assigned these luminescence to MMLCT excited states. In sharp contrast, complex **1** without the intramolecular Au^{I}-Au^{I} contact displays a higher energy emission band at λ_{em} = 486 nm,

in comparison to that of complexes **2-4** with intramolecular aurophilic interactions. While this phenomenon is in good agreement with the observation that an aurophilic contact can cause the emission band red-shifted.[22] Furthermore, the excitation spectra recorded by monitoring emission bands display excitation bands with almost same wavelength centered at λ_{exc} = 375 nm for all the complexes, which correspond nicely to their UV-vis absorption spectra, indicating that the origin of the photoluminescence process is same in both cases.

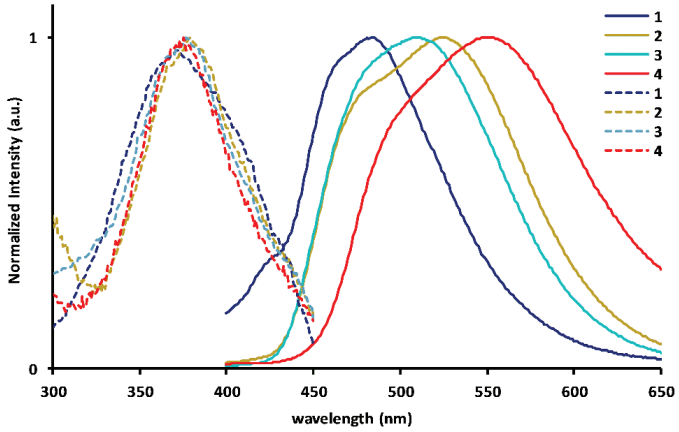

Figure 9. Normalized excitation (dash line) and emission (solid line) spectra of complexes **1-4** in CH_2Cl_2 solution at room temperature (2.0×10^{-5} M). Samples were excited at 345 nm. Photoluminescence excitation spectra were recorded by monitoring emissions at 485 nm (**1**), 510 nm (**3**), 520 nm (**2**) and 550 nm (**4**).

In the meantime, the measurement of luminescence properties of complexes **1-4** and free carbene **dpa^{P2}-NHC** in a different solvent, degassed 2-methyl-THF, was also conducted, and the result is shown in **Figure 10**. Judging from the obtained emission spectrum, we can find that variation of the solvent did not have any impact on their photoluminescence excitations as the excitation bands in both solvents are almost identical. This clearly suggests that the change of the solvent has approximately negligible influence on the photoluminescence excitation process of the studied complexes. Nevertheless, the emission spectrum shows a significant change compared to that in CH_2Cl_2 solution. In detail, all the investigated complexes **1-4** in degassed 2-methyl-THF display almost identical emission bands with the maximum centered at 500 nm, which are obviously different from that in CH_2Cl_2 as mentioned above. While it is worth noting that comparing with complexes **2-4**, **1** exhibits a blue shifted emission wavelength, which fits to the observation of these complexes in CH_2Cl_2. Compared to the emission band of the ligand dpa^{P2}-NHC, all the obtained gold complexes 1-4 showed negligible shift in terms of their emission bands, indicating these electronic transitions can be attributed to the ligand-centered transitions.

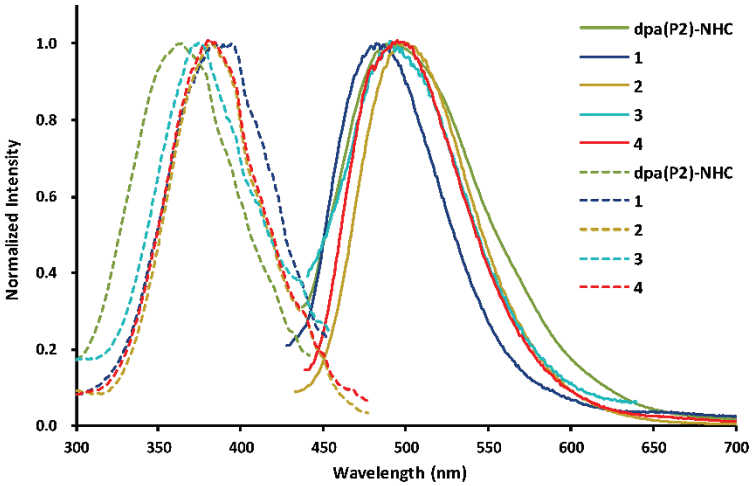

Figure 10. Photoluminescence excitation (dash line, normalized) and emission (solid line, normalized) spectra of complexes **1-4** in degassed 2-Me-THF at ambient temperature. Samples were excited at 375 nm (complexes **1-3**) and 420 nm (**dpa^{P2}-NHC** and **4**). Photoluminescence excitation spectra were recorded by monitoring emissions at 485 nm (**1** and **2**) and 500 nm (complexes **dpa^{P2}-NHC**, **3** and **4**).

All complexes are not phosphorescent at room temperature, but emit intense phosphorescence at 77K in glassy 2-methyl-THF. As shown in **Figure 11**, complexes **1-3** exhibit broad and structured phosphorescence spectra, in which both **1** and **2** show dual emissions at 579 and 617 nm, 603 and 659 nm, respectively. While **3** consists of three emission bands at 613, 639 and 667 nm, respectively, in contrast to which a broad phosphorescence at 648 nm was observed for complex **4**. Looking more closely to the spectrum, we can find that the phosphorescence bands of complexes **2-4** were slightly red-shifted from that of the free carbene **dpa^{P2}-NHC**, which was indicative of electronic perturbation of the gold cation to the triplet state of the carbene to a limited extent. Moreover, it is most likely that the two triplet states arising from different orbital parentages do not readily interconvert leading to the formation of two phosphorescent bands for **1** and **2**.[23]

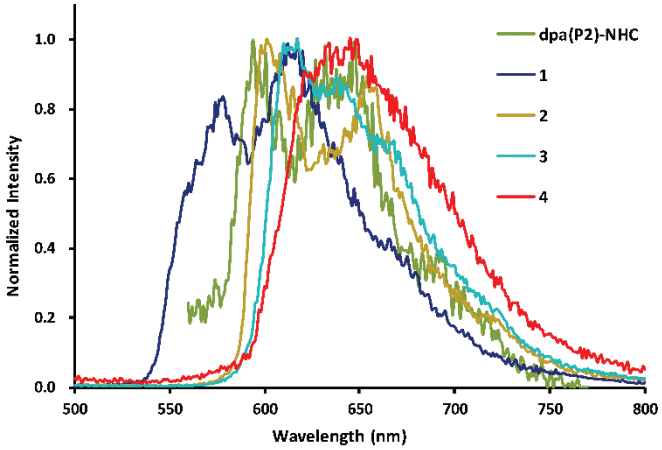

Figure 11. Normalized phosphorescence spectra of free carbene **dpa^{P2}-NHC** and gold complexes **1-4** at 77K in degassed glassy 2-methyl-THF (2.0×10^{-5} M). Samples were excited at 345 nm.

The phosphorescence decay profiles are depicted in **Figure 12**, from which the lifetimes of the free carbene **dpa^{P2}-NHC** and gold complexes **1-4** are calculated to be 772.0, 259.3, 89.1, 85.1 and 478.3 μs, respectively. Most likely, the long luminescence lifetimes for complexes **1** and **4** can be explained to originate from the lowest triplet states, while complexes **2** and **3** can be assigned as the lowest singlet state, based on their relatively long and short lifetimes.

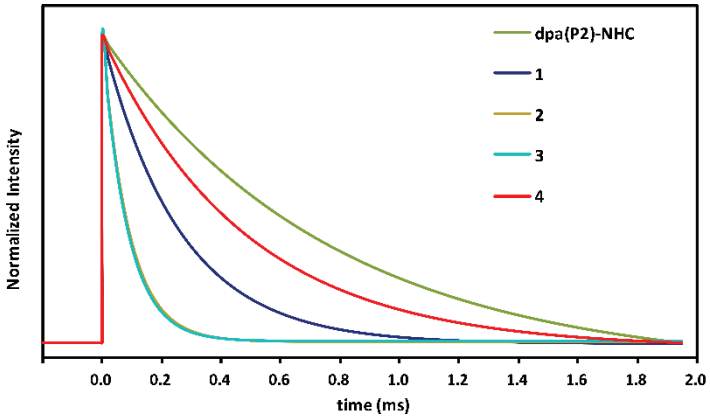

Figure 12. Phosphorescence decay traces for free carbene ligand **dpa^{P2}-NHC** and complexes **1-4** in 2-methyl-THF solution (2.0×10^{-5} M) at 77 K. The spectra were recorded by monitoring phosphorescence at 602 nm (**dpa^{P2}-NHC** and **2**), 615 nm (**1** and **3**) and 645 nm (**4**). The calculated lifetimes of **dpa^{P2}-NHC** and **1-4** are 771.97, 259.29, 89.14, 85.11 and 478.32 μs, respectively.

2-6. Conclusion and Outlook

In conclusion, di- and tetranuclear gold(I) complexes (complexes **2-4**) bearing diphenylphosphine-functionalized dipyrido-annulated NHC ligand were selectively synthesized from **dpa^{P2}-NHC** by changing the molar ratio between the gold(I) precursors and NHC ligand, as well as the anion associated with the former. Moreover, an interesting synthetic route has been developed together, that is, chloride abstraction of complex **2** with AgOTf gave rise to complex **3**, which subsequently reacted with $Au(tht)_2OTf$ affording complex **4** by the possible phosphine ligand transfer. Note that this alternative synthetic route provides nothing but an additional option for the syntheses of multinuclear metal NHC complexes. The room temperature NMR spectroscopy displaying possible coalescence indicated that complexes **2** and **4** underwent dynamic behavior in solution. X-ray analysis shows that complexes **3** and **4** display interesting coordination geometry: in **3**, both two gold centers are two-coordinate (neglecting the Au-Au interaction) and feature identical coordination sphere comprising an NHC and a phosphine donors belonging to two **dpa^{P2}-NHC** ligands; in **4**, the four gold(I) centers formed a planar ring which bridged two **dpa^{P2}-NHC** ligands in parallel.

All the gold complexes (**1-4**) show a variety of photoluminescence properties; in particular, these complexes exhibit totally different emission spectra when measured in different solvents. In 2-methyl-THF, complexes **1-4** exhibited almost same fluorescence bands with the free carbene ligand **dpa^{P2}-NHC**, suggesting that the electronic transmissions of these gold complexes are likely attributed to the ligand-centered (LC) transmissions. Furthermore, all the gold complexes are found to provide phosphorescence in degassed glassy 2-methyl-THF at 77 K, with the lifetime ranging from 89.1 μs to 772.0 μs. Since the investigation of gold part has been finished, we next turn our attention to investigating the coordination chemistry of **dpa^{P2}-NHC** towards silver(I) and copper(I) as well we the photophysical properties of concomitant complexes.

References

[1]. (a) J. C. Y. Lin, R. T. W. Huang, C. S. Lee, A. Bhattacharyya, W. S. Hwang, I. J. B. Lin, *Chem. Rev.* **2009**, 109,3561-3598. (b) S. P. Nolan, *Acc. Chem. Res.* **2011**, 44. 91-100. (c) N. Marion, S. P. Nolan, *Chem. Soc. Rev.* **2008**, 37, 1776-1782. (d) R. E. M. Brooner and R. A. Widenhoefer, *Angew. Chem. Int. Ed.* **2013**, 52, 11714-11724. (e) T. Wurm, A. M. Asiri, A. S. K. Hashmi, in *N-Heterocyclic Carbenes: Effective Tools for Organometallic Synthesis,* S. P. Nolan, Ed. Wiley-VCH Verlag GmbH & Co. KGaA. **2014**, pp. 243-270.

[2]. (a) H. G. Raubenheimer, S. Cronjie, *Chem. Soc. Rev.* **2008**, 37, 1998-2011. (b) K. M. Hindi, M. J. Panzner, C. A. Tessier, C. L. Cannon, W. J. Youngs, *Chem. Rev.* **2009**, 109, 3859-3884. (c) M. Porchia, M. Pellei, M. Marinelli, F. Tisato, F. Del Bello, C. Santini, *Eur. J. Med. Chem.* **2018**, 146, 709-746.

[3]. (a) E. E. Langdon-Jones and S. J. A. Pope, *Chem. Commun.* **2014**, 50, 10343-10354. (b) A. A. Penny, G. L. Starova, E. V. Grachova, V. V. Sizov, M. A. Kinzhalov, S. P. Tunik, *Inorg. Chem.* **2017**, 56, 14771-14787. (c) A. A. Penny, V. V. Sizov, E. V. Grachova, D. V. Krupenya, V. V. Gurzhiy, G. L. Starova, S. P. Tunik, *Inorg. Chem.* **2016**, 55, 4720-4732. (d) N. Sinha, L. Stegemann, T. T. Y. Tan, N. L. Doltsinis, C. A. Strassert, F. E. Hahn, *Angew. Chem. Int. Ed.* **2017**, 56, 2785-2789. (e) S. Bestgan, M. T. Gamer, S. Lebedkin, M. M. Kappes, P. W. Roesky, *Chem. Eur. J.* **2015**, 21, 601-614.

[4]. V. W. W. Yam and E. C. C. Cheng, *Chem. Soc. Rev.* **2008**, 37, 1806-1813.

[5]. H. M. J. Wang, C. Y. L. Chen, I. J. B. Lin, *Organometallics* **1999**, 18, 1216-1223.

[6]. (a) F. Mohr, *Gold Chemistry: Applications and Future Directions in the Life Sciences*; Wiley-VCH: Weinheim, Germany, **2009**. (b) P. Pyykko, *Chem. Rev.* **1997**, 97, 597−636. (c) P. Pyykko, N. Runeberg, F. Mendizabal, *Chem.-Eur. J.* **1997**, 3, 1451−1457. (d) P. Schwerdtfeger, *Heteroat. Chem.* **2002**, 13, 578−584. (e) J. Muñiz, C. Wang, P. Pyykkö, *Chem.-Eur. J.* **2011**, 17, 368−377. (f) H. Schmidbaur, A. Schier, *Chem. Soc. Rev.* **2012**, 41, 370−412.

[7]. (a) P. Ai, M. Mauro, L. D. Cola, A. A. Danopoulos, P. Braunstein, *Angew. Chem. Int. Ed.* **2016**, 55, 3338-3341. (b) P. Ai, M. Mauro, C. Gouristophe, S. Carrara, L. D. Cola, Y. Tobon, U. Giovanella, C. Botta, A. A. Danopoulos, P. Braunstein, *Inorg. Chem.* **2016**, 55, 8527-8542.

[8]. S. Gaillard, P. Nun, A. M. Z. Slawin, S. P. Nolan, *Organometallics* **2010**, 29, 5402-5408.

[9]. M. Hoshino, H. Uekusa, S. Ishii, T. Otsuka, Y. Kaizu, Y. Ozawa, K. Toriumi, *Inorg. Chem.* **2010**, 49, 7257-7265.

[10]. (a) P. Pyykko, *Chem. Rev.* **1997**, 97, 597-636. (b) E. R. T. Tiekink, *Coord. Chem. Rev.* **2014**, 275, 130-153. (c) H. Scjmidbaur, A. Schier, *Chem. Soc. Rev.* **2012**, 41, 370-412. (d) S. Sculfort and P. Braunstein, *Chem. Soc. Rev.* **2011**, 40, 2741-2760. (e) H. Scjmidbaur, A. Schier, *Chem. Soc. Rev.* **2008**, 37, 1931-1951.

[11]. P. De Frémont, N. M. Scott, E. D. Stevens, S. P. Nolan, *Organometallics* **2005**, 24, 2411-2418.

[12]. (a) H. M. J. Wang, I. J. B. Lin, *Organometallics* **2005**, 24, 1692-1702. (b) I. J. B. Lin, C. S. Vasam, *Can. J. Chem.* **2005**, 83, 812-825.

[13]. M. N. Hopkinson, C. Richter, M. Schedler, F. Glorius, *Nature.* **2014**, 510, 485-496.

[14]. P. G. Jones, J. Lautner, *Acta. Cryst.* **1988**, C44, 2091-2093.

[15]. Cambridge Structural Database: F. H. Allen, *Acta Crystallogr.* **2002**, B58, 380-388.

[16]. P. Ai, A. A. Danopoulos, P. Braunstein, *Inorg. Chem.* **2015**, 54, 3722-3724.

[17]. P. Ai, C. Gourlaouen, A. A. Danopoulos, P. Braunstein, *Inorg. Chem.* **2016**, 55, 1219-1229.

[18]. O. Rivada-Wheelaghan, S. L. Aristizabal, J. Lopez-Serrano, R. R. Fayzullin, J. R. Khusnutdinova, *Angew. Chem. Int. Ed.* **2017**, 56, 16267-16271.

[19]. (a) D. D. Zhukovsky, V. V. Sizov, G. L. Starova, S. P. Tunik, *J. Organomet. Chem.* **2018**, 867, 367-374; (b) Z. Wang, C. Zhang, W. Wang, C. Xu, B. Ji, X. Zhang, *Inorg. Chem.* **2016**, 55, 2157-2164; (c) A. K. Pal, A. F. Henwood, D. B. Cordes, A. M. Z. Slawin, I. D. W. Samuel, E. Zysman-Colman, *Inorg. Chem.* **2017**, 56, 7533-7544.

[20]. M. J. Leitl, V. A. Krylova, P. I. Djurovich, M. E. Thompson, H. Yersin, *J. Am. Chem. Soc.* **2014**, 136, 16032-16038.

[21]. (a) M. Osawa, M. Hoshino, M. Hashimoto, I. Kawata, S. Igawa, M. Yashima, *Dalton Trans.* **2015**, 44, 8369-8378; (b) M. Hashimoto, S. Igawa, M. Yashima, I. Kawata, M. Hoshino, M. Osawa, *J. Am. Chem. Soc.* **2011**, 133, 10348-103.

[22]. A. A. Penney, G. L. Starova, E. V. Grachova, V. V. Sizov, M. A. Kinzhalov, S. P. Tunik, *Inorg. Chem.* **2017**, 56, 14771-1478.

[23]. (a) C. K. Ryu, M. Vitale, P. C. Ford, *Inorg. Chem.* **1993**, 32, 869-874. (b) M. T. Buckner, T. G. Matthews, F. E. Lytle, D. R. MaMillin, *J. Am. Chem. Soc.* **1979**, 101, 5846-5848. (c) D. J. Casadonte, D. R. MaMillin, *J. Am. Chem. Soc.* **1987**, 109, 331-337.

Chapter 3

Multinuclear Cu, Ag, and Bimetallic Cu-Ag Complexes of Bis(diphenylphosphinyl)-functionalized Dipyrido-annulated N-heterocyclic Carbene

3-1. Introduction

Ag(I)-NHC complexes have been an active area of research for decades due to their multiple applications, for example, in NHC transfer reactions,[1] in catalysis[2] and in material science.[3] As excellent NHC transfer reagents, Ag(I)-NHC complexes have been utilized to successfully synthesize other transition metal-NHC complexes, in particular, those of the other two group 11 metals, Au and Cu, which largely benefits from the widespread nature that the coinage metal-NHC bond strength follows the order Au(I) > Cu(I) > Ag(I).[4] Meanwhile, along with the increasing interest in the functionalized NHCs that serve as the supporting ligands, multinuclear Ag(I) complexes bearing functionalized NHC ligands are also being intensively investigated owing to their diverse structures, as well as the concomitant interesting photoluminescence properties.[5] Many polynuclear silver complexes bearing functionalized NHC ligands with novel structures and metal-metal interactions have been reported recently.

Thanks to their excellent performance and great potential in some important catalytic transformations[6] and material science,[7] Cu(I)-NHC complexes are gathering increasing popularity in the recent past and particularly, an increasing number of groups recently start to investigate the luminescence properties of Cu(I)-NHC complexes.[8] In particular, the complexes featuring multi metals and strong inter- or intramolecular cuprophilic interactions have been experimentally and theoretically demonstrated to be able to provide a design methodology for highly efficient Cu(I)-based emitters.[9] Furthermore, owing to the cost and supply advantages, copper-based NHC complexes showing excellent luminescent properties seems to be the promising candidates of cyclometallated iridium complexes in terms of their application in organic light-emitting diodes (OLEDs).

Heterobimetallic complexes have gained increasing interest recently due to their distinct character of featuring two catalytically active sites.[10] While, the site-selective metallation seems to be a huge challenge that is hard to meet for achieving the heterobimetallic complexes. Few synthetic strategies which are not generally applicable have been used for the preparation of heterometallic complexes; for example, the stepwise deprotonation and metalation of the corresponding azolium salts,[11] the transmetallation from corresponding Ag(I)-NHC complexes benefiting from the difference in coordination chemistry of silver and the employed metals,[12] as well as the recently developed site-selective metallation based on the difference in reactivity of benzimidazole C2-Cl and imidazolium C2-H bonds.[13] While preparing heterobimetallic NHC complexes by taking advantage of the difference of coordination chemistry of the employed metals and the transmetallation aptitude of phosphine and NHC donors is extremely rare.[14]

Theoretical study[15] has shown that the coordination number of coinage metal ions is practically determined by the interaction energy and the energy of deformation of the metal coordination sphere. Accordingly, the gold complexes, having larger deformation energy in comparison with copper and silver ones, show an obvious predominance of dicoordination, compared to Cu^{I} and Ag^{I}. This notion

was also further corroborated by the synthesis of a series of dpa^{P2}-NHC Au^{I} complexes (**Chapter 2**), in which all the gold ions displayed dicoordination (neglecting the metal-metal interactions). Nonetheless, the dominant dicoordination, due to its relatively simple coordination mode, limits the structural diversity of Au complexes, to a large extent. In contrast, Cu^{I} and Ag^{I}, most commonly found as three- or four-coordinated species,[15] are expected to form complexes with more diversified structures for a given combination of metal ion and ligands.

In this chapter, we describe the coordination chemistry of bis(diphenylphosphinyl)-functionalized dipyrido-annulated N-heterocyclic carbene, **dpa^{P2}-NHC**, towards silver(I) and copper(I). Based on **dpa^{P2}-NHC**, two dinuclear silver (**Ag_2L_2**) and copper (**Cu_2L_2**) complexes, two tetranuclear copper complexes (**Cu_4LBr_4** and **$Cu_4L_2\cdot 2CH_3CN$**), a tetranuclear bimetallic silver/copper complex [**$Ag_2Cu_2L_2(O)$**] and a pentanuclear copper complex (**$Cu_5L_2Br_3$**) were achieved and characterized. NMR spectroscopy indicated that all the obtained complexes underwent dynamic behavior in solution at room temperature, which will be discussed in detail below. Furthermore, investigation into the photophysical properties of all the complexes showed that they are luminescent at room temperature, in which **Cu_4LBr_4**, **$Cu_4L_2\cdot 2CH_3CN$** and **$Cu_5L_2Br_3$** provided phosphorescence at 77 K with relatively long lifetimes ranging from 268.7 μs to 655.6 μs.

3-2. Syntheses of Dinuclear Silver Complex Ag_2L_2

As mentioned above, silver-NHC complexes can serve as the versatile carbene transfer reagents owing to their weaker Ag-NHC bond strength compared to those of gold and copper, thereby from which Au-NHC complexes can be synthesized. In contrast, the synthesis of Ag-NHC complexes from their gold analogues have never been reported. In this contribution, silver-NHC complexes are generally accessible via two synthetic methods: the reaction of the carbene precursor (usually imidazolium salt) with Ag_2O,[1a] or the coordination of the preformed free carbene to a labile silver precursor.[16] Considering the easy handle of **dpa^{P2}-NHC** (easy preparation and storage, stable for a long time), we choose the latter method. Meanwhile, ordinary silver salt AgOTf (OTf = triflate) for preparative purpose was chosen for this study. In view of this, a reaction of **dpa^{P2}-NHC** with AgOTf in a ratio of 1:1 in the absence of light was carried out, which led to the formation of a dinuclear silver complex **Ag_2L_2** as orange solid in a 79% isolated yield (**Scheme 1**). This compound is stable at ambient atmosphere for several hours and does not show any sign of decomposition.

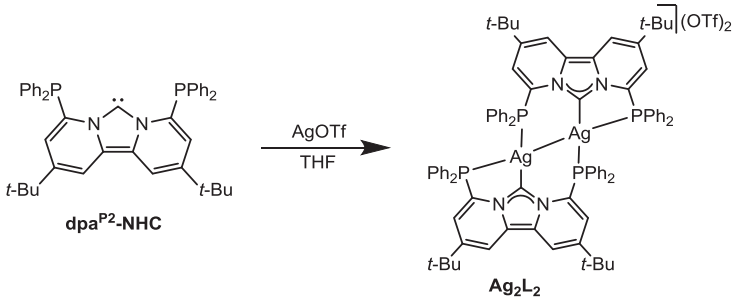

Scheme 1. Syntheses of dinuclear silver complex **Ag_2L_2** from **dpa^{P2}-NHC**.

Single crystals of **Ag_2L_2** suitable for X-ray diffraction analysis were obtained from a DMF solution overlayered with diethyl ether at -30 ˚C. Molecular structure of **Ag_2L_2** (**Figure 1**) shows a dimeric saddle-like structure. Actually, **Ag_2L_2** can be structurally regarded as two identical [Ag(dpa^{P2}-NHC)](OTf) monomers condensed together. Both two silver centers are three-coordinate (neglecting the Ag-Ag interaction) and exhibiting an identical coordination sphere comprising two phosphine donors from two dpa^{P2}-NHC ligands and one NHC donor. Different with its dinuclear Au analogue in which two of the phosphine donors remain dangling, all of the six σ-donors (two NHC and four phosphine donors) are respectively coordinating to one of the silver atoms. The bond distances between Ag(I) and C_{NHC} (C1-Ag1 2.166(3) Å, C44-Ag2 2.188(3) Å) lie in the typical range for silver-NHC complexes.[17] While interestingly, categorized by the bond length, two type of Ag-P bonds in **Ag_2L_2** were identified, that is, Ag1-P4 (2.4288(8) Å) and Ag2-P2 (2.4547(8) Å) with comparable bond lengths for typical silver-phosphine complexes,[14,16c,] Ag2-P3 (2.6694(9) Å) and Ag1-P1(2.6668(9) Å) with significant longer bond lengths compared to typical silver-phosphine complexes, respectively. These elongated bonds are most likely resulting from the strain and reduced orbital overlap within the

four-membered ring coming from the acute bite angle of 78.14(8)° (C44-Ag2-P3) and 77.80(9)° (C1-Ag1-P1), respectively. A strong d^{10}-d^{10} interaction is present based on the short distance between two silver atoms (Ag1-Ag2 2.8363(4) Å).[17,18]

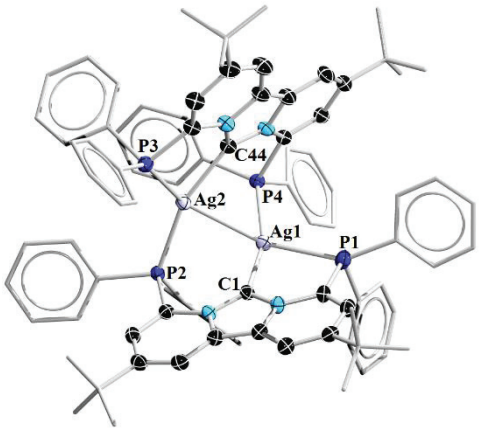

Figure 1. Thermal ellipsoid representation (50% probability level) of the structure of the cation in **Ag_2L_2**. Hydrogen atoms, two triflate anions and molecules of solvent of crystallization ($(CH3)_2NCHO$) are omitted for clarity. Selected bond lengths (Å) and angles [°]: Ag1-Ag2 2.8363(4), Ag1-P1 2.6668(9), Ag1-P4 2.4288(8), Ag1-C1 2.166(3), Ag2-P2 2.4547(8), Ag2-P3 2.6694(9), Ag2-C44 2.188(3); P1-Ag1-Ag2 135.53(2), P2-Ag2-Ag1 76.77(2), P2-Ag2-P3 122.68(3), P3-Ag2-Ag1 142.02(2), P4-Ag1-Ag2 78.28(2), P4-Ag1-P1 118.54(3), C1-Ag1-Ag2 84.02(8), C1-Ag1-P4 161.66(9), C1-Ag1-P1 77.80(9), C44-Ag2-Ag1 82.13(8), C44-Ag2-P2 158.10(9), C44-Ag2-P3 78.14(8).

Room temperature NMR spectra of **Ag_2L_2** showed a single and symmetrical dpa^{P2}-NHC ligand environment. In detail, three singlets at 8.71, 6.83 and 1.13 ppm corresponding to two kinds of pyridyl protons and *tert*-butyl protons, respectively, were detected; correspondingly, ^{13}C NMR spectrum shows only one set of resonance signals and only a broad singlet at -10.0 ppm was observed in ^{31}P NMR spectrum. Apparently, these solution data were inconsistent with the observation of its solid state structure since molecular structure of **Ag_2L_2** showed that two identical **dpa^{P2}-NHC** ligands are asymmetrical, that is, the four protons of dipyridyl groups and the two *tert*-butyl groups in each **dpa^{P2}-NHC** ligand are inequivalent. It is likely that these presumable NMR coalescences are the result of a fast fluxional behavior for **Ag_2L_2** in solution.

In order to explore the dynamic behavior of **Ag_2L_2** in solution, VT ^1H NMR study was performed. To our excitement, notable differences were observed between the ^1H NMR resonance of high temperature and low temperature. In other words, when the temperature was cooled down to below 203 K, the ^1H NMR spectrum of **Ag_2L_2** exhibited discernible decoalescence (**Figure 2**). In detail, upon cooling to 203 K, the singlet at 1.13 ppm assignable to the *tert*-butyl groups was split into two singlets.

Likewise, the pyridyl protons adjacent to the phosphine-substituted pyridyl carbons resonating as singlet at 8.71 ppm were found to give rise to two singlets starting from 203 K. Thus, at this temperature range, the resonance signals can be well resolved on the ^{1}H NMR timescale. And it is worth noting that those low temperature ^{1}H NMR spectra are in good agreement with the solid state structure.

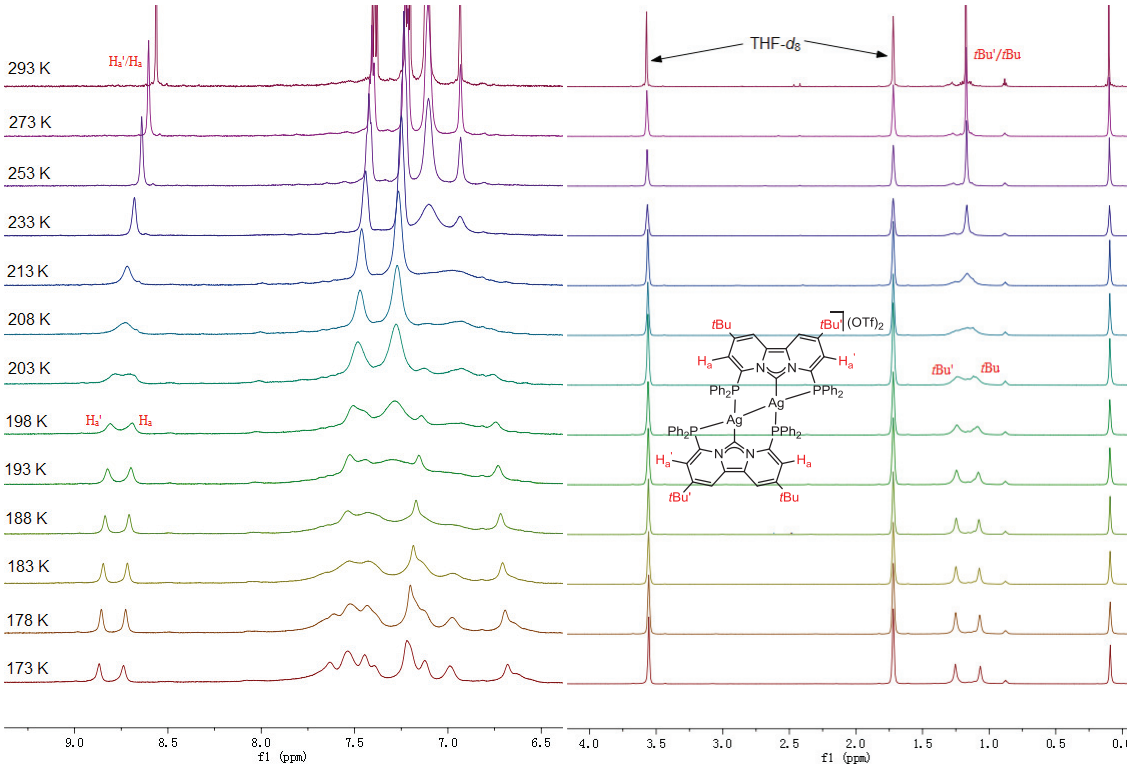

Figure 2. VT ^{1}H NMR spectrum of $\mathbf{Ag_2L_2}$ in THF-d_8 from 293 K to 173 K.

Meanwhile, we also conducted the VT ^{31}P NMR experiment for $\mathbf{Ag_2L_2}$ from 293 K to 178 K. Before our discussion, it is necessary to point out that a discernible room temperature ^{31}P NMR resonance for $\mathbf{Ag_2L_2}$ can be detected only after an overnight measurement or even longer. Due to our limited measuring condition, the VT NMR experiments at each set temperature can be running for no longer than 1 h. In other word, as shown in **Figure 3**, within 1 h no recognizable ^{31}P NMR resonance was observed from 293 K to 218 K, whereas discernible ^{31}P NMR resonance was detected below 218 K. On the other hand, owing to the silver element having two NMR active spin I = 1/2 isotopes (^{109}Ag and ^{107}Ag) with natural abundances of 48.18% and 51.82% respectively, after P-Ag coupling the standard ^{31}P NMR spectrum for P-NHC Ag complexes generally displays two close doublets with the coupling values ranging from 450-700 Hz.[14,16a,c,19]

A broad resonance signal at -10.0 ppm was observed for $\mathbf{Ag_2L_2}$ in the room temperature ^{31}P NMR spectrum, which is indicative of a possible coalescence and apparently inconsistent with the solid state structure which showed two different types of phosphine. While cooling down the temperature to 208

K led to decoalescence, where two multiplets at –5.1 ppm and –16.8 ppm, respectively, were observed (**Figure 3**). The ratio of these two multiplets in terms of their intensity are approximately 1:1; the downfield resonance and upfield resonance can be assigned to the inner two and outer two phosphines, respectively. Consequently, though the obtained low temperature ^{31}P NMR resonance were not well resolved likely due to the fast dynamic behavior of **Ag_2L_2** in solution, the conclusion can still be made that these spectral characteristics are roughly consistent with the solid state structure of **Ag_2L_2**.

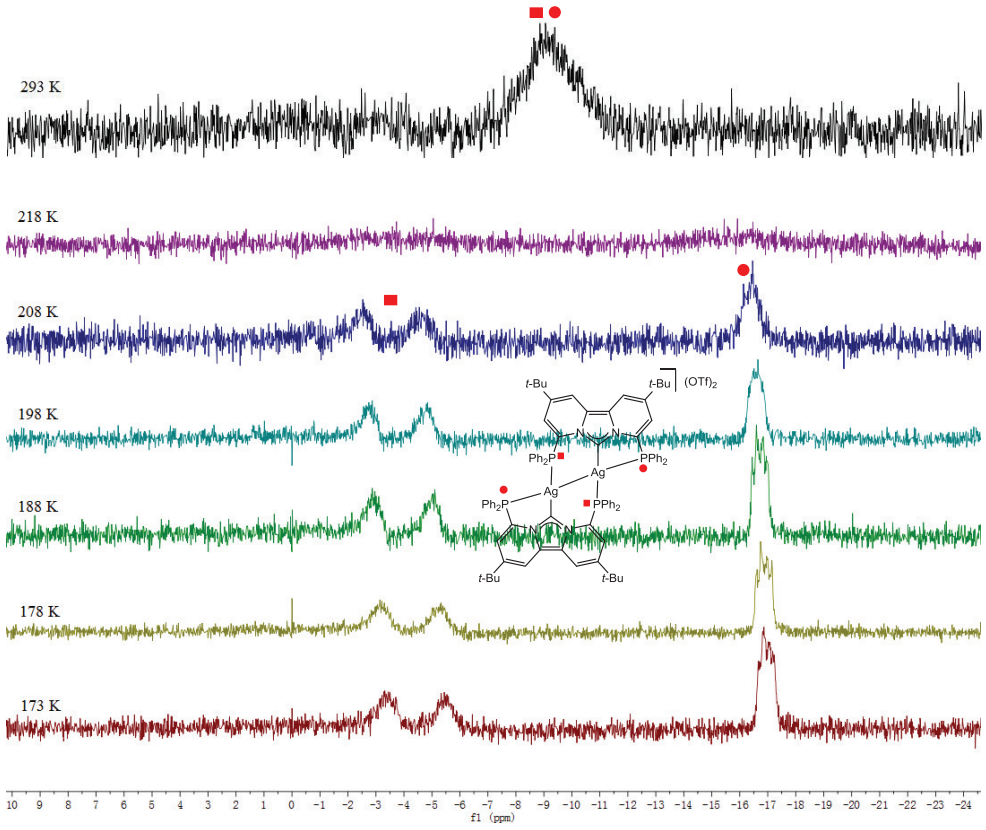

Figure 3. VT ^{31}P NMR spectrum of **Ag_2L_2** in THF-d_8 from 293 K to 173 K.

Given the obtained room temperature NMR spectroscopy of **Ag_2L_2**, two possibilities could describe its activities in solution. One is the dimeric species **Ag_2L_2** existing as a monomeric mononuclear species with symmetrical structure. The other one is the fast interconversion between two isomers (including **Ag_2L_2**). While the former one was less likely since a fairly broad room temperature ^{31}P {^{1}H} NMR resonance was observed: the postulated monomeric mononuclear silver species, likely featuring no interactions between the phosphine donors and silver center, is on the propensity to give rise to a sharp ^{31}P {^{1}H} NMR singlet. Furthermore, the latter hypothesis was eventually confirmed by the subsequent low temperature NMR experiments for **Ag_2L_2**. Careful simulation and kinetic analysis (**Kinetic Study of Ag_2L_2**, shown below) lead to a large positive entropy

($\Delta S^{\ddagger}$ = 68.6 cal mol^{-1} K^{-1}), indicative of a dissociative process with an energy barrio of ca. 25.3 kcal mol^{-1}. In addition, we proposed this dynamic behavior as shown below in **Scheme 2**.

Kinetic Study of Ag_2L_2

A JEOL JNM-ECA 600 NMR spectrometer was used for Variable Temperature (VT)-NMR studies of the solution behaviour of **Ag_2L_2**. The probe temperature was calibrated using standard methanol solution purchased from Sigma-Aldridge. The spectra were recorded at set temperatures, the corresponding probe temperatures from calibration curve were used for calculations. The gNMR Spectral Simulation Program (*version 4.1*) was used to simulate the obtained spectra.

From the calibration curve of our instrument, the real probe temperatures were calculated using the calibration equation: $y = -0.0014x^2 + 1.6451x - 63.72$

where x = Set Temperature, y = real probe temperatures.

Table 1. Temperature calibration: correlations between the set and real probe temperatures.

Set Temp /°C	Set Temp /K	Real Probe Temp /°C	Real Probe Temp /K
–65.0	208.2	–55.1	218.1
–70.0	203.2	–60.4	212.8
–75.0	198.2	–65.9	207.3
–80.0	193.2	–71.3	201.9
–85.0	188.2	–76.9	196.3

The hydrogen resonances corresponding to dipyridyl groups of **Ag_2L_2** are shifting depending on the temperature. We plotted chemical shifts against temperatures, and used the best approximation curve to assist the modeling of the chemical shifts (Hz) and half-width (Hz) of the resonances using gNMR. The simulated values for δ1, δ2 (in ppm) and half-width of signals (in Hz) as well as the rate constant k are listed below (the observed and simulated signals are attached at the end of this section).

Table 2. Simulated parameters from gNMR for an Eyring plot.

Temp. Calibration		gNMR Simulation					Eyring Plot	
Set Temp /°C	**Real Probe Temp /K**	**δ1 / ppm**	**$\nu_{1/2}$ (δ1) /Hz**	**δ2 / ppm**	**$\nu_{1/2}$ (δ2) /Hz**	**k / s^{-1}**	**1/T**	**ln(k/T)**
–65.0	218.1	8.732	48.00	8.720	48.00	205.60	0.00458	–0.06
–70.0	212.8	8.780	12.90	8.704	12.00	54.90	0.00470	–1.35
–75.0	207.3	8.809	25.80	8.695	24.00	10.98	0.00482	–2.94
–80.0	201.9	8.823	19.80	8.698	19.20	1.92	0.00495	–4.66
–85.0	196.3	8.836	12.20	8.708	12.00	0.30	0.00509	–6.48

With the simulated *k* values at different temperatures, an Eyring plot (ln(*k*/T) *v.s.* 1/T) was created to estimate the $\Delta G^{\ddagger}$, $\Delta S^{\ddagger}$ and $\Delta H^{\ddagger}$ values according to the equation:

$$\ln(\frac{k}{T}) = -(\frac{\Delta H^{\ddagger}}{R})\frac{1}{T} + (\frac{\Delta S^{\ddagger}}{R}) + \ln(\frac{k_B}{h})$$

where the slope of the plot = $-(\frac{\Delta H^{\ddagger}}{R})$, and the intercept = $(\frac{\Delta S^{\ddagger}}{R}) + \ln(\frac{k_B}{h})$

From the Eyring plot:

Slope = –12705, y-intercept = 58.282

Standard error and standard deviation of intercept: $\sigma_M = 0.958$, $\sigma = 2.143$

Standard error and standard deviation of X variable 1 (1/T): $\sigma_M = 198.238$, $\sigma = 443.274$

$\Delta S^{\ddagger}$ = 68.60 cal $mol^{-1}K^{-1}$ = 287.03 J $mol^{-1}K^{-1}$, $\Delta H^{\ddagger}$ = 25.30 kcal mol^{-1} = 105.64 kJ mol^{-1}

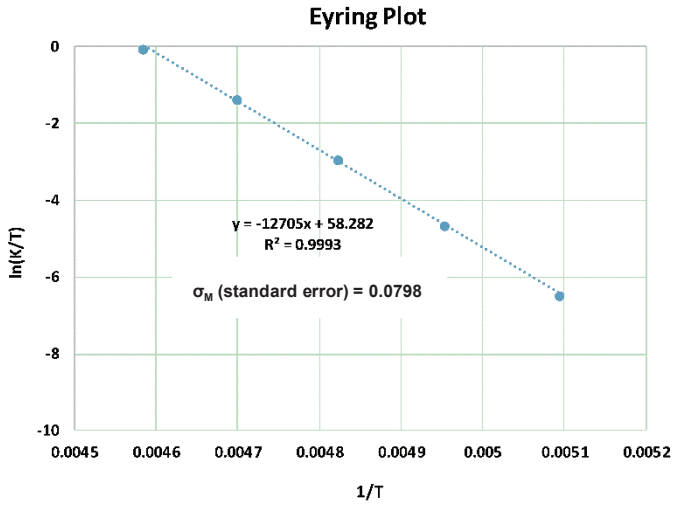

Figure 4. Eyring plot

To verify our simulation, the $\Delta G^{\ddagger}$ value at each temperature was calculated from the obtained $\Delta S^{\ddagger}$ and $\Delta H^{\ddagger}$ values, from which the corresponding k is also calculated according to the rearranged

equation:

$$k = (\frac{k_B T}{h}) e^{\frac{-\Delta G^{\ddagger}}{RT}}$$

The difference between the calculated k from the Eyring plot and the initial simulated k is within 10%.

Table 3. Calculated and simulated parameters for k at different temperatures.

Set Temp /°C	**Real Probe Temp /K**	**$\Delta G^{\ddagger}$ / kJ mol^{-1}**	**Calculated k** (Eyring plot) /s^{-1}	**Simulated k** (gNMR)/s^{-1}
–65.0	218.1	43.03	224.72	205.60
–70.0	212.8	44.56	50.73	54.90
–75.0	207.3	46.12	10.39	10.98
–80.0	201.9	47.69	1.91	1.92
–85.0	196.3	49.29	0.31	0.30

gNMR simulation:

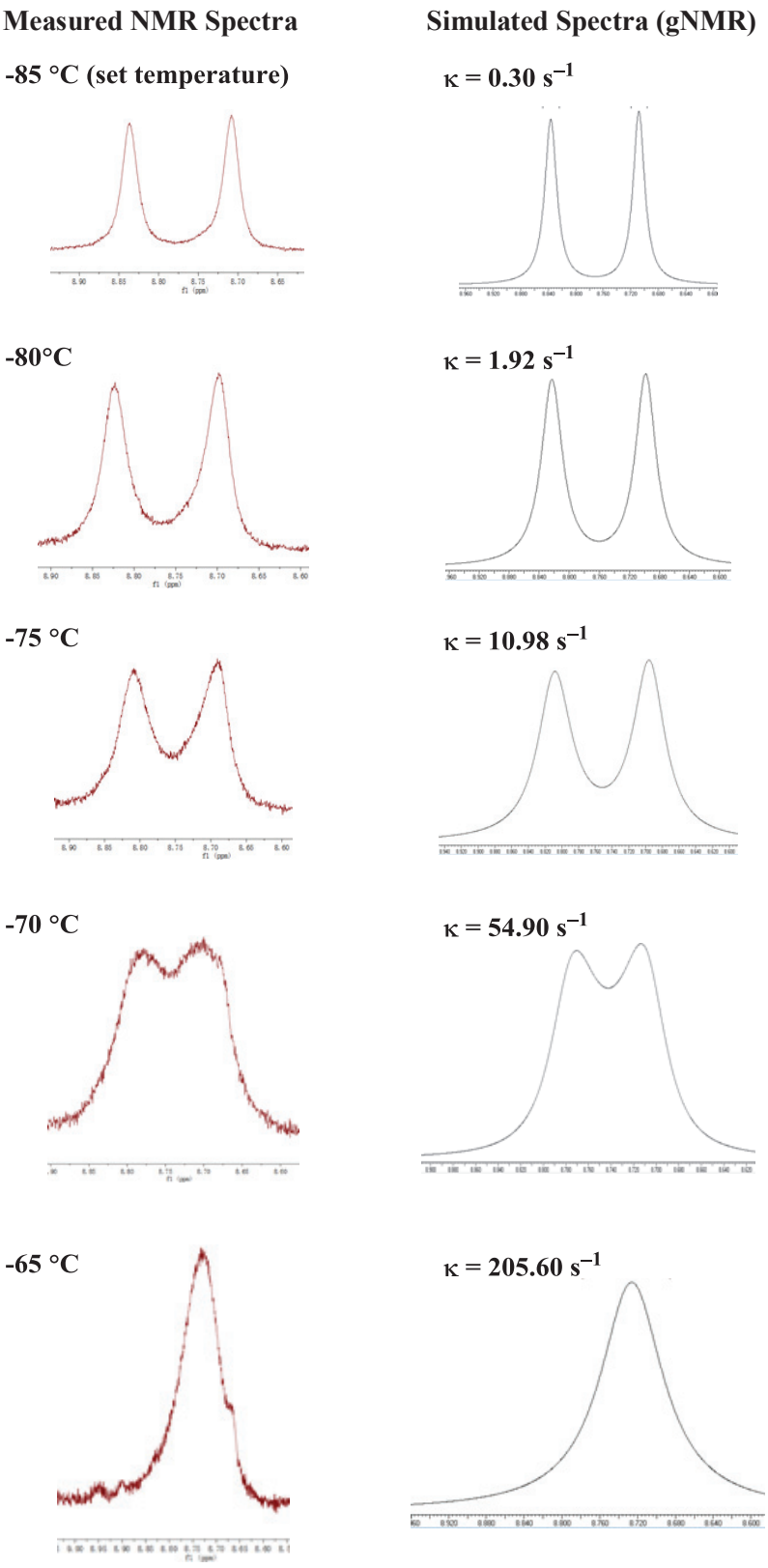

Figure 5. Comparison between measured and simulated spectra

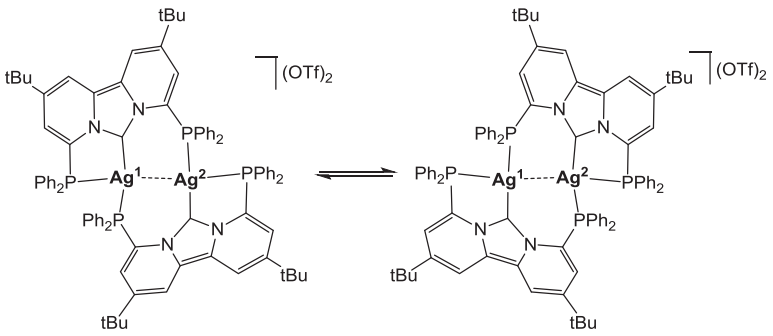

Scheme 2. Possible dynamic behavior of $\mathbf{Ag_2L_2}$ in solution

3-3. Syntheses of Neutral Tetranuclear Copper Complex Cu_4LBr_4

Generally, the Cu(I)-NHC complexes can be prepared via two commonly applied synthetic routes, that is, transmetallation from the corresponding Ag(I) complexes and the direct reaction of the (pre-formed) free carbene with labile Cu(I) precursor. Considering the cost and time factors, as well as the facile preparation and notable stability of **dpa^{P2}-NHC**, we prefer to use the latter method in the subsequent reactions.

As we have mentioned in chapter **2** that the products of the reactions of **dpa^{P2}-NHC** with gold(I) precursors are determined by the nature of the anions associated with the latter. Thus, we are curious about the outcome of the reactions between **dpa^{P2}-NHC** and copper(I) precursors with different associated anions.

Given the easy handle of [CuBr(tht)] (tht = tetrahydrothiophene) which is stable at ambient atmosphere, we preferred to carry out the reaction of **dpa^{P2}-NHC** with [CuBr(tht)]. And fortunately, a tetracopper complex **Cu_4LBr_4** with a novel and rare arrangement was produced when **dpa^{P2}-NHC** reacted with [CuBr(tht)] in the ratio of 1: 2.5 (**Scheme 3**). **Cu_4LBr_4**, existing as yellow solid, is stable at ambient atmosphere and shows good solubility in normal solvents, such as benzene, acetonitrile and dichloromethane; the reaction yield is 72% calculated based on the amount of [CuBr(tht)]. A single set of NMR signals indicates the highly symmetrical structure of **Cu_4LBr_4** in solution; in detail, the protons of dipyrido moiety and *tert*-butyl groups gave rise to three singlets at 8.55, 6.66 and 1.15 ppm, respectively, in ^{1}H NMR spectrum and simultaneously, $^{31}P\{^1H\}$ NMR spectrum showed only one resonance at −19.7 ppm as a broad singlet. These NMR data are broadly in agreement with the solid-state structure of **Cu_4LBr_4**. While one should keep in mind that the diphenylphosphinyl groups gave rise to a broad resonance ranging from 7.00 ppm to 7.60 ppm in the ^{1}H NMR spectrum, indicating a possible fluxional behavior of **Cu_4LBr_4** in solution. Cooling down the temperature to 233 K (–40˚C) did not lead to any decoalescence of these resonance but more broadening.

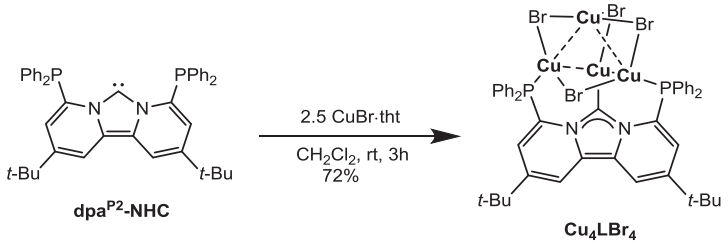

Scheme 3. Syntheses of the tetranuclear copper(I) complex **Cu_4L-Br_4**.

Single crystals suitable for X-ray diffraction analysis were obtained by slow diffusion of diethyl ether into the DMF solution of **Cu_4LBr_4**. Molecular structure (**Figure 6**) shows an inversion symmetry of complex **Cu_4LBr_4** which consists of a tetrahedral Cu^I core unit supported by one **dpa^{P2}-NHC** ligand and decorated by four bridging bromides in an μ_2 fashion with Cu-Br distances falling within the range

of 2.2579(8)-2.4422(8) Å; in the meantime, weak Cu^{I}-Cu^{I} interaction can be found between adjacent Cu^{I} atoms (Cu1-Cu2 2.6762(8) Å, Cu1-Cu3 2.6847 (9) Å, Cu2-Cu4 2.7074(9) Å, Cu3-Cu4 2.6849(9) Å), but not between the opposing Cu^{I} atoms (Cu1-Cu4 3.144 Å, Cu2-Cu3 3.165 Å).[7] It is most likely that the interaction between bromide and Cu^{I} results in the weak metal-metal interaction, as described in the literature: a stronger interaction between the anion or solvent and Cu^{I} atoms leads to the weakening of the metal-metal interaction.[20] The $C_{carbene}$-Cu bond distance of 1.886(5) Å is slightly shortened compared with the typical bond lengths in NHC-Cu complexes, indicating a stronger interaction between them.[21] That is tentatively due to the strong π donation from bromine which increasing the Cu-to-$C_{carbene}$ backdonation to strengthen the Cu-$C_{carbene}$ bond.[22] Moreover, the P-Cu bond distances of 2.2364(13) Å (P1-Cu2) and 2.2257(13) Å (P2-Cu3) are comparable to those for typical Cu^{I}-phosphine complexes.[21] Generally, for multinuclear coinage metal (+1 oxidation state) complexes bearing NHC ligands, the σ-donor groups from NHCs are essential for stabilizing the metal centers by direct interaction with them, situation like Cu4 that is stabilized without interacting with the σ-donors of NHC is extremely rare with only one example being described in which two of the four silver(I) metals are stabilized by their adjacent atoms (silver and iodide) in the Ag(I)-NHC complex.[23]

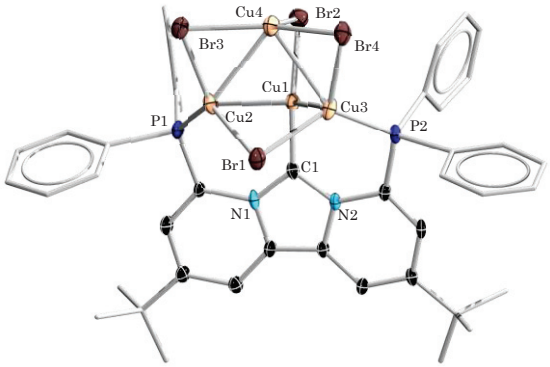

Figure 6. Molecular structure of complex **Cu_4LBr_4**. Ellipsoids are shown at the 50% probability level. Hydrogen atoms are omitted for clarity. Selected bond lengths (Å) and angles [˚]: Br1-Cu1 2.2579(8), Br1-Cu4 2.4150(11), Br2-Cu2 2.4422(8), Br2-Cu4 2.3556(8), Br3-Cu3 2.4282(8), Br3-Cu4 2.3526(8), Br4-Cu2 2.4344(8), Br4-Cu3 2.4305(8), Cu1-Cu2 2.6762(8), Cu1-Cu3 2.6847(9), Cu2-Cu4 2.7074(9), Cu3-Cu4 2.6849(9), Cu1-C1 1.886(5), Cu2-P1 2.2364(13), Cu3-P2 2.2257(13); Cu1-Br1-Cu4 85.19(3), Cu4-Br2-Cu2 68.68(3), Cu4-Br3-Cu3 68.31(3), Cu3-Br4-Cu2 80.51(3), Cu1-Cu2-Cu4 72.01(3), Cu1-Cu3-Cu4 72.23(3), Cu2-Cu1-Cu3 71.81(2), Cu3-Cu4-Cu2 71.33(3).

Looking more closely to the coordination sphere around the metal centers, it is easy to find that three of the Cu^{I} atoms are bridged by the **dpa^{P2}-NHC** ligand in a κP,κC,κP bonding mode which is a normal coordination sphere for polynuclear coinage metal NHC complexes, while the fourth one is

fixed, in a rare way, by two adjacent Cu^{I} atoms through metal-metal interaction together with three neighboring bromide ligands. In detail, the penta-coordinated Cu^{I} atom (Cu4) is in a trigonal-planar environment (Σ_aCu4 = 357.5°) formed by its three adjacent bromides (Br1, Br2, Br3), simultaneously by which two adjacent Cu^{I} centers (Cu2 and Cu3) are capped with cuprophilic interaction as discussed above. These two planes (Br1-Br2-Br3 plane and Cu2-Cu3-Cu4 plane) are at 54.5° and coincidently, in which Cu4 is the intersection. This special coordination environment leads to Cu4 being steadily fixed by virtue of its five adjacent atoms without the direct participation of σ-donors from **dpa^{P2}-NHC** ligand.

While it is worth noting that the ratio of copper(I) atoms to **dpa^{P2}-NHC** ligand (4:1) in complex **Cu_4LBr_4** is inconsistent with that of the copper(I) precursor to **dpa^{P2}-NHC** ligand (2.5:1), which were used as the starting materials in the reaction mentioned above. This thus prompted us to investigate what the product will be when **dpa^{P2}-NHC** reacts with [CuBr(tht)] under the same reaction condition as mentioned above except the ratio of the starting materials changed from 2.5:1 to 4:1. Interestingly, the combination of **dpa^{P2}-NHC** with copper(I) precursor [CuBr(tht)] in a ratio of 1:4 led to the formation of a pure species different from **Cu_4LBr_4** judging from the NMR spectroscopy (**Figure 7**). Similar to **Cu_4LBr_4**, the new obtained compound was found with only one set of NMR signals, which, however, show some slight chemical shifts compared with those of **Cu_4LBr_4**. In detail, the ^{1}H NMR resonances at 8.55 and 6.66 ppm assigned to the two sets of protons at dipyrido moiety for **Cu_4LBr_4** are down- and upfield shifted, respectively, to 8.60 and 6.58 ppm for the new obtained compound. Furthermore, the ^{31}P NMR singlet at −19.7 ppm for **Cu_4LBr_4** is downfield shifted to -18.5 ppm for the new compound.

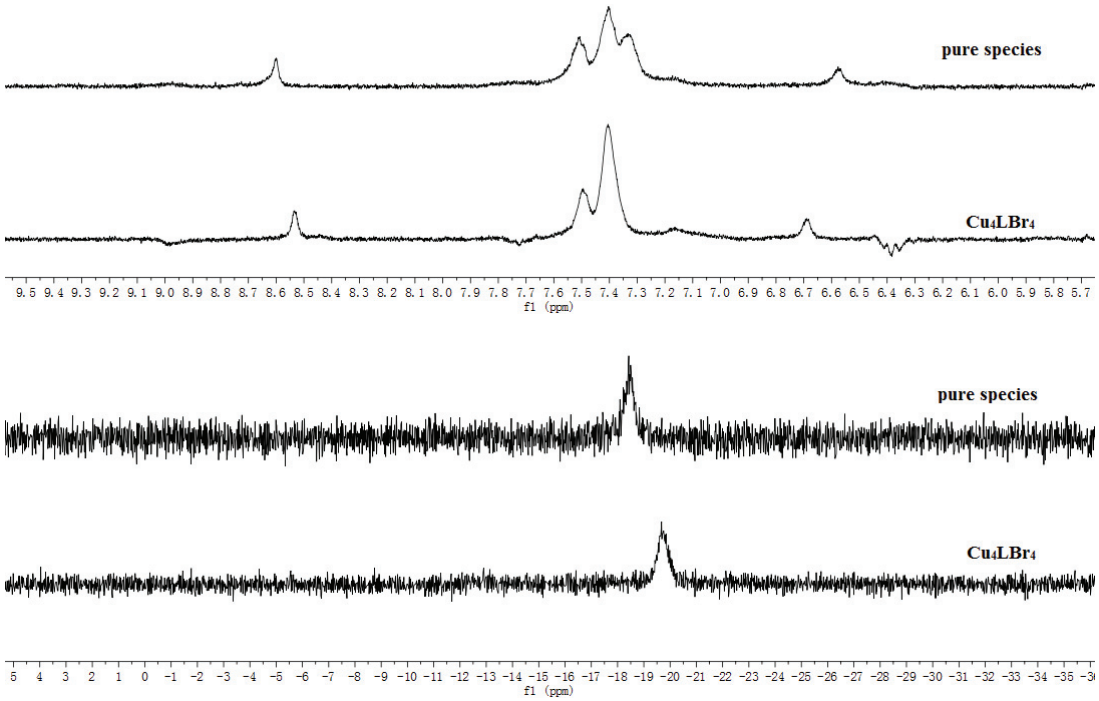

Figure 7. Comparison of ^{1}H (top) and ^{31}P (bottom) NMR spectra between the obtained pure species and **Cu_4LBr_4**.

Given the above mentioned NMR spectroscopy, a highly symmetrical structure for the new obtained compound is expected since only one set of NMR signals can be observed, which is similar to that of **Cu_4LBr_4**. To further prove this hypothesis, much efforts have been made to structurally characterize this compound. While unfortunately, attempts to obtain its solid-state structure by X-ray diffraction analysis failed due to its extremely poor solubility in normal solvents, such as THF, DMF and MeCN. Meanwhile, though it showed a good solubility in DMSO, single crystals suitable for X-ray study were not yet obtained after numerous recrystallization using DMSO/ether as the solvent.

3-4. Syntheses of Dinuclear Copper Complex Cu_2L_2

As mentioned in **Chapter 2** that the products of the reaction of **dpa^{P2}-NHC** with gold(I) precursors depend on the nature of the anions associated with the later, we were wondering if different outcomes will be generated when **dpa^{P2}-NHC** reacts with copper(I) precursors associated with different counter anions. The neutral tetranuclear copper(I) complex **Cu_4L-Br_4** has been produced from the reaction of **dpa^{P2}-NHC** with [CuBr(tht)], we next turned our attention to a different copper precursor, [Cu(MeCN)$_4$(OTf)]. The reason why we choose [Cu(MeCN)$_4$(OTf)] here is because that different with the associated anion Br^- which has been proved to possess a stronger coordination ability towards the metals, OTf would prefer to serve as disassociated counter anion in the formed metal complexes, which thereby will probably result in the formation of copper complexes with entirely different coordination geometry from **Cu_4L-Br_4**.

As expected, when **dpa^{P2}-NHC** reacted with [Cu(MeCN)$_4$(OTf)] in a ratio of 1:1 in THF, a dinuclear copper(I) complex **Cu_2L_2** was generated in a good yield (72%) as brown solid (**Scheme 4**). Single crystals suitable for X-ray diffraction analysis were obtained by slow diffusion of diethyl ether into the solution of **Cu_2L_2** in DMF (dimethylformamide) at room temperature. Molecular structure of **Cu_2L_2** (**Figure 8**) shows an unsymmetrical dimeric structure, with an extremely rare coordination sphere. In detail, two carbene carbons adopt entirely distinct bonding modes, with one (C1) simultaneously bound to two copper(I) atoms, yet the other one (C44) coordinating to only one (Cu2). Thus as expected, the C44-Cu2 bond length of 1.954(2) Å is comparable to the typical length for the terminal Cu^I-NHC complexes, whereas the C1-Cu1 and C1-Cu2 distances of 2.153(2) and 2.236(2) Å, respectively, are significantly longer. Meanwhile, both two copper(I) atoms are five-coordinate but in different coordination sphere: Cu1 is coordinated by two phosphine atoms belonging to two **dpa^{P2}-NHC** ligands, one carbene carbon (C1) and the neighboring copper atom Cu2 through intermetallic interaction, whose coordination sphere is completed by a DMF molecule; Cu2 is coordinated by two phosphine atoms and two carbene carbons belonging to two **dpa^{P2}-NHC** ligands, respectively, and the neighboring copper atom Cu1. A strong intramolecular Cu^I-Cu^I interaction is present based on the short distance between Cu1 and Cu2 (Cu1-Cu2 2.5182(5) Å).[24]

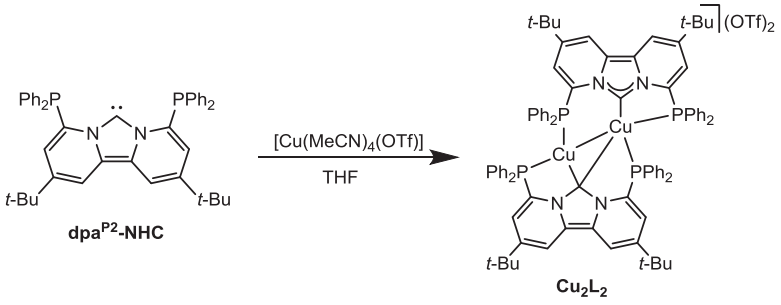

Scheme 4. Syntheses of dinuclear copper(I) complex **Cu_2L_2** from dpa^{P2}-NHC.

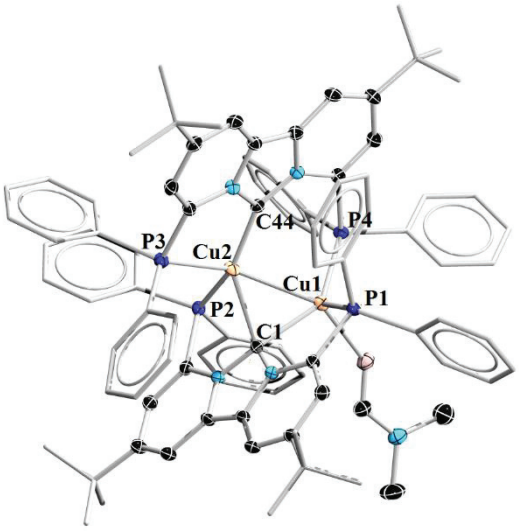

Figure 8. Molecular structures of the cation in **Cu_2L_2·DMF**. Hydrogen atoms, two dissociated triflate anions and molecules of crystallization solvent ($CH_3CH_2OCH_2CH_3$) are omitted for clarity. Selected bond lengths (Å) and angles [˚]: Cu1-Cu2 2.5812(5), Cu1-P1 2.3049(7), Cu1-P4 2.2873(7), Cu1-C1 2.154(2), Cu2-P2 2.2889(7), Cu2-P3 2.4006(7), Cu2-C1 2.236(2), Cu2-C44 1.954(2); P1-Cu1-Cu2 109.15(2), P2-Cu2-Cu1 99.19(2), P2-Cu2-P3 104.54(2), P3-Cu2-Cu1 141.29(2), P4-Cu1-Cu2 86.38(2), P4-Cu1-P1 117.50(3), C1-Cu1-Cu2 56.55(6), C1-Cu1-P1 87.20(6), C1-Cu1-P4 141.51(6), C1-Cu2-Cu1 53.47(6), C1-Cu2-P3 98.39(6), C1-Cu2-P2 85.04(6), C44-Cu2-Cu1 90.04(7), C44-Cu2-P3 86.42(7), C44-Cu2-P2 147.03(7), C44-Cu2-C1 124.67(9).

It is worth noting that the μ-bridging carbene in Cu^I-NHC complexes is extremely rare, and to the best of our knowledge, only two examples have been described to date.[25] Normally, in NHC-metal complexes presented as dimer or oligomer, the NHC ligands are in same coordination mode, that is, terminal carbene or bridging carbene. Structures like the dimer **Cu_2L_2**, in which two NHC ligands adopt totally different coordination sphere, that is, one is terminal carbene and the other one is bridging carbene, is unprecedented as we are aware of. Two possibilities seem to be reasonable to describe this novel binding mode. One is that one of the **dpa^{P2}-NHC** ligands (containing C1) was reduced to generate a bridging carbene carbon with sp^3 hybridization, which coordinates to two copper(II) atoms. Unfortunately, no literature has yet reported this situation to date. The other possibility involves an sp^2-hybridized μ_2-C_{NHC} and two copper(I) centers, namely, a σ–bonding interaction between μ_2-C_{NHC} and one of the two copper centers (in this case C1-Cu1) and an unconventional π-interaction between μ_2-C_{NHC} and another one (in this case C1-Cu2).[25a,26] According to the distances between μ_2-C_{NHC} and two copper atoms mentioned in the last paragraph, this description is quite reasonable.

While ^{1}H NMR spectrum of **Cu_2L_2** at room temperature shows a symmetrical and single dpa^{P2}-NHC ligand environment, namely, the protons of pyridyl and *tert*-butyl groups appear as three singlets

at δ 8.50, 6.99 and 1.20, respectively, which is inconsistent with the observation of its solid-state structure since, for instance, the four *tert*-butyl groups are obviously nonequivalent judging from its molecular structure. Correspondingly, only one ^{31}P NMR singlet was detected at δ -16.3, and the ^{13}C NMR spectrum shows only one set of resonance at ambient temperature. These NMR spectra data suggest that **Cu_2L_2** is likely to undergo a fast dynamic behavior in solution, or convert to a highly symmetric species once dissolved in solution.

If the former hypothesis which **Cu_2L_2** undergoes a dynamic process in solution is the fact, it is very possible that its NMR spectra or UV-vis spectrum will show some obvious or characteristic difference from those at ambient temperature, as long as the measuring temperature is low enough. Thus, to give an accurate explanation, variable temperature (VT) UV-Vis absorption experiment was first to be conducted. The VT UV-vis absorption spectrum (**Figure 9**) at ambient temperature in THF exhibits a broad band ranging from 360 nm to 550 nm with the maximum at 415 nm, which showed almost no any change when the temperature was gradually cooled to 183 K, except the slightly increasing intensity.

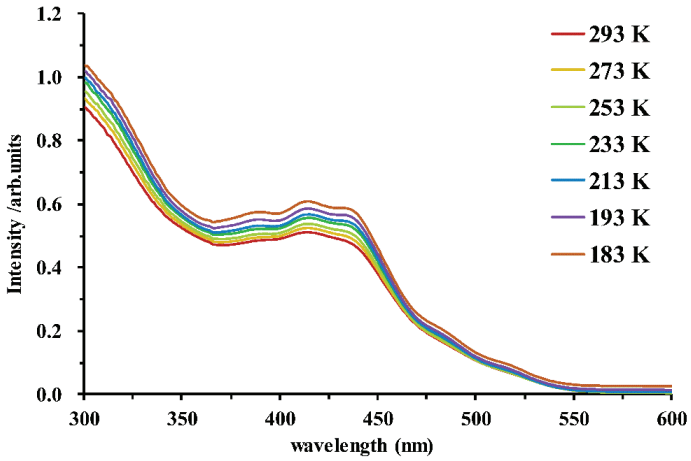

Figure 9. VT UV-vis absorption spectrum of **Cu_2L_2** in THF from 293 K to 183 K.

Thus, according to the obtained VT UV-vis spectrum, it seems like **Cu_2L_2** exists as a symmetrical species in solution in the temperature regime of 293 K-178 K. But we still can not exclude the possibility of **Cu_2L_2** undergoing a fast fluxional behavior in solution. To study further the behavior of **Cu_2L_2** in solution, we simultaneously conducted a VT ^{1}H NMR experiment. Gradually cooling down the temperature of ^{1}H NMR experiment from 293 K to 178 K for **Cu_2L_2** did not lead to any decoalescence of the NMR resonance (**Figure 10**), namely, the ^{1}H NMR spectrum of **Cu_2L_2** displays no significant change. Likewise, no obvious change was observed for the VT ^{31}P {^{1}H} NMR spectrum of **Cu_2L_2** from 293 K-178 K. Therefore, though a variety of experimental attempts have been conducted, the obtained results are not sufficient enough to support us to make a conclusion about the accurate state of **Cu_2L_2** in solution in the temperature range of 293 K-178 K.

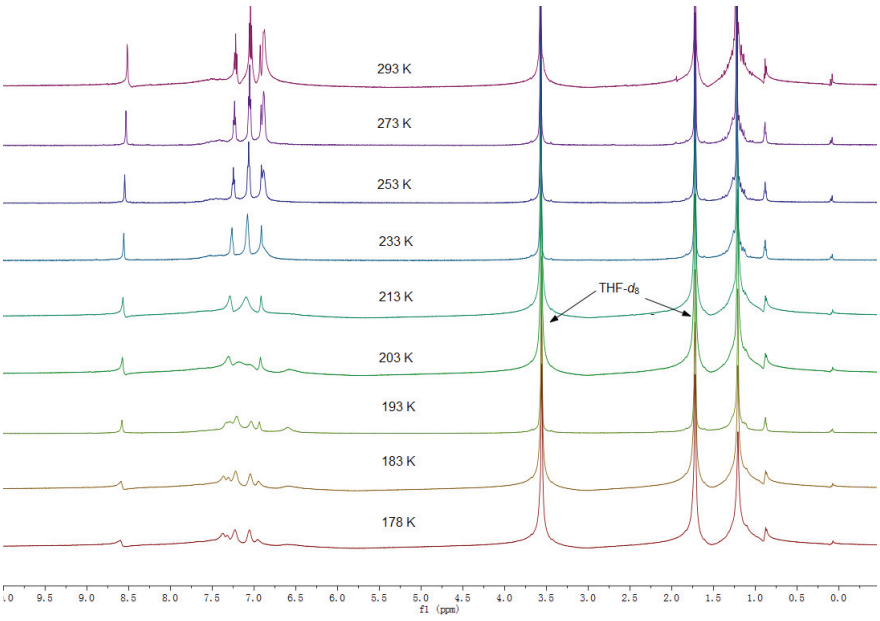

Figure 10. VT ^{1}H NMR spectrum of **Cu_2L_2** from 293 K to 178 K in THF-d_8.

While given the obtained solution data, there are two possibilities that could describe the state of **Cu_2L_2** in solution. The first possibility is that **Cu_2L_2** exists as a symmetrical species in solution. Here, we proposed this very symmetrical species to be a monomeric complex, **CuL** (**Scheme 5**), in which the only metal atom (Cu) is connected to the carbene carbon. The reasons why we provide this proposal here include: 1) the molecular structure of **CuL** is in good agreement with the observation of its NMR spectroscopy mentioned above; 2) the NMR resonance found in ^{13}C NMR spectrum at 198.3 ppm which corresponds to the carbene carbon of **dpa^{P2}-NHC** shifted significantly towards upfield to 153.5 ppm, indicating the existence of metal (Cu)-coordinated carbene carbon in **CuL**. The other possibility involves the fast interconversion between two dimeric species (**Scheme 5**), **Cu_2L_2** and **Cu_2L_2'**. For this hypothesis, the symmetrical NMR spectroscopy can be the result of the possible NMR coalescence. The origin of this dynamic behavior is likely involving the rapid μ_2-C_{arbene}-Cu and P-Cu bonds breaking/formation.

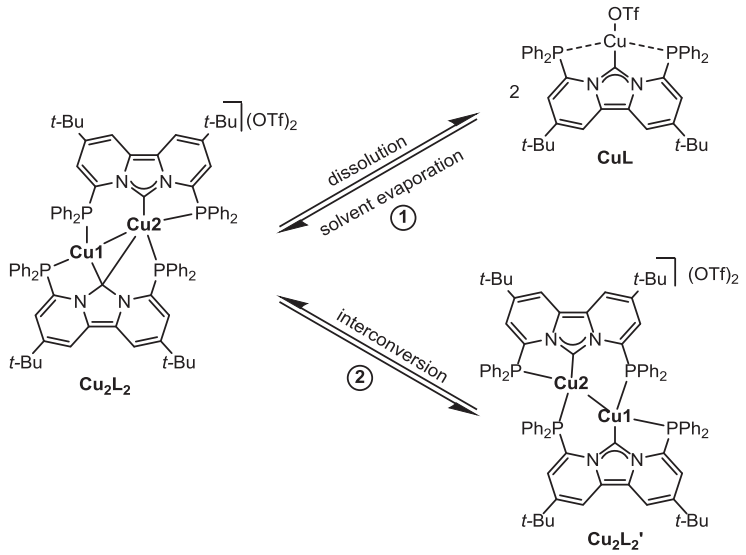

Scheme 5. Two possible fluxional behavior of $\mathbf{Cu_2L_2}$ in solution.

Even though the obtained solution data (VT NMR spectroscopy and VT UV-vis spectra) seem to be (in our view) reasonable for supporting the hypothesis of the fluxional behavior of $\mathbf{Cu_2L_2}$ in solution (① and ②) as mentioned above, this evidence is still not sufficient and convincible enough to enable us to conclude that these two proposed dynamic behavior are existing 100 percent, unless the precise structural assignment for **CuL** and $\mathbf{Cu_2L_2'}$ is performed. Thus, to achieve the rigorous proof, it seems to be necessary to establish the molecular structures of **CuL** and/or $\mathbf{Cu_2L_2'}$. We made some attempts to grow single crystals of **CuL** or $\mathbf{Cu_2L_2'}$ suitable for X-ray diffraction analysis by a DMF solution of $\mathbf{Cu_2L_2}$ overlayered by diethyl ether, at low temperature (below –30 ˚C). Unfortunately, rather than the expected molecular structure of **CuL** or $\mathbf{Cu_2L_2'}$, the obtained crystals were consistently proved to be the dimeric species, $\mathbf{Cu_2L_2}$. While in turn, these unsuccessful attempts demonstrate the stable existence of $\mathbf{Cu_2L_2}$ in the form of solid state.

3-5. Syntheses of Tetranuclear Bimetallic Ag-Cu Complex $Ag_2Cu_2L_2$ from Cu_2L_2

In **Chapter 2**, we have described the syntheses of tetranuclear gold complex **4** from the dinuclear gold complex **3**. Actually, both $\mathbf{Cu_2L_2}$ and $\mathbf{Cu_2L_2'}$ can be considered as the analogues of **3**. In this context, dpa^{P2}-NHC complexes containing higher metal nuclei than 2 are likely to be accessible from $\mathbf{Cu_2L_2}$. On the other hand, according to our previous hypothesis, the monomeric mononuclear complex **CuL** features two non-metallated phosphine donors, which implies the possibility of capturing extra metal centers. Therefore, it is very possible that multinuclear complexes (the number of metal beyond 2) can be afforded by reactions of the $\mathbf{Cu_2L_2}$ solution with metal precursors. Considering our research scope, the coinage metals (gold, silver and copper) will be checked in the next study.

In light of the synthesis of gold complexes **2-4**, trinuclear complexes based on dpa^{P2}-NHC are unlikely to be achieved. Therefore, we seek to achieve dpa^{P2}-NHC supported complexes with 4 or more metal nuclei instead of 3. Reaction of $\mathbf{Cu_2L_2}$ with two equivalents of AgOTf in THF under the protection of N_2 in the absence of light (**Scheme 6**) was carried out, which, after approximately 3 h, a heterobimetallic complex, $\mathbf{Ag_2Cu_2L_2}$, was isolated as the only product in the form of orange solid in a modest yield (47%).

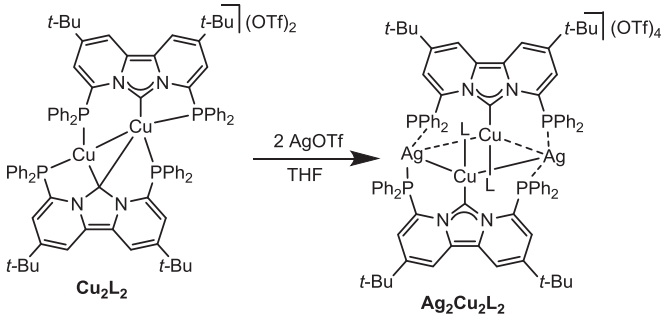

Scheme 6. Syntheses of heterobimetallic complex $\mathbf{Ag_2Cu_2L_2}$ from $\mathbf{Cu_2L_2}$.

The ^{1}H NMR spectrum of $\mathbf{Ag_2Cu_2L_2}$ showed a single and symmetrical $\mathbf{dpa^{P2}}$**-NHC** ligand environment. In detail, the protons of pyridyl groups give rise to only two singlets at 8.50 and 7.00 ppm, respectively; the protons of *t*Bu groups resonate as one singlet at 1.20 ppm. Correspondingly, only one set of signals was clearly observed in ^{13}C NMR spectrum, in which, unfortunately, the carbene carbon resonance signal was not detected, even after a three days' measurement in the solution of DMSO-d_6 at ambient temperature. Meanwhile, ^{31}P NMR spectrum shows a broad doublet at 2.6 and 4.2 ppm ($J_{P\text{-}^{107/109}Ag} \approx 273.8$ Hz), respectively, at 233 K, which is likely to be the result of a possible fluxional process.

Single crystals suitable for X-ray diffraction analysis were obtained by slow diffusion of diethyl ether into the solution of $\mathbf{Ag_2Cu_2L_2}$ in dimethylformamide (DMF). Interestingly, the obtained crystal structure showed an oxygenated species, $\mathbf{Ag_2Cu_2L_2(O)}$, which is different from our proposed structure. It is likely that in the course of crystallization, $\mathbf{Ag_2Cu_2L_2}$ was oxygenated by water contained in

solvents DMF/ether. While, satisfactory refinement of the structure was persistently unavailable. Even then, the connectivity of **$Ag_2Cu_2L_2(O)$** and its composition can be clearly deduced (**Figure 11**), but a detailed discussion of metrical data on this complex is impossible. Molecular structure of this complex shows a dimeric and roof-like structure with two **dpa^{P2}-NHC** ligands being bridged by a four-membered metallocycle (Ag-Cu-Ag-Cu) which is connected by intramolecular metal-metal interactions. Two outer Ag atoms are respectively coordinated by two phosphine donors from two **dpa^{P2}-NHC** ligands, while each of the two inner Cu atoms featuring an identical coordination sphere is bound to only one carbene carbon. Furthermore, two Cu atoms are capped by an oxygen atom located in the vertex of the geometry. The source of the oxygen atom of **$Ag_2Cu_2L_2(O)$** is arguably water contained in organic solvents which were used in the workup procedure. One of two counter anions, OTf, is dissociated from the cation and the other one is connected to an outer silver atom.

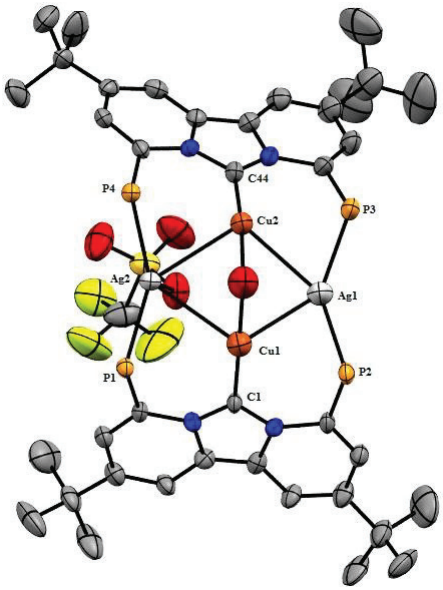

Figure 11. Thermal ellipsoid representation (50% probability level) of the structure of the cation in **$Ag_2Cu_2L_2(O)$**. Hydrogen atoms, phenyl groups and dissociated triflate anion are omitted for clarity.

The successful synthesis of **$Ag_2Cu_2L_2$** is important because it clearly demonstrates the existence of the dynamic behavior of **Cu_2L_2** in solution as we expected, although we cannot make sure which one (① and ②) the process is. Meanwhile, it also inspired us to check the reactions of **Cu_2L_2** with other two group 11 metals (Cu and Au).

3-6. Syntheses of Tetranuclear Cu(I) Complex $Cu_4L_2 \cdot 2CH_3CN$ from Cu_2L_2

Encouraged by the successful syntheses of the tetranuclear bimetallic Ag/Cu complex **$Ag_2Cu_2L_2$** from **Cu_2L_2**, we therefore sought to synthesize tetranuclear bimetallic Au/Cu complex and tetranuclear copper complex by treatment of **Cu_2L_2** with suitable gold and copper precursors, respectively.

We first conducted a reaction of **Cu_2L_2** with 2 equiv $[Au(tht)_2(OTf)]$ in inert atmosphere, unfortunately resulting in the formation of ill-defined mixture as judged by NMR spectroscopy. This is most likely due to the scrambling of the transmetallation from copper to gold of the NHC donor[27] and the coordination of gold directly by phosphine donors, which generate the admixture of gold-coordinated NHC and phosphine complexes. However, to be honest, the interpretation for the failed experiment cannot be currently identified since there is no pure product from the mixture that can be isolated yet.

Subsequently, a reaction of **Cu_2L_2** with 2 equiv $[Cu(MeCN)_4(OTf)]$ in the absence of light was performed (**Scheme 7**), which resulted in the formation of a tetranuclear copper complex **$Cu_4L_2 \cdot 2CH_3CN$** after a reaction time of approximately 3 h. The product was collected after work-up as a yellow solid and pure enough for the next analysis.

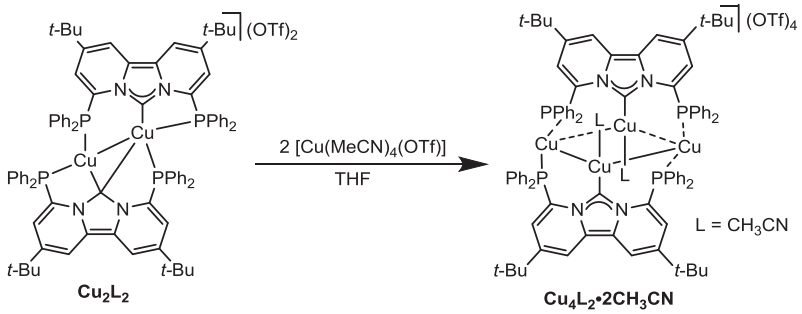

Scheme 7. Syntheses of tetranuclear copper(I) complex **$Cu_4L_2 \cdot 2CH_3CN$** from **Cu_2L_2**.

The ^{31}P NMR spectrum of **$Cu_4L_2 \cdot 2CH_3CN$** at room temperature showed only one singlet at −14.3 ppm, indicating the equivalence of all the phosphine ligands. Correspondingly, the ^1H NMR spectrum displays one set of resonance signals, which suggested a symmetrical and single ligand environment. In detail, the protons of dipyridyl groups adjacent to phosphine donors and *tert*-butyl groups gave rise to a downfield doublet at 8.09 nm ($^3J_{HP}$ = 1.8 Hz) and an upfield singlet at 1.22 ppm, respectively. Simultaneously, three kinds of phenyl protons appeared as three resonance signals, respectively, in the downfield (6.8-7.3 ppm). However, the left dipyridyl protons cannot be found in the room temperature ^1H NMR spectrum. This can be attributed to the overlap with the signals of phenyl protons. To ascertain our postulation such that achieving well-resolved ^1H NMR spectrum, VT ^1H NMR experiment for **$Cu_4L_2 \cdot 2CH_3CN$** was performed (**Figure 12**). Fortunately, cooling down the temperature to 253 K led to the appearance of the very dipyridyl protons, presenting as a singlet at

7.08 ppm. These spectral characteristics are indicative of a highly symmetrical structure of **$Cu_4L_2 \cdot 2CH_3CN$**.

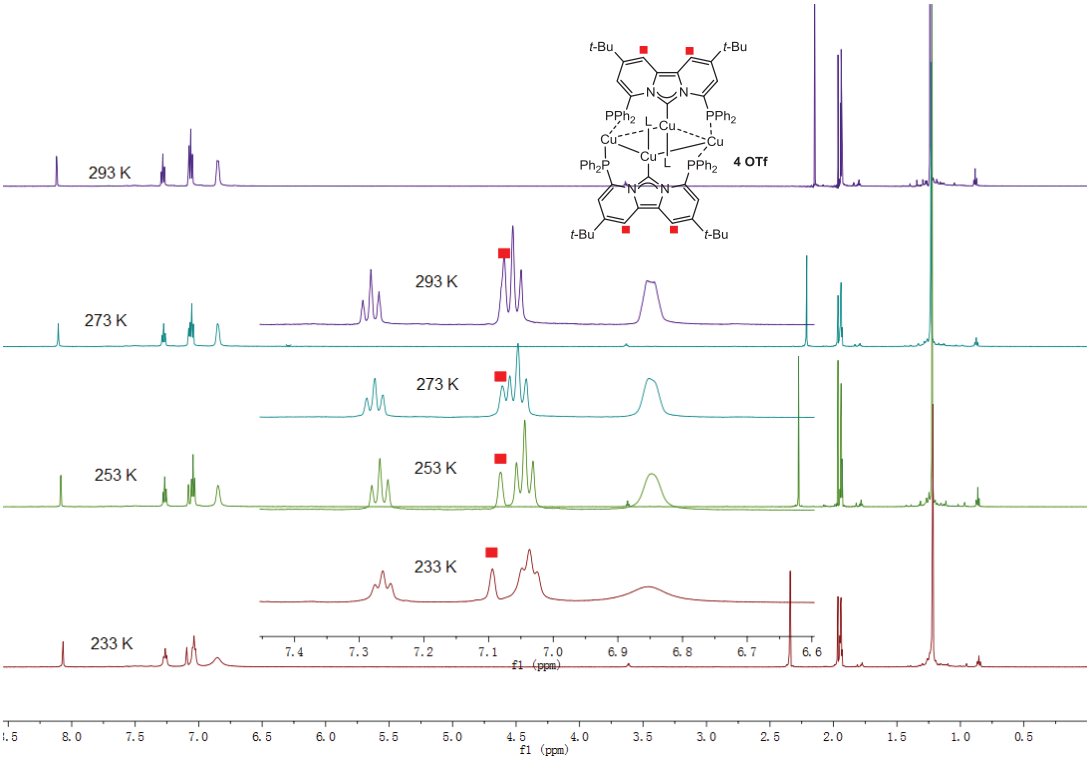

Figure 12. VT ^{1}H NMR spectrum of **$Cu_4L_2 \cdot 2CH_3CN$** in CD_3CN from 293 K to 233 K.

Single crystals suitable for X-ray diffraction analysis were obtained by slow diffusion of diethyl ether into the solution of **$Cu_4L_2 \cdot 2CH_3CN$** in DMF. While interestingly, instead of our proposed structure for **$Cu_4L_2 \cdot 2CH_3CN$**, X-ray diffraction analysis suggested an oxygenated tetranuclear **$Cu_4L_2(O)$** structure as shown in **Figure 13**, similar to **$Ag_2Cu_2L_2(O)$**. It is worth noting that satisfactory refinement of this structure was persistently unavailable due to the heavy disorder of the molecule, however, the connectivity of **$Cu_4L_2(O)$** and its composition can be clearly deduced, and a detailed discussion of metrical data on this complex is impossible. Molecular structure of **$Cu_4L_2(O)$** shows an almost same geometry with **$Ag_2Cu_2L_2(O)$**. The main difference between these two complexes is their two outer metal atoms, that is, in **$Ag_2Cu_2L_2(O)$** two silvers, in **$Cu_4L_2(O)$** two coppers.

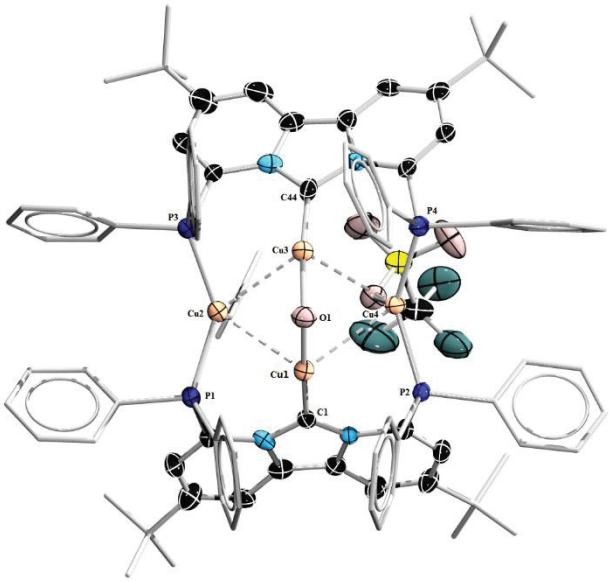

Figure 13. Thermal ellipsoid representation (50% probability level) of the structure of the cation in **Cu_4L_2(O)**. Hydrogen atoms, phenyl groups and a dissociated triflate anion are omitted for clarity.

Actually, the structure of **Cu_4L_2(O)** showed also consistency with the aforementioned NMR spectroscopy. Therefore, a question arises: is the bulk sample **$Cu_4L_2 \cdot 2CH_3CN$** or **Cu_4L_2(O)** (crystals has been identified as **Cu_4L_2(O)**)? To verify this, we performed a ^{19}F NMR experiment, since the fluorine content of equimolar amount of **$Cu_4L_2 \cdot 2CH_3CN$** and **Cu_4L_2(O)** are different. Here, we used the dinuclear gold complex **1** (**Chapter 2**) featuring a PF_6 anion as the standard sample and the sample for NMR experiment was the mixture of equimolar amount of **1** and bulk sample (bulk sample was presumed as **$Cu_4L_2 \cdot 2CH_3CN$**). The obtained ^{19}F NMR spectrum (**Figure 14**) displayed a doublet for **1** at –68.8 and –70.7 ppm with same intensity and a singlet for bulk sample at –77.4 ppm, whose ratio is 1:1:4. This revealed that the fluorine content of bulk sample is one time more than that of equimolar amount of **1**, suggesting that the bulk sample has four triflate anions. Consequently, we affirm that the bulk sample is **$Cu_4L_2 \cdot 2CH_3CN$**. The source of the oxygen atom of **Cu_4L_2(O)** is arguably water contained in recrystallization solvent DMF or diethyl ether.

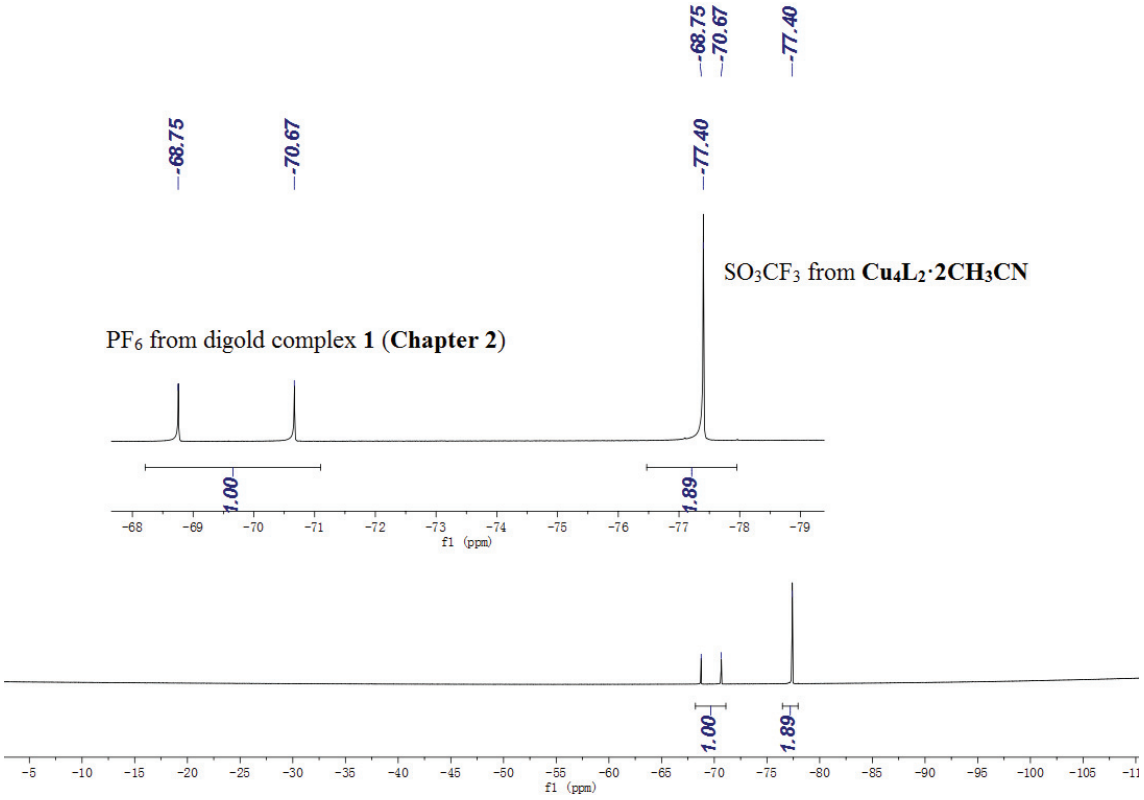

Figure 14. ^{19}F NMR spectrum of equimolar amount of complex **1** and bulk sample in DMSO-d_6 at room temperature.

3-7. Syntheses of Pentanuclear Cu(I) Complex $Cu_5L_2Br_3$ from Cu_2L_2

As described above, using the dinuclear species $\mathbf{Cu_2L_2}$ as the starting material, two tetranuclear species, $\mathbf{Ag_2Cu_2L_2}$ and $\mathbf{Cu_4L_2}$, have been cleanly achieved. We wonder if it is possible to generate multinuclear metal complexes, from $\mathbf{Cu_2L_2}$, whose number of nuclei is above 4. Keeping this in mind, we carried out a reaction of $\mathbf{Cu_2L_2}$ with 3 or 4 equivalents of [Cu(MeCN)$_4$(OTf)] in THF in the absence of light, which, unfortunately and consistently, led to the isolation of $\mathbf{Cu_4L_2}$ as the only product as judged by the obtained NMR spectra. In this context, four metals seem to be the highest metal content that **dpa^{P2}-NHC** is capable of capturing.

Nonetheless in 2016, Ai, P. et al.[8c] reported the syntheses of a hexanuclear copper(I) complex based on a diphhosphine-functionalized NHC ligand (*N,N'*-diphosphanyl-imidazol-2-ylidene), in which two adjacent copper(I) atoms connected by intramolecular cuprophilic interactions were capped by one or two iodides. With this arrangement, six coppers were captured and framed by two NHC ligands, together with five iodides. Triflate, as the sixth counter anion, is dissociative and does not show any obvious interactions with those six coppers. In this very compound, halides are likely playing an important role for stabilizing those six coppers. Accordingly, we attempted to introduce halide into the reaction so as to achieve multinuclear copper complex with a higher metal content in comparison to 4.

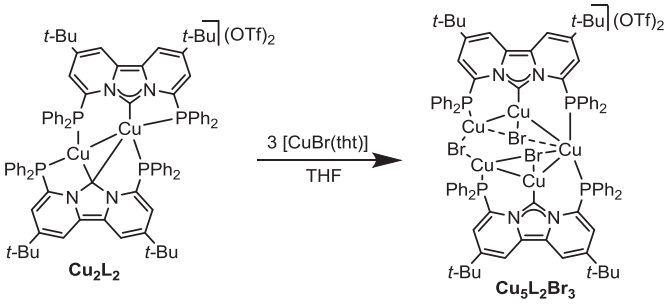

Scheme 8. Syntheses of pentanuclear copper(I) complex $\mathbf{Cu_5L_2Br_3}$ from $\mathbf{Cu_2L_2}$.

Considering the resource what we have at hand in our lab, bromide which is fixed in [CuBr(tht)] was chosen as the halide source. Subsequent reaction was carried out at ambient atmosphere since both reactants are air stable. Excitingly and expectedly, a pentanuclear copper complex $\mathbf{Cu_5L_2Br_3}$ was achieved as a yellow solid in a 52.5% yield when $\mathbf{Cu_2L_2}$ reacted with 3 equiv [CuBr(tht)] (**Scheme 8**), which shows no sign of decomposition when exposed, in the form of solid, to ambient atmosphere. NMR data implied a symmetrical ligand environment of $\mathbf{Cu_5L_2Br_3}$ in solution. In detail, two downfield singlets at 8.60 and 6.62 ppm, respectively, in the ^{1}H NMR spectrum were detected, corresponding to two type of dipyridyl protons. Meanwhile, only one upfield ^{1}H NMR singlet at 1.15 ppm assignable to the *tert*-butyl protons was detected. Correspondingly, the ^{31}P NMR spectrum of $\mathbf{Cu_5L_2Br_3}$ displayed a broad singlet at 18.7 ppm, indicating the equivalence of the phosphine groups.

The broadening of this copper-coordinated ^{31}P NMR singlet can be attributed to the fast quadrupole relaxation of the ^{63}Cu nucleus ($I = 3/2$).[28] While unfortunately, these solution data are inconsistent with the observation of its solid state structure (**Figure 15**). Cooling down the temperature to 193 K (–80˚C) had no effect for obtaining well resolved NMR spectra. We proposed the coalescence to be the result of dynamic behavior of **$Cu_5L_2Br_3$** in solution.

Single crystals suitable for X-ray diffraction analysis were obtained by slow diffusion of diethyl ether into a DMF solution of **$Cu_5L_2Br_3$**. Note that the obtained molecular structure **$Cu_5L_2Br_3$·2DMF** is solvated by two DMF molecules. While the comparison of the NMR spectra between **Cu_5L_2Br** and **$Cu_5L_2Br_3$·2DMF** which showed almost identical chemical shifts suggested that these two compounds are supposed to adopt the same coordination geometry in solution. In other words, the coordination sphere of **$Cu_5L_2Br_3$·2DMF** shown in **Figure** represents the structural assignment of **$Cu_5L_2Br_3$**. Molecular structure reveals that **$Cu_5L_2Br_3$·2DMF** contains two identical [Cu_3(dpa^{P2}-NHC)Br·DMF] subunits that are sharing one of five copper atoms (Cu3) and bridged by one of three bromides (Br3) through the interactions with two coppers (Br3-Cu4, Br3-Cu5), whereas pointing in the opposite directions. Five copper atoms found in a six-member metallocycle are connected via the Cu-Cu interactions (average Cu-Cu distance 2.5918 Å), which are slightly stronger in comparison to the typical cuprophilic interactions.[21] In each [Cu_3(dpa^{P2}-NHC)Br·DMF] subunit, three copper atoms connected through Cu-Cu interactions are spanned by one μ_3-**dpa^{P2}-NHC**,κP,κC,κP ligand and capped by one bromide. As a result, the interactions between bromide and respective three copper atoms are present and can be roughly grouped into two types based on the bond length, that is, Br1-Cu1 with a strong interaction (2.2789(11) Å), Br1-Cu4 and Br1-Cu3 with relatively weak interactions (2.6223(12) and 2.6947 (12) Å). This strong interaction can be attributed to the strong Br-to-Cu π-backdonation. Furthermore, it is worth noting that the bond lengths between Cu and C_{NHC} (Cu1-C1 1.883(7) Å and Cu2-C44 1.884(6) Å) are slightly shorter in comparison to the typical Cu^{I}-NHC complexes (>1.9 Å),[21] which is likely due to the strong copper-to-C_{NHC} π-backdonation. Furthermore, in comparison to tetranuclear gold complexes **4** (**Chapter 2**), there is one additional CuBr inserted between a metal-phosphine interaction.

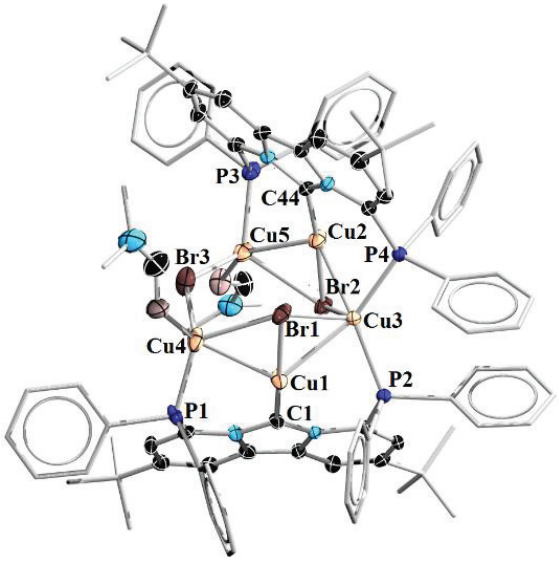

Figure 15. Thermal ellipsoid representation (50% probability level) of the structure of the cation in **$Cu_5L_2Br_3$·2DMF**. Hydrogen atoms and two triflate anions are omitted for clarity. Selected bond lengths (Å): Br1-Cu3 2.6947 (12), Br1-Cu1 2.2789(11), Br1-Cu4 2.6223(12), Br2-Cu3 2.6432(11), Br2-Cu2 2.2907(11), Br2-Cu5 2.6165(12), Br3-Cu4 2.4527(13), Br3-Cu5 2.4448(14), Cu1-Cu4 2.5752(13), Cu1-C1 1.883(7), Cu2-Cu5 2.5347(13), Cu2-C44 1.884(6), Cu2-Cu3 2.6333(12), Cu3-Cu1 2.6240(12), Cu3-P4 2.2618(19), Cu3-P2 2.2590(19), Cu4-P1 2.206(2), Cu5-P3 2.194(2).

We also made attempts to achieve hexanuclear complexes of dpa^{P2}-NHC by treatment of **Cu_2L_2** with 4 equiv [CuBr(tht)] but failed, with only **$Cu_5L_2Br_3$** being isolated from these reactions. This probably resulted from the combined effects of steric and electronic properties of dpa^{P2}-NHC.

3-8. Syntheses of Homonuclear Copper Complexes Cu_4L_2·2MeCN and $Cu_5L_2Br_3$ from dpa^{P2}-NHC and Heteronuclear Complexes $Ag_2Cu_2L_2(O)$ from Ag_2L_2

To be honest, it is unexpected and intriguing to have developed the synthetic routes to **Cu_4L_2·2MeCN**, **$Cu_5L_2Br_3$** and **$Ag_2Cu_2L_2$** from **Cu_2L_2**, since part of our initial plan was to achieve these multinuclear complexes straightforwardly from the free carbene ligand dpa^{P2}-NHC. We suspect that these established synthetic routes provide nothing but alternative syntheses of **Cu_4L_2·2MeCN**, **$Cu_5L_2Br_3$** and **$Ag_2Cu_2L_2$** (successful syntheses of **Cu_4L_2·2MeCN** and **$Cu_5L_2Br_3$** directly from dpa^{P2}-NHC and **$Ag_2Cu_2L_2$** from **Ag_2L_2** will be introduced in the following paragraph) and proof of **Cu_2L_2** undergoing fluxional process in solution. While in view of the efficiency of syntheses, one-step reaction is definitely more efficient comparing to two-step reaction when starting materials and target compounds are respectively same. Given this and in continuation of our initial objective, we next attempt to prepare **Cu_4L_2·2MeCN**, **$Cu_5L_2Br_3$** and **$Ag_2Cu_2L_2$** from dpa^{P2}-NHC by one-pot reaction.

Reaction of dpa^{P2}-NHC with two equivalents of $[Cu(MeCN)_4(OTf)]$ was prior to be carried out, leading to formation of the expected tetracopper complex **Cu_4L_2·2MeCN** as the only product in 73% yield (**Scheme 9**). Meanwhile, the pentanuclear copper complex **$Cu_5L_2Br_3$** was successfully generated by treatment of dpa^{P2}-NHC with $[Cu(MeCN)_4(OTf)]$ and [CuBr(tht)] in a ratio of 2:2:3, in 60% yield. Thus obviously, these two homonuclear copper complexes are accessible from dpa^{P2}-NHC in one step as we expected. Furthermore, the yield of one step reactions (73% for **Cu_4L_2·2MeCN** and 60% for **$Cu_5L_2Br_3$**) are significantly higher than those of two step reactions (50% for **Cu_4L_2·2MeCN** and 38% for **$Cu_5L_2Br_3$**).

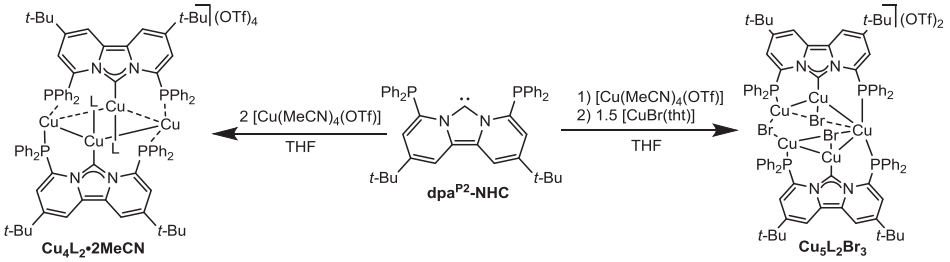

Scheme 9. Syntheses of homonuclear copper complexes **Cu_4L_2·2CH_3CN** and **$Cu_5L_2Br_3$** from **dpa^{P2}-NHC**.

While unfortunately, treatment of dpa^{P2}-NHC with $[Cu(MeCN)_4(OTf)]$ and AgOTf in a ratio of 1:1:1 did not give the desirable heteronuclear complex **$Ag_2Cu_2L_2$** but ill-defined mixture, as judged by NMR spectroscopy (**Scheme 10**). According to the analysis of proposed reaction mechanism, formation of **$Ag_2Cu_2L_2$** from dpa^{P2}-NHC by one pot reaction seems reasonable: NHC donor and one of two phosphine donors in dpa^{P2}-NHC coordinate to copper and silver ions, respectively, leading to the formation of **AgCuL** moiety, which is put together to give **$Ag_2Cu_2L_2$**. In addition, there should be no scrambling of the coordination of NHC or phosphine towards metals since we and others[14] have

proven that the NHC shows superior transmetallation aptitude to phosphine, and silver coordinated by NHC or phosphine tends to be substituted by other transition metals, including copper. More experiments and careful analysis are underway for figuring out the reason of the failure of this reaction.

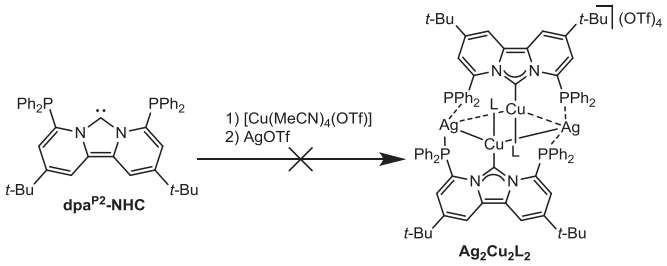

Scheme 10. Attempt to synthesize bimetallic Ag/Cu complex $\mathbf{Ag_2Cu_2L_2}$ from $\mathbf{dpa^{P2}}$**-NHC**.

Nonetheless, things are always unexpected. When the dinuclear silver complex $\mathbf{Ag_2L_2}$ reacted with equimolar amount of [Cu(MeCN)$_4$(OTf)] (**Scheme 11**), $\mathbf{Ag_2Cu_2L_2}$ was isolated as the only product in 64% yield after workup at ambient atmosphere. Concerning the process of the formation of $\mathbf{Ag_2Cu_2L_2}$, we proposed two steps, that is, prior C_{NHC} donors transmetallation from Ag to Cu and subsequently, an outward "sliding" movement of Ag. This reaction is significant because it corroborates that, in comparison to the phosphine ligand $Ph_2PC_{pyridyl}$, the NHC features superior transmetallation aptitude.[14]

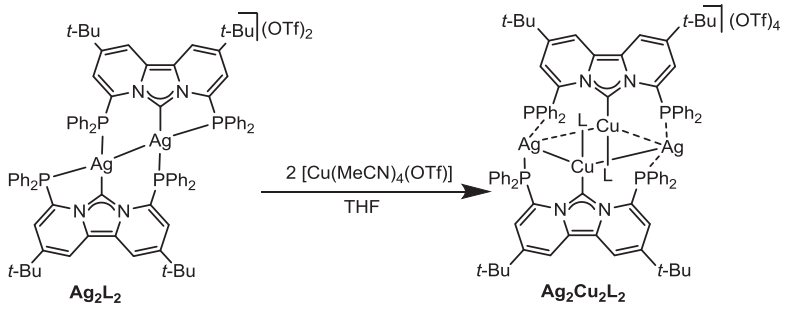

Scheme 11. Syntheses of heteronuclear bimetallic Ag/Cu complex $\mathbf{Ag_2Cu_2L_2}$ from $\mathbf{Ag_2L_2}$.

3-9. Photophysical Properties of the Obtained Silver, Copper and Bimetallic Silver/Copper Complexes

As described previously, luminescence properties of coinage metal complexes supported by NHC ligands have always been an interesting research subject.[29] With the silver and copper complexes in hand, we start to investigate their photophysical properties in degassed 2-methyl-THF, at room temperature (UV-vis absorption, photoluminescence excitation and emission) and 77 K (phosphorescence).

Figure 16 shows the obtained UV-vis absorption spectra of **Cu_4LBr_4**, **Cu_2L_2**, **$Ag_2Cu_2L_2$**, **$Cu_4L_2{\cdot}2CH_3CN$**, **$Cu_5L_2Br_3$** and **Ag_2L_2** at room temperature, whose absorption bands were found in the UV spectral range from 320 nm to 450 nm. These absorption bands compared well to those of gold complexes **1-4** (**Chapter 2**), which therefore can mainly be attributed to the ligand-centered (LC) transitions and metal-to-ligand charge transfer (MLCT) transitions.

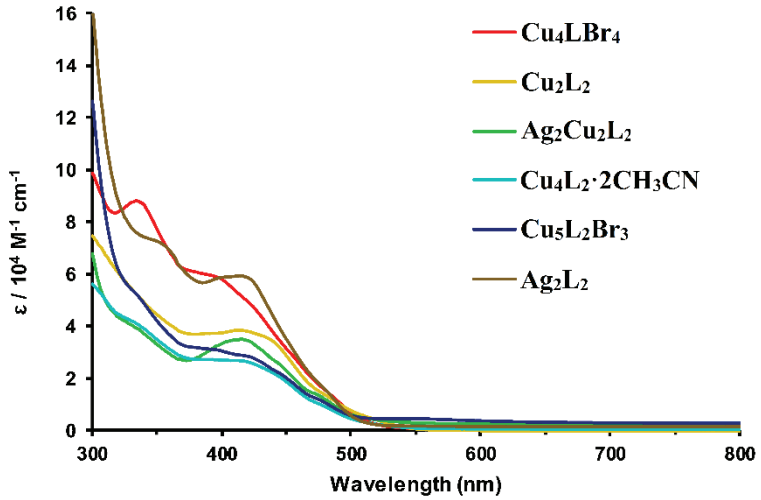

Figure 16. UV-vis absorption spectra of complexes **Cu_4LBr_4**, **Cu_2L_2**, **$Ag_2Cu_2L_2$**, **$Cu_4L_2{\cdot}2CH_3CN$**, **$Cu_5L_2Br_3$** and **Ag_2L_2** at room temperature in degassed 2-methyl-THF (2×10^{-5} M).

Photoluminescence excitation spectra (dash line) and emission spectra (solid line) acquired at room temperature were combined in **Figure 17**. All the obtained complexes are luminescent and display unstructured and almost same emission bands centered at about 500 nm. These emission bands are comparable to those of gold complexes **1-4** (**Chapter 2**), as well as, in particular, the free carbene ligand dpa^{P2}-NHC. Therefore, it suggests that the electronic transitions of these silver and copper complexes can be mostly attributed to the ligand-centered (LC) transitions. Meanwhile, once excited at 505 and 500 nm for **Ag_2L_2** and **Cu_4LBr_4**, **Cu_2L_2**, **$Ag_2Cu_2L_2$**, **$Cu_4L_2{\cdot}2CH_3CN$**, **$Cu_5L_2Br_3$**, respectively, all the complexes provided single excitation band centered at about 375 nm. The excitation spectra showed identical profiles to the corresponding UV-vis absorption spectra.

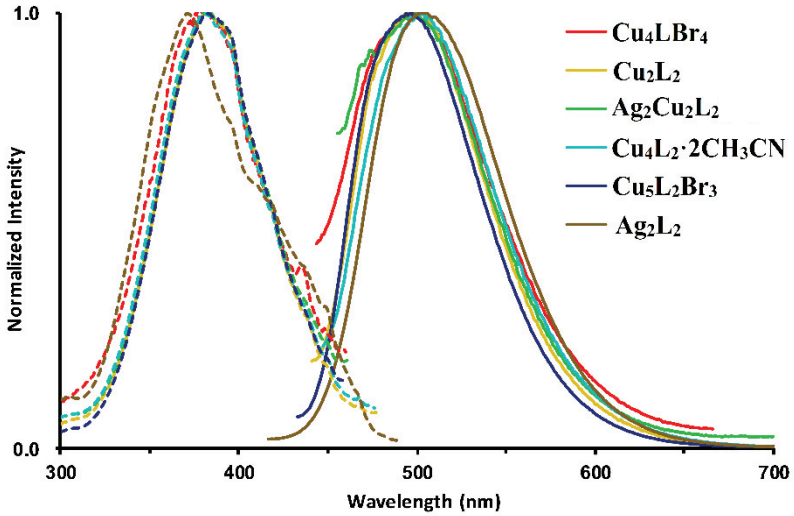

Figure 17. Normalized Excitation (dashed lines) and emission (solid line) spectra of complexes **Cu_4LBr_4**, **Cu_2L_2**, **$Ag_2Cu_2L_2$**, **$Cu_4L_2{\cdot}2CH_3CN$**, **$Cu_5L_2Br_3$** and **Ag_2L_2** at room temperature in degassed 2-methyl-THF (2×10^{-5} M). Samples were excited at 420 nm (**Cu_4LBr_4**, **Cu_2L_2**, **$Ag_2Cu_2L_2$**, **$Cu_4L_2{\cdot}2CH_3CN$** and **Ag_2L_2**) and 395 nm (**$Cu_5L_2Br_3$**). Photoluminescence excitation spectra were recorded by monitoring emissions at 505 nm (**Ag_2L_2**) and 500 nm (**Cu_4LBr_4**, **Cu_2L_2**, **$Ag_2Cu_2L_2$**, **$Cu_4L_2{\cdot}2CH_3CN$** and **$Cu_5L_2Br_3$**).

All the complexes have been investigated concerned with their phosphorescence at 77 K and only **Cu_4LBr_4**, **$Cu_4L_2{\cdot}2CH_3CN$** and **$Cu_5L_2Br_3$** were found to exhibit phosphorescence under this condition (**Figure 18**). Both **$Cu_4L_2{\cdot}2CH_3CN$** and **$Cu_5L_2Br_3$** showed a single phosphorescence band at about 640 nm; while interestingly, **Cu_4LBr_4** showed a dual phosphorescence at about 640 and 725 nm, which is likely stemming from the difficult interconversion of two triplet states arising from different orbital parentages. Compared with the free carbene ligand dpa^{P2}-NHC (**Chapter 2**), the phosphorescence bands of **Cu_4LBr_4**, **$Cu_4L_2{\cdot}2CH_3CN$** and **$Cu_5L_2Br_3$** were red-shifted, suggesting electronic perturbation of the copper cation to the triplet state of the carbene to a limited extent.

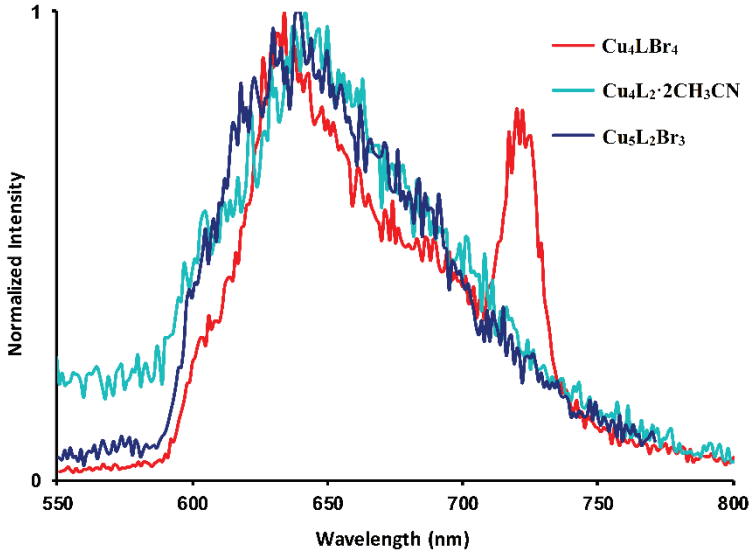

Figure 18. Normalized phosphorescence spectra of **Cu_4LBr_4**, **$Cu_4L_2{\cdot}2CH_3CN$** and **$Cu_5L_2Br_3$** in degassed 2-methyl-THF (2×10^{-5} M) at 77 K. Samples were excited at 420 nm (**Cu_4LBr_4** and **$Cu_4L_2{\cdot}2CH_3CN$**) and 395 nm (**$Cu_5L_2Br_3$**).

The phosphorescence decay profiles are depicted in **Figure 19**, from which the lifetimes of **Cu_4LBr_4**, **$Cu_4L_2{\cdot}2CH_3CN$** and **$Cu_5L_2Br_3$** are calculated to be 268.7, 571.9 and 655.6 μs, respectively. Most likely, these long luminescence lifetimes can be explained to originate from the lowest triplet states.

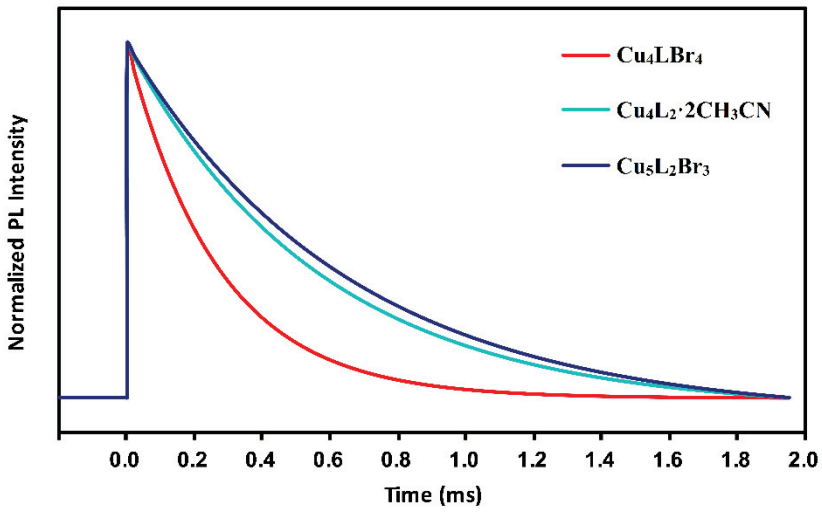

Figure 19. Phosphorescence decay traces for **Cu_4LBr_4**, **$Cu_4L_2{\cdot}2CH_3CN$** and **$Cu_5L_2Br_3$** in degassed 2-methyl-THF (2×10^{-5} M) monitoring at 640 nm at 77 K. The lifetimes of complexes **Cu_4LBr_4**, **$Cu_4L_2{\cdot}2CH_3CN$** and **$Cu_5L_2Br_3$** are 268.7, 571.9 and 655.6 μs, respectively.

3-10. Conclusion and Outlook

In conclusion, we have investigated the coordination chemistry of bis(diphenylphosphinyl)-functionalized dipyrido-annulated NHC (dpa^{P2}-NHC) towards silver(I) and copper(I). Based on dpa^{P2}-NHC, a series of multinuclear complexes featuring intramolecular d^{10}-d^{10} interactions have been achieved and characterized, including two dinuclear silver and copper complexes (**Ag_2L_2** and **Cu_2L_2**), a bimetallic tetranuclear complex (**$Ag_2Cu_2L_2$**), two tetranuclear copper complexes (**Cu_4LBr_4** and **$Cu_4L_2 \cdot 2CH_3CN$**) and a pentanuclear copper complex (**$Cu_5L_2Br_3$**). Judging by the obtained NMR spectra, all of the complexes underwent dynamic behavior in solution at room temperature. In particular, the room temperature NMR spectra of **Ag_2L_2** displaying a coalescence were well resolved at low temperature (below 208 K) and a dissociative process for **Ag_2L_2** was observed based on the calculated Eyring plot. In contrast, the possible coalesced NMR spectra of **Cu_2L_2** did not show any significant change with the temperature varying from 293 K to 173 K, indicating extremely low barrier of the fluxional process of **Cu_2L_2** in solution. **Ag_2L_2** showed a similar coordination sphere with its gold analogue **3** (**Chapter 2**). While differently, the dicopper complex **Cu_2L_2** contained two distinct carbenes, namely a terminal carbene and a bridging carbene. **Cu_4LBr_4** is neutral and monomeric, in which four copper centers were rigidly fixed by the tridentate ligand dpa^{P2}-NHC and additional bromide anions. **$Cu_5L_2Br_3$** showed a similar coordination sphere with the tetranuclear gold complex 4 (**Chapter 2**), except that one additional CuBr was inserted between a metal-phosphine interaction for **$Cu_5L_2Br_3$**.

All complexes obtained are luminescent, in which **$Cu_4L_2 \cdot 2CH_3CN$**, **Cu_4LBr_4** and **$Cu_5L_2Br_3$** are phosphorescent at 77 K. The metal centers and the different solid-state structures did not seem to change the solution photoluminescence properties of these dpa^{P2}-NHC complexes. This may be due to the dynamic processes in solution because of the rigidity of the ligand. Earlier group metal centers that prefer higher coordination numbers maybe more suitable for stronger non-dissociative coordination. This and their photophysical properties of the resulting complexes are our next research focus.

References

[1]. (a) I. J. B. Lin, C. S. Vasam, *Coord. Chem. Rev.* **2007**, 251, 642-670. (b) H. W. J. Wang, I. J. B. Lin, *Organometallics* **1998**, 17, 972-975. (c) H. M. Lee, J. Y. Zeng, C.-H, Hu, M.-T. Lee, *Inorg. Chem.* **2004**, 43, 6822-6829. (d) F. E. Hahn, M. C. Jahnke, T. Pape, *Organometallics* **2006**, 25, 5927-5936.

[2]. (a) L. Ray, V. Katiyar, S. Barman, M. J. Raihan, H. Nanavati, M. M. Shaikh, P. Ghosh, *J. Organomet. Chem.* **2007**, 692, 4259-4269. (b) M. K. Samantary, V. Katiyar, K. Pang, H. Nanavati, P. Ghosh, *J. Organomet. Chem.* **2007**, 692, 1672-1682. (c) A. C. Sentman, S. Csihony, G. W. Nyce, R. M. Waymouth, J. L. Hedrick. *J. Org. Chem.* **2005**, 70, 2391-2393. (d) M. K. Brown, T. L. May, C. A. Baxter, A. H. Hoveyda, *Angew. Chem. Int. Ed.* **2007**, 46, 1097-1100. (e) M. A. Kacprzynski, T. L. May, S. A. Kazane, A. H. Hoveyda, *Angew. Chem. Int. Ed.* **2007**, 46, 4554-4558. (f) Y. Lee, K. Akiyama, D. G. Gillingham, M. K. Brown, A. H. Hoveyda, *J. Am. Chem. Soc.* **2008**, 130, 446-447. (g) R. E. Douthwaite, *Coord. Chem. Rev.* **2007**, 251, 702-717.

[3]. K. H. Park, I. Ku, H. J. Kim, S. U. Son, *Chem. Mater.* **2008**, 20, 1673-1675.

[4]. (a) C. Boehme, G. Frenking, *Organometallics* **1998**, 17, 5801-5809. (b) D. Nemcsok, K. Wichmann, G. Frenking, *Organometallics* **2004**, 23, 3640-3646.

[5]. (a) K. M. Lee, H. M. J. Wang, I. J. B. Lin, *Chem. Soc. Dalton Trans.* **2002**, 2852-2856. (2) X. Zhang, S. Gu, Q. Xia, W. Chen, *J. Organomet. Chem.* **2009**, 694, 2359-2367. (c) Y. Zhou, X. Zhang, W. Chen, H. Qiu, *J. Organomet. Chem.* **2008**, 693, 205-215. (d) B. Liu, W. Chen, S. Jin, *Organometallics* **2007**, 26, 3660-3667. (e) V. J. Catalano, A. L. Moore, *Inorg. Chem.* 2005, 44, 6558-6566. (f) F. Gui, P. Yang, X. Huang, X.-J. Yang, B. Xu, *Organometallics* **2012**, 31, 3512-3518. (g) S. D. Adhikary, L. Jhulki, S. Seth, A. Kundu, V. Bertolasi, P. Mitra, A. Mahapatra, J. Dinda, *Inorg. Chim. Acta* **2012**, 384, 239-246. (h) S. D. Adhikary, S. K. Seth, M. R. Senapati, J. Dinda, *J. Mol. Struct.* **2013**, 1042, 123-128.

[6]. (a) F. Lazreg, F. Nahra, C. S. J. Cazin, *Coord. Chem. Rev.* **2015**, 293-294, 48-79. (b) J. D. Egbert, C. S. J. Cazin, S. P. Nolan, *Catal. Sci. Technol.* **2013**, 3, 912-926. (c) V. Jurkauskas, J. P. Sadighi, S. L. Buchwald, *Org. Lett.* **2003**, 5, 2417-2420. (d) G. Evano, N. Blanchard (Eds.), Copper-Mediated Cross-Coupling Reactions, Wiley, 2014.

[7]. (a) V. A. Krylova, P. I. Djurovich, M. T. Whited, M. E. Thompson, *Chem. Commun.* **2010**, 46, 6696-6698. (b) V. A. Krylova, P. I. Djurovich, J. W. Aronson, R. Haiges, M. T. Whited, M. E. Thompson, *Organometallics* **2012**, 31, 7983-7993.

[8]. (a) M. J. Leitl, V. A. Krylova, P. I. Djurovich, M. E. Thompson, H. Yersin, *J. Am. Chem. Soc.* **2014**, 136, 16032-16038. (b) Z. Wang, C. Zheng, W. Wang, C. Xu, B. Ji, X. Zhang, *Inorg. Chem.* **2016**, 55, 2157-2164. (c) P. Ai, M. Mauro, L. De cola, A. A. Danopoulos, P. Braunstein, *Angew. Chem. Int. Ed.* **2016**, 55, 3338-3341. (d) V. Gierz, A. Seyboldt, C. Maichle-Mössmer, K. W. Törnroos, M. T. Speidel, B. Speiser, K. Eichele, D. Kunz, *Organometallics* **2012**, 31, 7893-

7901. (e) R. Fränkel, J. Kniczek, W. Ponikwar, H. Nöth, K. Polborn, W. P. Fehlhammer, *Inorg. Chim. Acta* **2001**, 312, 23-39. (f) X. Hu, I. Castro-Rodriguez, K. Meyer, *J. Am. Chem. Soc.* **2003**, 125, 12237-12245. (g) C. Tubaro, A. Biffis, R. Gava, E. Scattolin, A. Volpe, M. Basato, M. M. Día z-Requejo, P. J. Perez, *Eur. J. Org. Chem.* **2012**, 2012, 1367-1372. (h) M. Poyatos, J. A. Mata, E. Peris, *Chem. Rev.* **2009**, 109, 36773707. (i) C. E. Ellul, G. Reed, M. F. Mahon, S. I. Pascu, M. K. Whittlesey, *Organometallics* **2010**, 29, 4097-4104. (j) K. Matsumoto, N. Matsumoto, A. Ishii, T. Tsukuda, M. Hasegawa, T. Tsubomura, *Dalton Trans.* **2009**, 6795-6801.

[9]. J. Nitsch, F. Lacemon, A. Lorbach, A. Eichhorn, F. Cisnetti, A. Steffen, *Chem. Commun.* **2016**, 52, 2932-2935.

[10]. (a) Y. Gu, X. Leng, Q. Shen, *Nat. Commun.* **2014**, 5, 5405. (b) J. M. Lee, Y. Na, H. Han, S. Chan, *Chem. Soc. Rev.* **2004**, 33, 302-312. (c) A. E. Allen, D. W. C. Macmillan, *Chem. Sci.* **2012**, 3, 633-658. (d) P. Buchwalter, J. Rosé, P. Braunstein, *Chem. Rev.* **2015**, 115, 28-126.

[11]. (a) A. Zanardi, R. Corbera´n, J. A. Mata, E. Peris, *Organometallics* **2008**, 27, 3570–3576. (b) S. Sabater, J. A. Mata, E. Peris, *Nat. Commun.* **2013**, 4, 2553. (c) A. Zanardi, J. A. Mata, E. Peris, *Chem. – Eur. J.* **2010**, 16, 13109–13115. (d) A. Zanardi, J. A. Mata, E. Peris, *J. Am. Chem. Soc.* **2009**, 131, 14531–15537.

[12]. (a) C. Schulte to Brinke, F. E. Hahn, *Eur. J. Inorg. Chem.* **2015**, 3227–3231. (b) R. Maity, H. Koppetz, A. Hepp, F. E. Hahn, *J. Am. Chem. Soc.* **2013**, 135, 4966–4969.

[13]. S. Bente, F. Kampert, T. T. Y. Tan, F. E. Hahn, *Chem. Commun.* **2018**, 54, 12887-12890.

[14]. T. Simler, P. Braunstein, A. A. Danopoulos, *Angew. Chem. Int. Ed.* **2015**, 54, 13691-13695.

[15]. M. A. Carvajal, J. J. Novoa, S. Alvarez, *J. Am. Chem. Soc.* **2004**, 126, 1465-1477.

[16]. (a) P. Ai, A. A. Danopoulos, P. Braunstein, *Chem. Commun.* **2014**, 50, 103-105. (b) A. Marchenko, H. Koidan, A. Hurieva, O. Kurpiieva, Y. Vlasenko, A. Kostyuk, C. Tubaro, A. Lenarda, A. Biffis, C. Graiff, *J. Organomet. Chem.* **2014**, 771, 14-23. (c) T. Simler, P. Braunstein, A. A. Danopoulos, *Dalton Trans.* **2016**, 45, 5122-5139.

[17]. S. Sculfort and P. Braunstein, *Chem. Soc. Rev.* **2011**, 40, 2741-2760.

[18]. H. Schmidbaur and A. Schier, *Angew. Chem. Int. Ed.* **2015**, 54, 746-784.

[19]. (a) X. Liu, P. Braunstein, *Inorg. Chem.* **2013**, 52, 7367-7379. (b) M. Brill, E. Kühnel, C. Scriban, F. Romingera, P. Hofmann, *Dalton Trans.* **2013**, 42, 12861-12864. (c) P. L. Chiu, H. M. Lee, *Organometallics* **2005**, 24, 1692-1702. (d) A. P. Marchenko, H. N. Koidan, A. N. Hurieva, O. V. Gutov, A. N. Kostyuk, C. Tubaro, S. Lollo, A. Lanza, F. Nestola, A. Biffis, *Organometallics* **2013**, 22, 718-721. (e) M. Raynal, X. Liu, R. Pattacini, C. Vallée, H. Olivier-Bourbigou, P. Braunstein, *Dalton Trans.* **2009**, 7288-7293. (f) A. P. Marchenko, H. N. Koidan, A. N. Huryeva, E. V. Zarudnitskii, A. A. Yurchenko, A. N. Kostyuk, *Organometallics* **2012**, 31, 8257-8264. (g) L. Cao, S. Huang, W. Liu, X. Yan, *Organometallics* **2018**, 37, 2010-2013.

[20]. D. L. Phillips, C.-M. Che, K. H. Leung, Z. Mao, M.-C. Tse, *Coord. Chem. Rev.* **2005**, 249, 1476-1490.

[21]. E. Kuhnel, I. V. Shishkov, F. Rominger, T. Oeser, P. Hofmann. *Organometallics* **2012**, 31, 8000-8011.

[22]. M. A. Legare, G. Belanger-Chabot, R. D. Dewhurst, E. Welz, I. Krummenacher, B. Engels, H. Braunschweig. *Science* **2018**, 359, 896-900.

[23]. L. Busetto, M. C. Cassani, C. Femoni, A. Macchioni, R. Mazzoni, D. Zuccaccia, *J. Organomet. Chem.* **2008**, 693, 2579-2591.

[24]. P. K. Mehrota, R. Hoffman, *Inorg. Chem.* **1978**, 17, 2187-2189.

[25]. (a) S. Gischig and A. Togni, *Organometallics* **2005**, 24, 203-205. (b) V. J. Catalano, L. B. Munro, C. E. Strasser, A. F. Samin, *Inorg. Chem.* **2011**, 50, 8465-8476.

[26]. (a) C. Garrison, R. S. Simons, W. G. Kofron, C. A. Tessier, W. J. Youngs, *Chem. Commun.* **2001**, 1780-1781. (b) J. C. Garrison, R. S. Simons, C. A. Tessier, W. J. Youngs, *J. Organomet. Chem.* **2003**, 673, 1-4.

[27]. (a) M. R. L. Furst and C. S. J. Cazin, *Chem. Commun.* **2010**, 46, 6924–6925. (b) F. Nahra, A. Gómez-Herrerab, C. S. J. Cazin, *Dalton Trans.* **2017**, 46, 628–631.

[28]. (a) H. Fribolin, Ein-zweidimensionale NMR-Spektroskopie, Wiley VCH, **2006**. (b) H. Fuji, M. Tomura, T. Kurahashi, M. Kujime, *Inorg. Chem.* **2007**, 46, 541-551.

[29]. (a) E. E. Langdon-Jones and S. J. A. Pope, *Chem. Commun.* **2014**, 50, 10343-10354. (b) R. Visbal and M. C. Gimeno, *Chem. Soc. Rev.* **2014**, 43, 3551-3574. (c) N. Sinha, L. Stegemann, T. T. Y. Tan, N. L. Doltsinis, C. A. Strassert, F. E. Hahn, *Angew. Chem. Int. Ed.* **2017**, 56, 2785-2789. (d) A. A. Penney, V. V. Sizov, E. V. Grachova, D. V. Krupenya, V. V. Gurzhiy, G. L. Starova, S. P. Tunik, *Inorg. Chem.* **2016**, 55, 4720-4732. (e) S. Kobialka, C. Müller-Tautges, M. T. S. Schmidt, G. Schnakenburg, O. Hollóczki, B. Kirchner, M. Engeser, *Inorg. Chem.* **2015**, 54, 6100-6111. (f) T. Lu, J-Y. Wang, D. Tu, Z.-N. Chen, X.-T. Chen, Z.-L. Xue, *Inorg. Chem.* **2018**, 57, 13618-13630. (g) A. M. Polgar, F. Weigend, A. Zhang, M. J. Stillman, J. F. Corrigan, *J. Am. Chem. Soc.* **2017**, 139, 14045-14048. (h) H. Ube, Q. Zhang, M. Shionoya, *Organometallics* **2018**, 37, 2007-2009. (i) Y. Zhou and W. Chen, *Organometallics* **2007**, 26, 2742-2746.

Chapter 4

Conclusion and Outlook

Since the spectroscopically and structurally characterization of the first isolable N-heterocyclic carbene by Arduengo and co-workers in 1991, NHCs have attracted considerable attention due to their numerous applications across a variety of fields. As part of our long-standing interests in the chemistry of pincer ligands, we designed and synthesized a diphosphine-functionalized hybrid NHC, bis(diphenylphosphinyl)-functionalized dipyrido-annulated NHC (**dpa^{P2}-NHC**). Closely following this, the coordination chemistry of **dpa^{P2}-NHC** towards coinage metal ions was investigated, from which exciting results were obtained.

Apprehensive of the potential experimental challenges to be met when dealing with the possible air- or light-sensitive silver carbene complexes, we were first to be focus on the coordination chemistry of **dpa^{P2}-NHC** towards Au^{I}.

At first, an air- and water-stable, monomeric dinuclear gold complex **1**, with two gold-coordinated phosphines and unactivated carbene, was achieved starting from the carbene precursor **L(H)I** via a two step reaction (**Scheme 1**). Considering the subsequent synthetic convenience, we attempted to isolate the free NHC **dpa^{P2}-NHC** at room temperature, which was successfully realized through the dehydrogenation reaction of **L(H)I** with *t*BuOK. **dpa^{P2}-NHC** is stable at inert atmosphere at room temperature for months, which is, to some extent, in favor of our next experimental work.

Shortly afterward, starting from the free carbene **dpa^{P2}-NHC**, we afforded two dinuclear gold complexes (**2-3**) and one tetranuclear gold complex (**4**) via respective one-step reactions (**Scheme 1**). While it is worth noting that two totally different digold complexes **2** and **3** were respectively generated from **dpa^{P2}-NHC**, when subjected to two different gold precursor ($AuCl(SMe_2)$ and $Au(tht)_2OTf$). Alternatively, complex **2** can serve as the precursor on the way to complexes **3** and **4** (**Scheme 1**) through the reactions of halide (chloride) abstraction and likely phosphine transfer, respectively. The obtained NMR spectra indicated that complexes **1** and **3** showed consistency in solid state and solution, while complexes **2** and **4** underwent possible dynamic behavior in solution.

The free carbene **dpa^{P2}-NHC** and complexes **1-4** were structurally characterized by X-ray diffraction analysis. Strong Au-Au interactions were found in complexes **2-4**. Especially, molecular structure of tetragold species **4** showed a novel and unprecedented coordination sphere, in which four gold cations connected by aurophilic interactions formed a planar metallocycle bridging two **dpa^{P2}-NHC** ligands, which are parallel to each other and point in the opposite direction. In the meantime, each of the central golds (NHC coordinated) lies in the plane of three σ-donors in each NHC ligand owing to the hindered rotation at the phosphines.

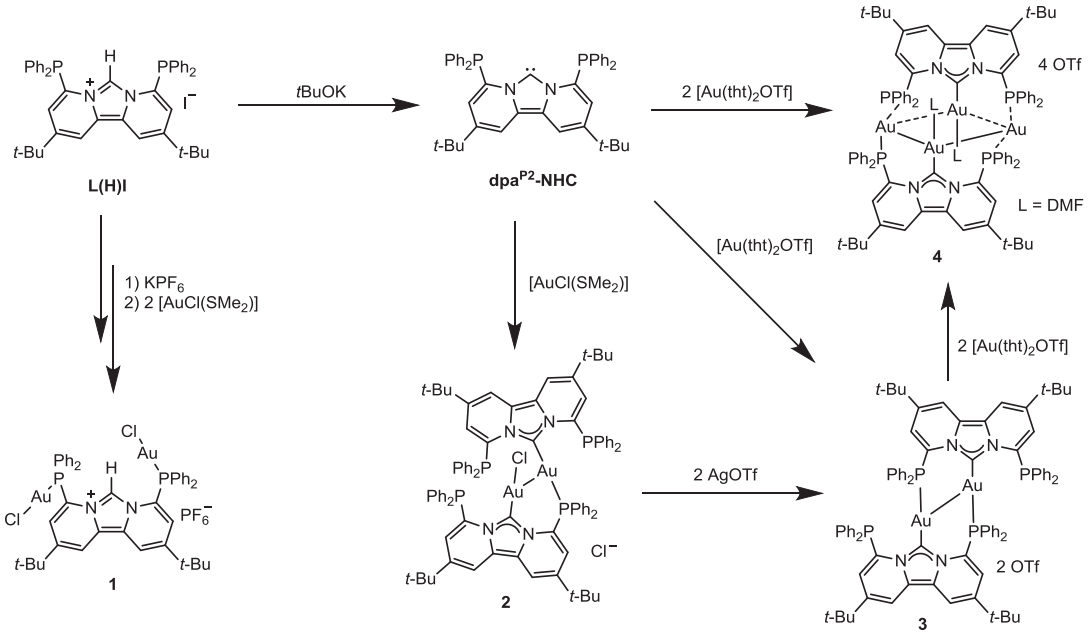

Scheme 1. Syntheses of di- and tetranuclear gold complexes (**1-4**) from **L(H)I**.

After finishing the gold part, we turned our attention to investigating the coordination chemistry of **dpa^{P2}-NHC** towards silver and copper. As a result, a series of homonuclear silver(I) and copper(I) complexes based on **dpa^{P2}-NHC** were synthesized and spectroscopically and structurally characterized, including two dinuclear complexes $\mathbf{Ag_2L_2}$ and $\mathbf{Cu_2L_2}$, two tetranuclear copper complexes $\mathbf{Cu_4LBr_4}$ and $\mathbf{Cu_4L_2{\cdot}2CH_3CN}$, and a pentanuclear copper(I) complex $\mathbf{Cu_5L_2Br_3}$ (**Scheme 2**).

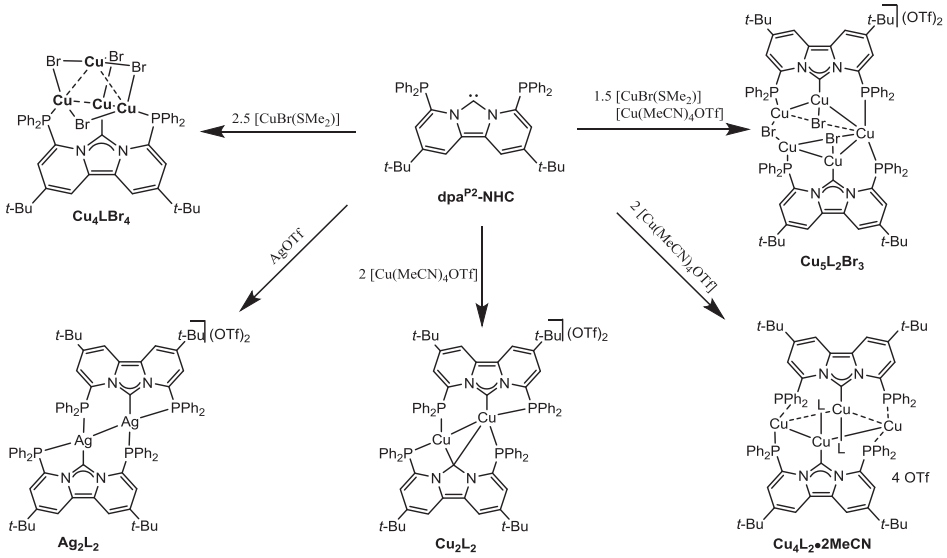

Scheme 2. Syntheses of homonulcear silver and copper complexes from **dpa^{P2}-NHC**

The two dinuclear complexes (**Ag_2L_2** and **Cu_2L_2**) were found to undergo fluxional behavior in solution judging from the obtained NMR spectroscopy, since both the room temperature NMR spectra of these two complexes showed a single and symmetric dpa^{P2}-NHC environment that contrasts with the observation of their solid state structure. For **Cu_2L_2**, cooling temperature to 193 K did not lead to the decoalescence of the NMR spectra. While the fluxional behavior can be directly corroborated by the successful synthesis of **$Cu_4L_2{\cdot}2CH_3CN$**, **$Ag_2Cu_2L_2$** and **$Cu_5L_2Br_3$** from **Cu_2L_2** via one step reaction (**Scheme 3**). For **Ag_2L_2**, well resolved NMR spectra can be observed on the ^{1}H and ^{31}P NMR timescale when the temperature is at <208 K. At this temperature range, the NMR spectra are in agreement with the solid state structure and a dissociative process was observed according to the calculated Eyring plot.

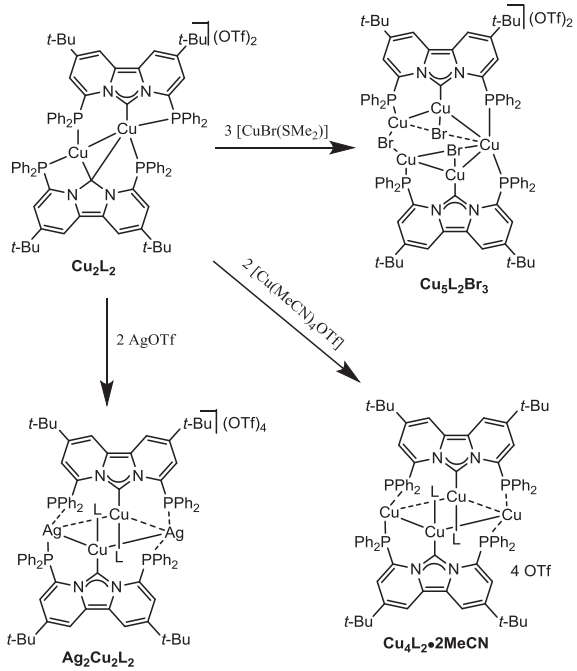

Scheme 3. Syntheses of homonulcear copper and heteronuclear silver/copper complexes from **Cu_2L_2**

Meanwhile, it is interesting to find that the bimetallic Ag/Cu complex **$Ag_2Cu_2L_2$** can be generated by reaction of **Cu_2L_2** with two equivalent of [Cu(MeCN)$_4$(OTf)] (**Scheme 4**). This reaction is likely to proceed via the transmetallation of the NHC donor from Ag(I) to Cu(I) and the following outward sliding movement of Ag(I) which is captured by two phosphine ligands from two dpa^{P2}-NHC ligands. This reaction is also significant because it corroborates that the NHC transmetallation aptitude is superior to that of the triarylphosphine.

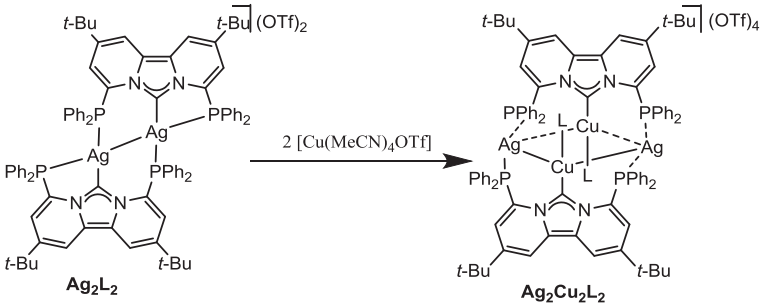

Scheme 4. Syntheses of heteronulcear silver/copper complexes $\mathbf{Ag_2Cu_2L_2}$ from $\mathbf{Ag_2L_2}$

The dicopper complex $\mathbf{Cu_2L_2}$ showed a novel coordination mode with two carbene carbons adopting two different bonding modes, namely one bound to only one copper atom and the other simultaneously bound to two copper atoms. Thus, two types of carbene carbons in terms of the hybridization can be expected, that is, the terminal carbene carbon in sp^2 hybridization and the bridging carbene carbon in sp^3 hybridization. $\mathbf{Ag_2L_2}$ displayed an entirely same coordination sphere compared to the obtained digold complex **3**. Interestingly, the tetranuclear copper complex $\mathbf{Cu_4L_2 \cdot 2CH_3CN}$ that are expected to adopt similar coordination sphere with the tetragold complex **4** likely underwent reactions with water contained in solvent (DMF) in the course of crystallization, resulting in the insertion of the oxygen atom in a form of bridging two central copper atoms. The neutral and monomeric complex $\mathbf{Cu_4LBr_4}$ showed a novel coordination mode with four copper centers of which are rigidly fixed by three σ donors (two phosphines and one NHC) and adjacent bromide anions. To our best knowledge, this coordination mode is unprecedented for phosphine-functionalized NHC supported coinage metal complexes. The pentanuclear copper complex $\mathbf{Cu_5L_2Br_3}$ comprised two same [$Cu_3Br(dpa^{P2}$-NHC)(DMF)] subunits sharing a hexacoordinated copper and bridged by one of the bromides through interactions with two phosphine-coordinated coppers, which point in opposite directions.

All the obtained complexes are luminescent in solution at room temperature. Of these, the gold complexes (**1-4**) and homonuclear copper complexes ($\mathbf{Cu_4LBr_4}$, $\mathbf{Cu_4L_2 \cdot 2CH_3CN}$ and $\mathbf{Cu_5L_2Br_3}$) emit phosphorescence at 77 K with long lifetimes ranging from 85.1 to 772.0 μs. While to be honest, the photoluminescence properties of these complexes were determined with no spectacular results, namely, all the complexes showed almost the same emission bands lying in the range of 450-600 nm. Given the comparison with the free carbene $\mathbf{dpa^{P2}}$**-NHC**, we can attribute the luminescence of these complexes to the ligand-centered (LC) transitions. In other words, the metal-metal interactions have no significant contribution to the enhancement of the photophysical properties of the obtained complexes in solution. This could be tentatively associated with the dynamic behavior of these complexes in solution, which lead to the possible disappearance of metal-metal interactions. Our next work is mainly focused on improving the stability of these complexes by replacing the dissociated

anion triflate with the anions with stronger coordinating ability, like halide anions, which are able to coordinate with the metal centers so that to stabilize the metal-metal interactions and keep the integrity of complexes in solution, to some extent.

The luminescence of complexes in solid state has been always an important parameter for measuring the physical properties of complexes. According to our original design, the strong metal-metal interactions and wide π-electron conjugation of the backbone as our obtained coinage metal **dpa^{P2}-NHC** complexes feature would contribute significantly to enhance the photophysical properties of the complexes. While unfortunately, due to the limited laboratory condition, measuring the luminescence of the obtained complexes in solid state cannot be carried out. We will do this work in the near future.

Given the reported excellent performance of gold- and copper-NHC complexes in a variety of chemical transformations as catalysts, we will also attempt to explore the catalytic uses of gold complexes (**2-4**) in cycloisomerization and C-H bond activation and copper complexes in cross-coupling reactions.

Experimental Section

General Procedure

Unless otherwise noted, all the manipulations were carried out using standard Schlenk techniques under an argon atmosphere. THF and hexane were purified by passing through a Glass Contour solvent dispensing system under an N_2 atmosphere; other solvents used were purified and dried by standard methods. The starting material **L(H)I** was prepared according to the literature procedure.[1-3] ^{1}H (400 MHz, 600 MHz), ^{13}C (100 MHz, 150 Hz), and ^{31}P (162 MHz, 243MHz) NMR spectra were recorded on JEOL AL-400S spectrometer and were referenced to $CDCl_3$ (^{1}H: δ=7.26 ppm; ^{13}C: δ=77.1 ppm), C_6D_6 (^{1}H: δ=7.16 ppm; ^{13}C: δ=128.0 ppm), DMSO-d_6 (^{1}H: δ=2.50 ppm; ^{13}C: δ=39.5 ppm) or CD_3CN (^{1}H: δ=1.94 ppm; ^{13}C: δ=118.26 ppm) as external standards. ^{31}P NMR spectra are referenced to 85% H_3PO_4 (δ=0.0 ppm) as external standards. UV-vis absorption spectra were recorded with a Shimadzu UV-1650PC spectrophotometer. Photoluminescence spectra were measured with a HORIBA FluoroMax-4 spectrophotometer.

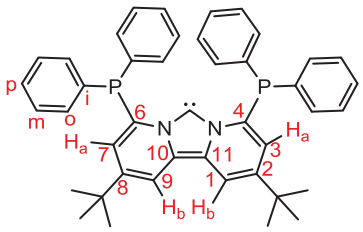

Figure S1. Atom numbering used for the assignment of the NMR resonances

Syntheses of L(H)I

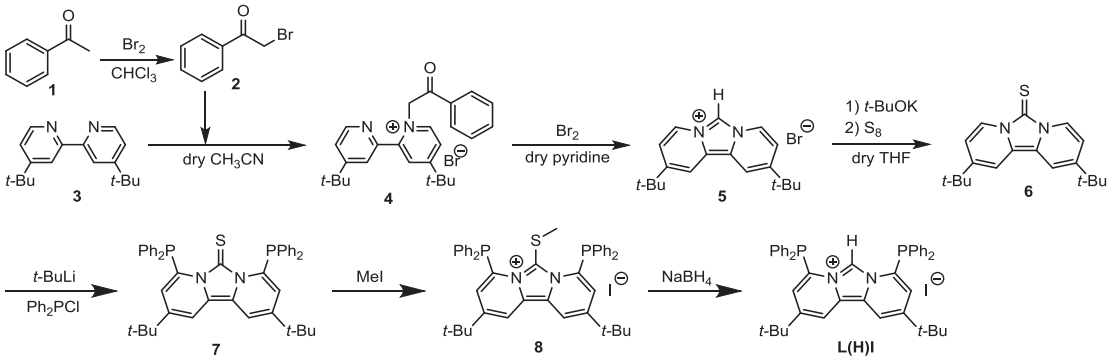

The carbene precursor **L(H)I** was afforded via a seven-step reaction according to the literature from us and other groups.[1-3]

Syntheses of dpa^{P2}-NHC

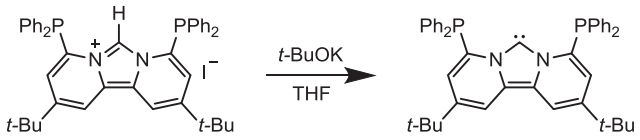

L(H)I **dpa^{P2}-NHC**

The solution of **L(H)I** (400.0 mg, 0.515 mmol) and *t*-BuOK (69.3 mg, 0.618 mmol) in THF (40 mL) was stirred at room temperature for 2 h and volatiles were then removed under reduced pressure. Hexane (60 mL) was added and the solution was filtered through Celite. After removal of the solvent, **dpa^{P2}-NHC** was obtained as a yellow solid. Yield: 68.7% (230.1 mg, 0.354 mmol). **^{1}H NMR** (600 MHz, C_6D_6): δ 1.08 (s, 18H, CH_3), 6.54 (s, 2H, H_a), 6.93-7.06 (m, 12H, *m-/p*-CH_{Ph}), 7.42 (m, 8H, *o*-CH_{Ph}), 7.53 (s, 2H, H_b). **^{31}P{^{1}H} NMR** (243 MHz, C_6D_6): δ -13.8. **^{13}C{^{1}H} NMR** (150 MHz, C_6D_6): δ 30.3 (CH_3), 34.7 ($C(CH_3)$), 111.5 (*C*1/*C*9), 121.1 (*C*3/*C*7), 122.7 (d, $^{1}J_{PC}$ = 2 Hz, *C*4/*C*6), 128.5 (d, $^{3}J_{PC}$ = 8 Hz, *m*-C_{Ph}), 128.8 (*p*-C_{Ph}), 134.7 (d, $^{1}J_{PC}$ = 21 Hz, *o*-C_{Ph}), 136.9 (d, $^{2}J_{PC}$ = 12 Hz, *i*-C_{Ph}), 140.3 (*C*10/*C*11), 142.0 (d, $^{3}J_{PC}$ = 14 Hz, *C*2/*C*8), 198.3 (t, $^{3}J_{PC}$ = 33 Hz, $C_{carbene}$). Element analysis calcd for $C_{43}H_{42}N_2P_2$ (648.77): C 79.61, H 6.53, N 4.32; found: C 79.37, H 6.20, N 4.84.

Syntheses of L(H)PF$_6$

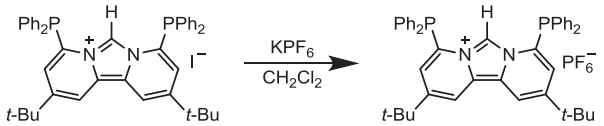

L(H)I **L(H)PF$_6$**

The solution of **L(H)I** (100 mg, 0.129 mmol) and KPF_6 (47.4 mg, 0.258 mmol) in CH_2Cl_2 (20 mL) was stirred at room temperature for 24 h. After the reaction solution being concentrated to 2-3 mL under reduced pressure, hexane (10 mL) was added to precipitate the yellow solid **L(H)PF$_6$** that was collected by filtration. Yield: 85.7% (87.8 mg, 0.111 mmol). **^{1}H NMR** (400 MHz, DMSO-d_6): δ 1.23 (s, 18H, CH_3), 6.97 (dd, $^{4}J_{HH}$ = 2.0 Hz, $^{3}J_{PH}$ = 2.4 Hz, 2H, H_a), 7.21-7.38 (m, 8H, *o*-CH_{Ph}), 7.39-7.67 (m, 12H, *m-/p*-CH_{Ph}), 8.64 (s, H, NC*H*N), 8.91 (d, $^{4}J_{HH}$ = 2.0 Hz, 2H, H_b). **^{31}P{^{1}H} NMR** (162 MHz, DMSO-d_6): δ -13.6 (s), -143.2 (sept, $^{1}J_{PF}$ = 720.9 Hz, *P*F_6). **^{13}C{^{1}H} NMR** (100 MHz, DMSO-d_6): δ 29.9 (CH_3), 35.1 ($C(CH_3)$), 110.2 (t, $^{3}J_{PC}$ = 16 Hz, N*C*HN), 114.8 (*C*1/ *C*9), 123.9 (*C*10/*C*11), 126.9 (d, $^{2}J_{PC}$ = 6 Hz, *C*6/*C*4), 129.0 (d, $^{1}J_{PC}$ = 6 Hz, *C*7/*C*3), 129.9 (d, $^{3}J_{PC}$ = 8 Hz, *m*-C_{Ph}), 131.2 (*p*-C_{Ph}), 133.1 (d, $^{1}J_{PC}$ = 25 Hz, *i*-C_{Ph}), 133.9 (d, $^{2}J_{PC}$ = 21 Hz, *o*-C_{Ph}), 146.0 (*C*2/*C*8). HRMS (ESI) m/z [M-PF_6]$^{+}$ 649.290. Element analysis calcd for $C_{43}H_{43}F_6N_2P_3$ (794.74): C 64.99, H 5.45, N 3.52; found: C 65.10, H 5.70, N 3.64.

Syntheses of complex 1

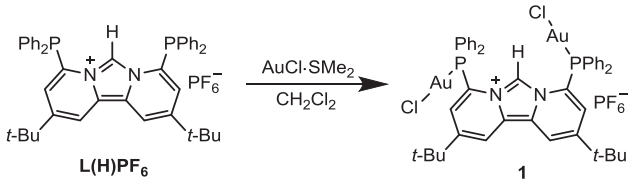

To a solution of **L(H)PF$_6$** (20.0 mg, 0.025 mmol) in CH_2Cl_2 (10 mL) was added [AuCl(SMe$_2$)] (14.8 mg, 0.051 mmol) and the resulting solution was stirred at room temperature for 1 h. After being concentrated to 2-3 mL under reduced pressure, hexane (15 mL) was added to precipitate the yellow solid complex **1** that was collected by filtration. Yield: 90.5% (28.5 mg, 0.023 mmol). Suitable crystals for X-ray analysis were obtained by slow diffusion of diethyl ether into the solution of **1** in dimethylformamide. **^{1}H NMR** (400 MHz, DMSO-d_6): δ 1.24 (s, 18H, CH_3), 7.14 (d, $^3J_{PH}$= 10.4 Hz, 2H, H_a), 7.59-7.89 (m, 20H, CH_{Ph}), 8.30 (s, H, NCHN), 9.23 (s, 2H, H_b). **^{31}P{^{1}H} NMR** (162 MHz, DMSO-d_6): δ 27.2 (s), -143.2 (sept, $^1J_{PF}$ = 720.9 Hz, PF$_6$). **^{13}C{^{1}H} NMR** (100 MHz, DMSO-d_6): δ 29.9 (CH$_3$), 35.3 (C(CH$_3$)), 110.0 (br s, 110.0), 118.1 ($C$1/$C$9), 122.7 (d, $^1J_{PC}$ = 65 Hz, $C$4/$C$6), 123.5 (d, $^1J_{PC}$ = 62 Hz, *i*-C_{Ph}), 125.1 (d, $^3J_{PC}$ = 2 Hz, $C$10/$C$11), 130.0 (d, $^2J_{PC}$ = 10 Hz, $C$3/$C$7), 131.0 (d, $^3J_{PC}$ = 13 Hz, *m*-C_{Ph}), 134.6 (d, $^4J_{PC}$ = 2 Hz, *p*-C_{Ph}), 134.8 (d, $^2J_{PC}$ = 10 Hz, *o*-C_{Ph}), 146.7 ($C$2/$C$8). HRMS (ESI) m/z [M-PF$_6$]$^+$ 1113.1609. Element analysis calcd for $C_{43}H_{43}Au_2Cl_2F_6N_2P_3$ (1259.58): C 41.00, H 3.44, N 2.22; found: C 40.58, H 3.24, N 2.13.

Syntheses of complex 2

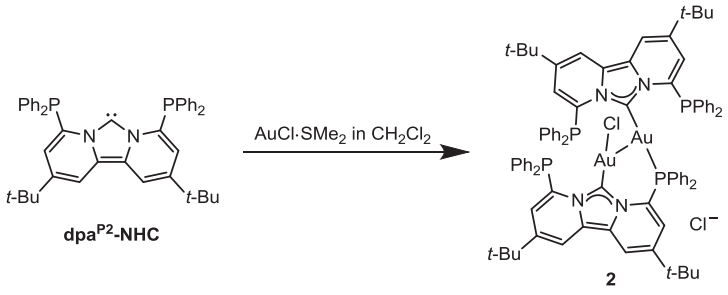

The approximately saturate solution of [AuCl(SMe$_2$)] (74.8 mg, 0.254 mmol) in CH_2Cl_2 (6 mL) was slowly added dropwise to a solution of free carbene **dpa^{P2}-NHC** (150.0 mg, 0.231 mmol) in hexane (80 mL) and the instantly formed yellow precipitate was collected by filtration. After recrystallization with THF at -18°C, desired product was collected as light yellow solid by filtration. Yield: 72.3% (147.2 mg, 0.084 mmol). Suitable crystals for X-ray analysis were obtained by slow diffusion of diethyl ether into the solution of **2** in dimethylformamide. Due to the fluxional process in solution, the proton resonance in ^{1}H NMR spectrum can not be clearly ascribed; ^{13}C{^{1}H} NMR spectrum could not be obtained due to the poor solubility and harsh measurement condition: long time (more than 1 days) and low temperature (around -10 °C). **^{31}P{^{1}H} NMR** (243 MHz, $CDCl_3$): δ26.2 (s),

27.3 (s), 28.5 (s), 30.3 (s). HRMS (ESI) m/z $[M\text{-}2Cl]^{2+}$ 845.2498. Element analysis calcd for $C_{86}H_{84}Au_2Cl_2N_4P_4$ (1762.37): C 58.61, H 4.80, N 3.18; found: C 58.37, H 4.99, N 3.18.

Syntheses of complex 3

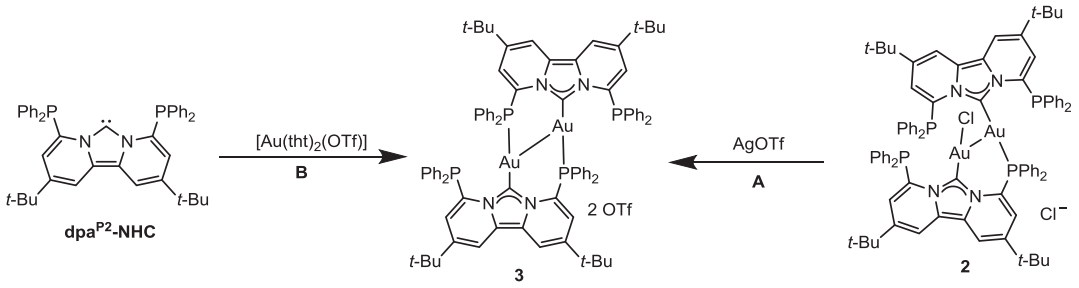

Method **A**: The solution of complex **2** (100.0 mg, 0.057 mmol) and AgOTf (29.3 mg, 0.114 mmol) in CH_2Cl_2 (15 mL) was stirred at room temperature over 1 h in the absence of light. Then the resulting solution was filtered through Celite and the filtrate was concentrated to 2-3 mL under reduced pressure; hexane (15 mL) was added to precipitate complex **3** that was collected as an orange solid by filtration. Yield: 64.3% (73.0 mg, 0.0367 mmol). Method **B**: The solution of free carbene **dpa^{P2}-NHC** (50.0 mg, 0.077 mmol) and $[Au(tht)_2(OTf)]$ (40.2 mg, 0.077 mmol) in THF (10 mL) was stirred at room temperature for 2 h and then concentrated to 2-3 mL under reduced pressure; hexane (15 mL) was added to precipitate complex **3** that was collected as an orange solid by filtration. Yield: 82.6% (63.3 mg, 0.0318 mmol). Suitable crystals for X-ray analysis were obtained by slow diffusion of diethyl ether into the solution of **3** in dimethylformamide. **^{1}H NMR** (400 MHz, DMSO-d_6): δ 1.04 (s, 18H, CH_3), 1.20 (s, 18H, CH_3), 6.76 (br s, 8H, CH_{Ph}), 6.88 (s, 4H, H_b), 7.10-7.70 (m, 32H, CH_{Ph}), 8.82 (s, 2H, H_a), 8.97 (s, 2H, H_a). **^{31}P{^{1}H} NMR** (162 MHz, DMSO-d_6): δ 29.7 (virtual triplet, J_{PP} = 31.5 Hz), 6.8 (virtual triplet, J_{PP} = 30.7 Hz). **^{13}C{^{1}H} NMR** (100 MHz, DMSO-d_6): δ 29.7 (*C*H$_3$), 29.8 (*C*H$_3$), 34.7 (*C*(CH$_3$)), 34.9 (*C*(CH$_3$)), 114.8 (*C*1), 118.1 (*C*9), 119.6 (q, $^1J_{CF}$ = 345.1 Hz, *C*F$_3$), 125.5 (*C*4), 126.2 (*C*6), 126.9 (*C*3), 128.8 (d, $^1J_{PC}$ = 7 Hz, *i'*-*C*$_{Ph}$), 129.2 (*m'*-*C*$_{Ph}$), 129.6 (br, *p'*-/*m*-*C*$_{Ph}$), 130.2 (*C*7), 130.8 (*p*-*C*$_{Ph}$),131.8 (d, $^1J_{PC}$ = 7 Hz, *i*-*C*$_{Ph}$), 132.7 (*o*-/*o'*-*C*$_{Ph}$), 135.4 (*C*10/*C*11), 142.5 (*C*2), 145.0 (*C*8), the carbene carbon could not be detected. HRMS (ESI) m/z $[M\text{-}2O_3SCF_3]^{2+}$ 845.2486. Element analysis calcd for $C_{88}H_{84}Au_2F_6N_4O_6P_4S_2$ (1989.60): C 53.12, H 4.26, N 2.82; found: C 54.24, H 4.12, N 2.87.

Syntheses of complex 4

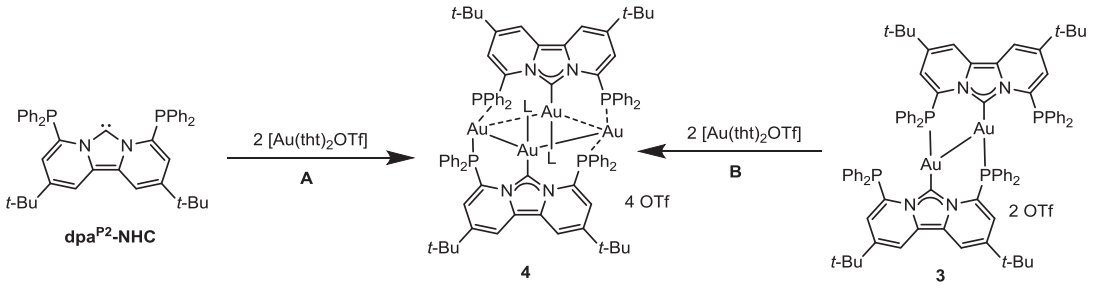

Method **A**: The solution of free carbene **dpa^{P2}-NHC** (25.0 mg, 0.0385 mmol) and [Au(tht)$_2$(OTf)] (40.2 mg, 0.077 mmol) in THF (10 mL) was stirred at room temperature for 2 h and concentrated to 2-3 mL under reduced pressure; hexane (15 mL) was added to precipitate complex **4** that was collected as an orange solid by filtration. Yield: 71.3% (36.7 mg, 0.0137 mmol). Method **B**: The solution of complex **3** (25.0 mg, 0.0126 mmol) and [Au(tht)$_2$(OTf)] (13.1 mg, 0.0252 mmol) in THF (15 mL) was stirred at room temperature for 3 h and concentrated to 2-3 mL under reduced pressure; hexane (15 mL) was added to precipitate complex **4** that was collected as an orange solid by filtration. Yield: 51.3% (16.1 mg, 0.006 mmol). Suitable crystals for X-ray analysis were obtained by slow diffusion of diethyl ether into the solution of **4** in dimethylformamide. **^{1}H NMR** (400 MHz, DMSO-d_6): δ 1.12 (s, 36H, CH_3), 6.65 (s, 4H, H_b), 6.91-8.21(m, 40H, CH_{Ph}), 9.06 (d, $^3J_{PH}$ = 22.0 Hz, 4H, H_a). **^{31}P{^{1}H} NMR** (162 MHz, DMSO-d_6): δ 36.3 (s). **^{13}C{^{1}H} NMR** (100 MHz, DMSO-d_6): δ 29.7 (*C*H$_3$), 34.7(*C*(CH$_3$)), 118.2 (*C*1/*C*9), 119.1 (*C*4/*C*6), 122.4 (*C*10/*C*11), 125.9 (*C*3/*C*7), 129.5 (*i*-*C*$_{Ph}$), 130.2 (*m*-*C*$_{Ph}$), 132.0 (*p*-*C*$_{Ph}$), 133.2 (*o*-*C*$_{Ph}$), 143.4 (*C*2/*C*8), the carbene carbon and carbons of triflates could not be detected. HRMS (ESI) m/z [M-4O$_3$SCF$_3$]$^{4+}$ 521.1086. Element analysis calcd for $C_{88}H_{84}Au_2F_6N_4O_6P_4S_2$ (2681.66): C 40.31, H 3.16, N 2.09; found: C 39.87, H 3.32, N 1.77.

Syntheses of Ag_2L_2

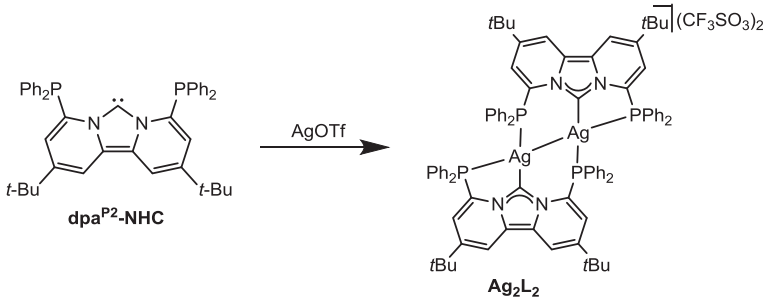

The solution of **dpa^{P2}-NHC** (50.0 mg, 0.077 mmol) and AgOTf (19.8 mg, 0.077 mmol) in THF (10 mL) was stirred at room temperature in the absence of light for 2 h and then concentrated to 2-3 mL; hexane (15 mL) was added to precipitate **Ag_2L_2** that was collected as a yellow solid by filtration. Yield: 78.9% (55.0 mg, 0.030 mmol). X-ray quality crystals were obtained by slow diffusion of diethyl

ether into the DMF solution of **Ag_2L_2**. Anal. Calcd. for $C_{88}H_{84}Ag_2F_6N_4O_6P_4S_2$: C 58.35, H 4.67, N 3.09. Found: C 58.29, H 4.71, N 3.15. **^{1}H NMR** (600 MHz, DMSO-d_6, 293K): δ 8.71 (s, 4H, H_a), 7.40-7.50, (m, 8H, *p*-CH_{Ph}), 7.20-7.35 (m, 16H, *m*-CH_{Ph}), 7.02 (br s, 16H, *o*-CH_{Ph}), 1.13 (s, 36H, C(CH_3)$_3$); **^{1}H NMR** (600 MHz, THF-d_8, 188 K): δ 8.87 (s, 2H, H_a), 8.74 (s, 2H, H_a), 8.15-6.88 (m, 40H, CH_{Ph}), 6.68 (s, 4H, H_b), 1.25 (s, 18H, C(CH_3)$_3$), 1.07 (s, 18H, C(CH_3)$_3$). **^{31}P{^{1}H} NMR** (243 MHz, DMSO-d_6, 293 K): δ -10.0 (br m); **^{31}P{^{1}H} NMR** (243 MHz, THF-d_8, 188 K): δ –16.76 (m), -5.11 (br d, $^1J_{p\text{-}^{107/109}Ag} \approx$ 527Hz). **^{13}C{^{1}H} NMR** (150 MHz, DMSO-d_6): δ 142.6 (*C*2/*C*8), 133.1 (*o*-C_{Ph}), 131.2 (*p*-C_{Ph}), 129.8 (*C*10/*C*11), 129.3 (*m*-C_{Ph}), 129.1 (*i*-C_{Ph}), 127.0 (*C*3/*C*7), 125.2 (*C*4/*C*6), 121.8 (q, $^1J_{CF}$ = 214 Hz, *C*F$_3$), 116.0 (*C*1/*C*9), 34.7 (*C*(CH$_3$)$_3$), 29.8 (*C*H$_3$), the carbene carbon *C*5 can not be detected.

Syntheses of Cu_4LBr_4

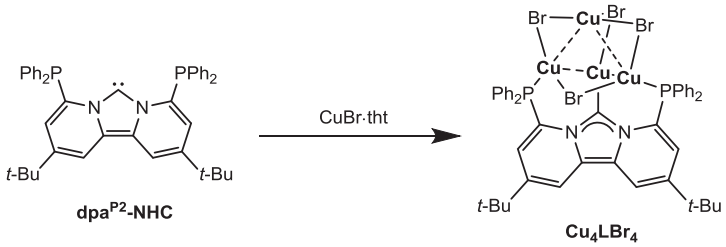

The solution of **dpa^{P2}-NHC** (20 mg, 0.031 mmol) and CuBr·tht (17.8 mg, 0.077 mmol) in THF (4 mL) was vigorously stirred at ambient temperature. After 3 h, hexane (15 mL) was added to precipitate the desired product **Cu_4LBr_4** as a bright yellow solid, which was collected by filtration. Yield: 72.3% (17 mg, 0.014 mmol) (yield was calculated based on CuBr·tht). X-ray quality crystals were obtained by slow diffusion of diethyl ether into the DMF solution of **Cu_4LBr_4**. Anal. Calcd. for $C_{43}H_{42}Br_4Cu_4N_2P_2$: C 42.24, H 3.46, N 2.29; found: C 42.68, H 3.09, N 2.56. **^{1}H NMR** (400 MHz, DMSO-d_6) δ 8.55 (s, 2H, H_a), 6.98-7.78 (br m, 20H, CH_{Ph}), 6.66 (s, 2H, H_b), 1.15 (s, 18H, C(CH_3)$_3$). **^{31}P{^{1}H} NMR** (162 MHz, DMSO-d_6) δ -19.7 (s). **^{13}C{^{1}H} NMR** (100 MHz, DMSO-d_6) δ142.5 (*C*2/*C*8), 133.8 (d, $^2J_{PC}$ = 16 Hz, *o*-C_{Ph}), 132.2 (*i*-C_{Ph}), 131.1 (*p*-C_{Ph}), 129.3 (d, $^3J_{PC}$ = 8 Hz, *m*-C_{Ph}), 125.8 (*C*3/*C*7), 123.6 (*C*4/*C*6), 115.1 (*C*1/*C*9), 34.7 (*C*(CH$_3$)$_3$), 29.9 (C(*C*H$_3$)$_3$), the carbene carbon *C*5 and *C*10/*C*11 can not be detected.

Syntheses of Cu_2L_2

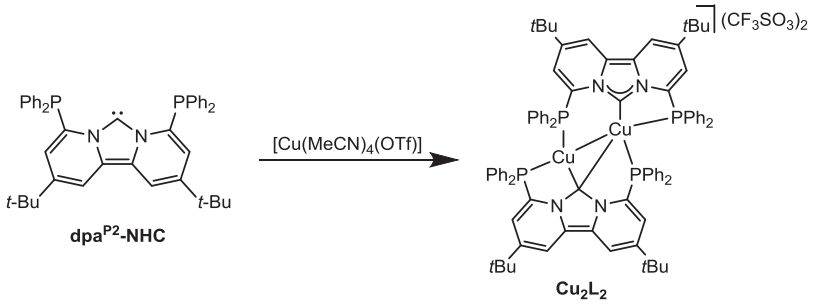

The solution of **dpa^{P2}-NHC** (50.0 mg, 0.077 mmol) and [Cu(MeCN)$_4$(OTf)] (29.0 mg, 0.077 mmol) in THF (10 mL) was stirred at room temperature in the absence of light. Two hours later, reaction solution was concentrated to 2-3 mL; hexane (15 mL) was added to precipitate **Cu_2L_2** that was collected as a brown solid by filtration. Yield: 71.5% (47.4 mg, 0.027 mmol). X-ray quality crystals were obtained by slow diffusion of diethyl ether into the DMF solution of **Cu_2L_2**. Anal. Calcd. for $C_{88}H_{86}Cu_2F_6N_4O_7P_4S_2$: C 60.72, H 4.98, N 3.22. Found: C 60.28, H 5.18, N 3.18. **^{1}H NMR** (600 MHz, DMSO-d_6): δ 8.50 (s, 4H, H_a), 7.38-7.28 (m, 8H, *p*-CH_{Ph}), 7.20-7.10 (m, 16H, *m*-CH_{Ph}), 6.99 (s, 4H, H_b), 6.88 (br s, 16H, *o*-CH_{Ph}), 1.20 (s, 36H, C(CH_3)$_3$). **^{31}P{^{1}H} NMR** (243 MHz, DMSO-d_6): δ -13.6. **^{13}C{^{1}H} NMR** (150 MHz, DMSO-d_6): δ 153.5 (*C*$_5$), 143.1 (*C*2/*C*8), 132.9 (*C*10/*C*11), 131.9 (*o*-*C*$_{Ph}$), 130.4 (*p*-*C*$_{Ph}$), 129.7 (*i*-*C*$_{Ph}$), 128.9 (*m*-*C*$_{Ph}$), 127.1 (*C*3/*C*7), 125.5 (*C*4/*C*6), 121.7 (q, $^1J_{CF}$ = 214.0 Hz, *C*F$_3$), 116.1 (*C*1/*C*9), 34.8 (*C*(CH$_3$)$_3$), 29.9 (*C*H$_3$).

Syntheses of $Ag_2Cu_2L_2$

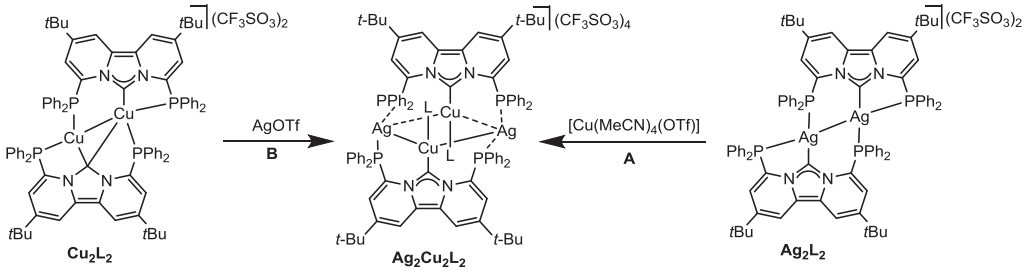

Method **A**: To the solution of **Ag_2L_2** (40.0 mg, 0.022 mmol) in CH_2Cl_2 (10 mL) was added [Cu(MeCN)$_4$(OTf)] (17.0 mg, 0.045 mmol) at room temperature and the resulting mixture was stirred for 2 h in the absence of light. After removal of the volatiles under reduced pressure, THF (3 mL) was added to dissolve the residual; desired product **$Ag_2Cu_2L_2$** was precipitated by the addition of hexane (did not undergo drying procedure) and collected as an orange solid by filtration. Yield: 63.9% (29.8 mg, 0.014 mmol); Method **B**: The solution of **Cu_2L_2** (24 mg, 0.015 mmol) and AgOTf (7.7 mg, 0.03 mmol) in THF (5 mL) was stirred at room temperature. Two hours later, hexane (15 mL) was added

to precipitate the desired product **$Ag_2Cu_2L_2$** as a yellow solid collected by filtration. Yield: 46.7% (15 mg, 0.007 mmol). X-ray quality crystals were obtained by slow diffusion of diethyl ether into the DMF solution of **$Ag_2Cu_2L_2$**. Anal. Calcd. for $C_{88}H_{84}Ag_2OCu_2F_6N_4O_7P_4S_2$[**$Ag_2Cu_2L_2$(O)**]: C 54.08, H 4.33, N 2.87. Found: C 54.54, H 4.55, N 3.13. **^{1}H NMR** (600 MHz, DMSO-d_6): δ 8.50 (s, 4H, H_a), 7.38-7.28 (m, 8H, *p*-CH_{Ph}), 7.20-7.08 (m, 16H, *m*-CH_{Ph}), 7.00 (s, 4H, H_b), 6.88 (br s, 16H, *o*-CH_{Ph}), 1.20 (s, 36H, C(CH_3)$_3$). **^{31}P{^{1}H} NMR** (243 MHz, DMSO-d_6): δ -4.24 (br d, $J_{P\text{-}107Ag/109Ag}$ ≈ 273.8 Hz). **^{13}C{^{1}H} NMR** (150 MHz, DMSO-d_6): δ 143.0 (*C*2/*C*8), 131.8 (*o*-C_{Ph}), 130.3 (*p*-C_{Ph}), 129.6 (*C*10/*C*11), 128.8 (*m*-C_{Ph}), 128.5 (*i*-C_{Ph}), 127.1 (*C*3/*C*7), 125.4 (*C*4/*C*6), 121.6 (q, $^1J_{CF}$ = 213.0 Hz, *C*F$_3$), 116.0 (*C*1/*C*9), 34.7 (*C*(CH$_3$)$_3$), 29.8 (*C*H$_3$), the carbene carbon *C*5 can not be detected.

Syntheses of Cu_4L_2·2CH_3CN

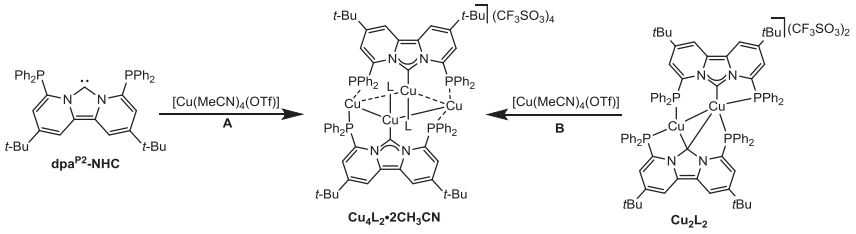

Method **A**: The solution of **dpa^{P2}-NHC** (20.0 mg, 0.031 mmol) and [Cu(MeCN)$_4$(OTf)] (22.7 mg, 0.062 mmol) in CH_2Cl_2 (10 mL) was stirred at room temperature in the absence of light for 2 h. After the removal of volatiles, desired product **Cu_4L_2·2CH_3CN** was obtained as an orange solid, Yield: 73.2% (23.1 mg, 0.011 mmol); Method **B**: The solution of **Cu_2L_2** (20.0 mg, 0.012 mmol) and [Cu(MeCN)$_4$(OTf)] (9.1 mg, 0.024 mmol) in CH_2Cl_2 (10 mL) was stirred at room temperature in the absence of light for 2 h. After the removal of volatiles, desired product **Cu_4L_2·2CH_3CN** was obtained as an orange solid, Yield: 69.9% (15.9 mg, 0.008 mmol). X-ray quality crystals were obtained by slow diffusion of diethyl ether into the DMF solution of **Cu_4L_2·2CH_3CN**. Anal. Calcd. for $C_{88}H_{84}OCu_4F_6N_4O_7P_4S_2$ [**Cu_4L_2(O)**]: C 56.65, H 4.54, N 3.00. Found: C 56.84, H 4.20, N 2.89. **^{1}H NMR** (600 MHz, CD_3CN): δ 8.09 (d, $^3J_{HP}$ = 1.8 Hz, 4H, H_a), 7.30-7.24 (m, 8H, *p*-CH_{Ph}), 7.08 (s, 4H, H_b), 7.07-7.01 (m, 16H, *m*-CH_{Ph}), 6.85 (br s, 16H, *o*-CH_{Ph}), 1.96 (s, 6H, CH_3CN), 1.22 (s, 36H, C(CH_3)$_3$). **^{31}P{^{1}H} NMR** (243 MHz, CD_3CN): δ -14.4. **^{13}C{^{1}H} NMR** (150 MHz, CD_3CN): δ 144.5 (*C*2/*C*8), 133.3 (*o*-C_{Ph}), 131.4 (*p*-C_{Ph}), 129.7 (*m*-C_{Ph}), 128.6 (*C*3/*C*7), 126.8 (*C*10/*C*11), 125.3 (*C*4/*C*6), 121.1 (q, $^1J_{CF}$ = 212.0 Hz, *C*F$_3$), 116.5 (*C*1/*C*9), 35.7 (*C*(CH$_3$)$_3$), 30.3 (*C*H$_3$), the carbene carbon *C*5 and *i*-C_{Ph} can not be detected.

Syntheses of $Cu_5L_2Br_3$

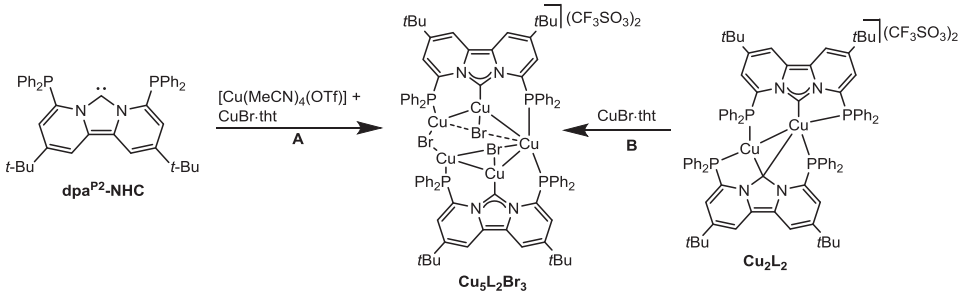

Method **A**: The solution of **dpa^{P2}-NHC** (50 mg, 0.077 mmol) in CH_2Cl_2 (5 mL) was added to a solution of CuBr·tht (23.7 mg, 0.115 mmol) and $[Cu(MeCN)_4(OTf)]$ (29.0 mg, 0.077 mmol) in CH_2Cl_2 (5 mL) and the resulting mixture was stirred for 3 h at room temperature in the absence of light. After removal of the volatiles under reduced pressure, the residue was dissolved with THF (10mL) and hexane (20 mL) was added to precipitate the desired product **$Cu_5L_2Br_3$** as a yellow solid collected by filtration. Yield: 60.3% (49.9 mg, 0.023 mmol); Method **B**: The solution of **Cu_2L_2** (15 mg, 0.0087 mmol) and CuBr·tht (6.1 mg, 0.0261 mmol) in CH_2Cl_2 was stirred at room temperature for 4 h. After removing the volatiles, the residual was dissolved with THF and hexane was added to precipitate the desired product **$Cu_5L_2Br_3$** as a yellow solid collected by filtration. Yield: 52.5% (10 mg, 0.00457 mmol). X-ray quality crystals were obtained by slow diffusion of diethyl ether into the DMF solution of **$Cu_5L_2Br_3$**. Anal. Calcd. for $C_{88}H_{84}Br_3Cu_5F_6N_4O_6P_4S_2$: C 49.09, H 3.93, N 2.60. Found: C 44.81, H 3.84, N 2.46. Element analysis were consistently found to be low in carbon. **^{1}H NMR** (600 MHz, DMSO-d_6): δ 8.68 (s, 4H, H_a), 7.74-6.92 (m, 40H, CH_{Ph}), 6.56 (s, 4H, H_b), 1.14 (s, 36H, C(CH_3)$_3$). **^{31}P{^{1}H} NMR** (243 MHz, DMSO-d_6): δ −16.8 (br s). **^{13}C{^{1}H} NMR** (150 MHz, DMSO-d_6): δ 142.8 (*C*2/*C*8), 133.7 (*o*-C_{Ph}), 131.7 (*p*-C_{Ph}), 129.51 (*m*-C_{Ph}), 129.45 (*i*-C_{Ph}), 126.3 (*C*3/*C*7), 123.7 (*C*10/*C*11), 121.7 (q, $^1J_{CF}$ = 213.0 Hz, *C*F$_3$), 118.1 (*C*4/*C*6), 115.6 (*C*1/*C*9), 34.7 (*C*(CH$_3$)$_3$), 29.8 (*C*H$_3$), the carbene carbon *C*5 can not be detected.

NMR Spectra

NMR Spectra of ***dpa^{P2}-NHC***

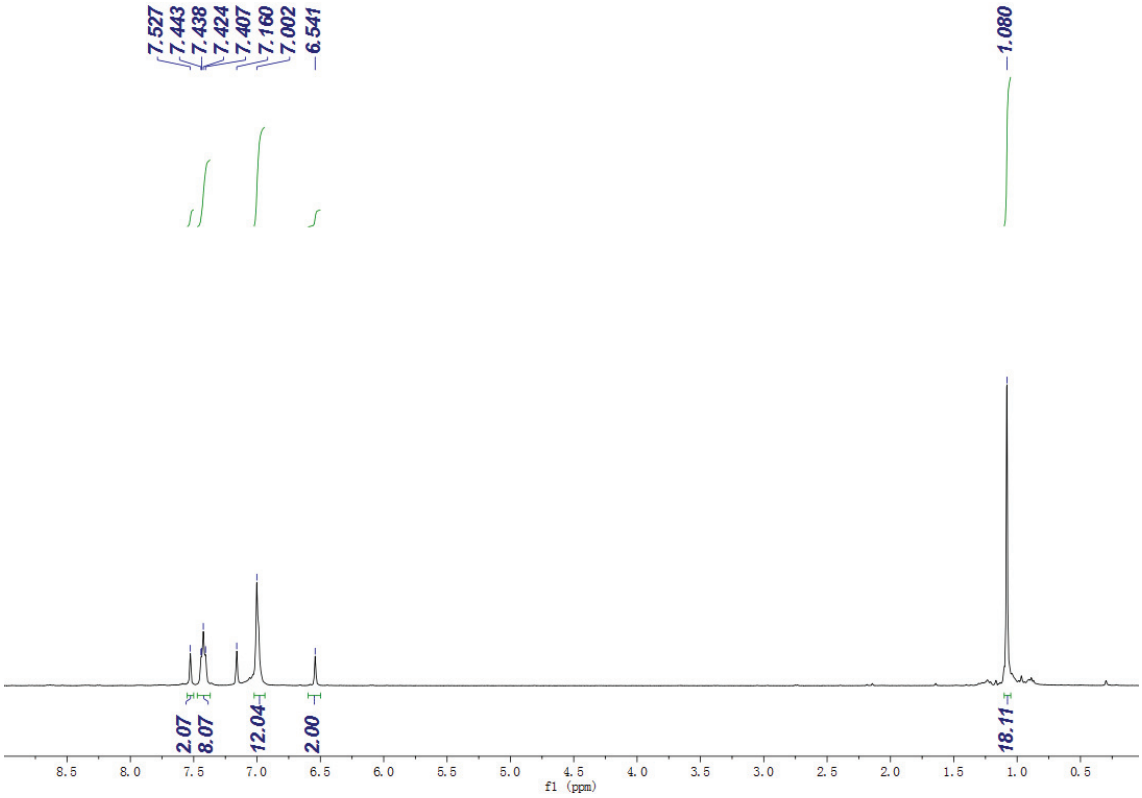

Figure S2. ^{1}H NMR spectrum (600 MHz) of **dpa^{P2}-NHC** in C_6D_6.

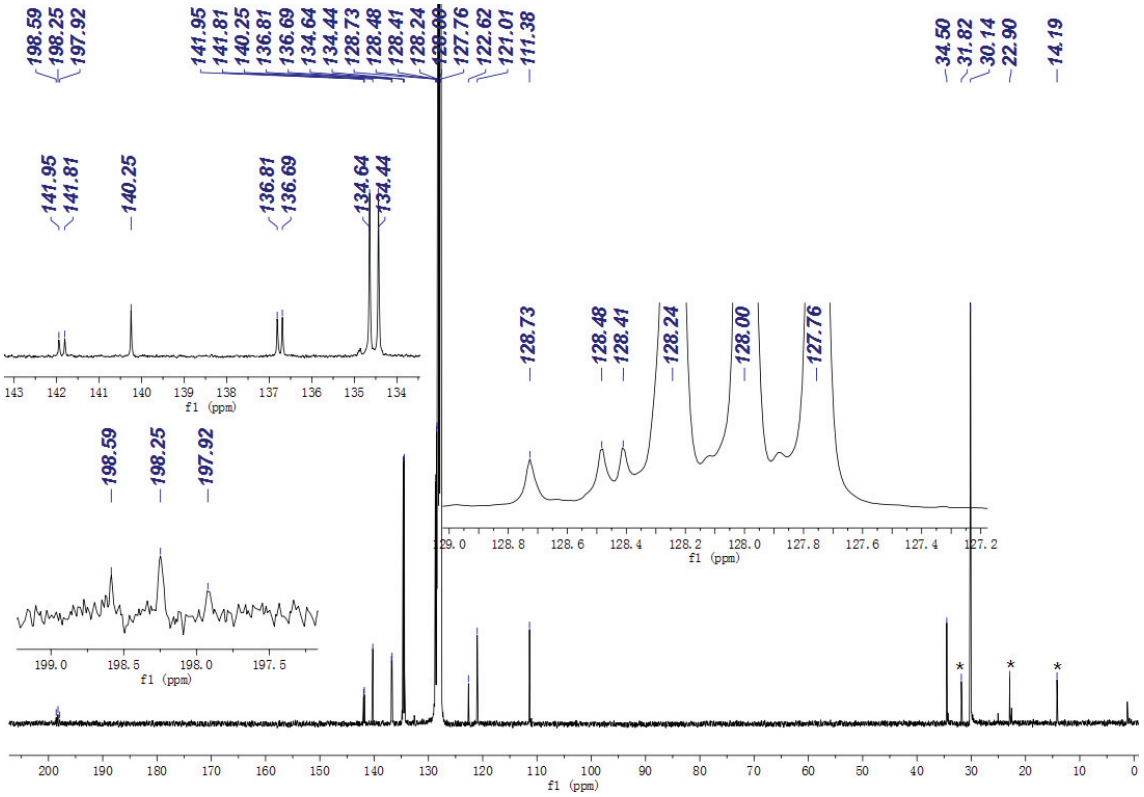

Figure S3. ^{13}C NMR spectrum (150 MHz) of **dpa^{P2}-NHC** in C_6D_6 (* = hexane).

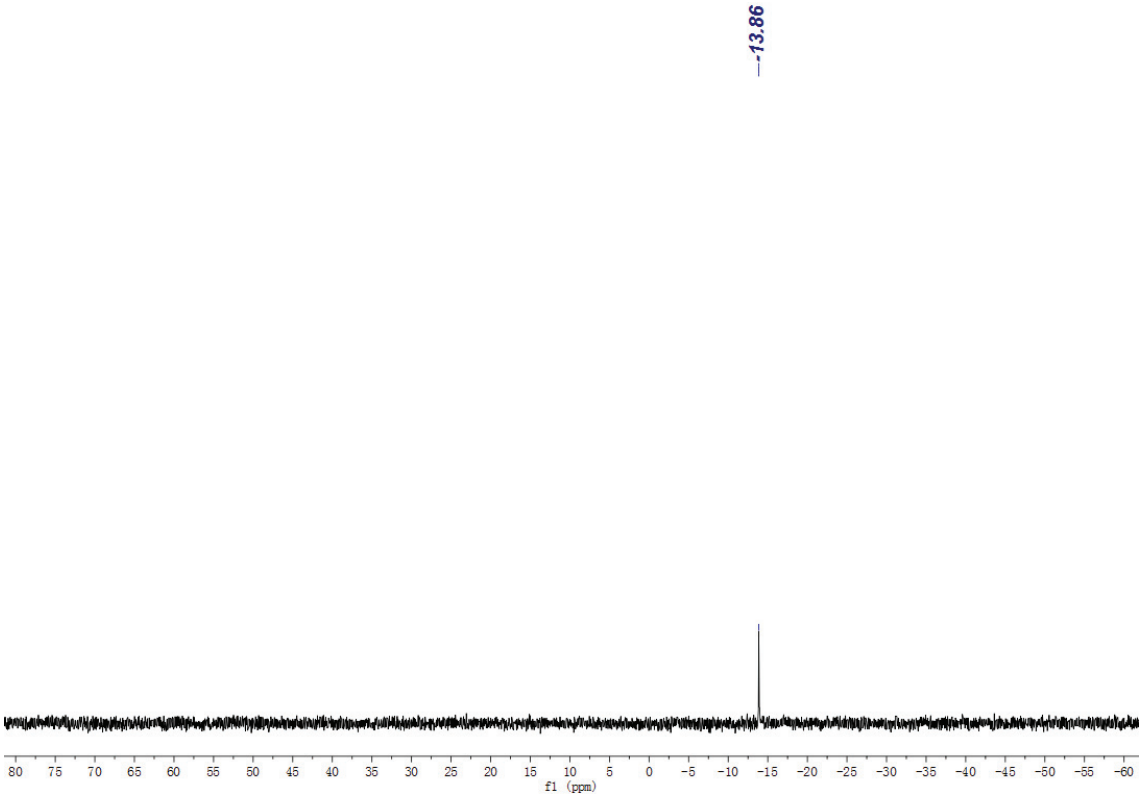

Figure S4. ^{31}P NMR spectrum (243 MHz) of **dpa^{P2}-NHC** in C_6D_6.

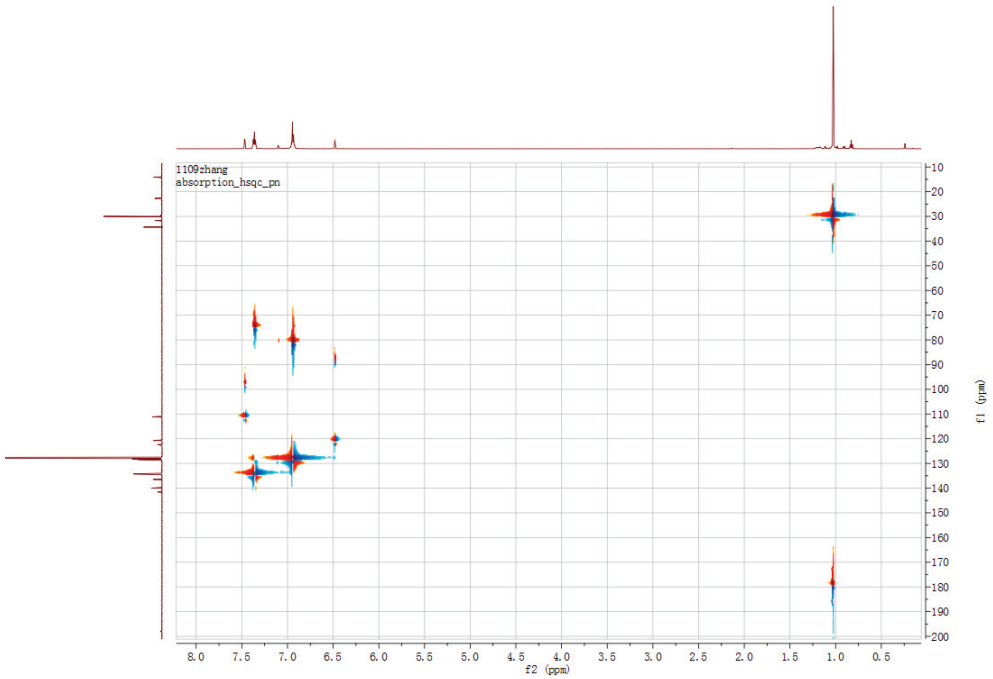

Figure S5. H-C HSQC spectrum of the free carbene **dpa^{P2}-NHC** (C_6D_6)

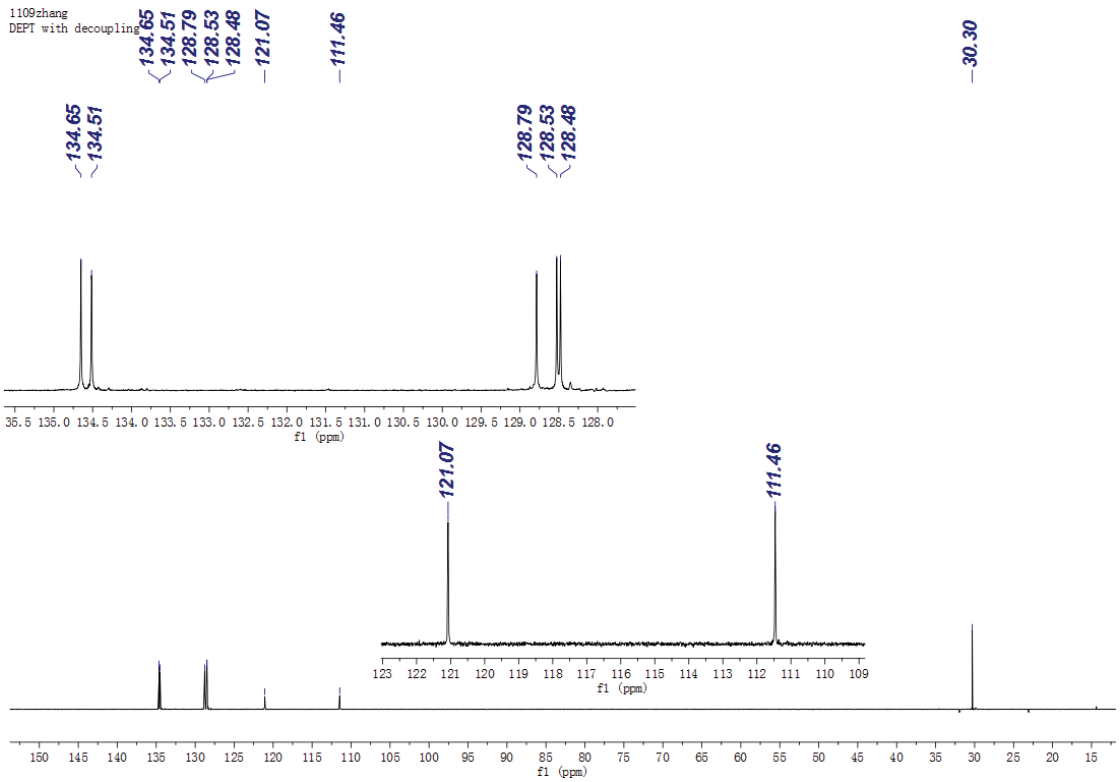

Figure S6. DEPT 135 spectrum of free carbene **dpa^{P2}-NHC**

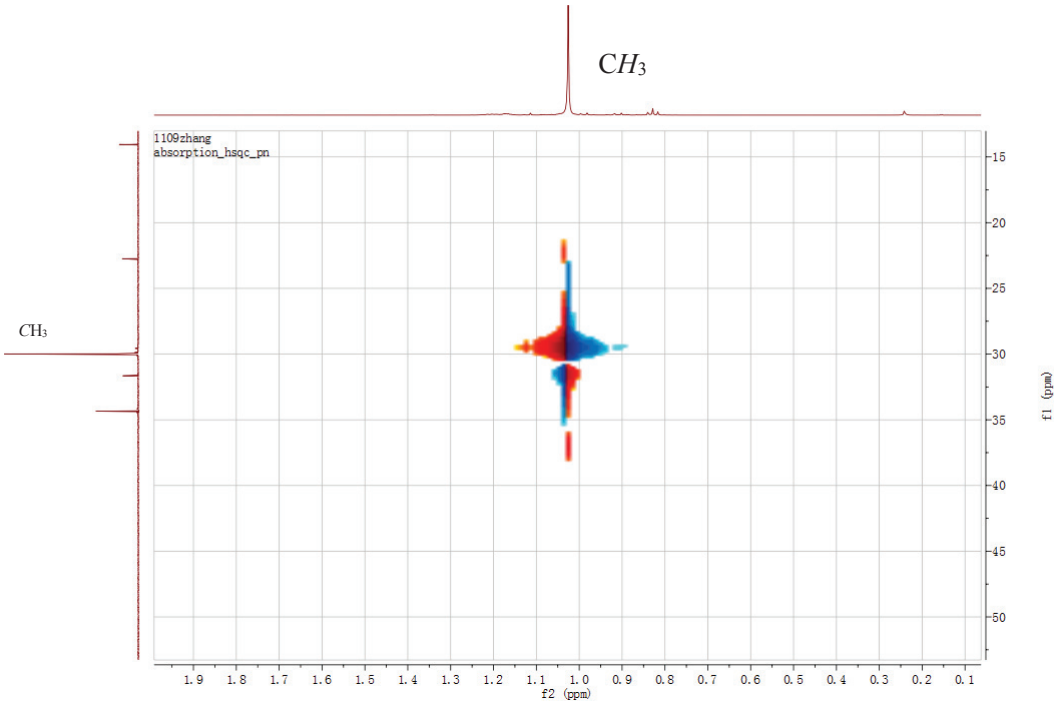

Figure S7. Selected region (part 1) of H-C HSQC spectrum of the free carbene **dpa^{P2}-NHC**

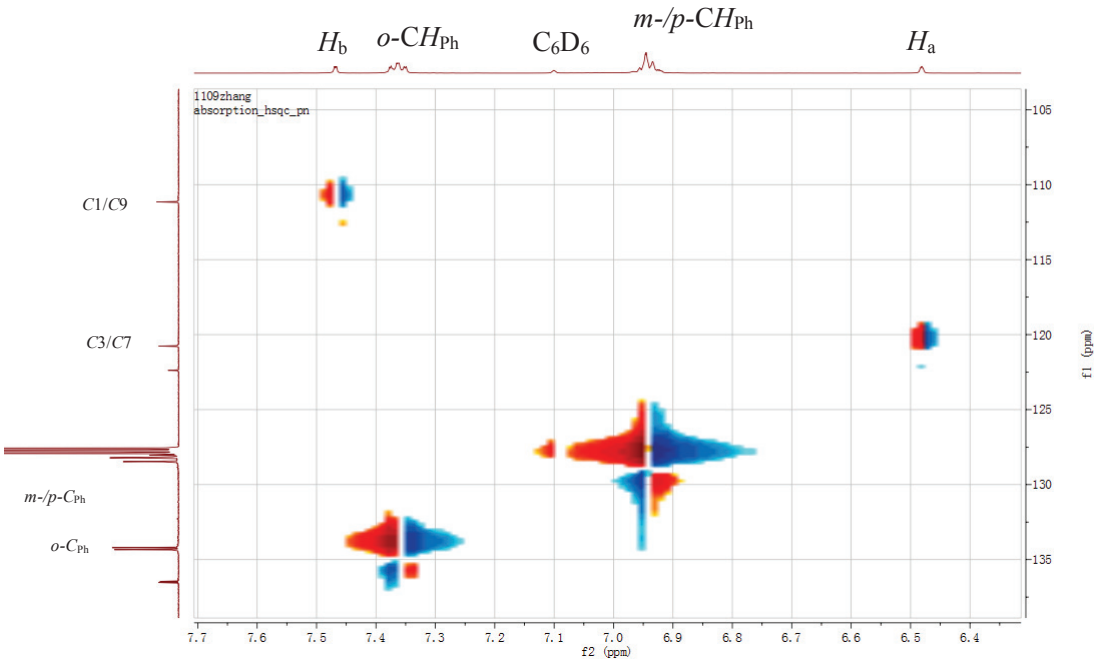

Figure S8. Selected region (part 2) of H-C HSQC spectrum of the free carbene **dpa^{P2}-NHC**

NMR Spectra of ***L(H)PF$_6$***

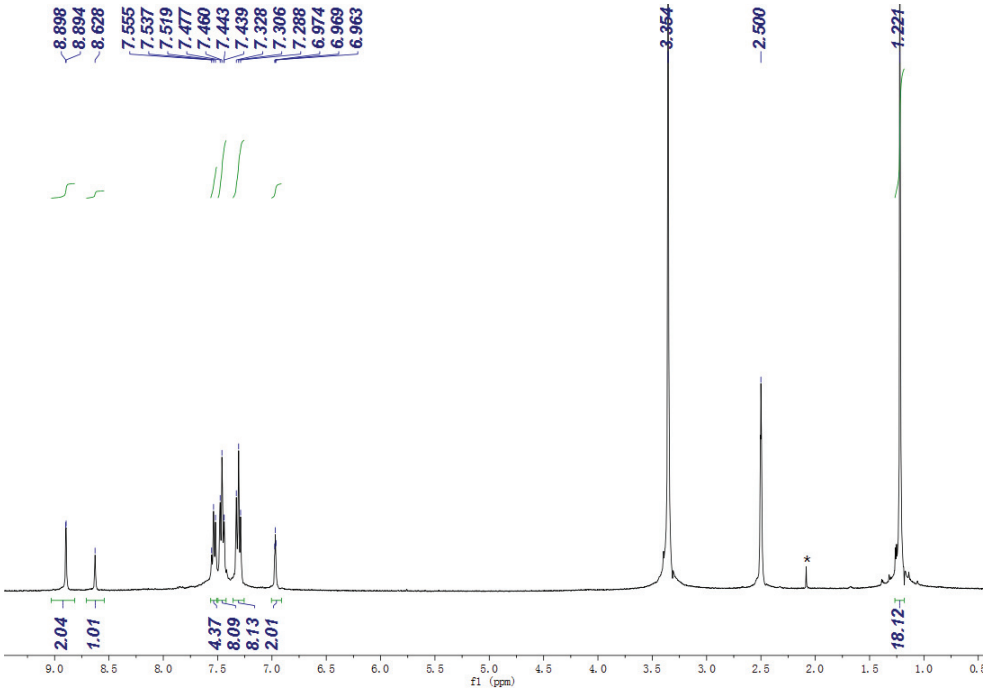

Figure S9. ^{1}H NMR spectrum (400 MHz) of **L(H)PF$_6$** in DMSO-d$_6$ (* = acetone)

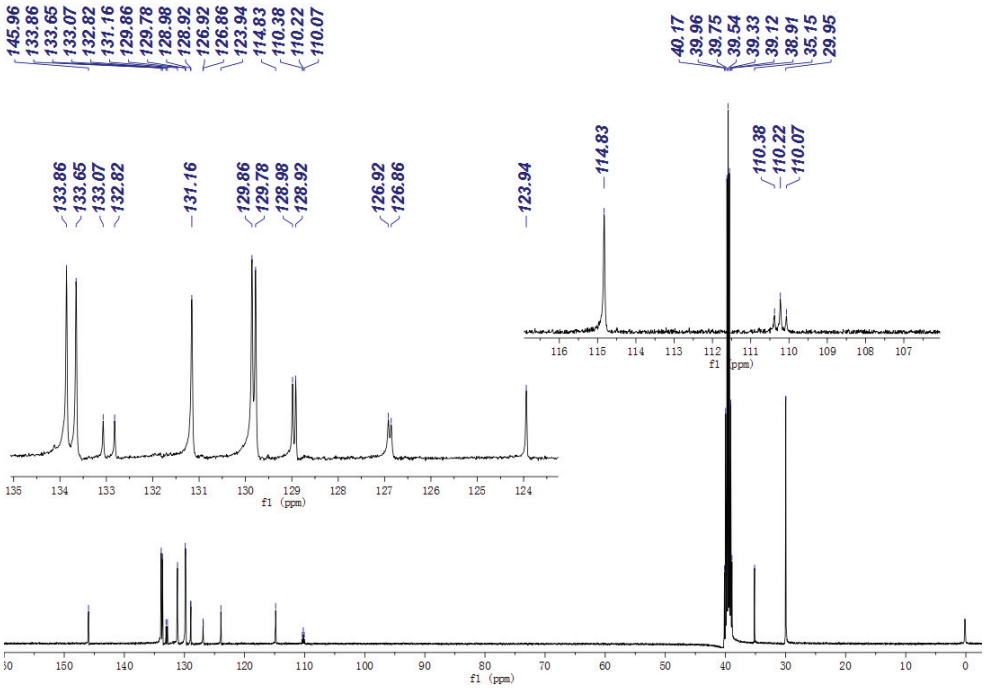

Figure S10. ^{13}C{^{1}H} NMR spectrum (100 MHz) of **L(H)PF$_6$** in DMSO-d$_6$

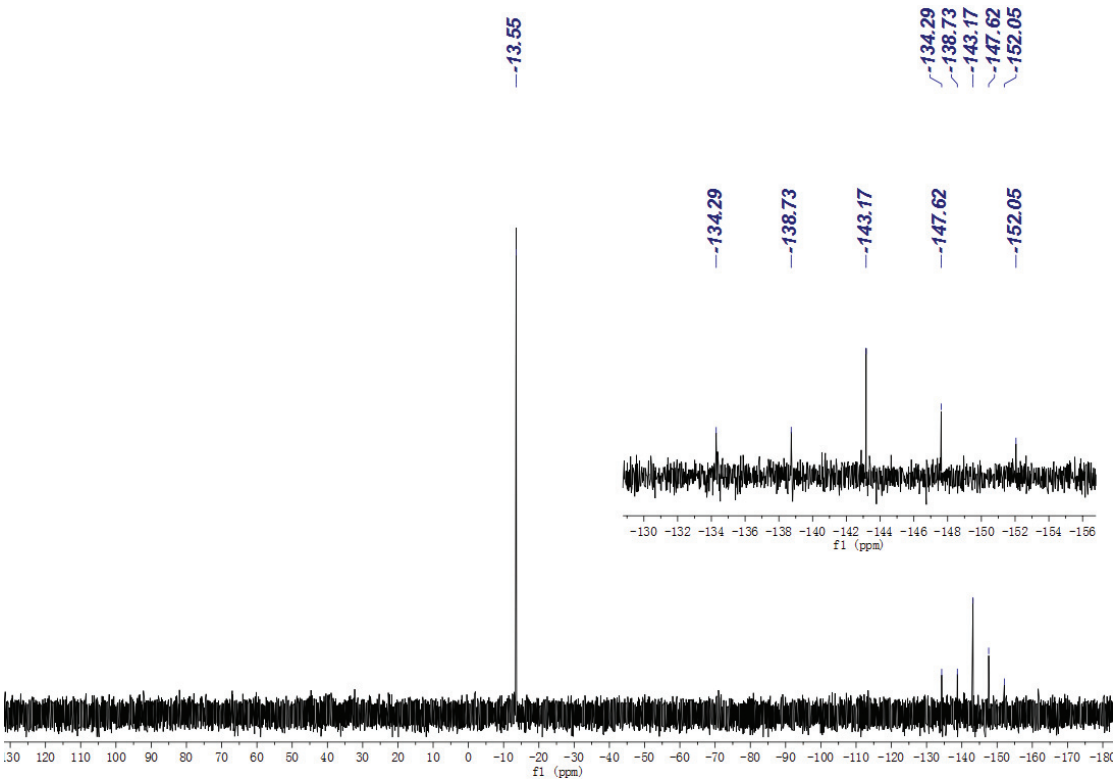

Figure S11. $^{31}P\{^{1}H\}$ NMR spectrum (162 MHz) of **L(H)PF$_6$** in DMSO-d$_6$

*NMR Spectra of complex **1***

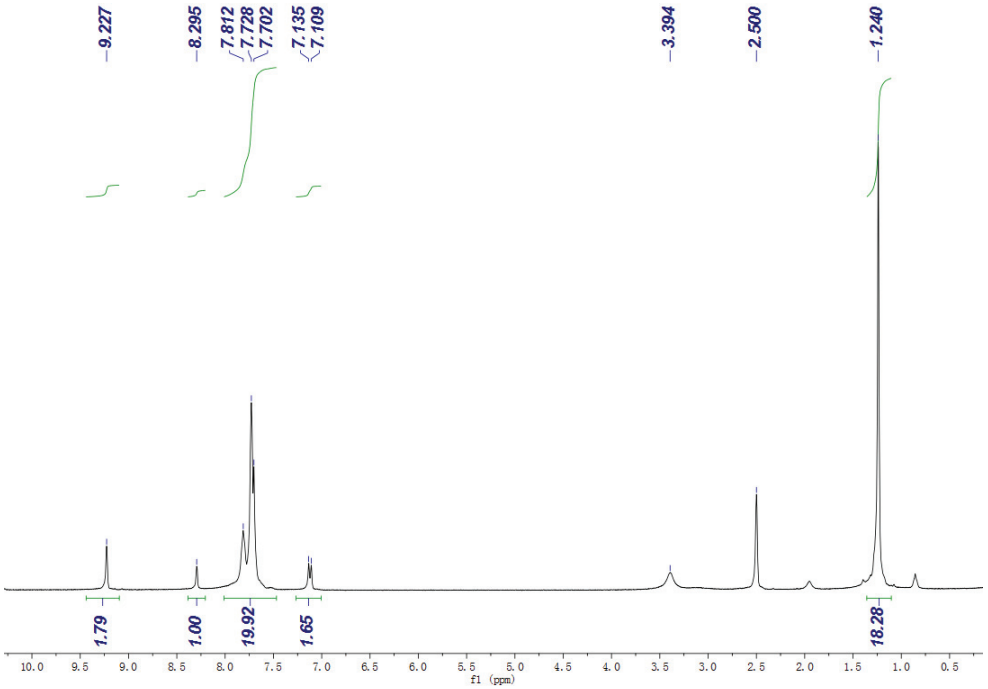

Figure S12. ^{1}H NMR spectrum (400 MHz) of complex **1** in DMSO-d$_6$

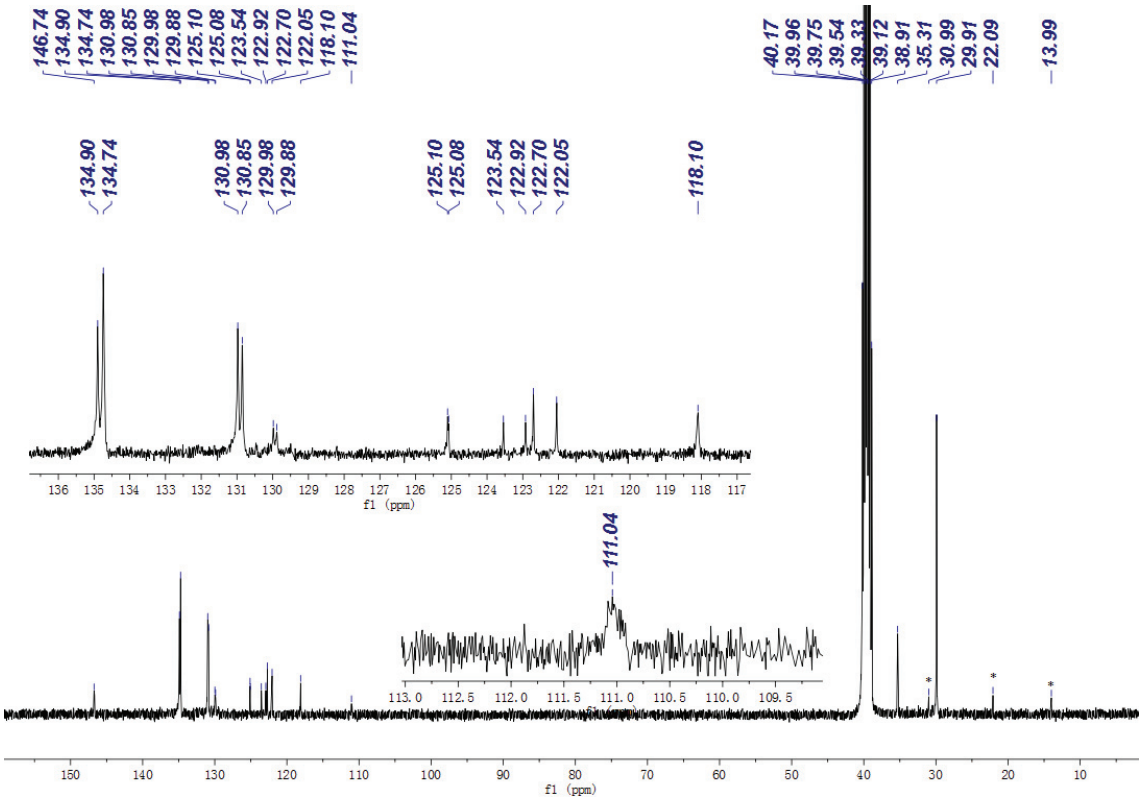

Figure S13. $^{13}C\{^{1}H\}$ NMR spectrum (100 MHz) of complex **1** in DMSO-d_6 (* = hexane)

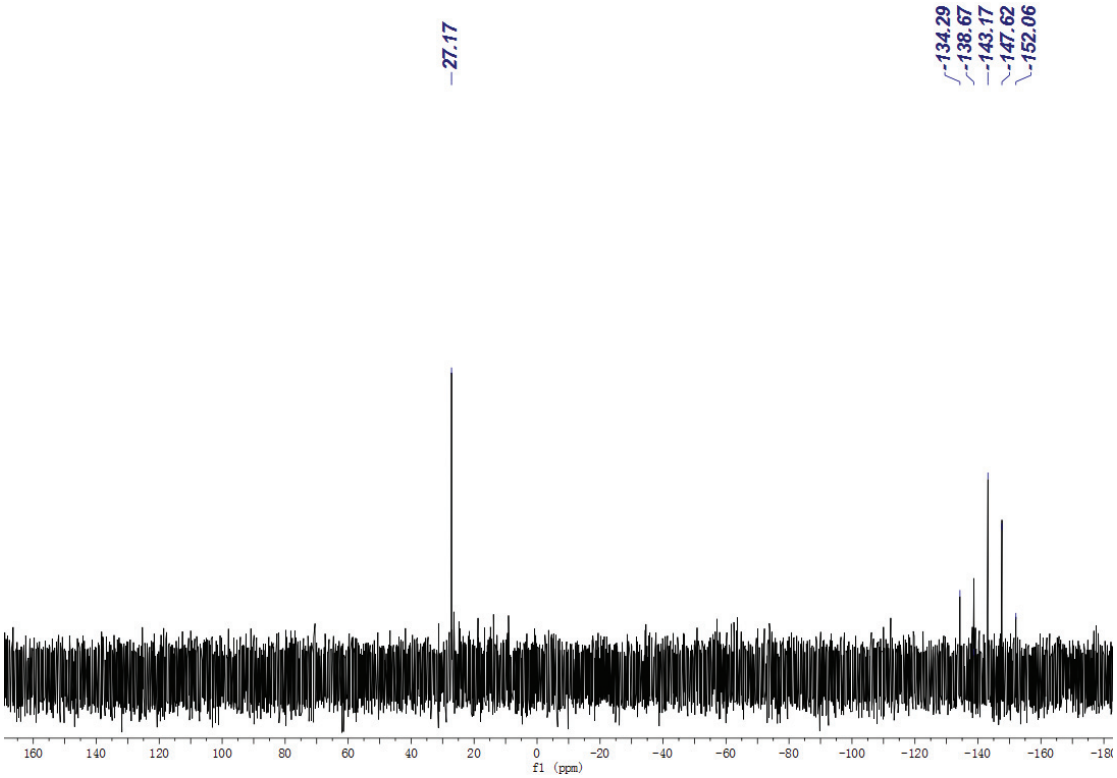

Figure S14. $^{31}P\{^{1}H\}$ NMR spectrum (162 MHz) of complex **1** in DMSO-d_6

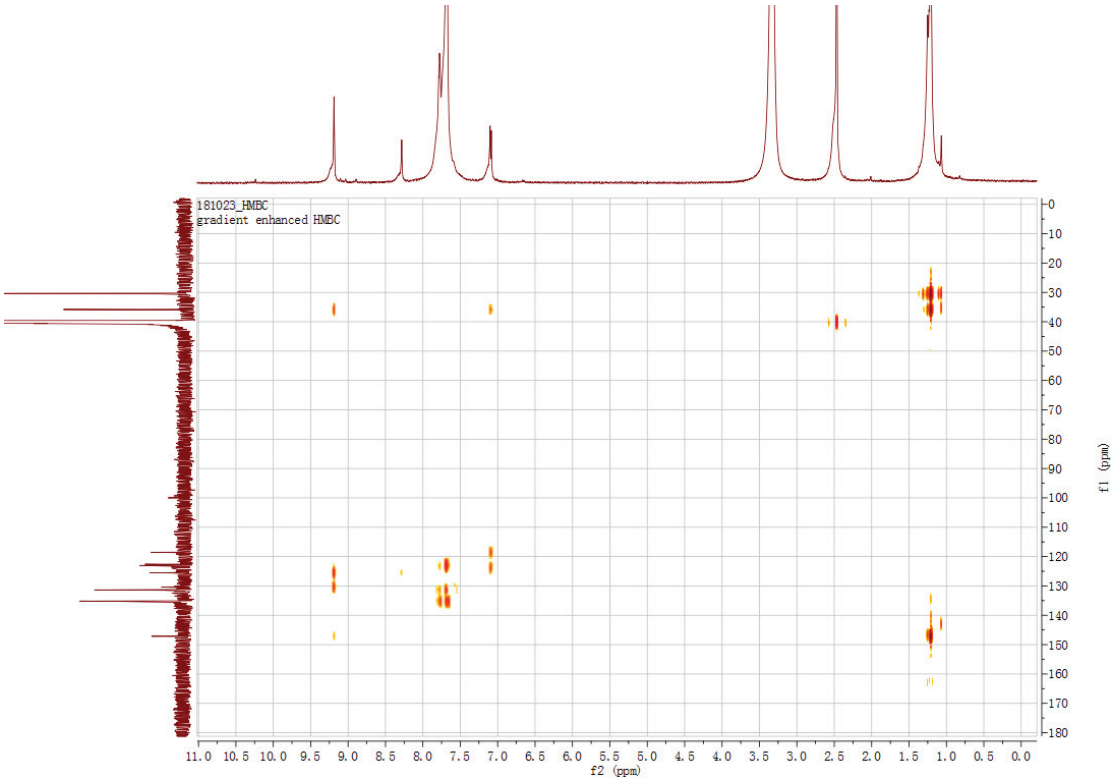

Figure S15. H-C HMBC spectrum of complex **1** in DMSO-d_6

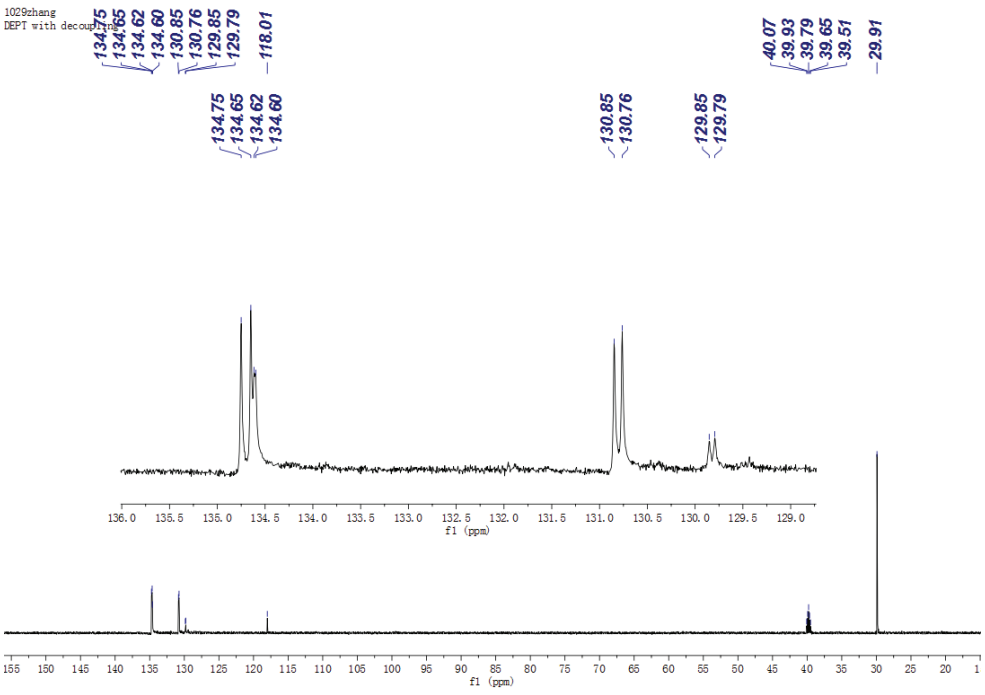

Figure S16. DEPT(135) spectrum of complex **1** in DMSO-d_6

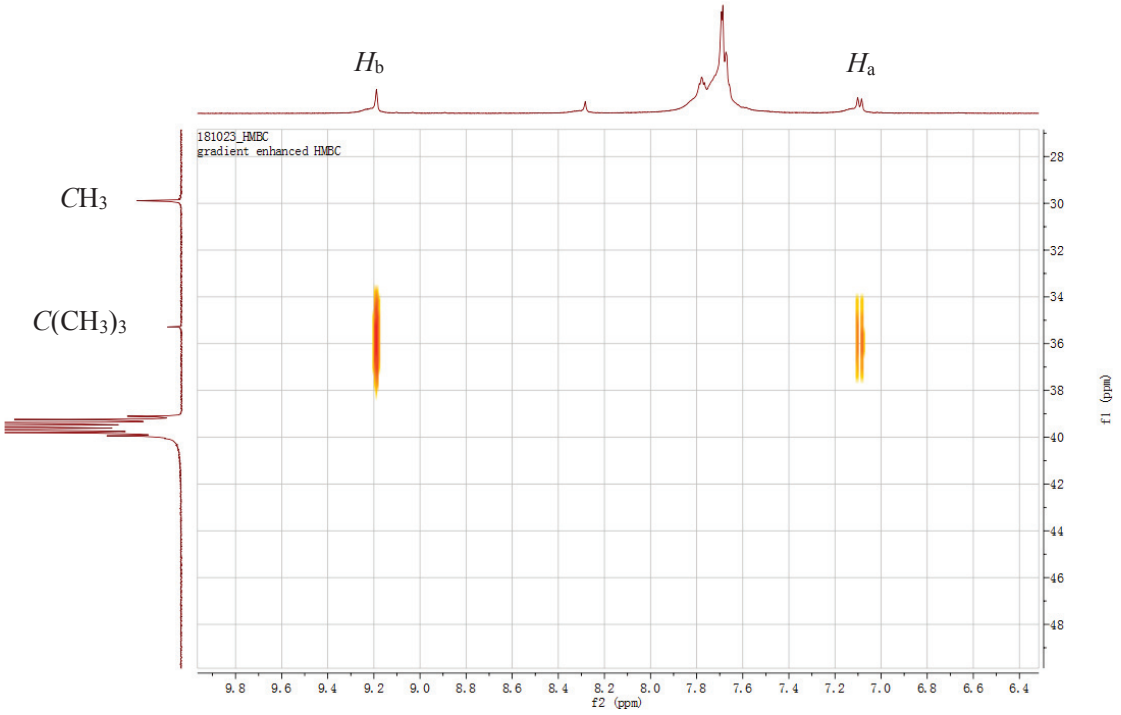

Figure S17. Selected region (**part 1**) of H-C HMBC spectrum of complex **1** in DMSO-d_6

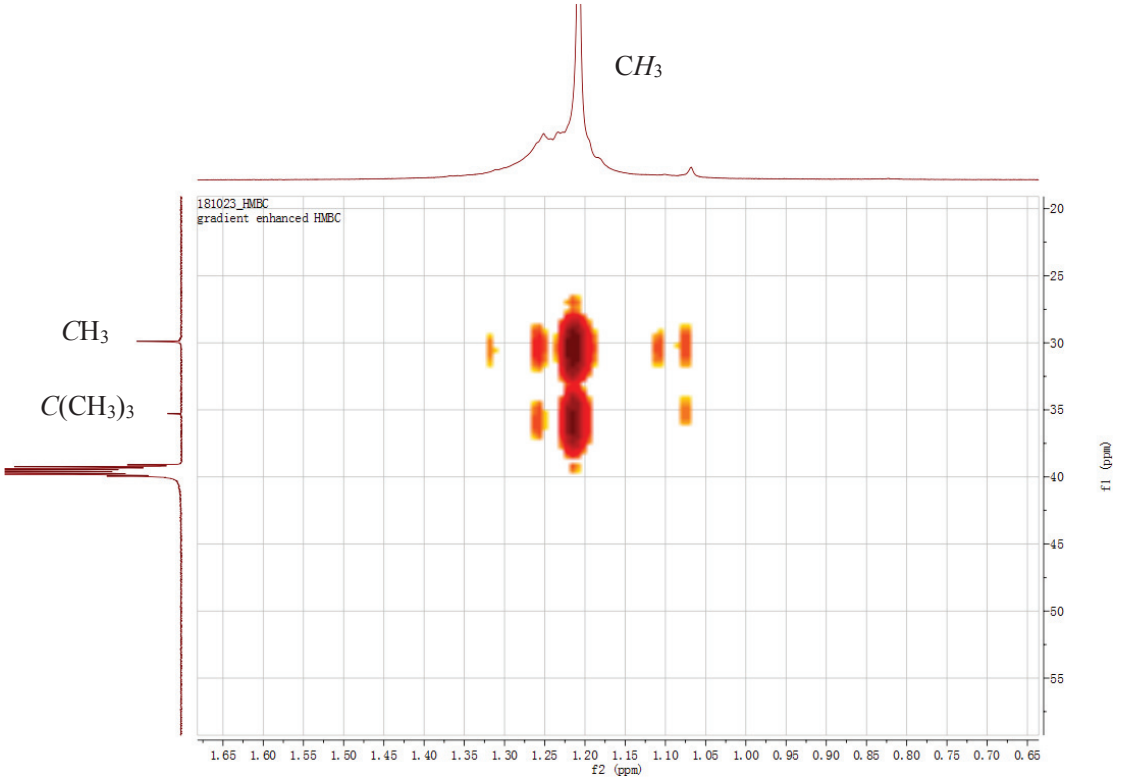

Figure S18. Selected region (**part 2**) of H-C HMBC spectrum of complex **1** in DMSO-d_6

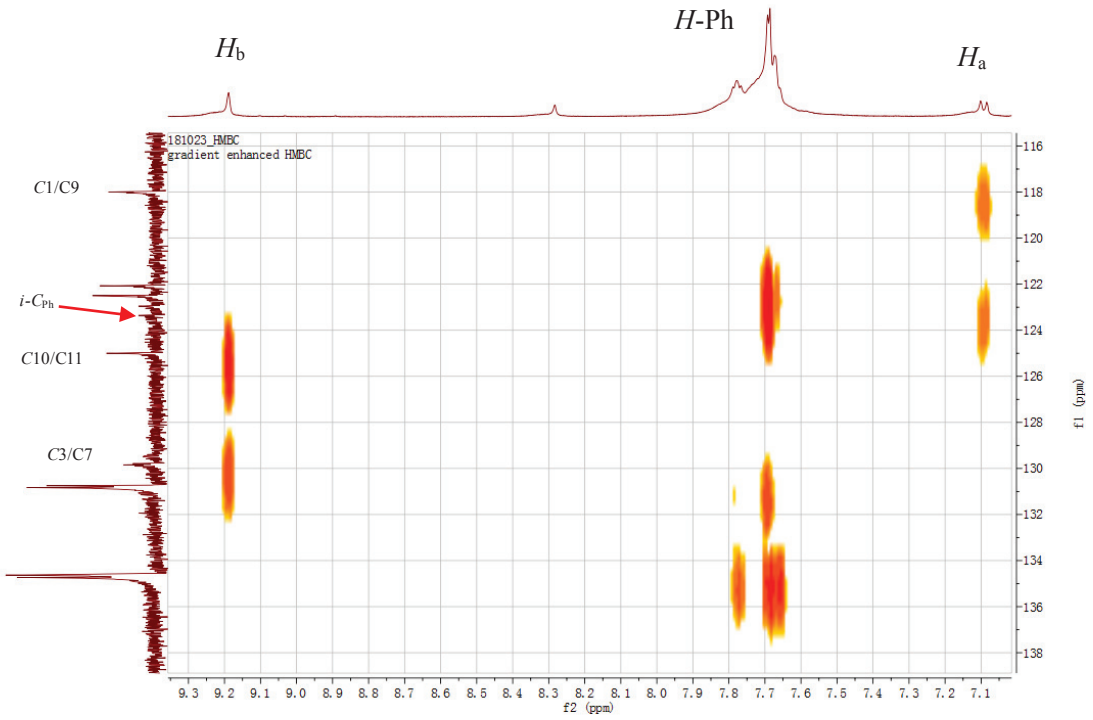

Figure S19. Selected region (**part 3**) of H-C HMBC spectrum of complex **1** in DMSO-d_6

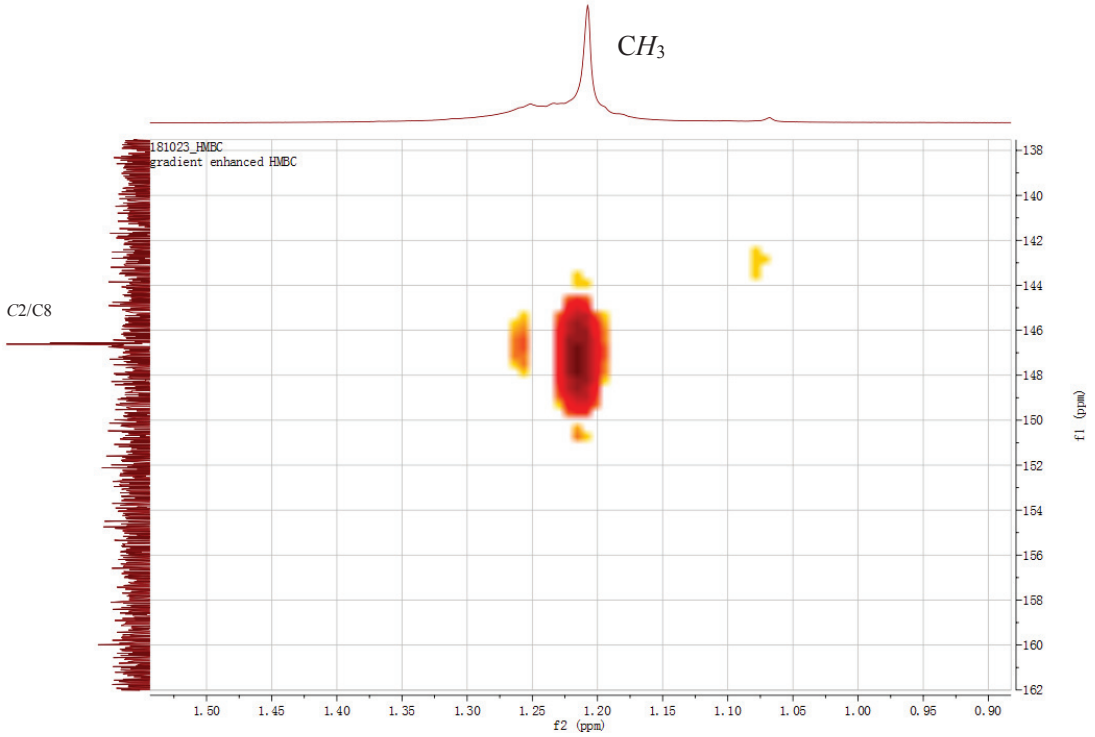

Figure S20. Selected region (**part 4**) of H-C HMBC spectrum of complex **1** in DMSO-d_6

*Variable temperature (VT) NMR spectra of complex **2** in $CDCl_3$*

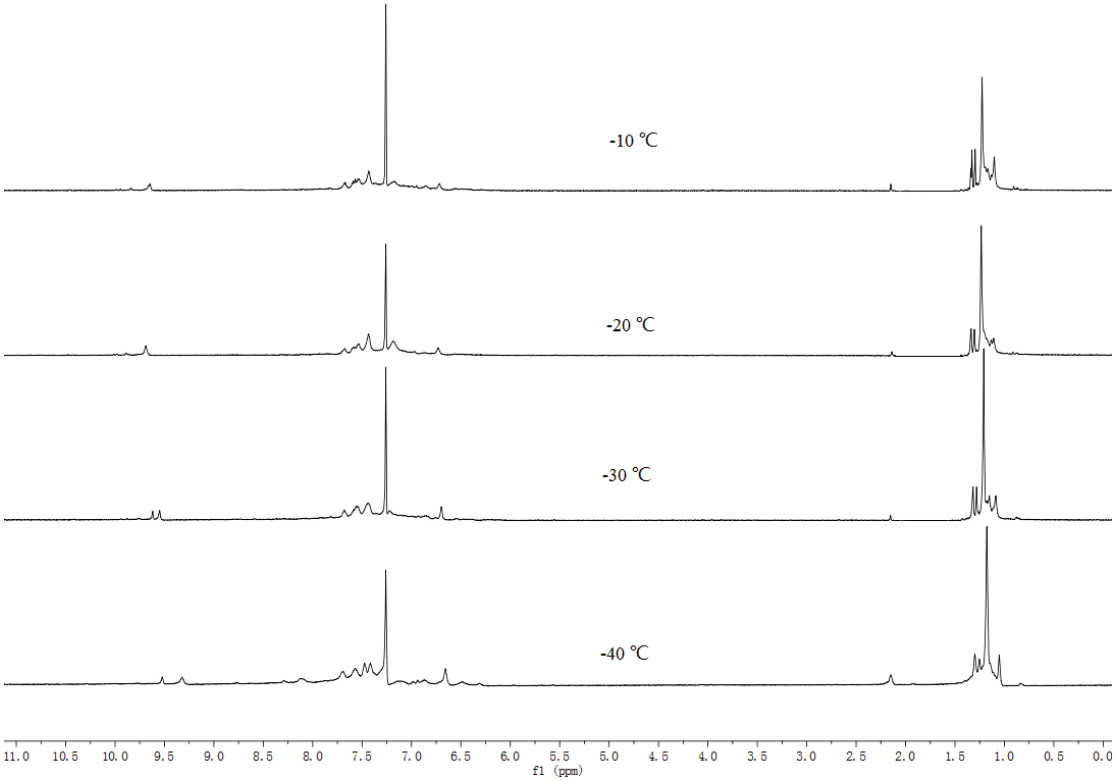

Figure S21. VT ^{1}H NMR spectra (600 MHz) of complex **2** in $CDCl_3$ from -10℃ to -40℃

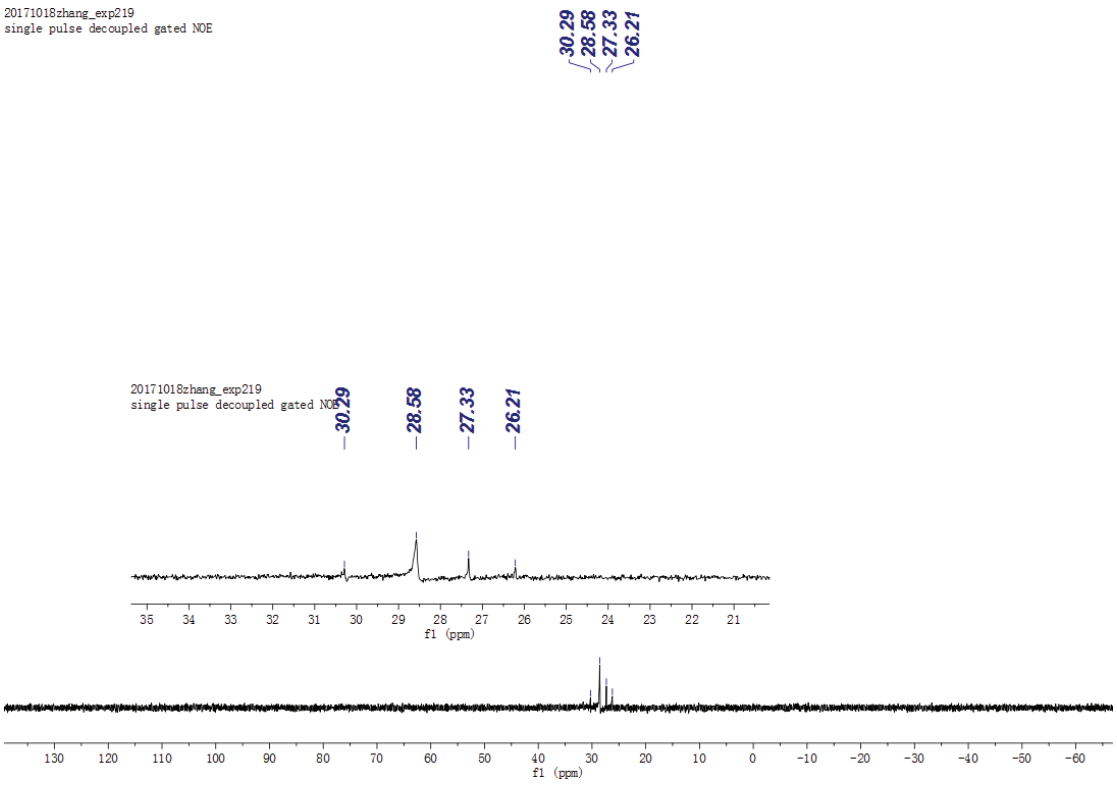

Figure S22. $^{31}P\{^{1}H\}$ NMR spectrum (243 MHz) of complex **2** in $CDCl_3$ at -10℃

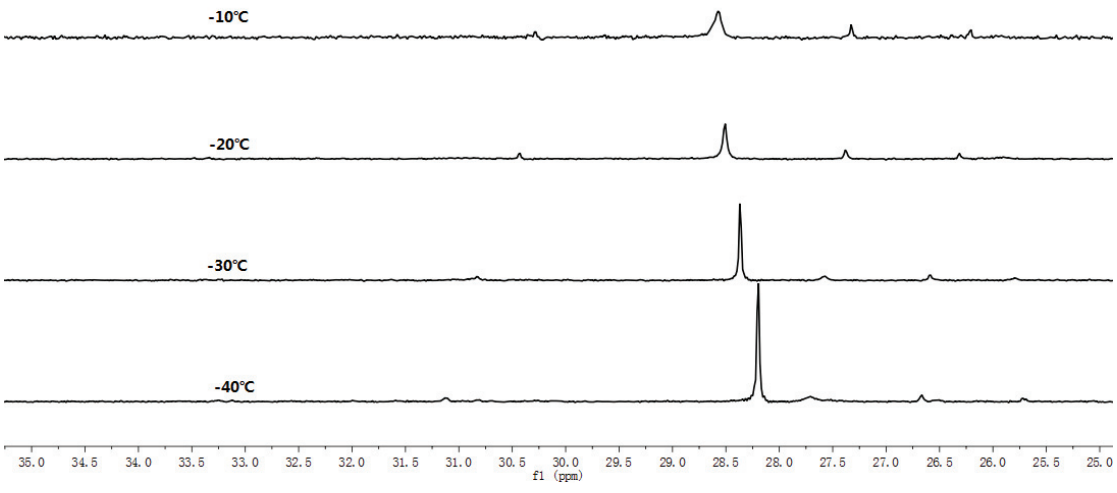

Figure S23. VT $^{31}P\{^{1}H\}$ NMR spectrum (243 MHz) of complex **2** in $CDCl_3$ from -10℃ to -40℃

*NMR spectra of complex **3***

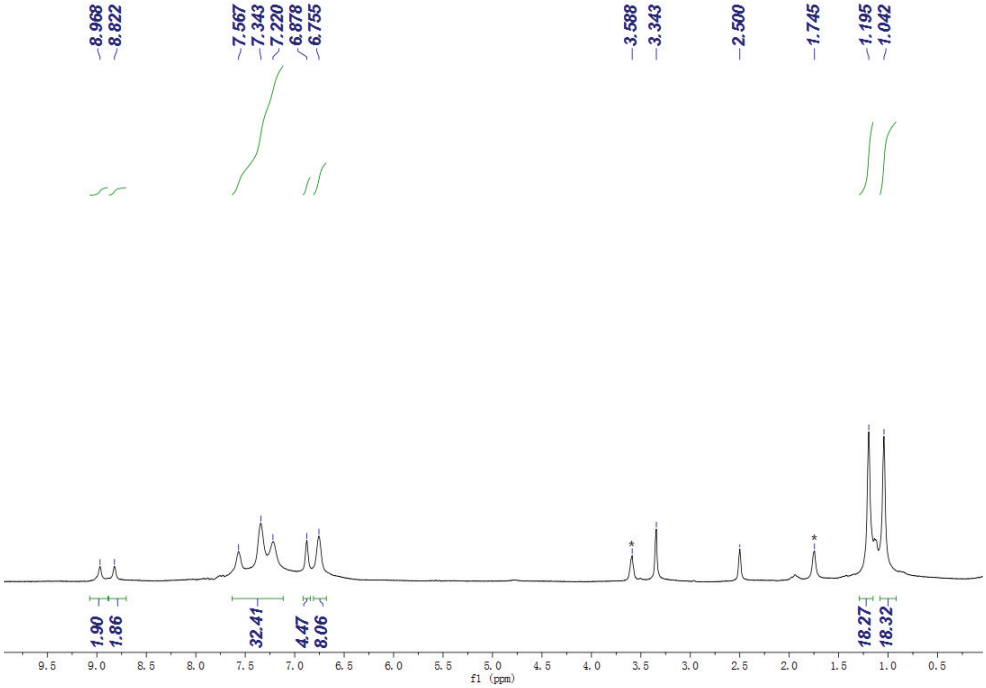

Figure S24. ^{1}H NMR spectrum (400 MHz) of complex **3** in DMSO-d_6 (* = THF)

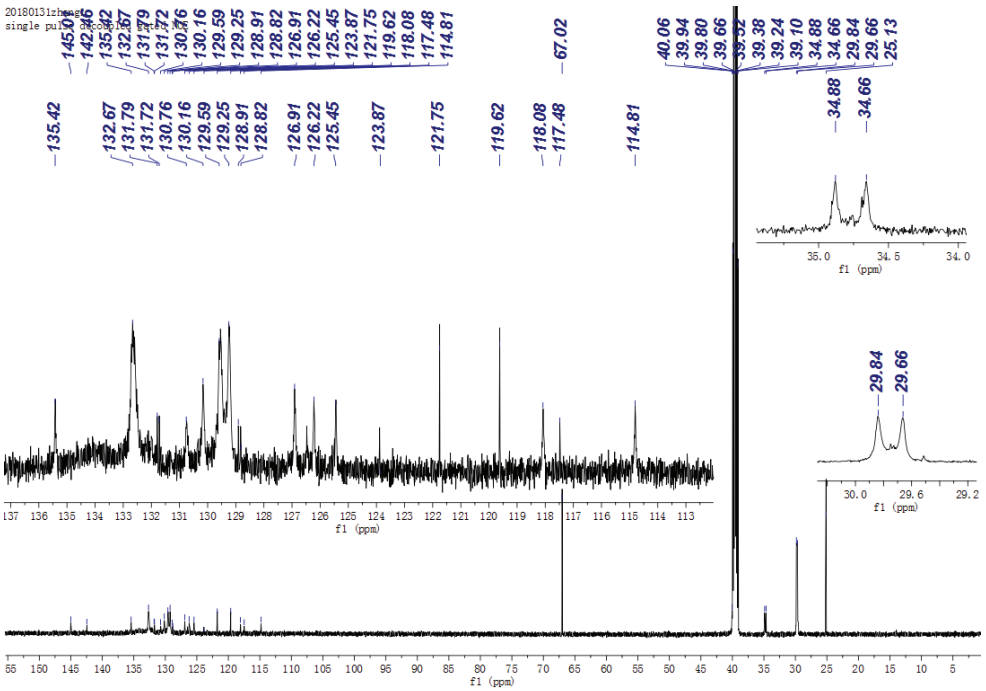

Figure S25. ^{13}C{^{1}H} NMR spectrum (100 MHz) of complex **3** in DMSO-d_6 (* = THF)

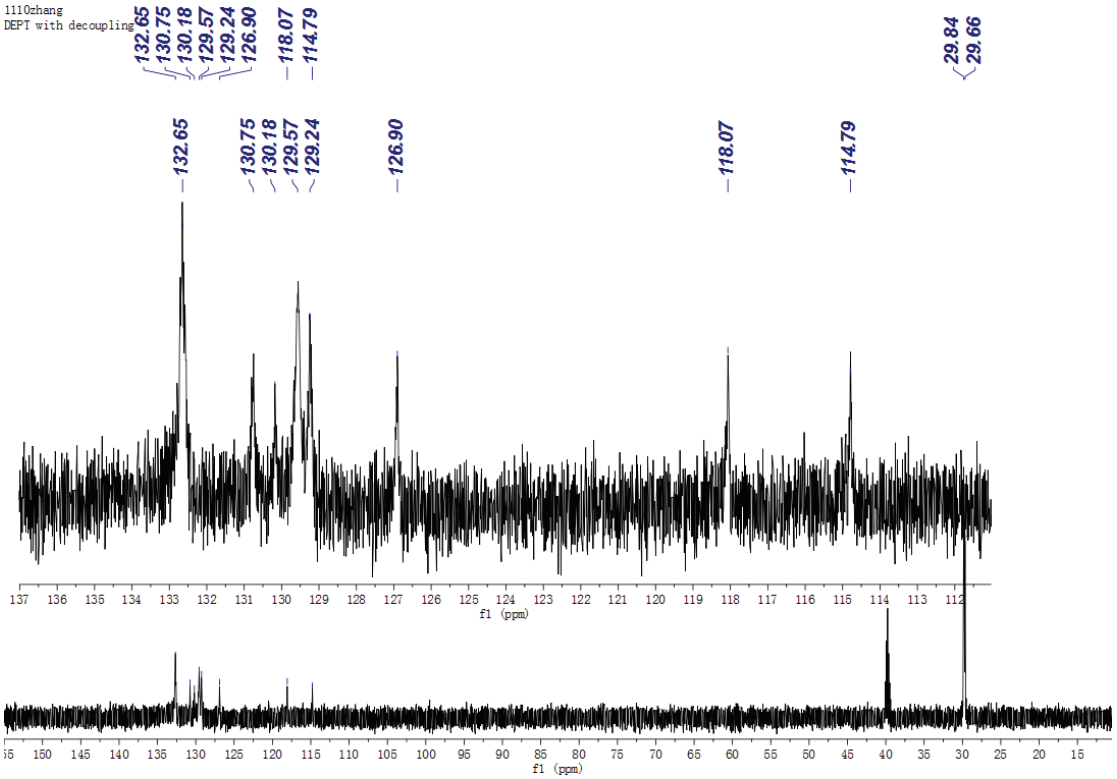

Figure S26. DEPT(135) spectrum of complex **3** in DMSO-d_6

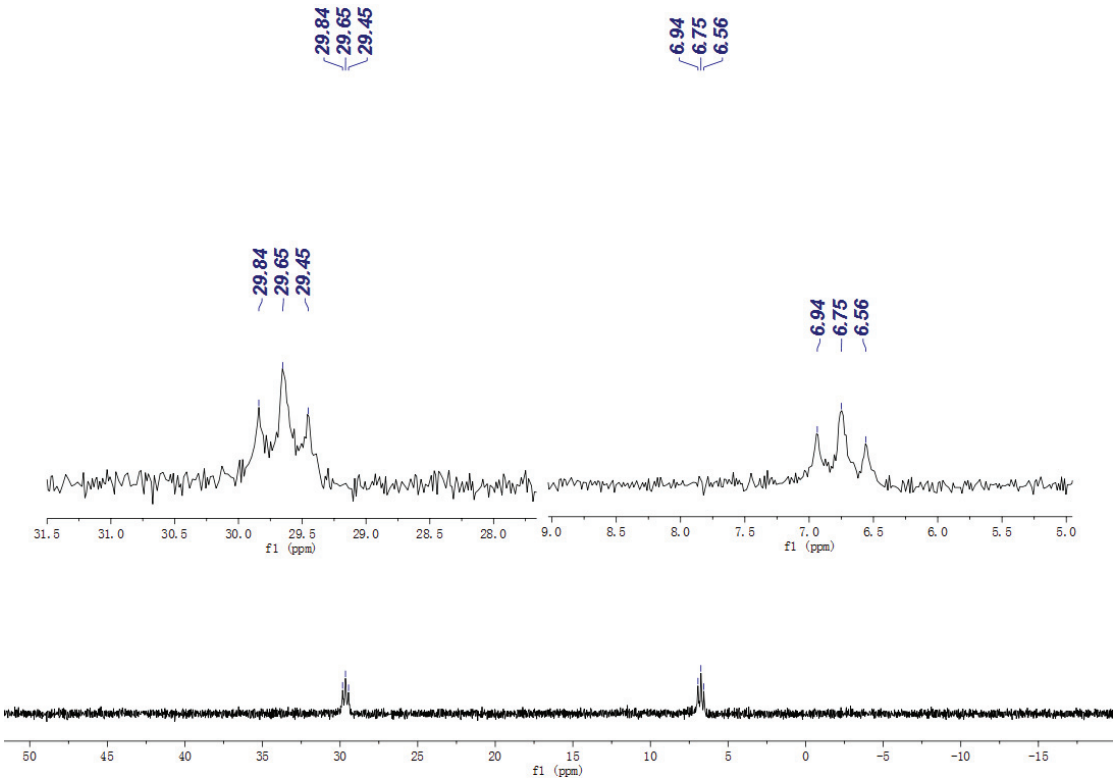

Figure S27. $^{31}P\{^{1}H\}$ NMR spectrum (162 MHz) of complex **3** in DMSO-d_6

*NMR spectra of complex **4***

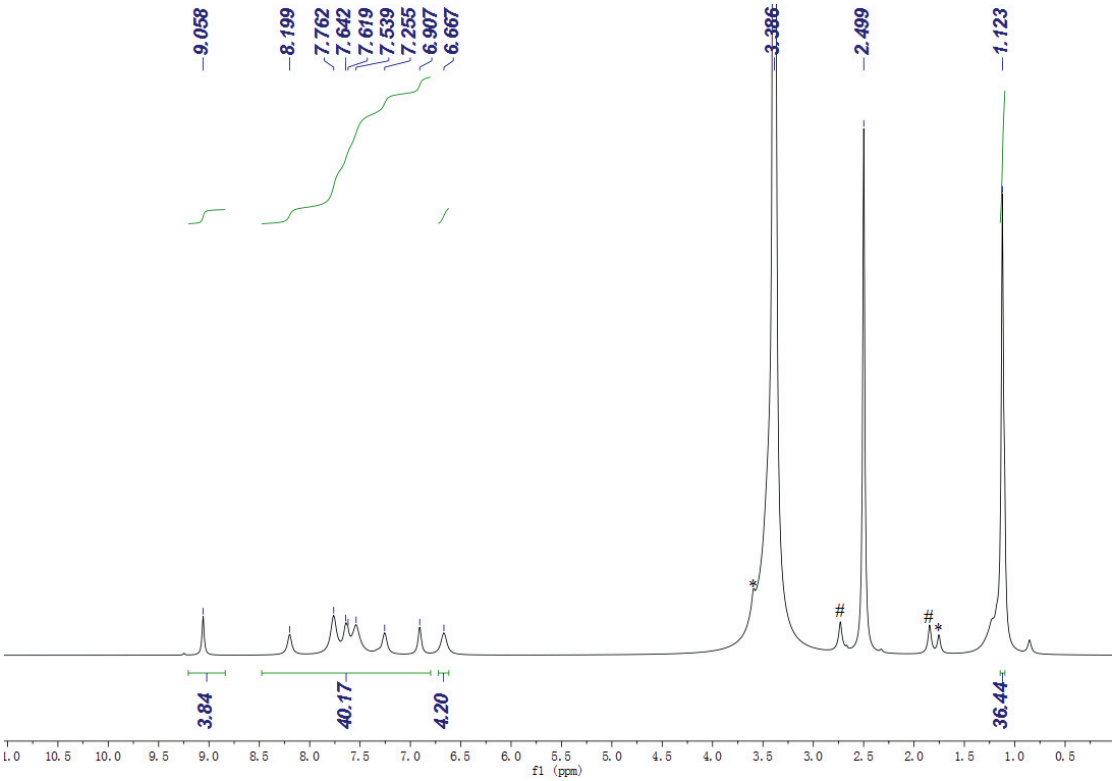

Figure S28. ^{1}H NMR spectrum (400 MHz) of complex **4** in DMSO-d_6 (* = THF, # = tht)

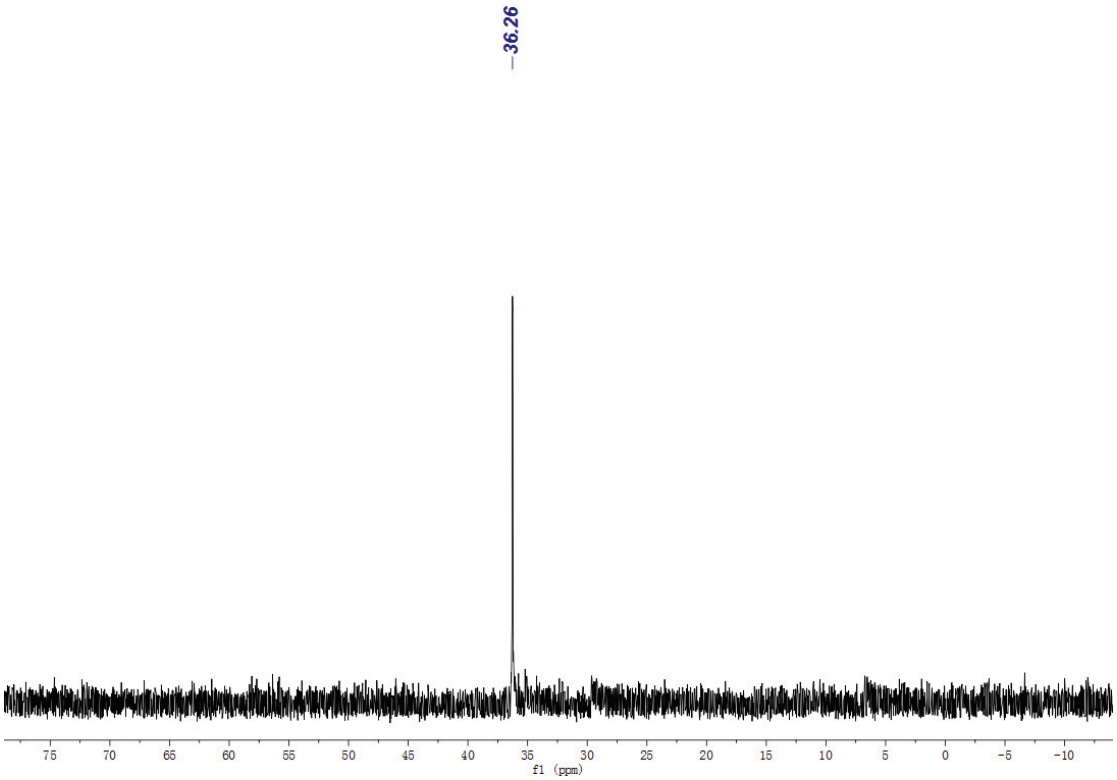

Figure S29. ^{31}P{^{1}H} NMR spectrum (162 MHz) of complex **4** in DMSO-d_6

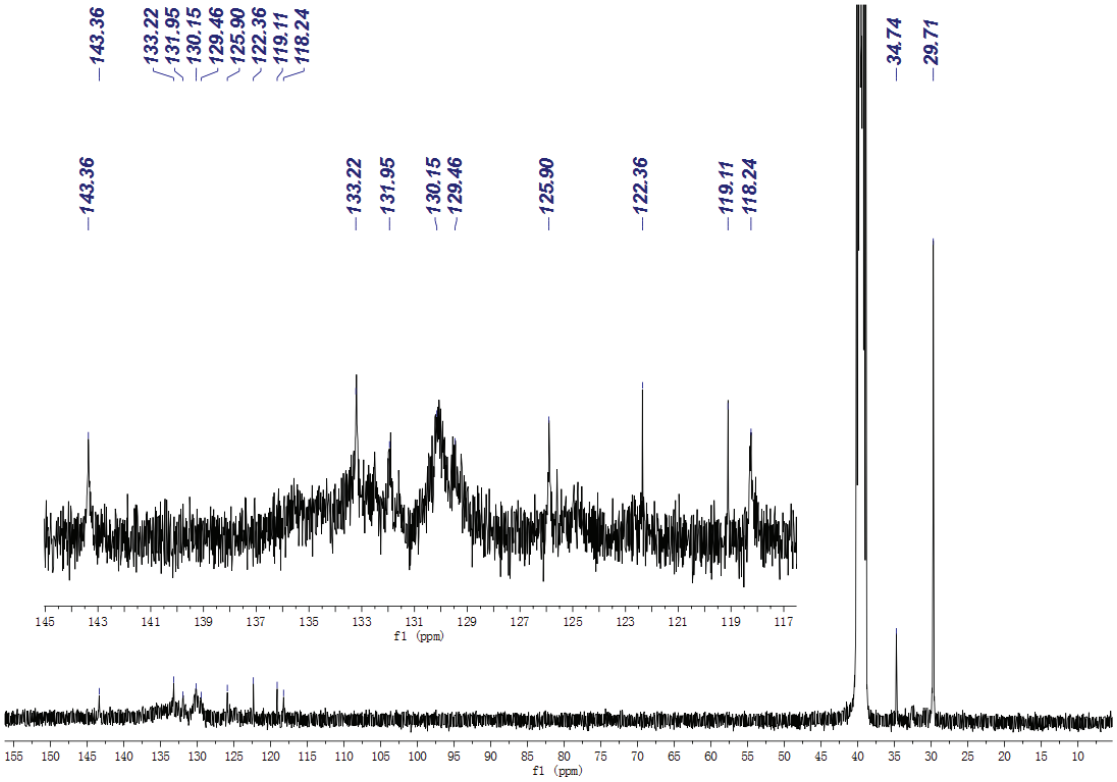

Figure S30. $^{13}C\{^{1}H\}$ NMR spectrum (100 MHz) of complex **4** in DMSO-d_6

NMR Spectra of ***Ag₂L₂***

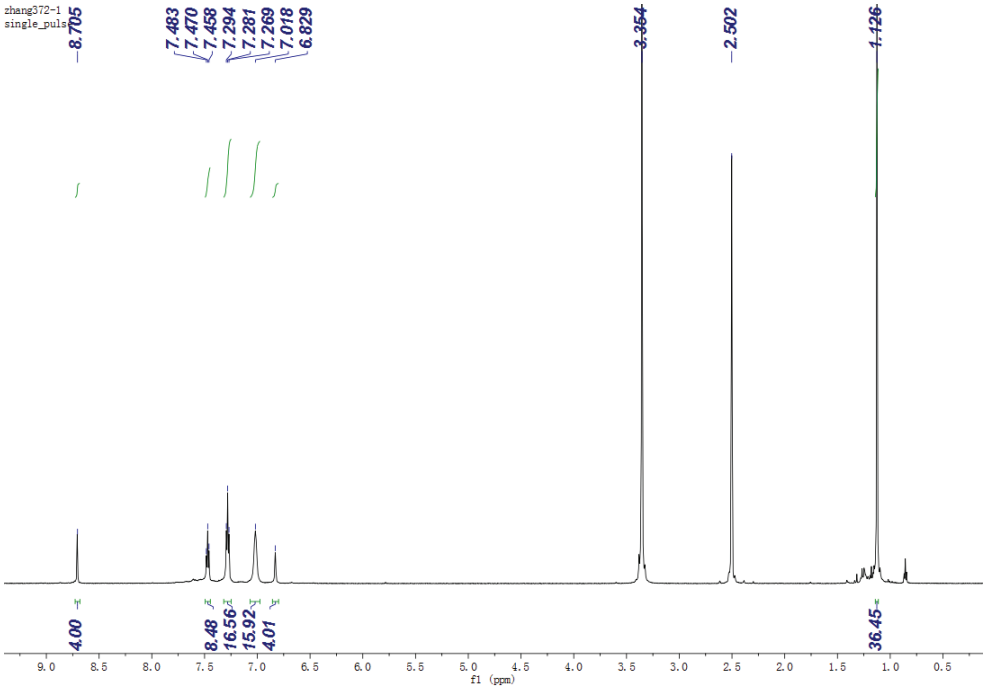

Figure S31. ^{1}H NMR spectrum (600 MHz) of $\mathbf{Ag_2L_2}$ in DMSO-d_6

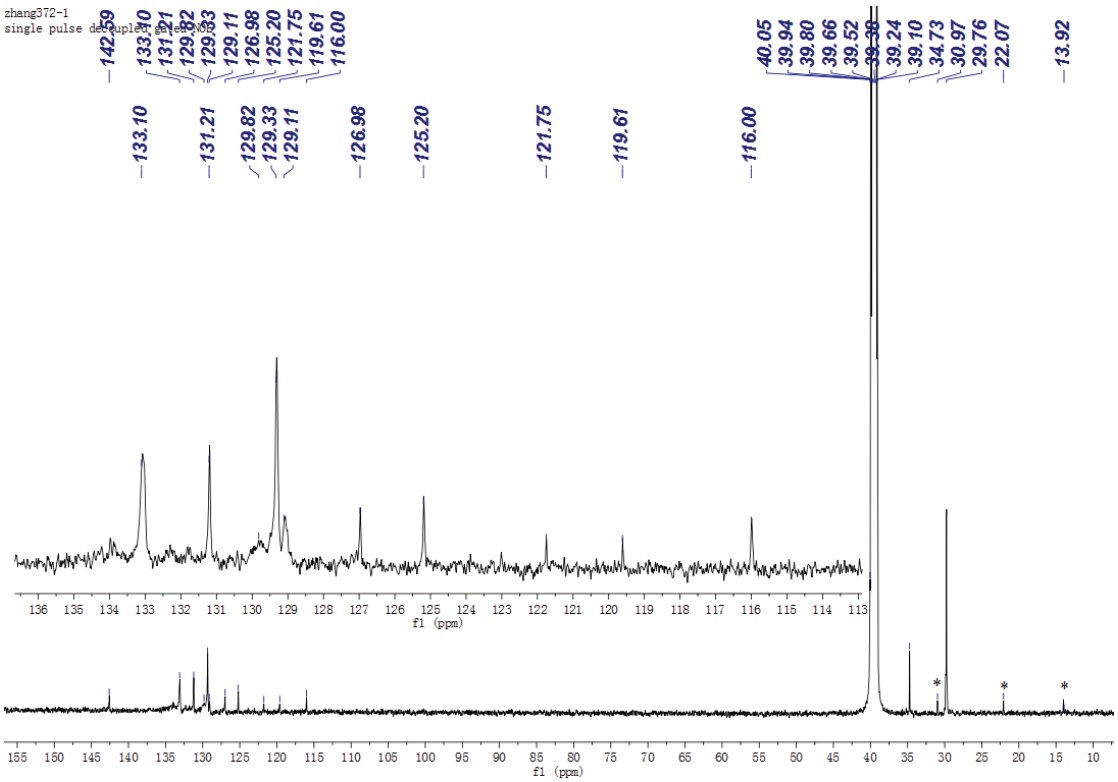

Figure S32. $^{13}C\{^{1}H\}$ NMR spectrum (150 MHz) of $\mathbf{Ag_2L_2}$ in DMSO-d_6 (* = hexane)

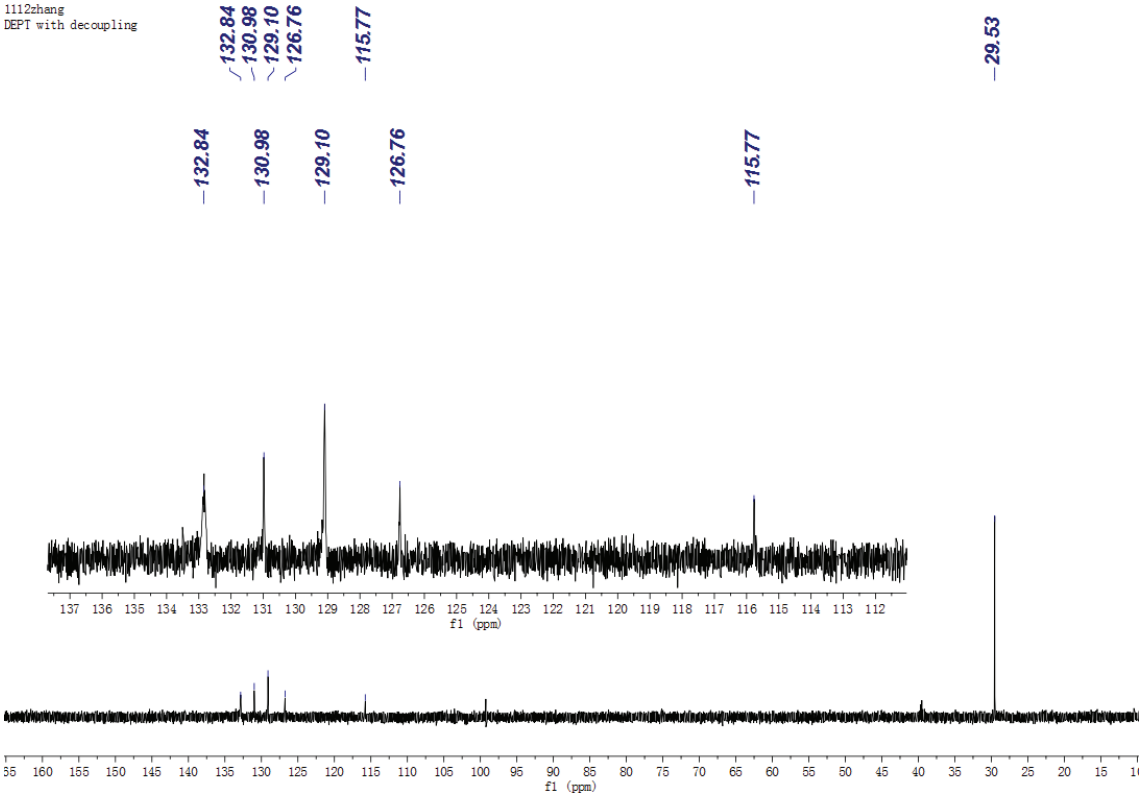

Figure S33. DEPT (135) spectrum of $\mathbf{Ag_2L_2}$ in DMSO-d_6

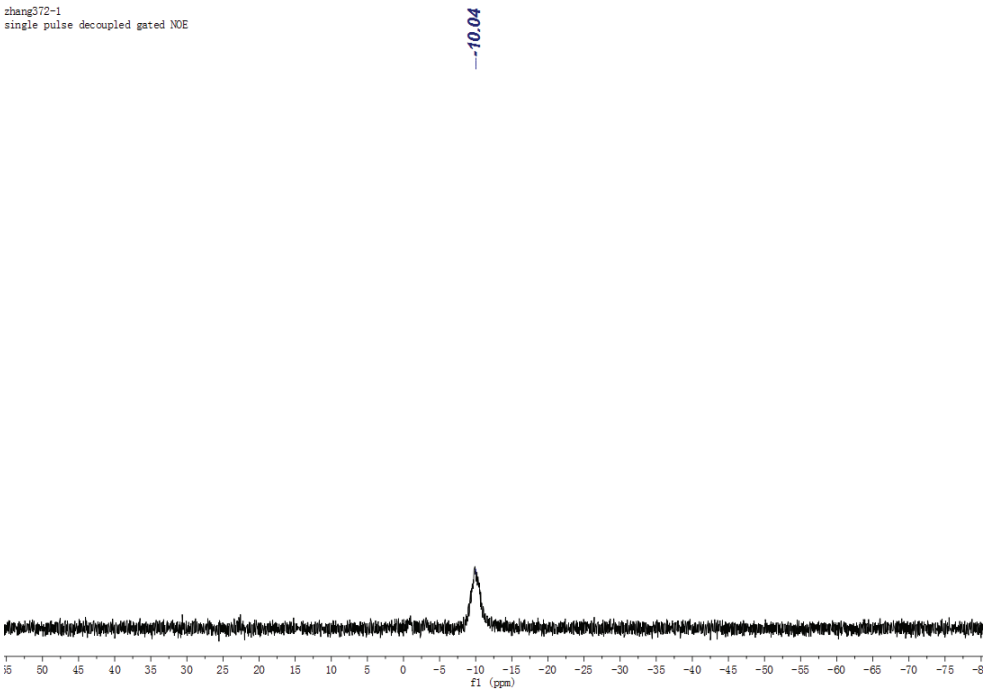

Figure S34. $^{31}P\{^{1}H\}$ NMR spectrum (243 MHz) of $\mathbf{Ag_2L_2}$ in DMSO-d_6

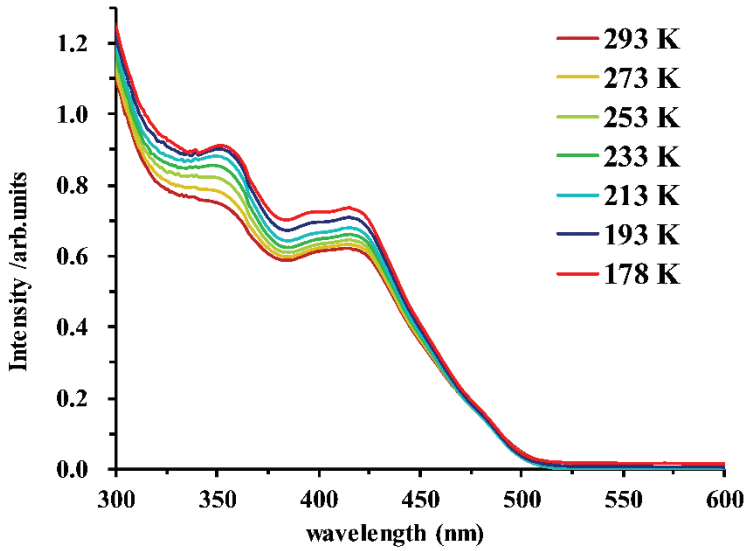

Figure S35. VT UV-Vis spectra of complex $\mathbf{Ag_2L_2}$ in THF from 293 K to 178 K at concentration of 2.0×10^{-5} M

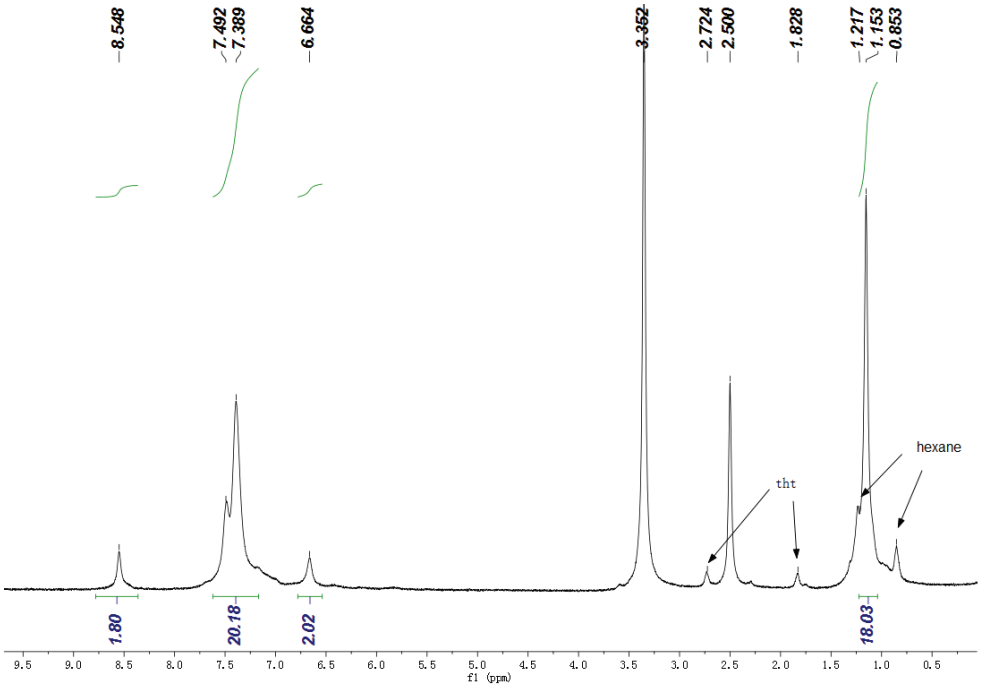

Figure S36. ^{1}H NMR spectrum (400 MHz) of **Cu$_4$LBr$_4$** in DMSO-d_6

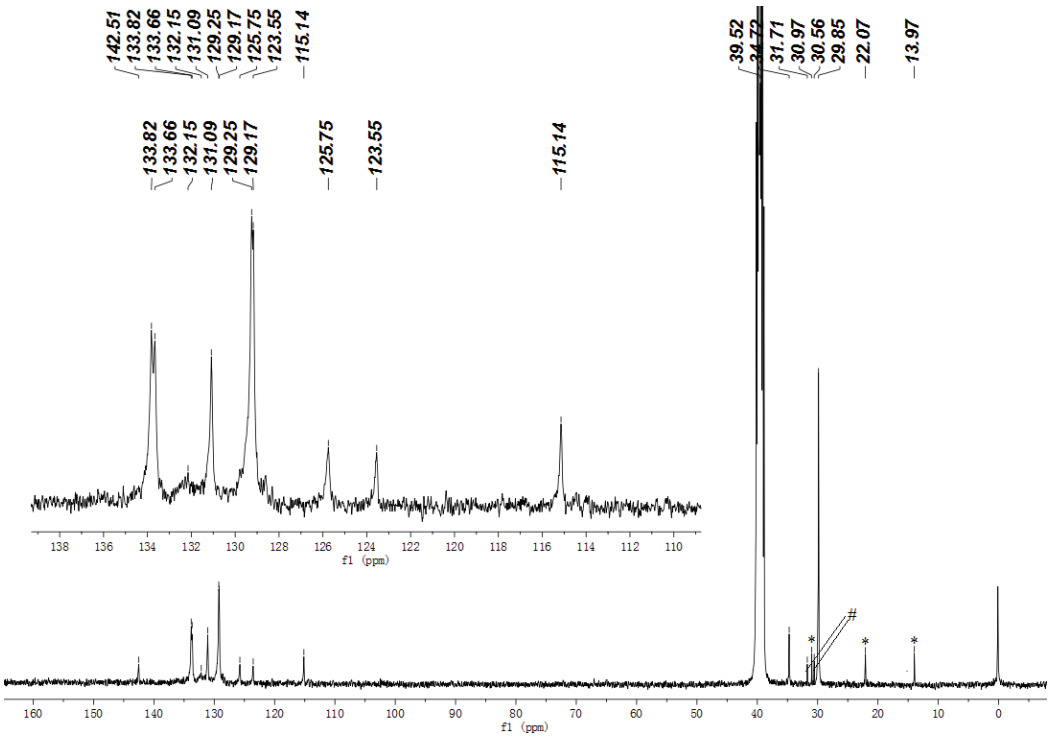

Figure S37. ^{13}C{^{1}H} NMR spectrum (150 MHz) of **Cu$_4$LBr$_4$** in DMSO-d_6 (* = hexane, # = tht)

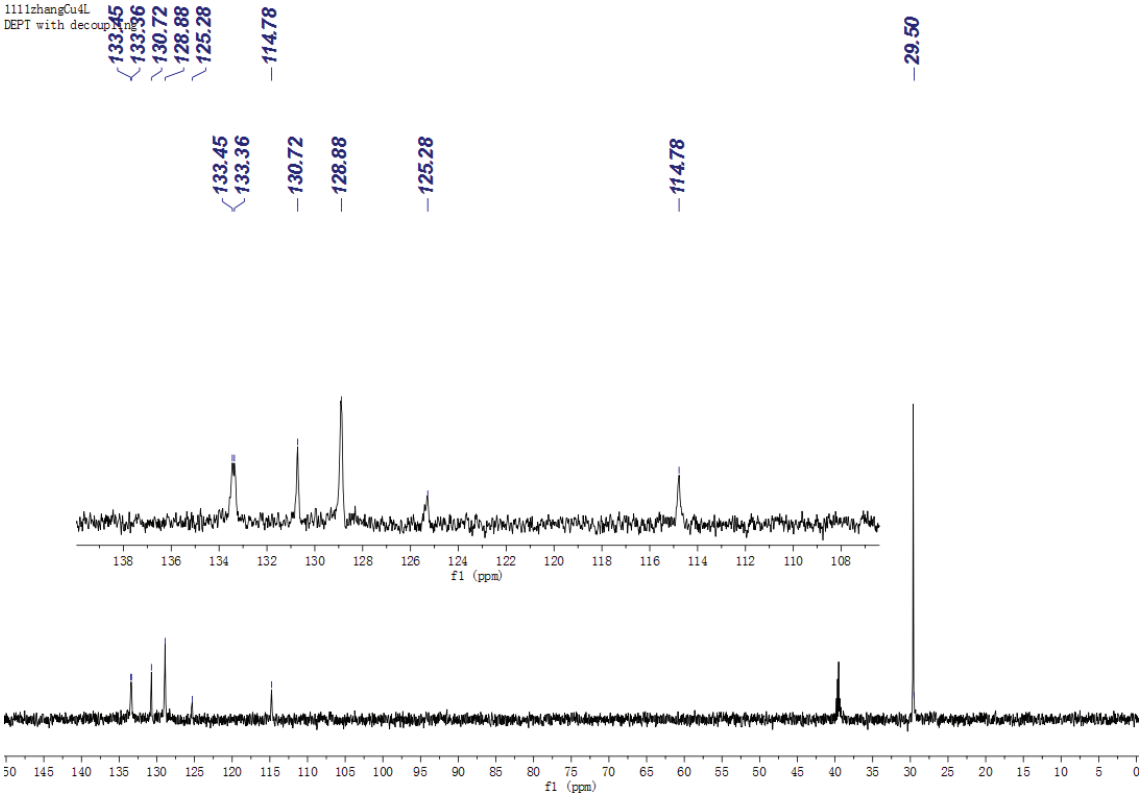

Figure S38. DEPT (135) spectrum of **Cu_4LBr_4** in DMSO-d_6

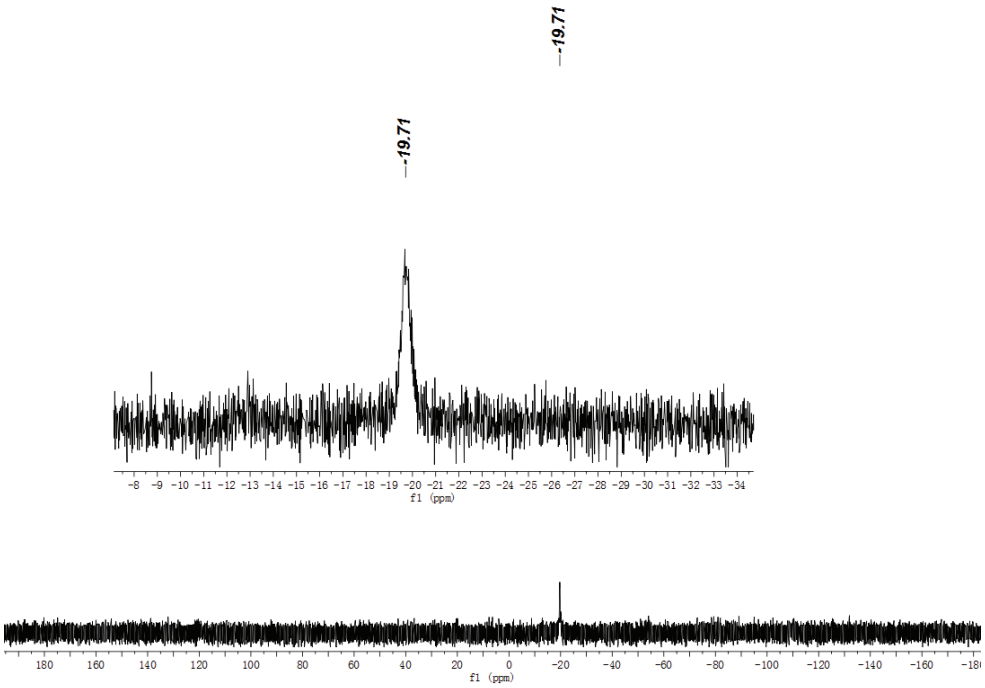

Figure S39. $^{31}P\{^1H\}$ NMR spectrum (243 MHz) of **Cu_4LBr_4** in DMSO-d_6

NMR Spectra of ***Cu₂L₂***

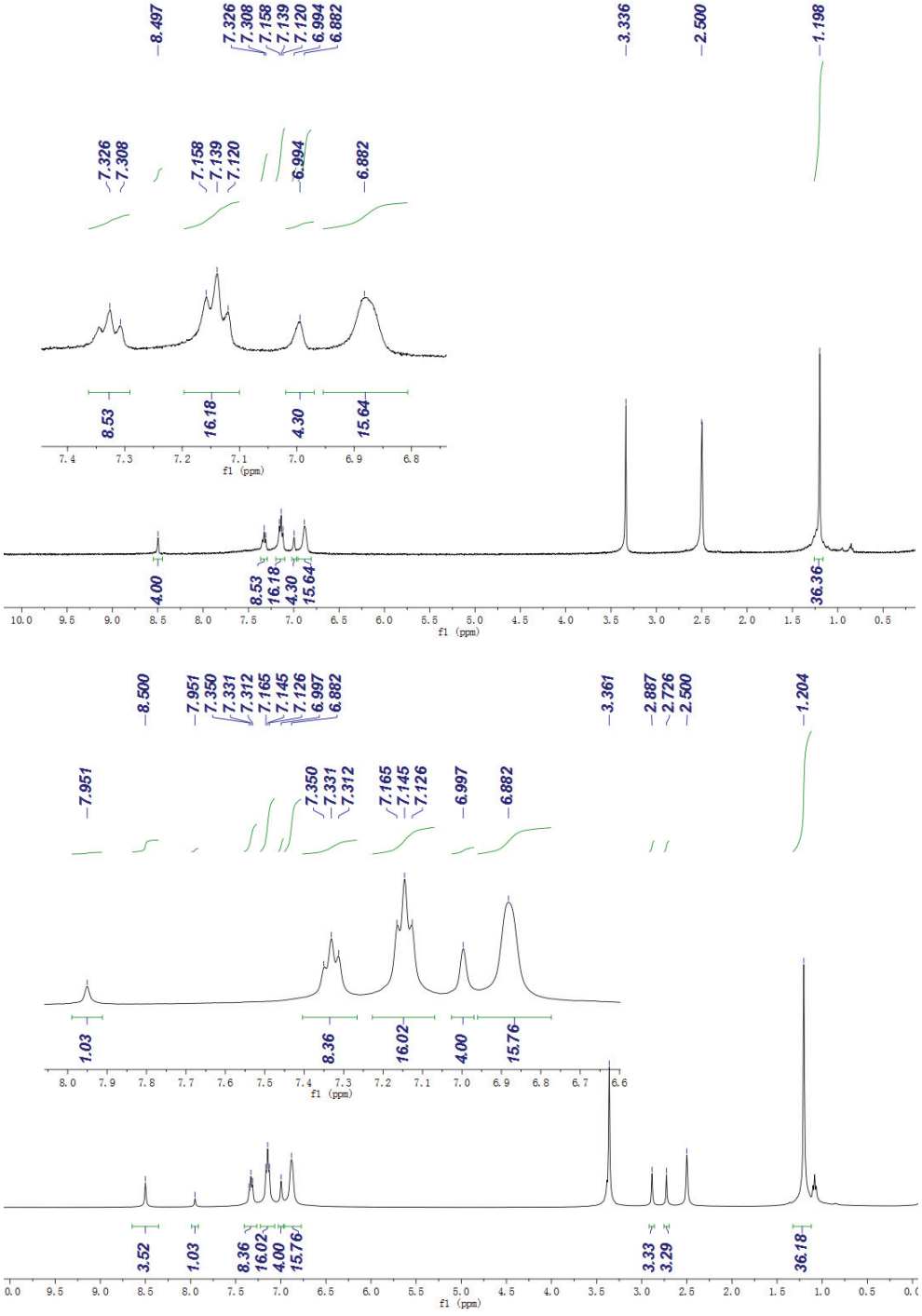

Figure S40. ^{1}H NMR spectra (600 MHz) of **Cu_2L_2** (bulk sample, top) and **Cu_2L_2·DMF** (crystals, bottom) in DMSO-d_6

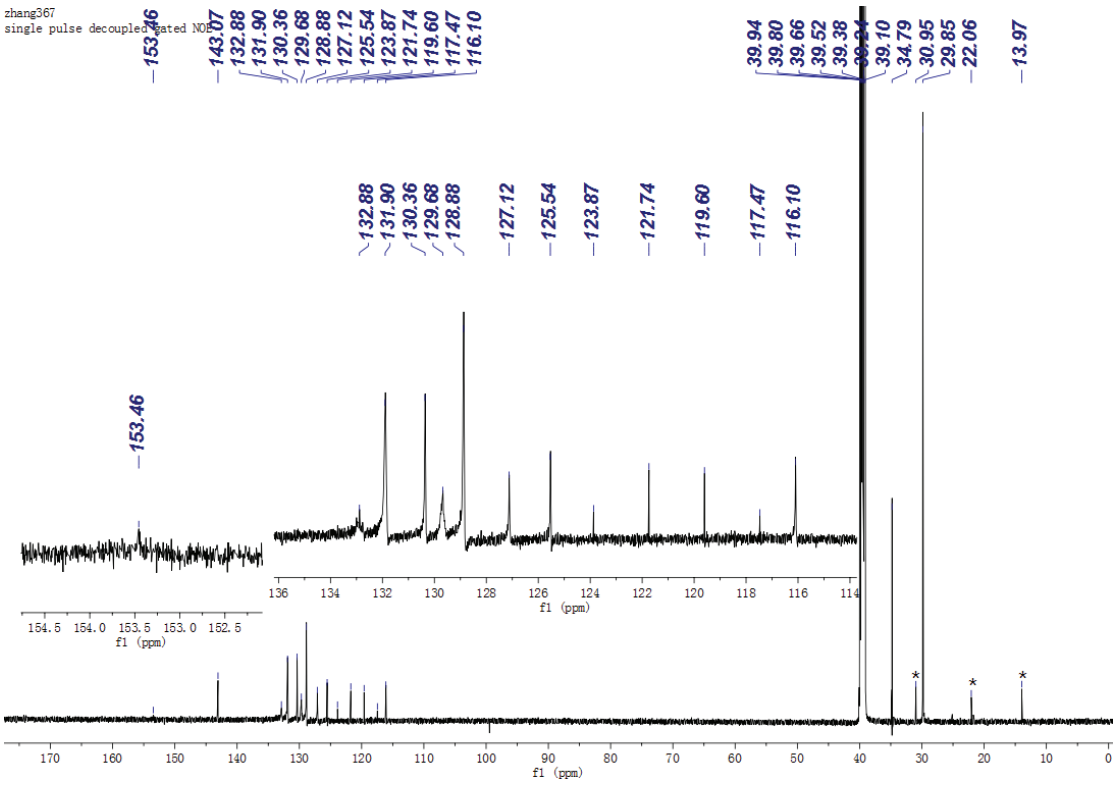

Figure S41. $^{13}C\{^{1}H\}$ NMR spectrum (150 MHz) of $\mathbf{Cu_2L_2}$ in DMSO-d_6 (* = hexane)

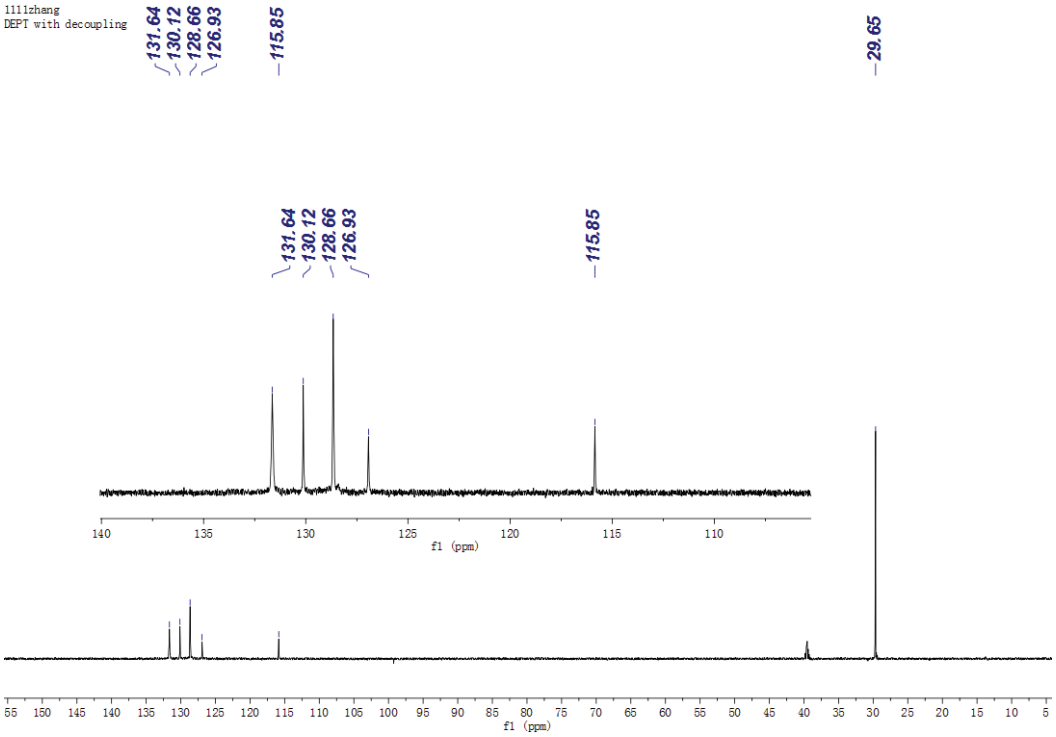

Figure S42. DEPT (135) spectrum of $\mathbf{Cu_2L_2}$ in DMSO-d_6

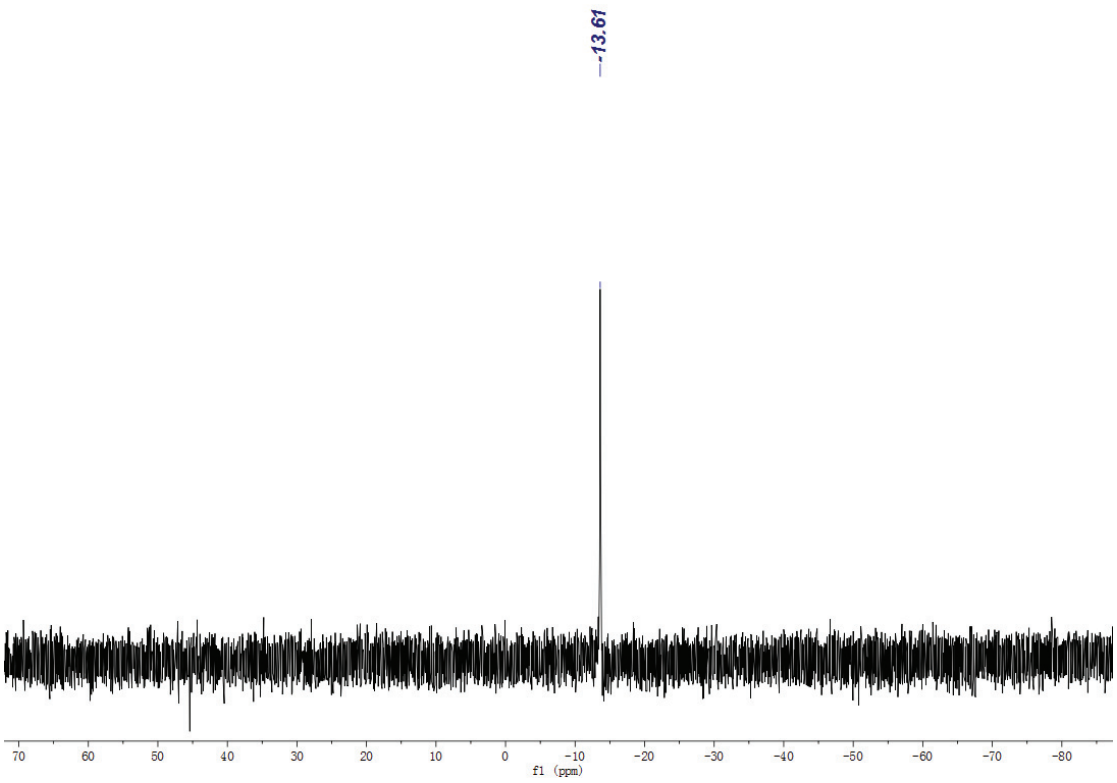

Figure S43. $^{31}P\{^{1}H\}$ NMR spectrum (243 MHz) of $\mathbf{Cu_2L_2}$ in DMSO-d_6

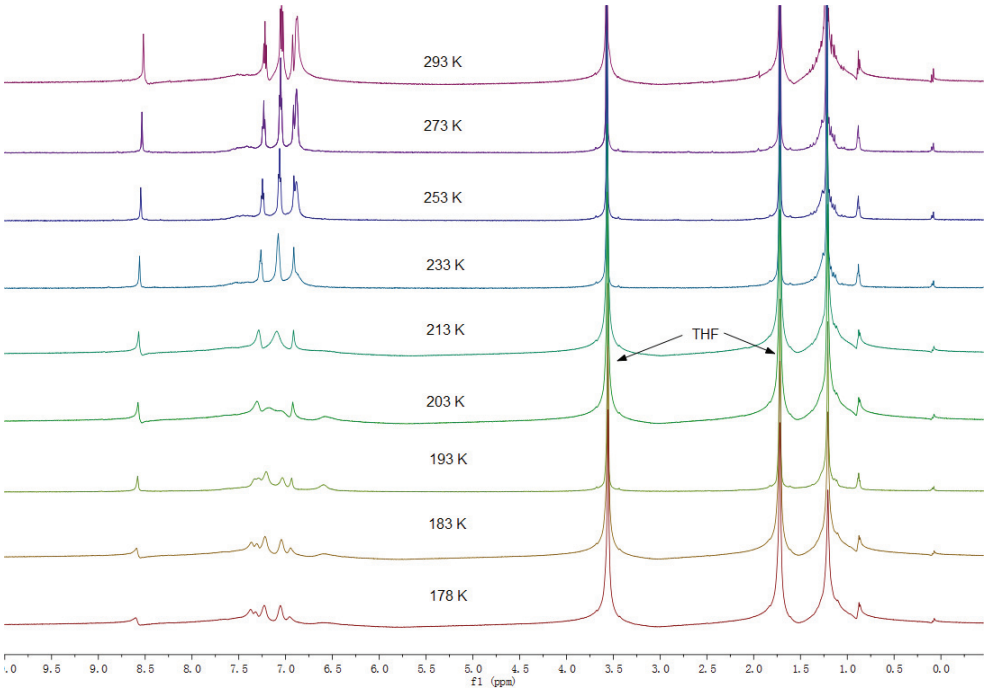

Figure S44. VT ^{1}H NMR spectra (600 MHz) of $\mathbf{Cu_2L_2}$ in THF-d_8

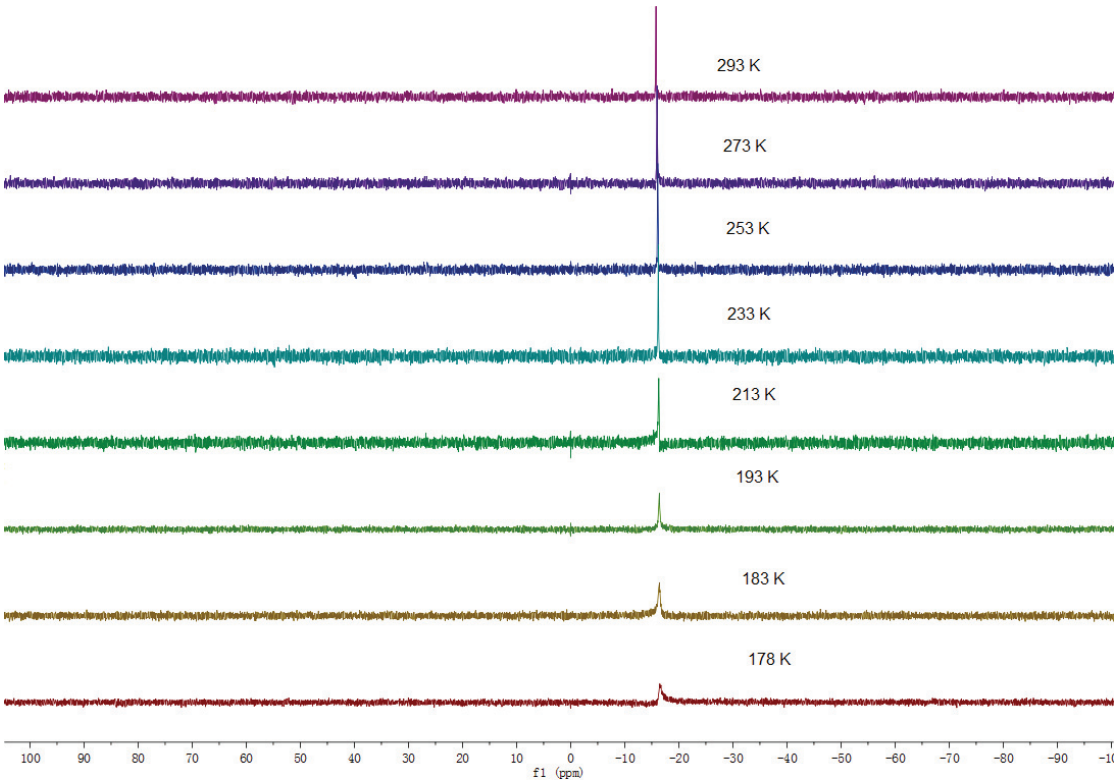

Figure S45. VT $^{31}P\{^{1}H\}$ NMR spectra (243 MHz) of $\mathbf{Cu_2L_2}$ in THF-d_8

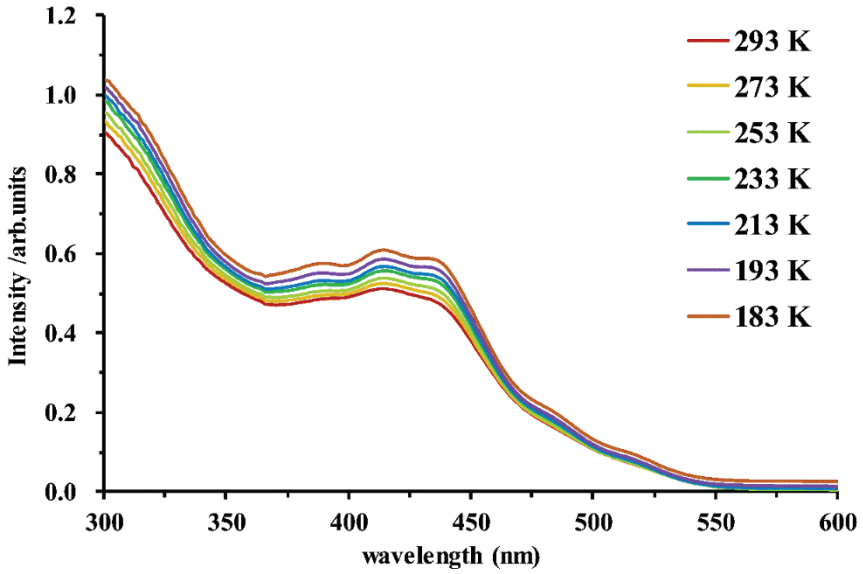

Figure S46. VT UV-Vis spectra of complex $\mathbf{Cu_2L_2}$ in THF from 293 K to 183 K at concentration of 2.0×10^{-5} M

NMR Spectra of ***$Ag_2Cu_2L_2(O)$***

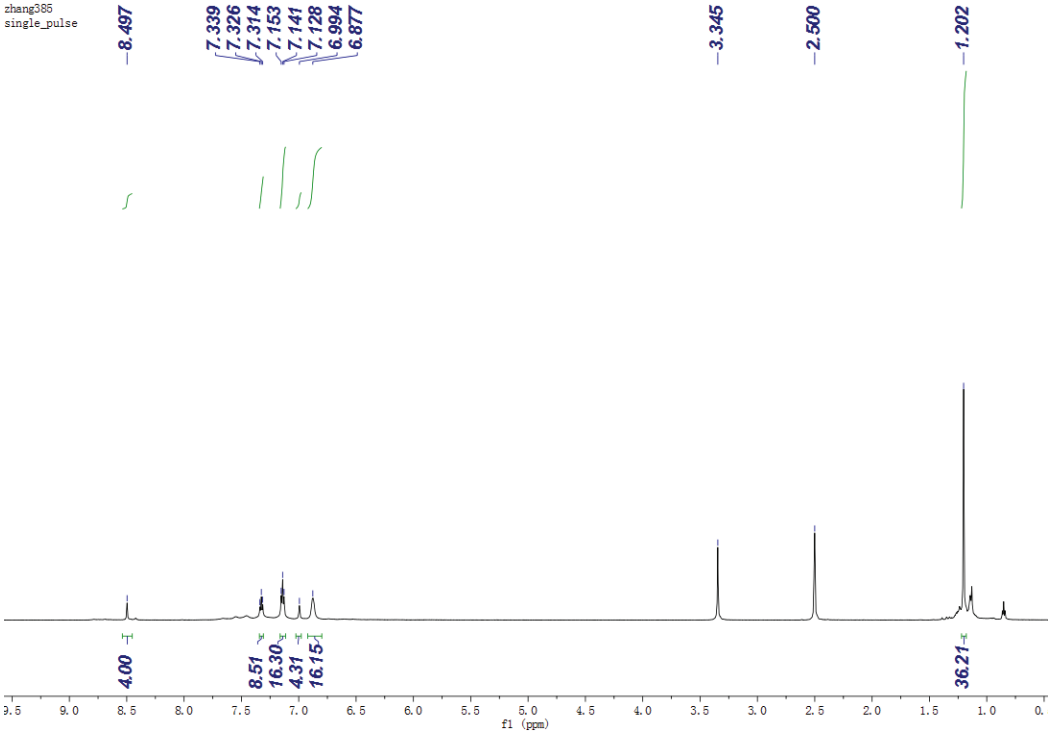

Figure S47. ^{1}H NMR spectrum (600 MHz) of **$Ag_2Cu_2L_2(O)$** in DMSO-d_6

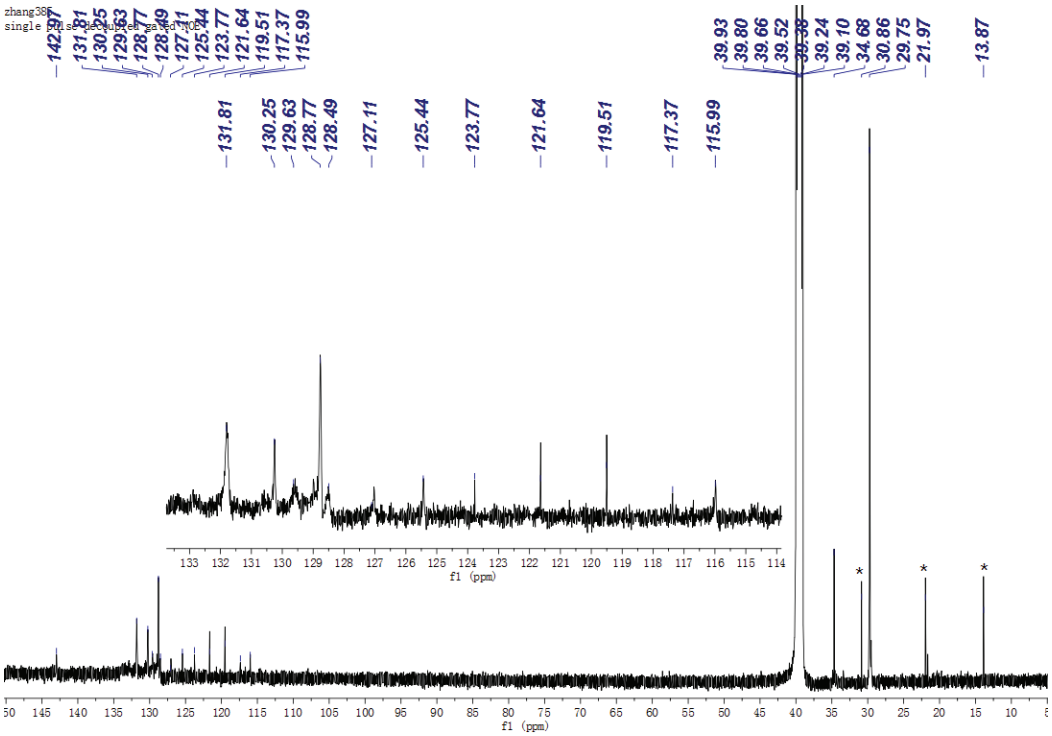

Figure S48. ^{13}C{^{1}H} NMR spectrum (150 MHz) of **$Ag_2Cu_2L_2(O)$** in DMSO-d_6 (* = hexane)

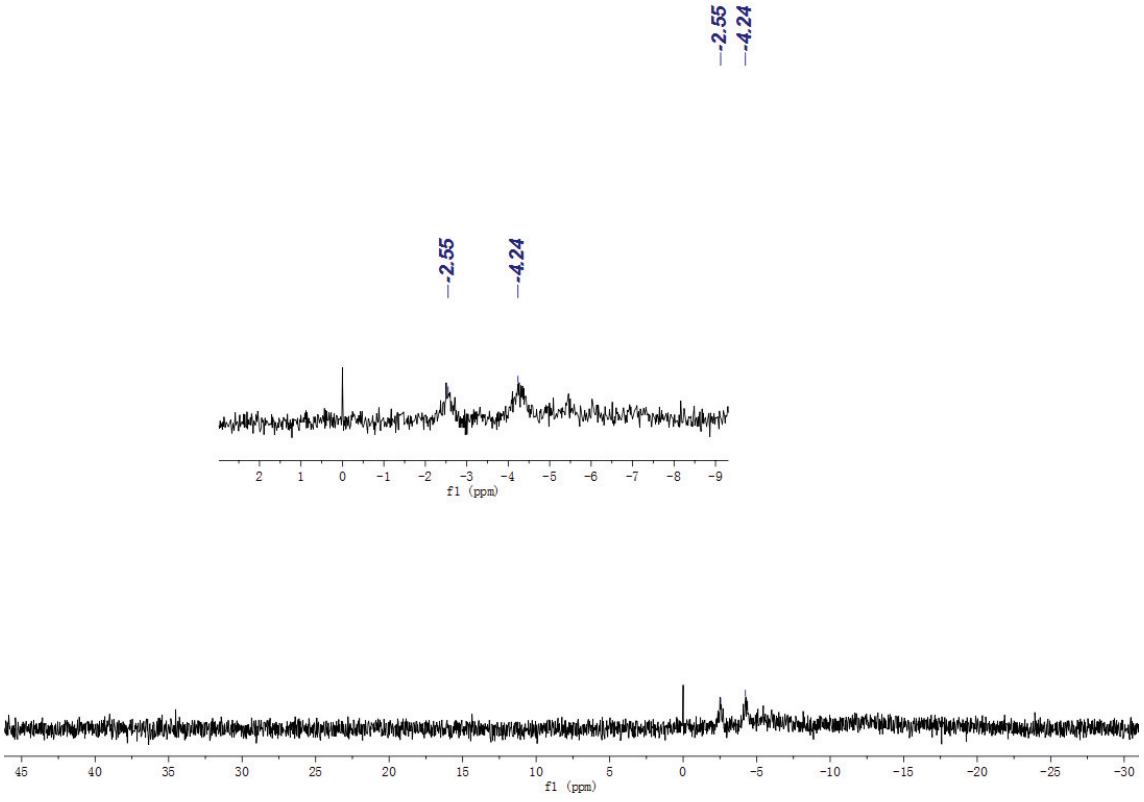

Figure S49. $^{31}P\{^{1}H\}$ NMR spectrum (243 MHz) of **$Ag_2Cu_2L_2(O)$** in DMSO-d_6

NMR Spectra of ***$Cu_4L_2 \cdot 2CH_3CN$***

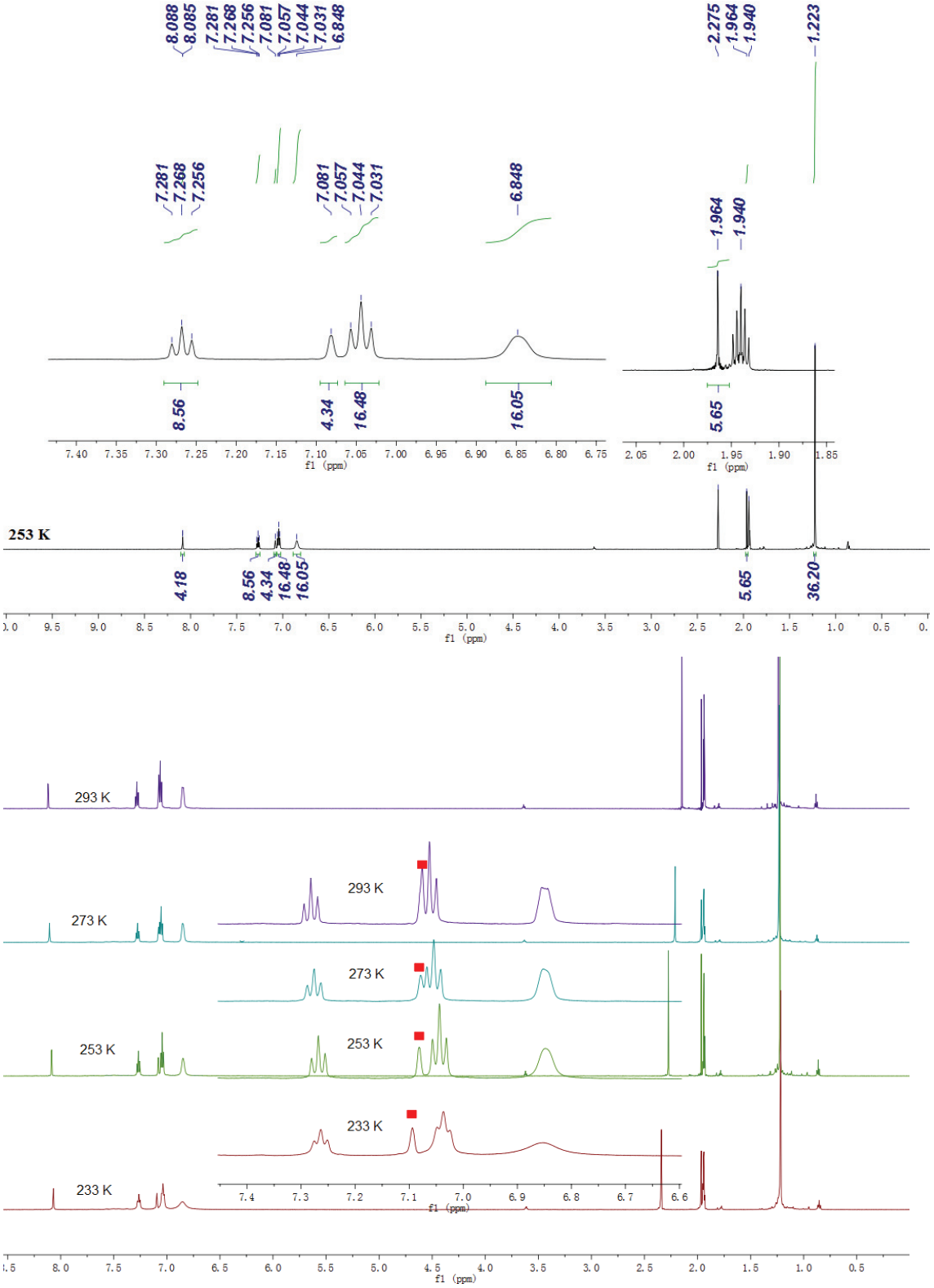

Figure S50. ^{1}H NMR spectra (600 MHz) at 253 K (top) and VT ^{1}H NMR spectra from 293 to 233 K (bottom) of $\mathbf{Cu_4L_2 \cdot 2CH_3CN}$ in CD_3CN

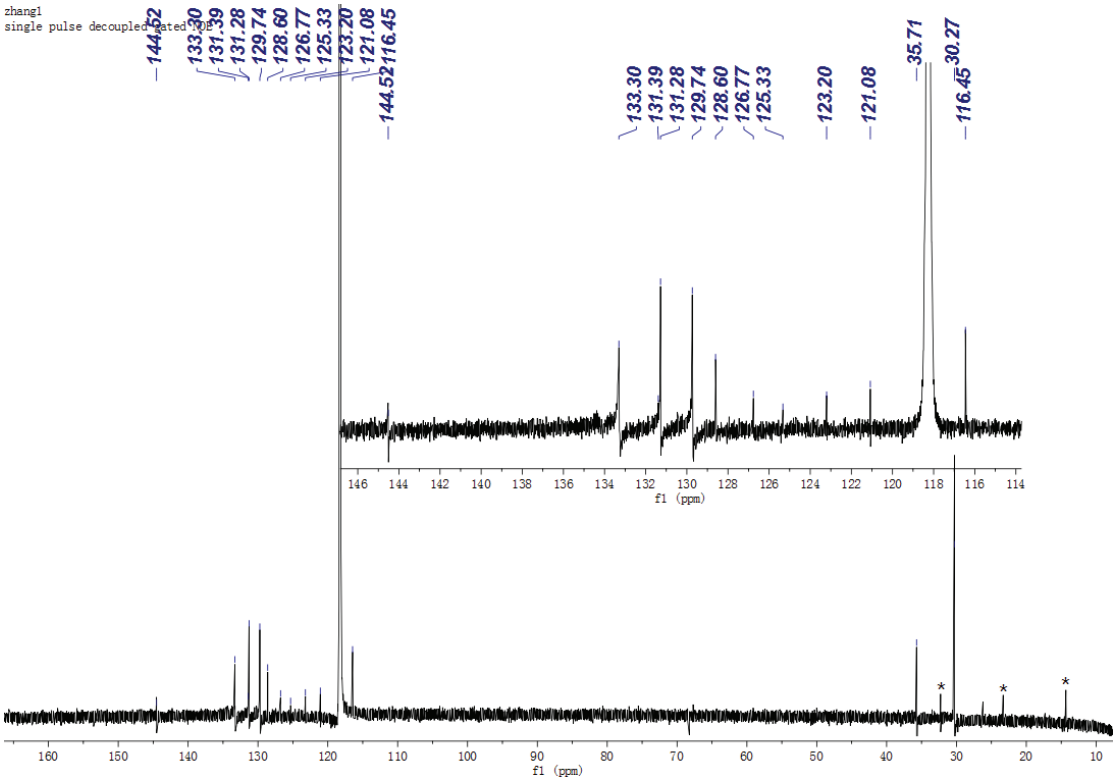

Figure S51. $^{13}C\{^{1}H\}$ NMR spectrum (150 MHz) of **Cu_4L_2·2CH_3CN** in CD_3CN (* = hexane)

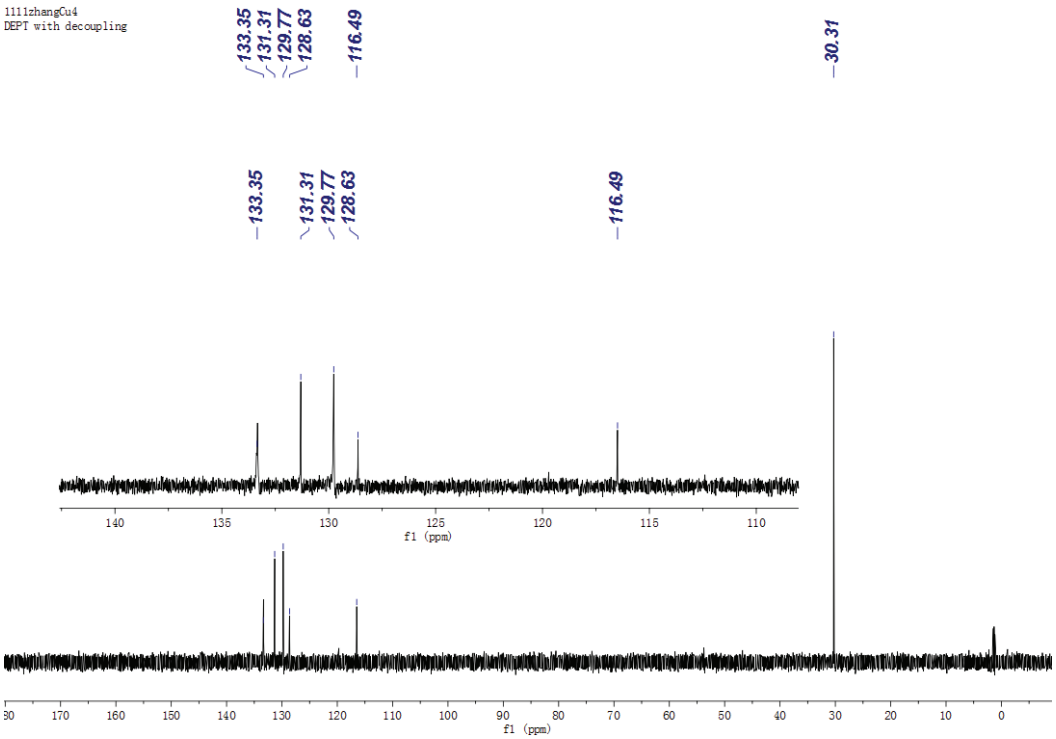

Figure S52. DEPT (135) spectrum of **Cu_4L_2·2CH_3CN** in DMSO-d_6

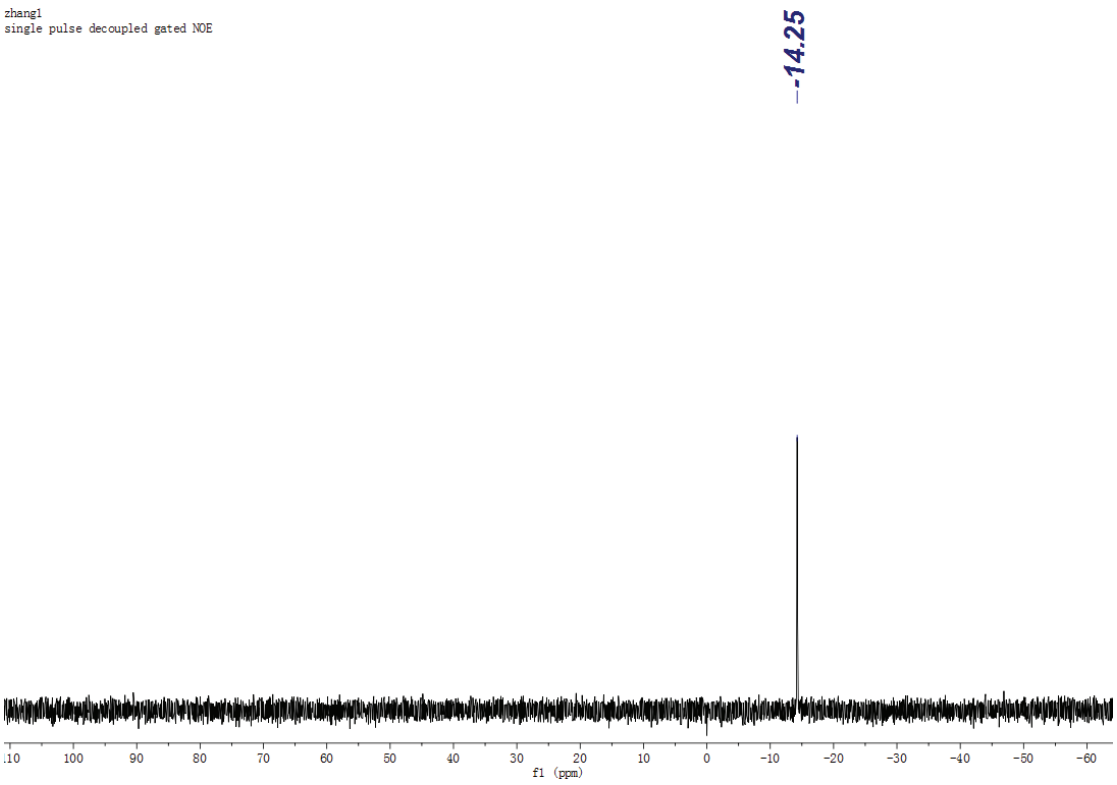

Figure S53. $^{31}P\{^{1}H\}$ NMR spectrum (243 MHz) of **$Cu_4L_2 \cdot 2CH_3CN$** in CD_3CN

NMR Spectra of ***Cu$_5$L$_2$-Br$_3$***

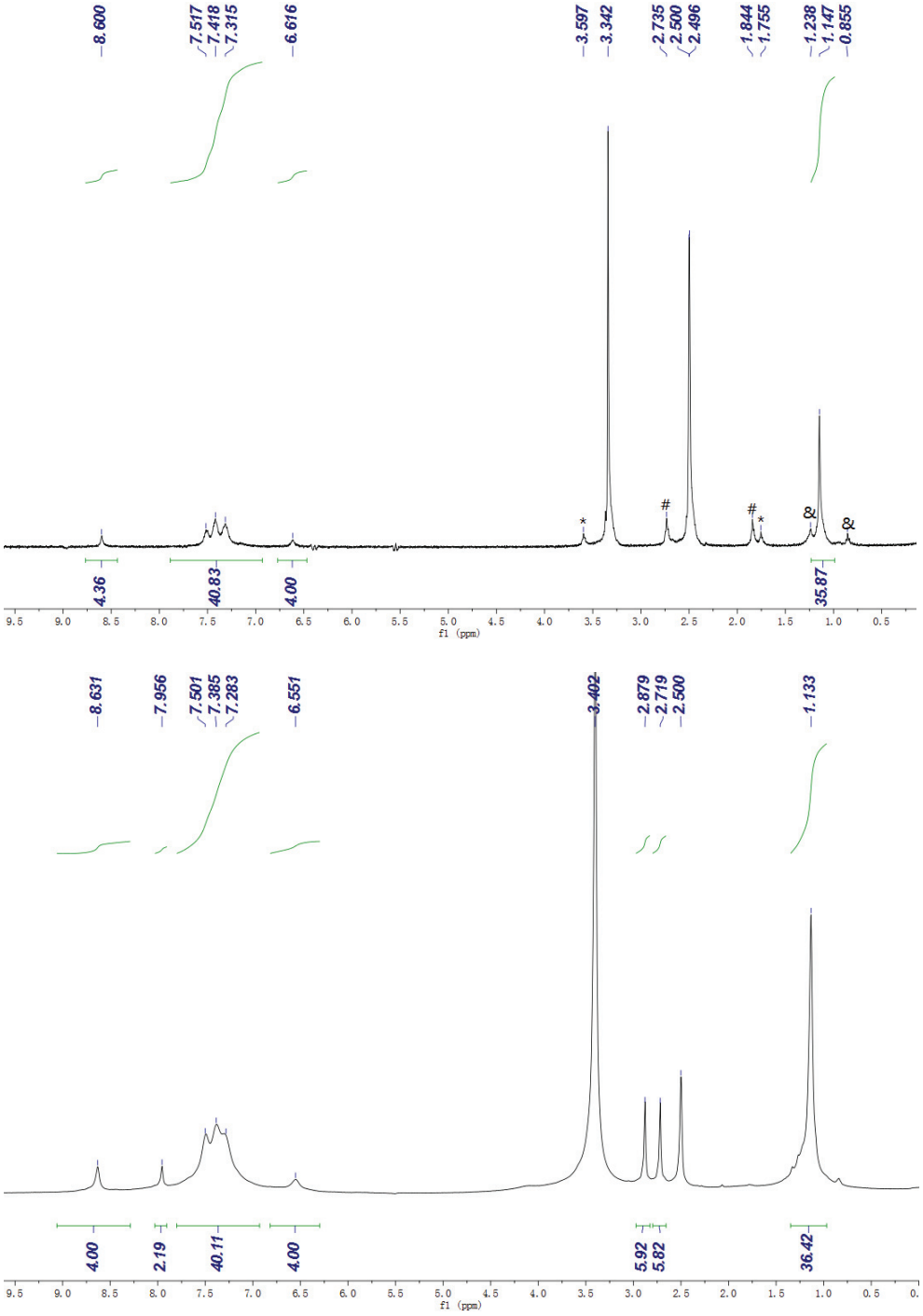

Figure S54. ^{1}H NMR spectrum (600 MHz) of **Cu$_5$L$_2$Br$_3$** (bulk sample, top) and **Cu$_5$L$_2$Br$_3$·2DMF** (crystals, bottom) in DMSO-d_6 (* = THF, # = tht, & = hexane)

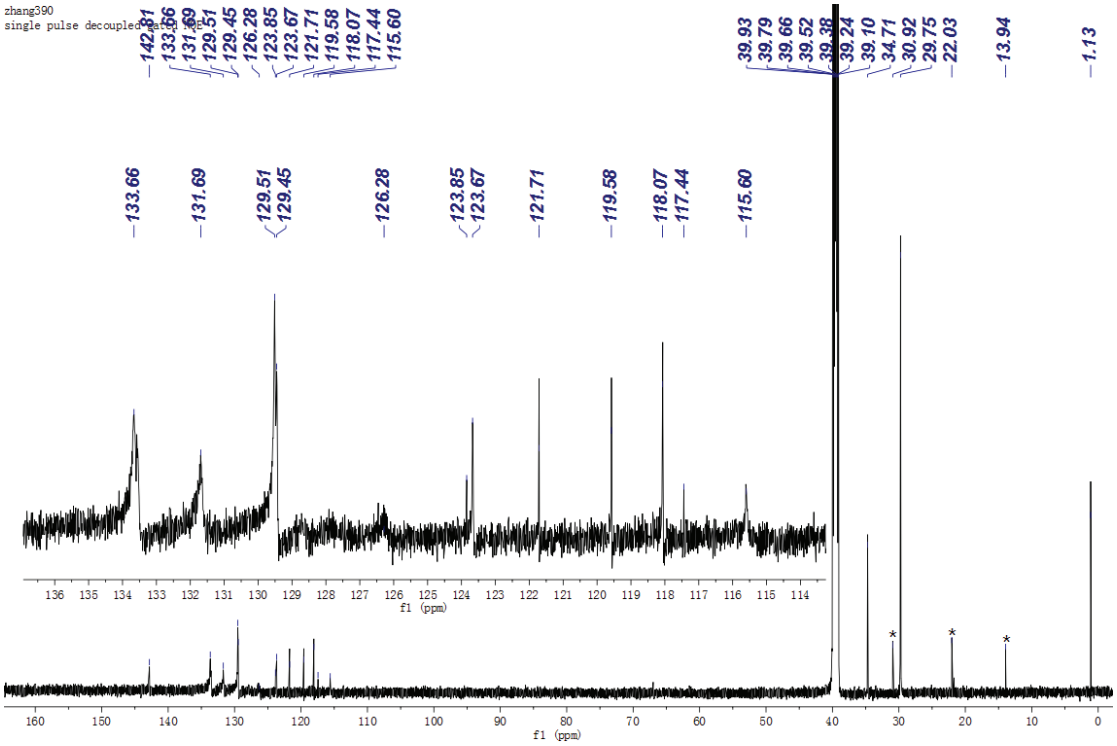

Figure S55. $^{13}C\{^{1}H\}$ NMR spectrum (150 MHz) of **$Cu_5L_2Br_3$** in DMSO-d_6 (* = hexane)

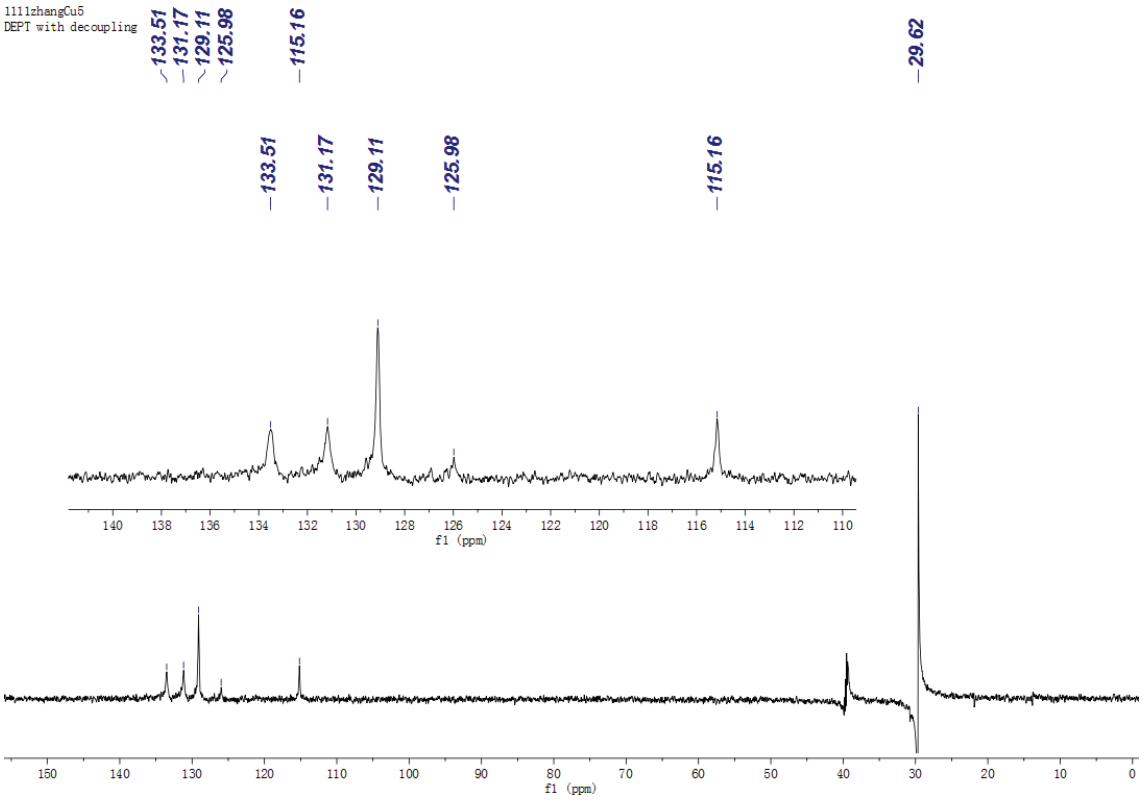

Figure S56. DEPT (135) spectrum of **$Cu_5L_2Br_3$** in DMSO-d_6

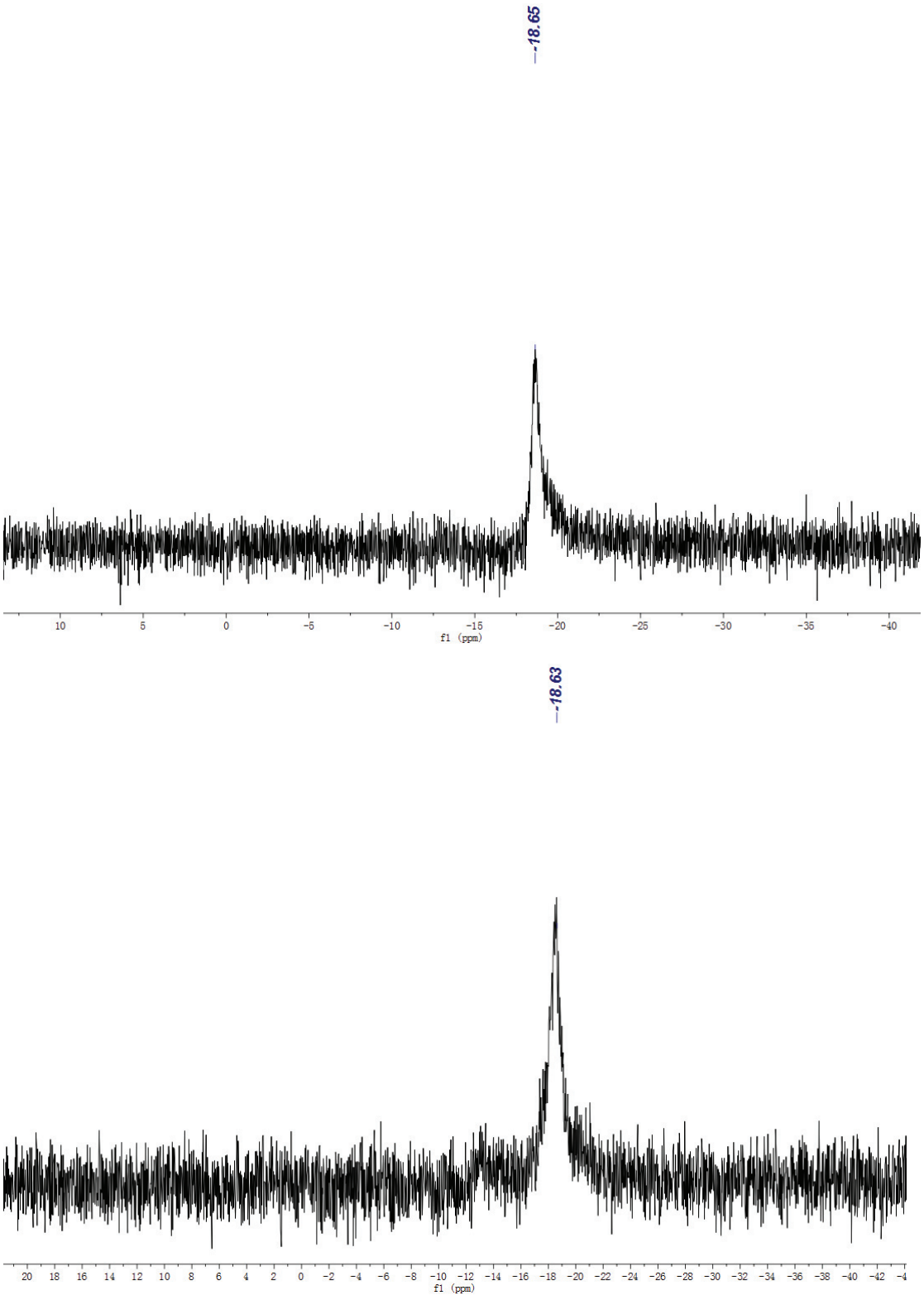

Figure S57. $^{31}P\{^{1}H\}$ NMR spectrum (243 MHz) of **$Cu_5L_2Br_3$** (bulk sample, top) and **$Cu_5L_2Br_3$·2DMF** (crystals, bottom) in DMSO-d_6

Crystal Structure Determination

Crystals suitable for X-ray structural determination were mounted on a *Bruker SMART APEXII* CCD diffractometer. Samples were irradiated with graphite monochromated Mo-Kα radiation (λ= 0.71073 Å) at 173 K for data collection. The data were processed using the *APEX* program suite. Using Olex2,[4] the structures were solved with the ShelXT[5] structure solution program using Intrinsic Phasing and refined with the ShelXL[6] refinement package using Least Squares minimization. Refinement was performed on F^2 anisotropically for all the non-hydrogen atoms by the full-matrix least-squares method. The hydrogen atoms were assigned to idealized geometric positions and included in the refinement with isotropic thermal parameters. The pictures of molecules were prepared using *Pov-Ray* 3.7.0.[7] The crystallographic data are summarized in **Table S1-S5**.

Table S1. Crystallographic data for compound **dpa^{P2}-NHC**

Compound	**dpa^{P2}-NHC**
Formula	$C_{43}H_{42}N_2P_2$
Molecular weight	648.72
Crystal system	orthorhombic
Space group	*Pbca*
Color	brown
Habit	plate
Crystal dimens, mm	0.50×0.16×0.08
a, Å	14.093(2)
b, Å	16.545(2)
c, Å	30.850(5)
α, deg	90
β, deg	90
γ, deg	90
V, Å^3	7193.3(18)
Z	8
D_{calc}, g cm^{-3}	1.198
Abs coeff, mm^{-1}	0.153
F(000)	2752
Radiation; *λ,* Å	Mo Kα, 0.71073
Temp, K	123(2)
Reflections	32784
Independent	6331

Data/restraints/parameters	6331 / 0 / 430
R_{int}	0.0829
R_1 [$I > 2\sigma(I)$]	0.0429
wR_2 (all data)	0.1005
GOF	0.957
solv. for crystallization	THF / hexane

CCDC-1894301 (**dpa^{P2}-NHC**) contains the supplementary crystallographic data. The data can be obtained free of charge from the Cambridge Crystallographic Data Centre via www.ccdc.cam.ac.uk/data_request/cif

Table S2. Crystal data for complexes **1** and **2**.

Compound	**1**	**2**
Formula	$C_{43}H_{43}Au_2Cl_2F_6N_2O_6P_3 \cdot 4(CH_3)_2NCHO$	$C_{86}H_{84}Au_2Cl_2N_4P_4 \cdot 2(CH_3)_2NCHO$
Molecular weight	1551.92	1908.47
Crystal system	Monoclinic	Monoclinic
Space group	*C*2/*c*	$P2_1/n$
Color	yellow	yellow
Habit	block	block
Crystal dimens, mm	0.06×0.06×0.05	0.13×0.13×0.075
a, Å	22.392(5)	14.259(11)
b, Å	16.519(4)	31.08(2)
c, Å	16.628(4)	20.805(16)
α, deg	90	90
β, deg	98.342(3)	99.714(13)
γ, deg	90	90
V, Å^3	6086(2)	9088(12)
Z	4	4
D_{calc}, g cm^{-3}	1.694	1.395
Abs coeff, mm^{-1}	5.049	3.402
F(000)	3064	3840
Radiation; *λ,* Å	Mo Kα, 0.71073	Mo Kα, 0.71073

Temp, K	173(2)	123(2)
Reflections	15774	54785
Independent	6215	22722
Data/restraints/parameters	6215/0/361	19462/150/1067
R_{int}	0.0274	0.0311
R_1 [$I > 2\sigma(I)$]	0.0351	0.0384
wR_2 (all data)	0.1005	0.0930
GOF	1.087	1.019
solv. for crystallization	DMF/ether	DMF/ether

CCDC-1894302 (**1**) and 1894303 (**2**) contain the supplementary crystallographic data. The data can be obtained free of charge from the Cambridge Crystallographic Data Centre via www.ccdc.cam.ac.uk/data_request/cif

Table S3. Crystal data for complexes **3** and **4**.

Compound	**3**	**4**
Formula	$C_{88}H_{84}Au_2F_6N_4O_6P_4S_2\cdot(CH_3)_2NCHO\cdot CH_3CH_2OCH_2CH_3$	$C_{90}H_{84}Au_4F_{12}N_4O_{12}P_4S_4\cdot 4(CH_3)_2NCHO$
Molecular weight	2135.73	2964.90
Crystal system	Monoclinic	Triclinic
Space group	$P2_1/c$	P-1
Color	brown	yellow
Habit	block	plate
Crystal dimens, mm	0.10×0.10×0.08	0.05×0.05×0.02
a, Å	15.779(12)	15.762(2)
b, Å	25.547(19)	15.767(2)
c, Å	24.151(19)	23.977(4)
α, deg	90	82.204(2)
β, deg	97.082(15)	78.435(2)
γ, deg	90	85.067(2)
V, Å^3	9662(13)	5773.2(15)
Z	4	2
D_{calc}, g cm^{-3}	1.519	1.620

Abs coeff, mm^{-1}	3.213	5.270
F(000)	4456	2744
Radiation; *λ,* Å	Mo Kα, 0.71073	Mo Kα, 0.71073
Temp, K	123(2)	123(2)
Reflections	58187	30206
Independent	24011	22790
Data/restraints/parameters	19652/9/1116	19890/99/1368
R_{int}	0.0240	0.0287
R_1 [$I > 2\sigma(I)$]	0.0341	0.0612
wR_2 (all data)	0.0921	0. 1975
GOF	1.016	1.033
solv. for crystallization	DMF/ether	DMF/ether

CCDC-1894304 (**3**) and 1894305 (**4**) contain the supplementary crystallographic data. The data can be obtained free of charge from the Cambridge Crystallographic Data Centre via www.ccdc.cam.ac.uk/data_request/cif

Table S4. Crystal data for complexes **Cu_4LBr_4** and **Cu_2L_2·DMF**.

Compound	**Cu_4LBr_4**	**Cu_2L_2·DMF**
Formula	$C_{43}H_{42}N_2P_2Br_4Cu_4$	$C_{88}H_{84}Cu_2F_6N_4O_6P_4S_2$·[$(CH_3)_2NCHO$+$2CH_3CH_2OCH_2CH_3$]
Molecular weight	1222.57	1906.94
Crystal system	Monoclinic	Monoclinic
Space group	$P2_1/c$	$P2_1/c$
Color	yellow	brown
Habit	block	block
Crystal dimens, mm	0.38×0.25×0.06	0.194×0.118×0.071
a, Å	9.3808(6)	13.0789(17)
b, Å	25.6046(17)	20.410(3)
c, Å	18.5364(12)	34.694(5)
α, deg	90	90
β, deg	97.090(1)	92.526(2)
γ, deg	90	90

V, Å^3	4418.2(5)	9252(2)
Z	2	4
D_{calc}, g cm^{-3}	1.838	1.369
Abs coeff, mm^{-1}	5.622	0.645
F(000)	2400	3980
Radiation; λ, Å	Mo Kα, 0.71073	Mo Kα, 0.71073
Temp, K	123(2)	123(2)
Reflections	23849	48648
Independent	9337	18706
Data/restraints/parameters	9337/6/502	18706/0/1162
R_{int}	0.1118	0.0573
R_1 [$I > 2\sigma(I)$]	0.0556	0.0444
wR_2 (all data)	0.1674	0.1242
GOF	1.022	1.021
solv. for crystallization	DMF/ether	DMF/ether

CCDC-1920385 (**Cu_4LBr_4**) and 1920383 (**Cu_2L_2·DMF**) contain the supplementary crystallographic data. The data can be obtained free of charge from the Cambridge Crystallographic Data Centre via www.ccdc.cam.ac.uk/data_request/cif

Table S5. Crystal data for complexes **Ag_2L_2** and **$Cu_5L_2Br_3$·2DMF**.

Compound	**Ag_2L_2**	**$Cu_5L_2Br_3$·2DMF**
Formula	$C_{88}H_{84}Ag_2F_6N_4O_6P_4S_2$·$(CH_3)_2NCHO$	$C_{88}H_{84}Br_3Cu_2F_6N_4O_6P_4S_2$ ·2$(CH_3)_2NCHO$
Molecular weight	1884.42	2299.21
Crystal system	Monoclinic	Monoclinic
Space group	$P2_1/c$	$P2_1/c$
Color	brown	yellow
Habit	block	plate
Crystal dimens, mm	0.234×0.202×0.056	0.160×0.160×0.073
a, Å	14.6842(8)	29.878(2)
b, Å	28.1889(16)	13.1902(10)
c, Å	21.6554(12)	28.148(2)
α, deg	90	90

β, deg	106.563(1)	117.060(1)
γ, deg	90	90
V, Å^3	8591.9(8)	9878.7(12)
Z	4	4
D_{calc}, g cm^{-3}	1.457	1.546
Abs coeff, mm^{-1}	0.650	2.447
F(000)	3872	4656
Radiation; λ, Å	Mo Kα, 0.71073	Mo Kα, 0.71073
Temp, K	123(2)	123(2)
Reflections	45485	51294
Independent	17532	20103
Data/restraints/parameters	17532/360/1142	20103/0/1169
R_{int}	0.0282	0.0393
R_1 [$I > 2\sigma(I)$]	0.0441	0.0795
wR_2 (all data)	0.1233	0.2276
GOF	1.025	1.093
solv. for crystallization	DMF/ether	DMF/ether

CCDC-1920382 (**Ag_2L_2**) and 1920384 (**$Cu_5L_2Br_3 \cdot 2DMF$**) contain the supplementary crystallographic data. The data can be obtained free of charge from the Cambridge Crystallographic Data Centre via www.ccdc.cam.ac.uk/data_request/cif

References

[1]. S. Fuku-en, J. Yamamoto, M. Minoura, S. Kojima, Y. Yamamoto, *Inorg. Chem.* **2013**, 52, 11700-11702.

[2]. S. Fuku-en, J. Yamamoto, S. Kojima, Y. Yamamoto, *Chem. Lett.* **2014**, 43, 468-470.

[3]. M. Nonnenmacher, D. Kunz, F. Rominger, T. Oser, *Chem. Commun.* **2006**, 1378-1380.

[4]. O. V. Dolomanov, L. J. Bourhis, R. J. Gildea, J. A. K. Howard, H. Puschmann. *J. Appl. Cryst.* **2009**, 42, 339-341.

[5]. G. M. Sheldrick. *Acta Cryst. A* **2015**, 71, 3-8.

[6]. G. M. Sheldrick. *Acta Cryst. C* **2015**, 71, 3-8.

[7]. Persistence of Vision Raytracer (*ver.* 3.7.0); Persistence of Vision Pty. Ltd., 2016; Retrieved from http://www.povray.org/download/

Publications

Publications

(1) Luminescent Di- and Tetranuclear Gold Complexes of Bis(diphenylphosphinyl)-functionalized Dipyrido-annulated N-heterocyclic Carbene
S. Zhang, R. Shang, M. Nakamoto, Y. Yamamoto, Y. Adachi and J. Ohshita
Inorganic Chemistry **2019**, 58(9), 6328–6335.

(2) Bis(diphenylphosphinyl)-functionalized Dipyrido-annulated N-heterocyclic Carbene towards Silver(I) and Copper(I)
S. Zhang, R. Shang, M. Nakamoto, Y. Yamamoto, Y. Adachi and J. Ohshita
Dalton Transactions **2019**, accepted.

Acknowledgements

The studies described in this dissertation have been carried out under the direction of Prof. Yohsuke Yamamoto and Assist. Prof. Rong Shang at the Department of Chemistry, Graduate School of Science, Hiroshima University.

The author sincerely wishes to express his appreciation to Prof. Yohsuke Yamamoto for his continuing guidance, valuable discussions and encouragement throughout the course of studies. Grateful acknowledgment is made to Associate Prof. Masaaki Nakamoto and Assist. Prof. Dr. Rong Shang for their helpful discussions and suggestions.

The author is grateful to Prof. Joji Ohshita (Hiroshima University) and Assist. Prof. Yohei Adachi (Hiroshima University) for their helpful discussions and valuable suggestions.

The author appreciates the kindly help and professional guidance from Prof. Tsutomu Mizuta and Prof. Manabu Abe.

The author also thanks all the members of Prof. Yamamoto's group, past and present, who have provided author great help, not only in research but also in life, in the last three and half years at Hiroshima University.

The author also would like to express appreciations to some of the staff at Hiroshima University. Without their help, the author can not carry out his research such smoothly. In particular, thanks to the NMR staff, Fujikata san, the X-ray staff, Kawata san, and the MS staff, Amimoto san, for their kindly and professional help.

July, 2019

Sihan Zhang

Department of Chemistry, Graduate School of Science

Hiroshima University